Assessing the techno-economic feasibility of battery-electric trucks in Europe: A model-based analysis of lithium-ion batteries and public charging infrastructure

Zur Erlangung des akademischen Grades eines

DOKTORS DER INGENIEURWISSENSCHAFTEN (Dr.-Ing.)

von der KIT-Fakultät für Elektrotechnik und Informationstechnik
des Karlsruher Instituts für Technologie (KIT)

angenommene

DISSERTATION

von

M.Sc. Steffen Fabian Link
geboren in Karlsruhe

Tag der mündlichen Prüfung:	02.10.2025
Hauptreferent:	Prof. Dr.-Ing. Martin Doppelbauer
Korreferent:	Prof. Dr. Martin Wietschel

Karlsruhe, November 2025

Danksagung

Die vorliegende Dissertation entstand im Rahmen meiner Tätigkeit als wissenschaftlicher Mitarbeiter am Fraunhofer-Institut für System- und Innovationsforschung ISI. An dieser Stelle möchte ich allen danken, die mich in vielfältiger Weise bei der Erstellung dieser Arbeit unterstützt haben.

Mein besonderer Dank gilt Herrn Prof. Dr.-Ing. Martin Doppelbauer für die Betreuung dieser Dissertation, für das mir entgegengebrachte Vertrauen sowie für die stets konstruktive und wertschätzende Zusammenarbeit von Beginn bis zum Abschluss dieser Arbeit. Ebenso danke ich meinem Zweitgutachter und Mentor, Herrn Prof. Dr. Martin Wietschel, für den regelmäßigen und intensiven Austausch sowie für seine wertvollen und motivierenden Hinweise, die maßgeblich zum Gelingen dieser Arbeit beigetragen haben.

Darüber hinaus danke ich Prof. Dr.-Ing. Ulrike Krewer und Prof. Dr.-Ing. Thomas Leibfried für ihre Teilnahme am Prüfungsausschuss sowie Prof. Dr.-Ing. John Jelonnek für den Vorsitz der Prüfungskommission.

Mein Dank gilt auch allen Kolleginnen und Kollegen sowie meinen studentischen Hilfskräften, die mich in dieser Zeit unterstützt und mir im Projektalltag den notwendigen Freiraum eingeräumt haben, um mit Freude und Hingabe an meinen Forschungsthemen zu arbeiten. Besonders dankbar bin ich Prof. Dr. Patrick Plötz und Dr. Annegret Stephan für ihre wertvolle Unterstützung und die vielen inspirierenden Gespräche und Anregungen.

Nicht zuletzt gilt mein tief empfundener Dank meiner Freundin, meiner Familie und meinen Freunden für ihre Geduld, ihr Verständnis und ihre unermüdliche Unterstützung während der Erstellung dieser Arbeit.

Kurzfassung

Der schwere Straßengüterverkehr verursacht in Europa etwa 7% der energiebedingten Treibhausgasemissionen, weshalb ein schneller Umstieg auf emissionsfreie Lkw notwendig wird. Hierfür sind batterieelektrische Lkw, gegenüber anderen Technologien zur Dekarbonisierung, sehr wahrscheinlich die vielversprechendste Option. Jedoch äußern Flottenbetreiber nach wie vor Bedenken hinsichtlich der Eignung von batterieelektrischen Lkw für ihren spezifischen Einsatz, während die Vielfalt im Lkw-Markt allgemeingültige Aussagen erschwert. Diese Arbeit nutzt einen simulationsbasierten Ansatz um die techno-ökonomische Machbarkeit von batterieelektrischen Lkw in Europa (EU-27, EFTA und Großbritannien) zwischen 2025 und 2030 zu untersuchen. Hierbei werden die vielfältigen Einsatzbedingungen von Lkw und Wechselwirkungen zwischen der individuellen Nutzung und Kaufentscheidung einzelner Besitzer, den Lkw- und Batteriespezifikationen, und der Ladeinfrastruktur berücksichtigt.

Zu diesem Zweck wurden fünf sequenzielle Simulationsmodelle auf Basis umfangreicher Realdaten entwickelt. Zu Beginn steht die neuartige, wahrscheinlichkeitsbasierte Simulation von Fahrprofilen, welche detaillierte mehrjährige Einsatzpläne von Lkw mit wechselnden Nutzungsbedingung abbildet. Benötigte Informationen wie Energieverbrauch und Batterieeigenschaften werden dann über nachfolgende Simulationsmodelle ergänzt. Die technische Machbarkeit wird durch die Batteriedimensionierung sowie Zwischenladen sichergestellt und mittels verschiedener Metriken und drei Ladeszenarien evaluiert. Für jeden Einsatzplan wird die Wirtschaftlichkeit von batterieelektrischen Lkw anhand von länderspezifischen Gesamtbetriebskosten in drei Kostenszenarien bewertet und gegenüber Diesel-Lkw verglichen. Abschließend werden mögliche reale Standorte für öffentliche Ladeinfrastruktur entlang des europäischen TEN-T Straßennetzes identifiziert.

Die Ergebnisse zeigen, dass die große Bandbreite an Einsatzbedingungen sowie wenige extreme Touren/Tage pro Einsatzplan die technische Machbarkeit von batterieelektrischen Lkw einschränken. Länderspezifische Faktoren wie Mautgebühren und das Kostenverhältnis von Strom zu Diesel wirken im Besonderen auf die Wirtschaftlichkeit ein. Bei einem strikten 1:1 Ersatz von Diesel-Lkw wird die technische Machbarkeit vermutlich auch weiterhin eingeschränkt bleiben. Allerdings können nahezu alle Einsatzpläne bereits heute elektrifiziert werden, insofern geringfügige Anpassungen zugelassen und die richtige Ladestrategie und Batteriegröße (500–700 kWh) kombiniert werden. LFP-Batterien stellen sehr wahrscheinlich die vielversprechendste Technologie dar, ergänzt von nickelreichen Chemien – vor allem für schwere Anwendungen oder bei unzureichender Ladeinfrastruktur. Bereits heute können batterieelektrische Lkw in einigen Ländern profitabel betrieben werden und erzielen im Jahr 2030 mit hoher Wahrscheinlichkeit einen Kostenvorteil gegenüber Diesel-Lkw in allen untersuchten Ländern.

Diese Dissertation basiert auf meiner Forschung am Fraunhofer-Institut für System- und Innovationsforschung ISI unter der Betreuung von Prof. Dr.-Ing. Martin Doppelbauer am Elektrotechnischen Institut (ETI) sowie Prof. Dr. Martin Wietschel am Institut für Industriebetriebslehre und Industrielle Produktion (IIP) des Karlsruher Instituts für Technologie (KIT).

Abstract

Reducing greenhouse gas emissions from road transport requires a fast transition to zero-emission trucks, with heavy road freight transport responsible for approximately 7% of energy-related emissions in Europe. Battery-electric trucks are very likely the most promising solution for decarbonizing European road freight since series models are available and numerous studies confirm their techno-economic supremacy over alternative decarbonization pathways. However, fleet operators still cite concerns about the viability of battery-electric trucks for their specific operations, and the truck market heterogeneity complicates generalized conclusions. This thesis addresses these challenges through simulations that consider the variety of truck operations and related interdependencies between individual truck owner purchase decisions, truck and battery specifications, and charging infrastructure. The analysis focuses on the European truck market (EU-27, EFTA, and the UK) between 2025 and the early 2030s.

To evaluate the techno-economic feasibility of battery-electric trucks, this thesis developed five consecutive simulation models based on extensive real-world datasets. Central to this is the novel probabilistic driving profile simulation that generates detailed operating schedules throughout the first-user service life for each truck, capturing real-world variations in trip distances, cargo weights, and ambient conditions tailored to different truck classes and regions. Complementary information such as energy consumption and battery characteristics is added via respective simulation models. The technical feasibility is ensured via appropriate battery sizing and interim charging and evaluated via different metrices and for three charging scenarios. For each schedule, country-specific total costs of ownership (TCO) are used to compare the profitability of battery-electric trucks with that of their diesel counterparts in three cost scenarios. Finally, specific real-world locations for public charging infrastructure along the European TEN-T highway network are identified.

The results indicate that the wide range of operational patterns in Europe and a few extreme tours/days per schedule complicate the technical feasibility of battery-electric trucks. Country-specific factors, such as toll rates and differential costs of diesel and electricity, further impact profitability. When replacing diesel trucks one by one, the technical feasibility remains limited. However, almost all schedules can be electrified by allowing minor schedule adjustments and combining the right charging strategy and battery choice, with 500-700 kWh needed the most. LFP batteries seem the most promising technology in almost all applications because of their aging resistance and better fast charging capability, complemented by nickel-rich chemistries, especially in the early market stages. Plus, the latter are favorable for heavily loaded applications, if charging infrastructure is limiting, or if truck owner continue striving for oversized batteries to increase flexibility. Even today, using battery-electric trucks can be profitable in some countries, and by 2030 thery are likely to beat diesel trucks in terms of costs in most cases.

This thesis is based on my research conducted at the Fraunhofer Institute for Systems and Innovation Research ISI under the supervision of Prof. Dr.-Ing. Martin Doppelbauer at the Institute of Electrical Engineering (ETI) and Prof. Dr. Martin Wietschel at the Institute for Industrial Production (IIP), both at the Karlsruhe Institute of Technology (KIT).

Contributing publications

This thesis is based on my research conducted at the Fraunhofer Institute for Systems and Innovation Research ISI and accompanied by six publications, listed below. A full list of publications is given at the end.

- **Link, S.**, & Plötz, P. (2022): Technical Feasibility of Heavy-Duty Battery-Electric Trucks for Urban and Regional Delivery in Germany -A Real-World Case Study. *World Electric Vehicle Journal*, 13 (9), 161. https://doi.org/10.3390/wevj13090161

- **Link, S.**, Neef, C., & Wicke, T. (2023): Trends in Automotive Battery Cell Design: A Statistical Analysis of Empirical Data. *Batteries*, 9 (5), 261. https://doi.org/10.3390/batteries9050261

- Teichert, O., **Link, S.**, Schneider, J., Wolff, S., Lienkamp, M. (2023): Techno-economic cell selection for battery-electric long-haul trucks. *eTransportation Journal*, Volume 16. https://doi.org/10.1016/j.etran.2022.100225

- **Link, S.** & Plötz, P. (2024). Geospatial truck parking locations data for Europe. *Data in Brief Journal*, Volume 54. https://doi.org/10.1016/j.dib.2024.110277

- **Link, S.**, Stephan, A., Speth, D., Plötz P. (2024): Rapidly declining costs of truck batteries and fuel cells enable large-scale road freight electrification. *Nature Energy* 9, 1032–1039 (2024). https://doi.org/10.1038/s41560-024-01531-9

- **Link, S.**, Schneider, L., Stephan, A., Weymann, L., Plötz, P. (2025): Feasibility of meeting future battery demand via domestic cell production in Europe. *Nature Energy* 10, 526–534 (2025). https://doi.org/10.1038/s41560-025-01722-y

Contents

List of Figures

List of Tables

List of Abbreviations

AAM	Anode active material
AC	Alternating current
AFIR	Alternative Fuels Infrastructure Regulation
ANOVA	Analysis of variance
BET	Battery-electric truck
BMS	Battery management system
BTMS	Battery thermal management system
BN	Bayesian Networks
CAM	Cathode active material
CAPEX	Capital expenditure
CCS	Combined Charging System
COP	Coefficient of Performance
CPE	Constant Phase Element
DC	Direct current
DOD	Depth of discharge
DT	Diesel truck
EC	European Commission
ECM	Equivalent circuit model
ECDF	Empirical cumulative density function
EU	European Union
EMS	European Modular System
ERFT	European road freight transport
FCET	Fuel cell electric truck
FCLM	Flow Capturing Location Model
FRLM	Flow Refuelling Location Model
GAN	Generative Adversarial Networks
GHG	Greenhouse gas
GNLM	General Non-Linear Models
GVW	Gross vehicle weight
HDT	Heavy-duty trucks
HDV	Heavy-duty vehicles
IQR	Interquartile range
LAM	Loss of active material
LC	Loss of conductivity
LCC	Life cylce costs
LFP	Lithium iron phosphate
LH	Long haul
LIB	Lithium-ion battery
LLI	Loss of lithium inventory
LOE	Loss of electrolyte
MHDT	Medium- and heavy-duty trucks
MCMC	Markov Chain Monte Carlo
MCLM	Maximum Cover Location Problem
MCS	Megawatt Charging System
NCA	Lithium nickel cobalt aluminium oxides
NMC	Lithium nickel manganese cobalt oxides
NST	Nomenclature for transport statistics
NUTS	Nomenclature of territorial units for statistics
OCV	Open circuit voltage
OD	Origin-destination
OPEX	Operational expenditure
OSM	OpenStreetMap
PCA	Principal Component Analysis
PDF	Probability density function
PNGV	Partnership for a New Generation of Vehicles
RD	Regional delivery
RPE	Retail price equivalent
SCLM	Set Cover Location Problem
SD	Standard deviation
SEI	Solid electrolyte interphase
SOC	State of charge
SOH	State of health
SSTPA	Safe and Secure Truck Parking Area
TEN-T	Trans-European Transport Network
TCO	Total costs of ownership
UD	Urban delivery
VC	VECTO class
VECTO	Vehicle energy consumption calculation Tool
WHVC	World Harmonized Vehicle Cycle

List of Symbols

Battery modeling:

Formula symbol	Unit	Description
$c_{p,bat}$	$J\,kg^{-1}K^{-1}$	Specific heat capacity of the battery system
C_1	F	Capacitance of first RC element (Thevenin)
C_{DL}	F	Capacitance (double layer) in RC-element
C_{SEI}	F	Capacitance (solid electrolyte interface) in RC-element
C_{ch}, C_{dch}	h^{-1}	Battery charge (ch) / discharge (dch) C-rate
DOD	$-$	Depth of discharge
E_{bat}	kWh	Total battery capacity (gross)
ϵ_{grav}	$Wh\,kg^{-1}$	Specific energy (system-level)
ϵ_{vol}	$Wh\,l^{-1}$	Volumetric energy density (system-level)
$\eta_{bat,ch}, \eta_{bat,dch}$	$-$	Battery charge (ch) / discharge (dch) efficiency
f_i	$-$	Generic functional relation i
FEC	$-$	Full equivalent cycles (FEC)
FEC_{cert}	$-$	Certified number of FEC for an 80% SOC window
I_{cell}	A	Cell current
m_{bat}	kg	Total battery weight
Q_{cell}	Ah	Cell capacity
Q_{loss}	$-$	Capacity loss (relative)
$Q_{loss,cal}$, $Q_{loss,cyc}$	$-$	Capacity loss due to calendar (cal) or cyclic (cyc) aging
r_{SOC}	$-$	SOC operating window for service life
R_0	Ω	Series resistance
$R_{0,ch}, R_{0,dch}$	Ω	Series charging (ch) / discharging (dch) resistance
R_1	Ω	Resistance of first RC-element (Thevenin)
R_{inc}	$-$	Cell resistance increase
$R_{inc,cal}, R_{inc,cyc}$	$-$	Cell resistance increase due to calendar (cal) or cyclic (cyc) aging
R_{CT}	Ω	Resistance (charge transfer) in RC-element
R_{ref}	Ω	Cell reference resistance (20°C, 50% SOC, 1s pulse duration)
R_{SEI}	Ω	Resistance (solid electrolyte interface) in RC-element
SOC	$-$	State of Charge (SOC)
$\overline{SOC}$	$-$	Average SoC operating window
SOH	$-$	State of Health (SOH)
t	s	time
$t_{cert,cal}$	$years$	Certified battery age (with or without utilization)
T_{cell}	$°C$	Cell temperature
τ_{SOH}	$-$	Remaining battery life
U_{nom}	V	Nominal cell voltage
U_{OCV}	V	Cell Open Circuit Voltage (OCV)
U_T	V	Cell terminal voltage
$z_{Q,cal}, z_{Q,cyc}$	$-$	Aging exponents for capacity loss
$z_{R,cal}, z_{R,cyc}$	$-$	Aging exponents for resistance increase
$z_{useable}$	$-$	Share of usable battery capacity
Z_W	Ω	Warburg impedance

Vehicle simulation:

Formula symbol	Unit	Description
a	m/s^2	Applied acceleration
a_{acc}, a_{dec}	m/s^2	Acceleration (acc) / deceleration (dec) limit
a_{mot}	m/s^2	Acceleration limit by the available motor power
α	rad	Road slope
α_{cab}	W/K	Cabin heat losses
A_{drag}	m^2	Truck air drag (frontal area x drag coefficient)
$COP_{HVAC,C}, COP_{HVAC,H}$	$-$	COP of the HVAC system for heating (H) and cooling (C)
c_{rr}	$-$	Tire rolling resistance coefficient
ec_{BET}, ec_{DT}	kWh/km	Energy consumption electric truck (BET) and diesel truck (DT)
$\eta_{ICE}, \eta_{EM}, \eta_{TM}, \eta_{AX}$	$-$	Component efficiencies: Engine (ICE), electric motor (EM), transmission (TM), and axle (AX)
η_{EDT}, η_{DDT}	$-$	Drivetrain efficiencies: Electric (EDT) and diesel (DDT)
F_{Drag}	N	Aerodynamic resistance
F_{Grad}	N	Inclination resistance
F_{Roll}	N	Rolling resistance
F_{Tot}	N	Total driving resistance
g	m/s^2	Gravitational constant
j	$-$	Simulation step index
J_{wheels}	$kg * m^2$	Total inertia of all tires
k	$-$	Driving cycle step index
k_{dec}	$-$	Driving cycle index with target speed reduction
l_{wb}	mm	Truck wheelbase
m_{DT}, m_{BET}	kg	Total truck weight: diesel (DT) or battery-electric (BET)
m_{DTCM}, m_{BETCM}	kg	Diesel or battery-electric truck curb mass
m_{DPT}, m_{eAx}	kg	Weight of the diesel powertrain (DPT) or electric axle (eAx)
$m_{payload}$	kg	Payload weight
$m_{trailer}$	kg	Weight of trailer (rigid trucks) or semitrailer(tractors)
m_{Total}	kg	Total vehicle weight
v	m/s	Truck driving speed
$\bar{v}$	m/s	Average truck driving speed
v_{cycle}	m/s	Target speed defined by the driving cycle
v_{target}	m/s	Target speed incl. deceleration phases
P_{aux}	W	Total auxiliary power
P_{bat}	W	Total power drawn or supplied to the battery
P_{BTMS}	W	Electric power demand for the BTMS
P_{HVAC}	W	Electric power demand for the HVAC system
$P_{H,max}$	W	Maximum heating power of the HVAC system
P_{mot}	W	Applied motor power
P_{rated}	W	Rated motor power
r_{dyn}	mm	Dynamic tire radius
r_{wheel}	mm	Tire radius (incl. housing)
ρ	kg/m^3	Air density
s	m	Distance along the driving cycle
S_{Truck}	$-$	Total truck specification
t	s	Time
t_{stop}	s	Stop duration
T_{amb}, T_{cab}	$°C$	Temperature: Ambient (amb) or driver cabin (cab)
$V_{cabin}, V_{Tank}, V_{Frame}$	mm^3	Available installation spaces for the battery
$\omega_1, \omega_2, \omega_3$	$-$	BTMS regression coefficients

Cost model:

Formula symbol	Unit	Description
$\beta_1, \dots, \beta_5$	–	Regression coefficients for truck resale values
C_{CAPEX}	$€_{2020}$	Total capital expenditures
C_{OPEX}	$€_{2020}$	Total operating expenditures
C_{truck}	$€_{2020}$	Truck purchase costs
$C_{energy,t}$	$€_{2020}$	Energy costs in year *t*
$C_{toll,t}$	$€_{2020}$	Toll costs in year *t*
$C_{ms,t}$	$€_{2020}$	Maintenance costs in year *t*
$C_{in,t}$	$€_{2020}$	Insurance costs in year t
CRF	–	Capital recovery factor
$c_{chassis}$	$€_{2020}$	Truck chassis costs
c_{ICE}, c_{EAT}	$€_{2020}$/kW	Specific component costs in the diesel powertrain
c_{BAT}, c_{EM}, c_{HV}	$€_{2020}$/kW	Specific component costs in the electric powertrain
$c_{ms,BET}, c_{ms,DT}$	$€_{2020}$/km	Specific maintenance costs by truck technology (DT or BET)
$c_{toll,i}$	$€_{2020}$/km	Specific toll rate per trip *i*
$c_{diesel,t}$	$€_{2020}$/l	Diesel costs in year *t*
$c_{ch,dpt,t}, c_{ch,pub,t}$	$€_{2020}$/kWh	Total charging costs for depot (dpt) or public (pub) in year *t*
$c_{elec,dpt,t}, c_{elec,pub,t}$	$€_{2020}$/kWh	Electricity costs for depot (dpt) or public (pub) in year *t*
$c_{charger,dpt,t}, c_{charger,pub,t}$	$€_{2020}$/kWh	Costs of infrastructure for depot (dpt) or public (pub) in year *t*
$c_{grid,dpt,t}, c_{grid,pub,t}$	$€_{2020}$/kWh	Costs of grid extension for depot (dpt) or public (pub) in year *t*
$d_{annual,t}$	km	Total distance in year *t*
d_{tot}	km	Total distance until end of ownership
$e_{DT,i}, e_{BET,i}$	kWh	Energy consumption for trip *i* by truck technology (DT or BET)
N_{trips}	–	Total number of trips until end of ownership
r	–	Discount rate
$r_{toll,i}$	–	Proportion of toll road use per trip *i*
RPE	–	Retail price equivalent factor
RV_{truck}	$€_{2020}$	Resale value of the truck
RV_{bat}	$€_{2020}$	Resale value of the battery
t_{tot}	yr	Total ownership period
$p_{bat,scr}$	–	Battery scrappage value

Stochastic modeling and driving profile simulation:

Formula symbol	Unit	Description
$\mathrm{B}, \mathrm{E}, \Gamma$	–	Conditional distribution function: Beta, Empirical, Gamma
$\mathrm{C}(\cdots)$	–	Copula function
cty	–	Country variable
$\mathrm{d}_{\mathrm{trip}}, \mathrm{d}_{\mathrm{day}}, \mathrm{d}_{\mathrm{week}}$	km	Distance information per trip, per day, and per week
$\mathrm{d}_{\mathrm{old}}$	km	Previous weekly distance
D_x	–	General conditional distribution function for parameter x
f_i	–	Generic functional relation i
γ, κ, λ	–	Distribution parameters: shift, shape, scale
$\widehat{\mathrm{M}}_{\mathrm{TKM},w}$	tkm	Targeted transport performance for week w
$\mathrm{m}_{\mathrm{tripPL},i}$	kg	Payload for trip i
$\mathrm{m}_{\mathrm{PL,max},w}$	kg	Maximum payload among all trips per week w
$\mathrm{M}_{\mathrm{nst}}$	–	NST transition matrix from previous to next week
$\mathrm{n}_{\mathrm{empty},w}, \mathrm{n}_{\mathrm{loaded},w}$	–	Number of empty / loaded trips per week w
$\mathrm{n}_{\mathrm{subtrip},i}$	–	Number of subtrips/microtrips per trip i
$\mathrm{n}_{\mathrm{trips},w}$	–	Number of total trips per week w
nst_w	–	NST variable (goods classification) per week w
$\mathrm{nst}_{\mathrm{old}}$	–	Previous NST variable
$\mathrm{NST}_{\mathrm{All}}$	–	All possible NST classes
ops_w	–	Operation variable per week w
$\mathrm{OPS}_{\mathrm{All}}$	–	All possible operation types (
$\mathrm{p}(\mathrm{x})$	–	Probability density function of random variable X (continuous)
$\mathrm{P}(\mathrm{x})$	–	Probability that random variable X takes the value x (discrete)
$\mathrm{p}_{\mathrm{norm}}, \mathrm{P}_{\mathrm{norm}}$	–	Normalized probabilities
$\mathrm{r}_{\mathrm{driving},d}$	–	Ratio of driving time to total operating time per day d
s_x	–	Weighting function for parameter x
$\mathrm{t}_{\mathrm{ARR},d}, \mathrm{t}_{\mathrm{ARR},i}$	hh: mm	Arrival time per day d (last trip of the day) or per trip i
$\mathrm{t}_{\mathrm{break},i}, \mathrm{t}_{\mathrm{load},i}, \mathrm{t}_{\mathrm{unload},i}, \mathrm{t}_{\mathrm{rest},i}, \mathrm{t}_{\mathrm{stop},i}, \mathrm{t}_{\mathrm{idle},i}$	min	Time per trip i for driving break (break), cargo loading(load), cargo unloading (unload), rest period (rest), stopps at customers (stop), and idling (idle)
$\mathrm{t}_{\mathrm{drive},i}$	min	Driving time per trip i
$\mathrm{t}_{\mathrm{DEP},d}, \mathrm{t}_{\mathrm{DEP},i}$	hh: mm	Departure time per day d (first trip of the day) or per trip i
tc_w	–	Truck class variable per week w
$\mathrm{TC}_{\mathrm{All}}$	–	All truck classes
$\mathrm{TC}_{\mathrm{VG}}$	–	All selectable truck classes limited by the defined VECTO group
$\mathrm{type}_{\mathrm{trip},i}$	–	Trip type variable per trip i
$\mathrm{TT}_{\mathrm{All}}$	–	All selectable trip types
v_d	km h^{-1}	Average driving speed per day d
X_{i}	–	Random variable i
$\mathrm{z}_{\mathrm{tollRoad},d}$	–	Share of driving on toll roads per day d

1 Introduction

1.1 Motivation

Reducing greenhouse gas (GHG) emissions is pivotal in limiting global warming in line with the Paris Climate Agreement and reaching European climate neutrality by 2050 (Jaramillo et al. 2023; Plötz et al. 2023b). However, decarbonization poses substantial difficulties for many sectors, such as transport and particularly heavy road freight (Creutzig et al. 2015). European freight transport has experienced strong growth recently, a trend expected to persist, amounting to more than 15 billion tons of freight per year and with trucks as flexible, responsive and cost-effective transport solution handling about three-quarters of all transported freight (EC 2024). With annual sales of more than 400,000 units and over 7 million medium- and heavy-duty trucks (MHDTs[1]) in operations on European roads, these vehicles account for about 220 Mt CO_2eq or 7% of Europe`s total GHG emissions per year (EC 2024[2], **Table S1**, **Table S2**).

Global key markets have instituted specific CO_2 reduction targets for newly sold heavy-duty vehicles (HDVs) to accelerate road freight decarbonization. Notably, the European Union (EU) has agreed on ambitious tailpipe emission reduction targets of -43% by 2030, -65% by 2035, and -90% by 2040 for newly sold trucks compared with 2019/20 levels (Regulation (EU) 2024/1610). Accordingly, all European truck manufacturers expressed their commitment to low-carbon solutions by announcing a 100% zero-emission truck (ZET) sales target by 2040 and high interim targets of up to 60% by 2030 (Mulholland et al. 2023). California imposed the phase-out of conventional combustion trucks by 2036 (Newsom 2023), with certain US states expected to follow and nationally strenghened emission reduction standards in the introduction (Phase 3 – EPA 2024). Last, China is also anticipated to tighten its tailpipe emission reduction targets soon to comply with its near-zero emission target by 2060 (Khanna et al. 2021; Zhang et al. 2023).

While achieving these targets necessitates the fast deployment of ZETs, there is still an active and cross-national debate among industry, politics, and academia about different measures and technological pathways for decarbonizing HDVs (Link et al. 2024c). Specifically, this debate concerns the respective roles – from low-volume product for specialist applications to the prevalent mass-market technology – of battery-electric trucks (BETs) and fuel cell electric trucks (FCETs) in future truck fleets (Plötz 2022). However, there is increasing evidence that prospects for BETs as the leading future truck technology and no-regret option seem more favorable at higher confidence, with BET series models available from all major European truck manufacturers (ITF 2023; Link et al. 2024b).

[1] Defined as trucks with a gross vehicle weight above 3.5 tons
[2] Reported for the EU-27 and EFTA member states, excluding the UK

In fact, an increasing number of studies[3] confirm the technical feasibility and profitable operations for BETs in almost all applications as of today. However, the market shares of BETs were less than 2% in Europe by 2022-2024 (Ananda et al. 2024; Mulholland et al. 2024), even though the European Commission (EC) and several member states grant certain ZET privileges such as purchase subsidies, toll exemptions or higher permissible weights. In addition, the European Commission promotes the deployment of the newly required charging infrastructure along highways with fixed targets. However, only a few charging locations are available today. Thus, complying with the CO_2 reduction targets and meeting the announced manufacturer targets will require a sharp boost in the market diffusion of BETs and their required charging infrastructure until 2030 and beyond.

A critical factor influencing this market skepticism is the heterogeneous nature of both the logistics systems and the accompanying truck markets. While trucks are primarily used for transporting goods from urban delivery to international long-haul, different industries – from agriculture and timber industry to food retail or construction and mining – require specialized body types, specific axle configurations, power take-offs, or auxiliary power units (Hilgers 2023). Additionally, truck owners and fleet operators continue to question the technical feasibility of BETs for their specific needs and individual schedules with distinct delivery times and varying tours. Accordingly, surveys reflect concerns about limited vehicle range, restricted routing, reduced operational flexibility, inadequate charging infrastructure, questionable durability beyond one million kilometers, potential payload penalties, or the necessity for operating private charging infrastructure for overnight charging at their depots (Anderhofstadt et al. 2019; Bae et al. 2022; Göckeler et al. 2022; Ragon et al. 2022b; Spiller et al. 2023). These technical to operational challenges are further accentuated by a pronounced cost sensitivity in the logistics sector, where narrow profit margins complicate the profitability of BETs.

Given this background, it can be summarized that: (1) BETs are most likely the prevalent technology to decarbonize heavy road freight transport and comply with legally binding climate targets; (2) truck owners express numerous concerns toward operating BETs, ranging from limited vehicle ranges to missing charging infrastructure and high costs; and (3) the heterogeneity of the truck market renders standardized solutions or generalizations about the techno-economic feasibility of BETs both challenging and potentially inadequate.

1.2 Problem definition and research gap

This thesis aims to assess the techno-economic feasibility of BETs for the European truck market (EU-27, EFTA, and the UK) around 2025 to the early 2030s using simulation and various empirical datasets to address electrification issues and current shortcomings, particularly those emerging from truck heterogeneity and variety of operations.

[3] See full overview in Subchapter 2.2

The large-scale success of BETs relies on profitable operations, technical feasibility, and broad operational availability given the specific utilization patterns of individual truck owners, all of which are highly affected by battery characteristics and available charging infrastructure. Accordingly, this simplified constellation involves three general players: (1) Truck owners select BETs and the required battery capacity according to their operating schedules, facing techno-economic trade-offs among costs, flexibility or operational compliance, payload sensitivity, or available charging infrastructure. (2) Truck manufacturers anticipate and incorporate individual customer requirements in their tailored battery design (capacities, chemistries, formats) to optimally serve most truck owners in the market. (3) Local charging infrastructure providers strategically identify attractive locations with likely high charging demand and anticipate chosen battery characteristics in the BET fleet to accommodate local charging needs and set prices that make their operations profitable. These interdependent dynamics, which have – to the best of the author's knowledge – not been thoroughly analyzed to date, are illustrated in **Figure 1**.

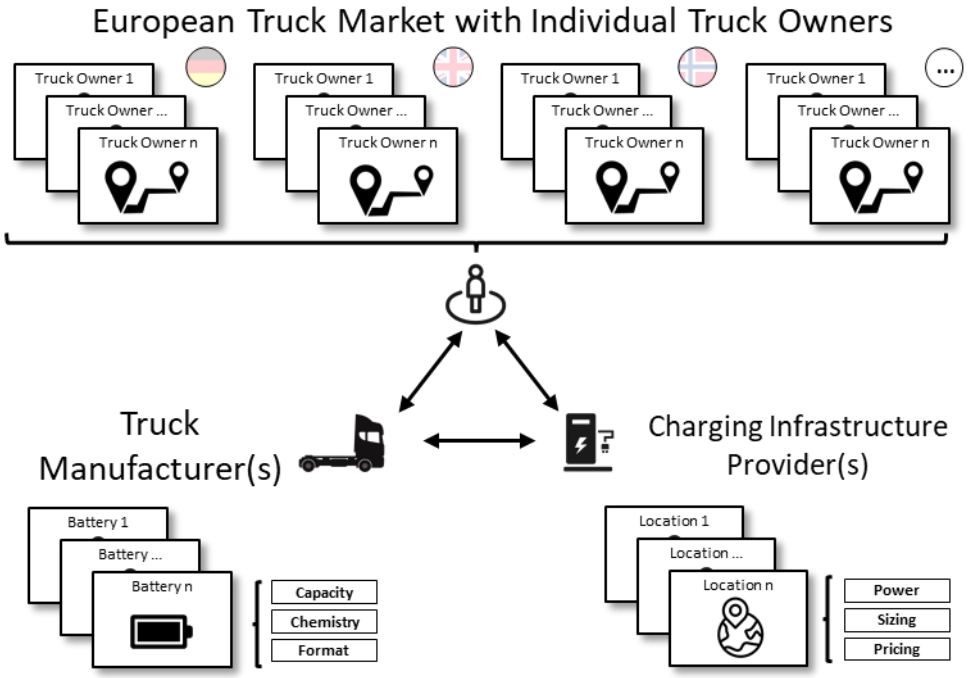

Figure 1: Interaction scheme in the techno-economic BET feasibility

Accordingly, two specific research gaps can be identified: (1) Insuffiencies in modeling truck operating patterns in the techno-economic assessment of BETs with individual operating schedules, and (2) missing joint evaluations for dynamics between truck batteries and charging infrastructure. Hence, two main research questions and corresponding subquestions are identified:

> *Q1: Which factors distinguish the operating patterns of trucks in Europe and how can such operations be modeled to specifically assess the techno-economic feasibility of battery-electric trucks?*

Initially, this involves developing a suitable simulation model and compiling corresponding datasets. Different submodels should be able to cover critical elements for an accurate techno-economic assessment of BETs amidst the European market heterogeneity and large variability: (1) a driving profile simulation should create individual operational schedules that reflect truck-specific utilization over an extended period; (2) a vehicle simulation should determine the energy consumption for each trip planned in the operational schedule; (3) a battery simulation should reflect the electrical and aging characteristics; (4) a cost model should reflect regionalized cost patterns for purchasing and operating trucks by individual ownerns; and (5) an infrastructure model should reflect the costs and availability of charging infrastructure. Accordingly, different modeling approaches need to be harmonized, with balancing complexity and runtime versus accuracy. Model dependencies and parameterization follow from analyses of similar models, literature and surveys, and statistical evaluations of real-world datasets. The first research question is further operationalized in two subquestions:

> *Q1-1: What energy requirements emerge in daily operating schedules and what battery capacities are required to mimic current driving patterns in different European countries?*

> *Q1-2: Which battery technology is preferable and what battery capacities can be installed without impacting the truck's payload?*

The second research question (Q2) extends to the first one and focuses on the interdependent dynamics between charging infrastructures and the battery selection of BETs in more detail, analyzing potential strategies and best responses to different possible actions. As part of this, potential locations for charging infrastructure in Europe will be identified.

> *Q2: How do truck battery capacities and the available charging infrastructure interact and how to consider both in the techno-economic feasibility?*

This question is operationalized in two subquestions:

> *Q2-1: What impact do public charging prices have on the cost-effective choice of battery capacities for individual trucks?*

> *Q2-2: Where to locate public truck charging facilities in Europe?*

Accordingly, this thesis offers four main contributions to the interdependent dynamics between customer-specific operating patterns and requirements, electric trucks and their battery design, and truck charging infrastructure: (1) clarify different truck operating patterns across Europe; (2) help individual truck owners choosing the suitable battery capacities for their specific needs and individual schedules; (3) support truck and battery engineers in developing tailored and requirements-oriented product designs for the European market; and (4) help federal planning and private entities to identify attractive locations for the deployment of public truck charging infrastructure, which is also crucial for proactive grid planning.

1.3 Outline and scope

The structure of this thesis is organized as follows: **Chapter 2** starts by introducing background information on trucks and regulations and proceeds by summarizing related literature on BETs, batteries, charging infrastructure planning, and activity modeling. These summaries involve both thematic findings and methodological elements. **Chapter 3** introduces the core datasets for this thesis and closes with related limitations. **Chapter 4** details the model development process, starting with an overview, advancing through the individual simulation models, and closing with related limitations. **Chapter 5** outlines the modeling results, addresses the related research questions, and closes with a discussion of limitations and future research. The thesis concludes in **Chapter 6** with a summary of conclusions and implications.

Figure 2 summarizes the general scope and limitations of this thesis. The analysis focuses on the European market (EU-27, EFTA, and the UK) and its specic truck design concerning the period 2025 to the early 2030s and the corresponding available lithium-ion battery (LIB) technologies and charging systems. Uncertainties and special effects of early market diffusion phases are not addressed. Current logistic requirements and truck operating patterns serve as the baseline because of the availability of data. Assessments are centered on the techno-economic feasibility of BETs in Europe for initial customers (first-user perspective), with a focus on comparable pan-European assessments rather than highlighting single countries. Heavy-duty trucks (HDTs) with a gross vehicle weight (GVW) above 12 tons (class N3) constitute the core segment. Other alternative decarbonization pathways are out of scope, except for potential biogenic or synthetic diesel blends as a benchmark for cost parity calculations of BETs versus diesel trucks (DTs). The consideration of charging technologies is limited to stationary plug-in solutions.

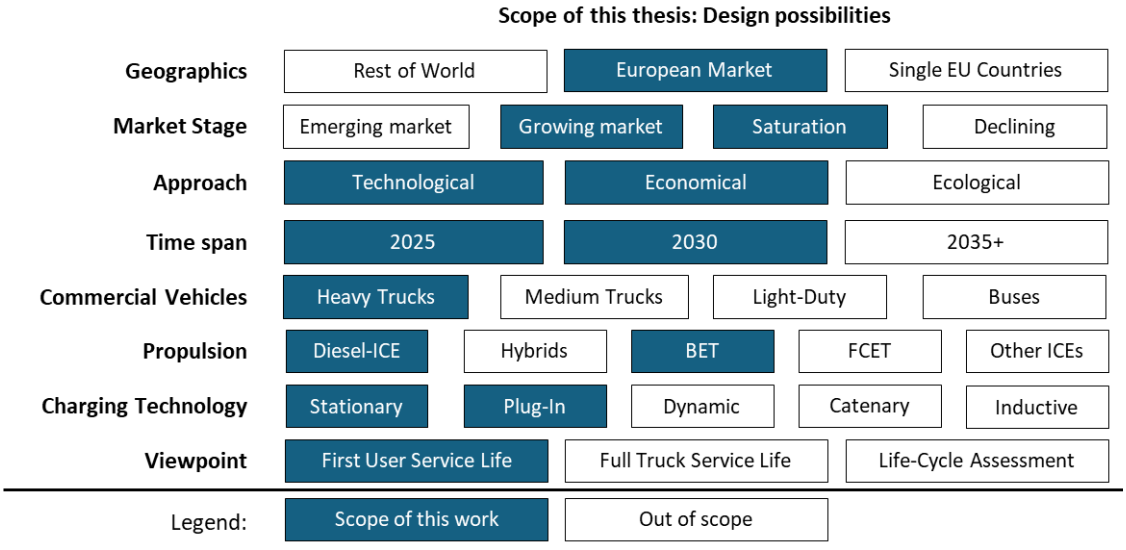

Figure 2: Morphological box. Scope of this thesis

2 Background and literature

The following chapter summarizes the current state of research relevant to this thesis. **Subchapter 2.1** introduces background information on trucks and regulations. **Subchapter 2.2** reviews current research on battery-electric trucks. **Subchapter 2.3** introduces the basics of battery design and battery modeling. **Subchapter 2.4** summarizes the current research on infrastructure modeling, with an emphasis on truck charging facilities. **Subchapter 2.5** introduces approaches to modeling vehicle operating patterns and driving profiles.

2.1 Introduction to commercial vehicles

Vehicle classification

Trucks function as adaptable transport vehicles, customizable through specific body types, auxiliary power take-offs (electrical, pneumatic, or hydraulic), or chassis/suspension modifications. Basic categorizations generally differentiate between application profiles, truck types, and axle configurations (Hilgers 2016; Hoepke et al. 2016):

- Application profiles are diverse. Such profiles vary from urban delivery (UD) and regional distribution (RD) to national and international long-haul (LH), cross-border traffic, intermodal transport, or construction (CO). Typically, longer trips necessitate larger trucks equipped with more powerful engines and specialized sleeper cabins.
- Two basic truck types exist. Rigid trucks (or shortly: rigids) operate either independently or with an articulated trailer to form so-called road trains. Rigids can be configured as chassis or feature special bodies. In contrast, tractors have no ability to transport goods but are designed to tow semitrailers, typically denoted as articulated trucks. Tractors are thus more flexible and the prevalent truck type in Europe.
- Axle configurations categorize trucks by the total number of axles (*TA*) and number of driven axles (*DA*), typically denoted as *TAxDA*. Driven axles typically use twin-tire setups.

Relevant regulations

European legislation, which is partially supported by the United Nations Economic Commission for Europe (UNECE), aims to harmonize certification procedures as well as vehicle regulations to ease pan-European operations and promote standardized, safe vehicle designs for European manufacturers or to set specific targets for Member States or manufacturers. Within the context of trucks and electrifying road freight transport, the following documents are most relevant:

Truck categories - Regulation (EU) 2018/858: European trucks are classified as light commercial vehicles (class N1, up to 3.5t), medium-duty vehicles (class N2, 3.5-12t), or heavy-duty vehicles (class N3, >12t) based on their GVW.

CO_2 emission performance standards - Regulation (EU) 2024/1610: The European certification process requires the determination of CO_2 emissions and fuel consumption of new HDVs. The stated emission reduction targets are -43% by 2030, -65% by 2035, and -90% by 2040 for newly sold trucks (compared with 2019/20 levels). This regulation covers more than 90% of HDV sales, with exceptions for some vocational trucks. The official values are determined following standardized test procedures and using the so-called VECTO software, which is a component-based vehicle simulation that includes five designated distance-based driving cycles (so-called mission profiles: urban delivery (UD), regional delivery (RD), long-haul (LH), construction (CO), and municipality). Trucks are segmented into 17 groups based on their axle configuration, truck type, and GVW (see ***Table S3***). The CO_2 monitoring process requires that the reported data must be available for download as prescribed in *Regulation (EU) 2018/956*.

Vehicle weight limits - Directive 96/53/EC: Weight limits vary on the basis of truck/trailer combination and axle count and must be observed during operations. In general, two-axle trucks must not exceed 18/19 tons, three-axle trucks must not exceed 25/27 tons, and trucks with four or more axles must not exceed 32 tons. Combinations with four axles are limited to 36-38 tons, and those with five or more axles must not exceed 40 tons. Exceptions exist for intermodal transport and cross-border traffic (42-44 tons). Under *Regulation (EU) 2019/1242*, these limits increase by up to two tons for ZETs. However, national peculiarities and derogations remain (see overview in **Table S4**).

Axle weight limits - Directive 96/53/EC: In addition to total weight limits, axle load limits must not be violated, which depend on the technical specification of the axle, single-tire or twin-tire configuration, wheelbase, total number of adjacent axles, and suspension types. In general, nondriven single-tire axles are restricted to 10 tons, whereas driven twin-tire axles are restricted to 11.5 tons. There are currently no specified exemptions or higher axle weight limits for ZETs. The two-axle trailer limits vary from 11 to 20 tons, and three-axle trailer limits range from 21 to 24 tons, depending on the wheelbase.

Restrictions on truck dimensions - Directive 96/53/EC: Rigids and trailers are capped at 12 meters in length, whereas road trains are limited to 18.75 meters. Tractor and semitrailer combinations have a maximum length of 16.5 meters, thus offering less cargo volume than road trains. The standard width is around 2.55-2.60 meters, allowing to transport euro-pallets side by side and complying with European road widths. The maximum height is usually around four meters. However, national peculiarities and derogations remain (see overview in **Table S5**).

European Modular System (EMS) - Directive 96/53/EC: Since countries such as Sweden and Finland allow heavier and longer trucks than the standard configurations above, the EMS formulation allows two extended truck-trailer combinations at some parts of the European road network to create equal and standardized conditions. However, the allowance is still subject to

approval by the Member States. This system permits extended combinations of up to 25.25 meters in length and weight limits between 50 and 65 tons via two configurations: (1) 6x2 tractors with three-axle semitrailers and an additional two-axle trailer, or (2) 6x2 rigids with a two-axle dolly to tow a three-axle semitrailer.

European driving times and rest periods - Regulation (EC) 561/2006: This regulation sets maximum daily and fortnightly driving hours, as well as minimum daily and weekly rest periods. However, specified exceptions and national derogations exist. In general, daily driving periods are capped at nine hours, which can be extended to ten hours twice a week. Driving breaks of at least 45 minutes (separable into 15 minutes followed by 30 minutes) are required after a maximum of 4.5 hours.

The Alternative Fuels Infrastructure Regulation (AFIR) - Regulation (EU) 2023/1804: The AFIR mandates the deployment of public truck charging facilities along the Trans-European Transport (TEN-T) network, which represents major European highways and freight corridors. This network is separated into the TEN-T Core and TEN-T Comprehensive network, covering over 136,000 km and approximately 420 urban nodes (cities with more than 100,000 residents). Coverage along this network and nodes must be completed by 2030 to establish an initial charging network that also pioneers for further private investments, with interim targets by 2025 and 2027. The regulation also specifies that charging stations on the TEN-T Core network should be placed every 60 km and every 100 km on the TEN-T Comprehensive network, including requirements on minimum power per station.

Eurovignette Directive - Directive (EU) 2022/362: The 2022 reform of the Eurovignette directive mandates that all Member States harmonize their tolling scheme or update concession agreements to include CO_2-based charges, air pollution charges, and distance-based rates on all TEN-T Core network segments. This must happen within the 2020s for most countries with exceptions until 2030 for smaller countries. The CO_2-based component foresees an exemption for all ZETs until 2025 and minimum reductions between 50% and 75% thereafter. However, current toll schemes are country-specific and very heterogeneous, involving rates per kilometer, per time spent in a country, or per tonne-kilometer.

2.2 Truck electrification

This subchapter starts by providing an overview of available BET models and proceeds with a literature review, with BETs defined as electric trucks that exclusively rely on electrical energy from an on-board battery system to power an electric powertrain for propulsion. The review section opens with eight headlines that summarize key findings and implications, followed by short outlines of selected studies to highlight approaches and details, and concludes by summarizing methodological differences and similarities. **Table 2** (at the end of this subchapter) provides an overview of current studies and positions this thesis in context.

Available BET models

First BET series models have been available since the early 2020s, and second-generation models have already started their commercial rollout, with a strong rise toward 2025. **Table 1** presents selected BET models and their specifications, illustrating that the stated ranges have increased from below 400 km to approximately 600 km. Battery design strategies differ in terms of their pack capacity and chemistry, and involve either lithium iron phosphates (LFP) or nickel-rich chemistries such as lithium nickel manganese cobalt oxides (NMC) or lithium nickel cobalt aluminum oxides (NCA).

Table 1: Specifications of current and announced battery-electric truck models.

Truck	**Model year**	**Curb mass**	**Battery capacity** (packs, usable energy)	**Battery chemistry**	**Stated range**
Volvo FHe Gen1	Q4 2022	10.55 t	540 kWh (6 packs, 70%)	NCA	300 km
Daimler eActros 300	2022/23	N/A	336 kWh (3 packs, 90%)	NMC	220 km
Designwerk HC Semi	2023	N/A	508 kWh (2 packs, 85%)	NMC	360 km
Scania 45R	Q3 2023	10.7 t	624 kWh (6 packs, 75%)	NMC	350 km
DAF XF Electric FT	Q2 2023	9.8 t	525 kWh (5 packs, 88%)	LFP	300 km
Daimler eActros 600	Q4 2024	11.0 t	621 kWh (3 packs, 95%)	LFP	500 km
MAN eTGX/eTGS	Q4 2024	10.3 t	534 kWh (6 packs, 90%)	NMC	400-600 km
Volvo FHe Gen2	Q1 2026	N/A	780 kWh (8 packs, N/A)	NMC/NCA	600 km

Note: Only tractors with 4x2 axle configuration for comparability. N/A: Not available.
This market excerpt (incomplete) extends from Teichert (2024). Further data is available at Calstart (2024).

Summary of key findings and implications

The following eight headlines summarize key findings and implications from recent studies:

1. While early studies identified the greatest potential for BETs in urban and regional delivery with daily ranges below 400 km, most recent research considers heavy long-haul transport even above 500 km to be technically feasible and profitable, if fast charging options are available, which is attributable to rapid battery advances due to synergies with passenger cars (Nykvist et al. 2021; Phadke et al. 2021).
2. The technical feasibility of BETs generally declines with increasing distance, but profitability improves as higher acquisition costs can amortize during operations, yiedling respective intervals (daily ranges, annual mileages, and periods of ownership) where BETs are affordable and technically feasible (Link et al. 2021; Tol et al. 2022).

3. Minimizing BET energy consumption is crucial for extending their operational range and avoiding larger batteries, which is influenced mainly by technical truck characteristics (road load: air drag, rolling resistance, weight), ambient temperatures, payload weights, driving profiles (trip dynamics and speed), elevation change, and driver behavior (Basma et al. 2021a; Earl et al. 2018; Mareev et al. 2018; Sripad et al. 2019; Wolff et al. 2021).
4. Fast charging during mandatory driving breaks or upon reaching the destination enhances the effective (daily) range and promotes full electrification, ideally without changing operations, thus enabling substantial reductions in the required battery capacity and shifting away from the previous paradigm of matching DT ranges (Basma et al. 2021b; Nykvist et al. 2021; Shoman et al. 2023; Teichert et al. 2023).
5. The optimal battery capacity depends on individual driving patterns and should be synchronized to the availability and prices of fast charging, resulting in a wide spectrum of required battery capacities; however, average mileages can be misleading, as the impacts of trip variations and infrequent long trips are ignored (Karlsson et al. 2023b; Link et al. 2021; Tol et al. 2022).
6. Battery characteristics critically impact the techno-economic feasibility of BETs, necessitating precise battery cell selection and tailored system designs, with cheaper LFP emerging as promising technology for most applications owing to its durability and pricier NMC for weight-constrained transport (Mauler et al. 2022; Schneider et al. 2024; Teichert et al. 2023).
7. Regional variations in the transportation of specific commodities over specific distance intervals via locally preferred or custom truck types substantially influence the electrification potential (Liimatainen et al. 2019).
8. Local taxation and policy settings strongly affect the amortization of BETs compared with DTs, particularly through the differential costs of diesel versus electricity and road toll regulations (Aryanpur et al. 2024; Basma et al. 2021b; Noll et al. 2022; Tol et al. 2022).

Literature review

The following section outlines relevant studies, ascending by year of publication and grouped by affiliation:

Sripad et al. (2017) utilized Monte-Carlo simulations with a simplified longitudinal dynamics model to estimate the battery capacity, mass, cost, and payload capacity for Class-8 trucks with 300-900 miles (480-1,450 km) of range, finding substantial cost and payload limitations for long-range BETs with current LIBs. However, their revisited results (Sripad et al. 2019) suggest that 500-mile range BETs (1,000 kWh) can compete with DTs in the 2020s, if vehicle aerodynamics improve to lower required battery capacities, charging infrastructure above 500 kW is available at below $0.20 per kWh, battery pack prices fall below $150 per kWh, and selected batteries are resistant to aging.

Mareev et al. (2018) assessed the techno-economic feasibility of long-haul transport in Germany by using the 45 min driving break for fast charging and a total cost of ownership (TCO) analysis. Their technical model included a route, driver, longitudinal dynamics, and drivetrain model, alongside a detailed battery model[1] that compared two high-energy battery cells. Based on two synthetic driving cycles composed of important German highway segments, the required battery capacity ranged from 600 kWh (high-efficiency configuration with low air drag and rolling resistance: 1.33 kWh per km) with 22 t of payload to 900 kWh (low-efficiency configuration: 1.83 kWh per km) at 19 t of payload. Their results indicate that BETs can compete with DTs if required battery capacities decrease, charging infrastructure above 800 kW is available, battery pack costs fall below €150 per kWh, and selected battery cells are resistant to aging.

Liimatainen et al. (2019) analyzed the technical potential for electrification by using trip data from road freight transport surveys in Switzerland (N=8,500) and Finland (N=10,000). With BET electricity consumption derived from converted weight-dependent DT fuel consumption values, several scenarios vary the availability of on-route fast charging (50-400 kW), and battery sizes are 150-350 kWh for rigids and 400-800 kWh for combinations. Their results highlight that regional truck usage patterns (driving patterns, truck types, transported commodities, and payload utilization) substantially affect the technical BET feasibility, varying notably between Switzerland (71%) and Finland (35%).

Nykvist et al. (2021) analyzed the techno-economic impacts of using smaller battery packs (290 km) with frequent fast charging during breaks, avoiding the need to match current DT ranges. Their model used a simplified longitudinal dynamics model yet no battery model to account for the potential effects of accelerated battery degradation through frequent fast charging. Their results indicate that current battery technologies ($200 per kWh, 3000 cycles, 150 Wh/kg) are marginally sufficient for BET feasibility and profitability, with higher sensitivity toward battery aging than battery prices.

Basma et al. (2021a) used parameterized models from commercial software to analyze BET technologies for tractors via VECTO mission profiles. The authors employed a complex vehicle model and detailed battery models (electrical, thermal, and aging) to assess three cell chemistries in two drivetrain topologies[2]. Their results highlight that achieving a 500 km range with 700 kWh, sufficient to cover 70% (w/o charging) to 95% (with charging) of all daily ranges in Europe, is feasible within the 2020s without payload penalties, if road-load reduction technologies (reduced air drag, rolling resistance, and weight) are employed, decreasing the average energy consumption from 1.5 to 1.1 kWh/km. However, extreme temperatures more significantly affect the driving range (up to 9%) than the cell chemistry or drivetrain topology. Building on these findings, Basma et al. (2021b) analyzed the TCO of long-haul BET

[1] Holistic battery model - electric (impedance-based), thermal, and semi-empircal aging – adopted from Schmalstieg et al. (2014).

[2] Asynchronous induction motor (ASM) versus permanent magnet synchronous motor (PMSM) implemented via distinct efficiency maps, torque characteristics, and associated gear ratios and shift strategies.

configurations for seven European countries. Their results highlight that TCO parity is feasible as of today and can be reached within the 2020s for all seven countries but varies due to local policies such as road toll reductions, purchase incentives, or additional CO_2 pricing on diesel.

Link et al. (2021) analyzed the techno-economic feasibility of BETs for food retail in Germany using real-world tour data (N=9,500 tours to 543 stores by 224 trucks over one month) and assuming BETs exactly mimic the current DT operations. Extending the longitudinal dynamics model from Sripad et al. (2017) and calculating truck-specific TCOs, their results highlight that electrifying urban delivery was technically feasible but often not profitable due to low mileages; the opposite was true for regional delivery. Plus, substantial tour variations and a few extralong tours heavily affected battery sizing. Link et al. (2022) further examined the technical feasibility through Monte-Carlo simulations and allowed intermediate charging. Their findings suggest that intermediate charging below 200 kW facilitates full electrification, but appropriate battery capacities (200-800 kWh) vary across truck classes, which stresses the need for truck-specific battery size analyses.

Mauler et al. (2022) assessed the techno-economic feasibility of BETs for long-haul transport in the US, using the regulatory break of 30 min after eight hours for charging. Their technical model used a simplified longitudinal dynamics model and a simplified battery model to compare LFP and NMC cells, and the TCO model included forgone profits and extra costs from additional stops or reduced payload capacity. The findings suggest that cheaper LFP batteries are advantageous for volume-constrained transport below 300 km, whereas costly NMC batteries perform better in weight-constrained transport up to 600-700 km despite penalty costs.

Tol et al. (2022) assessed the techno-economic potential of BETs between 2020 and 2040 in the EU-27 and the UK for four truck classes. Their technical model used simplified longitudinal dynamics and auxiliary units, simplified battery considerations, and their TCO model used local settings. An analysis of Dutch fleet data indicated a relative standard deviation of 20-40% in daily distances up to 1,000 km, prompting a model cutoff so that only 90% of all tours per truck had to be feasible. While highlighting that BETs are likely the most cost-effective option for all truck classes, regional European differences could delay profitability by up to three years, with CO_2 pricing in tolls and diesel fuels required to enhance the BET potential before 2030.

Noll et al. (2022) conducted a Monte-Carlo TCO analysis for five alternative powertrain technologies, two HDT use cases (regional and long-haul) and ten European countries. Their results highlight that regional (168 kWh) and long-haul (1,354 kWh) BETs can be cost competitiveness as of today, especially in countries with supportive policies. The key factors affecting TCO include road tolls, energy cost differences between electricity and diesel, and purchase subsidies, yet there is higher sensitivity to operating costs.

Karlsson et al. (2023a) evaluated the techno-economic feasibility of BETs for a Swedish line-haul case. Their approach featured battery sizing based on energy throughput and State of Charge (SOC) operating windows to accommodate the corresponding Full Equivalent Cycles (FEC) over the truck service life. Specific costs for charging were calculated based on charger utilization.

Extended by Karlsson et al. (2023b), who introduced the concept of energy distribution diagrams to visually analyze usage patterns based on the daily energy needs, their results highlighted the mutual dependence of battery capacity choice and fast charging to accomplish all days. Their findings suggest that low variations in daily energy consumption favor the replaceability of DTs with BETs.

A series of consecutive studies have been published in association with the TUM. Wolff et al. (2021) used simulations to analyze the effect of drivetrain topologies on truck efficiency over different driving cycles, finding drivetrain efficiencies around 87-95%, with the highest for PMSM central motor concepts, yet higher sensitivity to the underlying driving cycle than the chosen motor concept and topology. Teichert et al. (2023) developed a techno-economic cell selection tool for long-haul tractors in Germany, using battery datasheet information from 160 commercial cells and assuming a generic driving pattern (drive: 4.5h - break: 45min - drive: 4.5h) over the VECTO LH profile. Their technical model featured a static longitudinal dynamics model and a battery sizing algorithm that uses battery characteristics (cycle life and specified charge/discharge rates, share of useable energy, and SOC window). The results highlight that higher charging powers (350 kW versus 1,000 kW) improve the cost-competitiveness of long-haul BETs, and that TCO parity is affected mainly by cycle life of the battery, charging prices and energy consumption. Matching DT payload capacities is feasible for best-in-class cells and via optimized system integration. Building on this, Schneider et al. (2023) explored the techno-economic interaction of higher charging powers (up to 3,750 kW) and three generic operations, all approximately lasting 10h and with 1-3 charging stops. The results indicate that NMC cells seem more favorable for 1-stop-strategies (smallest battery: 798 kWh) and LFP for multiple-stop operations. Schneider et al. (2024) extended this approach by exploring the techno-economic interaction of battery sizing and charging strategy for one generic use case and using an updated battery model[3]. Their results suggest that LFP is the cost-optimal choice in most applications and at higher charging levels (700 kW), although NMC can be more economical for weight-constrained transport at low charging powers (300 kW).

Summary of methodological differences and similarities

The previous section highlighted that the approaches and scopes of previous studies differ substantially. This thesis compares these studies based on five characteristics: (1) the scope of the assessment; (2) cost analysis; (3) BET modeling and energy simulation; (4) battery modeling; and (5) truck application and use case. **Table 2** presents this comparison, which includes 35 earlier publications.

[3] The combined battery model (electric, thermal, and semi-empircal aging) is adopted from Teichert et al. (2022). Different aging characteristics are implemented for NMC (Schmalstieg et al. 2014) and LFP (Naumann et al. 2018; Naumann et al. 2020). Different electrical characteristics are implemented for NMC (VW ID.3 cell based on Wassiliadis et al. 2022) and LFP (Tesla Model 3 cell based on Stock et al. 2023).

(1) Most studies assess the technical feasibility, profitability or techno-economic feasibility of BETs for the US or European truck market in general, without considering national differences, or conduct generalized single-country assessments. In contrast, others conduct local company-specific case studies (e.g., Karlsson et al. 2023a; Link et al. 2021), while only a few consistently account for local factors impacting BET operations and profitability across multiple countries (e.g., Basma et al. 2021b; Noll et al. 2022; Tol et al. 2022). Typically, deterministic models are employed, which benefit from simplicity and reproducibility with using fixed technical or economic parameter values and scenarios or sensitivity analyses to ensure robustness (e.g., Mareev et al. 2018; Teichert et al. 2023). In contrast, probabilistic models such as Monte-Carlo simulations are less common but address parameter ranges and inevitable uncertainties more effectively by capturing nonlinear, simultaneous interactions, albeit at the expense of greater computational effort (e.g., Craglia 2022; Gray et al. 2022; Noll et al. 2022; Sripad et al. 2017).

(2) Cost competitiveness between BETs and DTs is often evaluated via TCO calculations that utilize detailed bottom-up cost models. This approach covers all relevant costs over the vehicle service life, allowing BETs to amortize higher acquisition costs with cheaper operations compared to DTs. Costs are categorized into capital expenditures (CAPEX), such as vehicle purchase and resale, and operational expenditures (OPEX), which usually include energy costs, insurance, road tolls, maintenance and tire costs, driver wages, and taxes. Few studies specifically analyze the costs associated with public fast-charging or depot charging stations (e.g., Basma et al. 2021b; Karlsson et al. 2023a; Mareev et al. 2018), yet most employ electricity price surcharges or adopt standard charging tariffs. Few studies explicitly price in potential profit losses due to payload constraints or increased operational times from more frequent charging breaks (e.g., Aryanpur et al. 2024; Gray et al. 2022; Mauler et al. 2022).

(3) Assessing the techno-economic feasibility of BETs usually involves energy consumption modeling and payload considerations. Energy consumption modeling primarily utilizes physics-based longitudinal dynamics models (driving resistances and drivetrain efficiencies) for accurate propulsion power calculations, which are partially supplemented by empirical models for additional power demands from onboard systems, thermal management, and auxiliary units. Simulations may employ distance- or time-based driving cycles (e.g., Basma et al. 2021a; Mareev et al. 2018; Teichert et al. 2023) or use simplified approaches for entire tours (e.g., Link et al. 2022; Nykvist et al. 2021; Phadke et al. 2021 Mauler et al. 2022). Treating simulation parameters as constant generally provides sufficient accuracy in terms of energy consumption. Payload analysis usually focuses on comparing component weights and ensuring GVW compliance, with less frequent detailed packaging assessments (e.g., Teichert et al. 2023) or consideration of permissible axle loads.

(4) Battery modeling typically focuses on SOC considerations based on energy throughput. Battery dimensioning usually considers at least single constraints such as Depth of Discharge (DOD), share of usable energy at the pack-level, fast charging capability based on SOC-windows, or battery aging via State of Health (SOH) and FEC considerations (e.g., Karlsson et al. 2023a; Teichert et al. 2023). Few studies have used parametrized battery models to simulate the

electrical, thermal or aging behavior (calendar and cyclic) in greater detail (e.g., Baek et al. 2020; Mareev et al. 2018; Schneider et al. 2024). Few studies have explored battery size variations in synergy with the charging strategies (e.g., Karlsson et al. 2023b; Link et al. 2022; Nykvist et al. 2021; Zähringer et al. 2024).

(5) Assessing the techno-economic feasibility of BETs is usually limited to single truck types or classes (e.g., Basma et al. 2021b; Teichert et al. 2023). Others distinguish between rigids and tractors (e.g., Noll et al. 2022; Plötz et al. 2023a) or even account for multiple truck classes (e.g., Craglia 2022; Tol et al. 2022). Assessments rely mainly on single day assessments based on distributions of daily driving ranges (e.g., Basma et al. 2021b) or archetypal utilization patterns that rely on driving time regulations (e.g. Schneider et al. 2023; Teichert et al. 2023). Few case studies analyze extended time periods and use real-world driving schedules that also include tour variations (e.g., Baek et al. 2020; Hildermeier et al. 2020; Link et al. 2021).

Interim conclusion

Despite varying methods and scopes, recent literature reveals consistent findings and trends in the techno-economic feasibility of BETs in Europe. However, the actual interplay between battery designs and required capacities, realistic truck operations with diverse utilization patterns, varying schedules and trip-specific energy requirements, country specifics or different truck types, and charging infrastructure (cf. **Subchapter 2.4**) remains insufficiently addressed, which might alter respective findings.

To evaluate BET prospects in more realistic detail, this thesis develops five consecutive simulation models and large-scale empirical datasets. This involves truck-specific operating schedules with hundreds of back-to-back trips as time series data (see **Subchapter 4.1**), truck and trip-specific energy consumption values through a physics-based longitudinal dynamics model (see **Subchapter 4.2**), electrical battery characteristics as well as battery dimensioning and space requirements (see **Subchapter 4.3**), TCO with detailed cost structures and regionalized cost patterns comparing the profitability of BETs versus DTs (see **Subchapter 4.4**), as well as costs for charging infrastructure and potential infrastructure locations (see **Subchapter 4.5**).

Table 2: Comparison of previous literature on heavy-duty battery-electric trucks

	Scope					Costs				Truck					Battery						Application				
	Region	#Countries / Regions	Technical / Economic	Deterministic	Probabilistic	Detailed cost model	TCO / LCC	Penalty or replace costs	Charging price model	Techn. specifications	Simplified / Empirical	Static / Dynamic	Component simulation	Paackaging & payload	Multiple chemistries	SOC / energy-based	Usage limits (DOD, etc.)	Advanced models	Battery size variations	Charging strategies	#Truck types / classes	Daily range	Generic operation(s)	Schedules / trip plans	Real-world data
Boer et al. (2013)	EU	-	TE	x			x				x				(x)		x				2	x			
Sripad et al. (2017)	US	-	T		x					x	x			x	x	x	x				1	x			
Çabukoglu et al. (2018)	CH	1	T	x								S				x	x				9				x
Mareev et al. (2018)	DE	-	TE	x		x	x		x	x		S		x			x	x	x		1		x		
Earl et al. (2018)	EU	-	TE	x			x		(x)		x			x		x	x				1	x			
Liimatainen et al. (2019)	EU	2	T	x						(x)	x					x			(x)	(x)	5				(x)
Depcik et al. (2019)	US	-	T	x								D	x	x	x		x	x			1		x		
Sripad et al. (2019)	US	-	E		x	x	x														1	x			
Baek et al. (2020)	IT	1	TE	x				(x)				S					x	x					x	x	
Hildermeier et al. (2020)	EU	-	TE		x				x		x					x				x	2			x	x
Basma et al. (2021a)	EU	-	T	x								D	x	x	x		x	x			1	x			
Basma et al. (2021b)	EU	7	E	x		x	x	x	x												1	x			(x)
Link et al. (2021)	DE	1	TE	x		x	x		x		x					x	x		x	(x)	4			x	x
Phadke et al. (2021)	US	-	TE	x			x		(x)		x					x	x				1	x			
Nykvist et al. (2021)	EU	-	TE	x		x	x	x	x		x				x	x	x		x	x					
Wolff et al. (2021)	EU	-	T	x						x		D	x								1	x			
Noll et al. (2022)	EU	10	E		x	x	x		(x)	x	x										2	x			
Link et al. (2022)	DE	1	T		x					x	x					x	x		x	x	4			x	x
Craglia (2022)	EU	-	E		x	x	x	(x)	(x)												9	x			
Gray et al. (2022)	EU	-	E		x	x	x	(x)	x	x	x			x							1	x			
Tol et al. (2022)	EU	28	TE	x		x	x		(x)	x	x	S		x		x	x		(x)	(x)	4	x			(x)
Mauler et al. (2022)	US	-	TE	x		x	x	x	(x)	x	x			x	x	x	x				1		x		
Ragon et al. (2022a)	EU	27	TE		x		x			x						x				x	1		x		
Karlsson et al. (2023a)	SE	1	TE	x		x			x		x					x	x	(x)	x	x	1			x	
Karlsson et al. (2023b)	SE	1	TE	x		x			x		x					x	x	(x)	x	x	1		x		
Teichert et al. (2023)	DE	1	TE	x		x	x	x				S		x	x	x	x		(x)		1		x		
Schneider et al. (2023)	EU	-	TE	x		x	x	x				S		x	x		x	x	x	x	1		x		
Plötz et al. (2023a)	EU	7	TE	x		x	x		x	x	x					x	x		x		2	x			
Wang et al. (2024)	UK	1	E		x	x	x												(x)		2	x			
Schneider et al. (2024)	EU	-	TE	x		x	x	x	(x)			S		x	x		x	x	x	x	1		x		
Suneson et al. (2024)	EU	1	E	x			x														1	x			
Neuhausen et al. (2024)	EU	-	E	x			x		(x)												1	x			
Zhao et al. (2024)	CN	-	E	x			x		(x)																x
Zähringer et al. (2024)	DE	1	T	x							x					x	x		x	x	1			x	
Cheng et al. (2024)	US	-	TE	x		x	x	x			x					x	x				1		x		
This thesis: General / Case	**EU**	**30/13**	**TE**		**x**	**x**	**x**	**(x)**	**x**		**x**	**SD**		**x**		**x**	**x**	**x**	**x**	**x**	**17/4**			**x**	**x**

Legend: x=covered; (x)=partially covered; S=static; D=dynamic

2.3 Lithium-ion batteries and battery modeling

This subchapter starts with battery designs, focusing on different types of lithium-ion batteries (LIBs) as prevalent high-energy automotive technology (Deng et al. 2020), and proceeds with summarizing battery modeling to properly address battery characteristics in the BET simulation.

Battery design parameters

Batteries are electrochemical energy storage systems, with their design and performance influenced at three distinct levels, ranging from (1) interior cell design to (2) exterior cell-level design to (3) system-level design (Lain et al. 2019). Among others, interior cell design involves electrode design with the selection of cathode and anode active materials (CAMs and AAMs) and related coating properties, separator choices, electrolyte mixing with distinct additives, and current collector design, along with electrode stacking. The cell-level parameters include the cell format, cell housing, and dimensions (width, length, and height). System-level parameters heavily depend on cell characteristics and involve the integration and packaging of single cells (series and parallel wiring, and module or pack design and housing), battery thermal management system (BTMS), battery management software (BMS), and safety devices.

System-level assessments and cosimulations concerning batteries in applications typically center on specifics related to cathode chemistries and formats (refer to the prior section). Thus, the focus is on effective system-level properties such as specific costs (in €/kWh), specific energy (ϵ_{grav} in Wh/kg), energy density (ϵ_{vol} in Wh/L), temperature stability and operating windows, voltage levels, electrical current levels, self-discharge, or aging (cyclic and calendar).

With respect to cathodes, three chemistries are most relevant for automotive LIB applications (Doppelbauer 2020; Hettesheimer et al. 2022; Link et al. 2023): (1) Lithium iron phosphates (LFP - ideally $LiFePO_4$: 150-160 mAh/g and 3.2 V) offer high safety, thermal stability, long cycle life, high C-ratings, and low costs but lower energy density, which can be partially mitigated at the pack level due to reduced cooling and safety requirements. (2) Lithium nickel manganese cobalt oxides (NMC[4]: 150-190 mAh/g and 3.5-3.7 V) are prevalent in modern electric vehicles, featuring a fair trade-off between moderate energy and power densities, lifespans, and costs but limited thermal stability. (3) Lithium nickel cobalt aluminium oxides (NCA[5]: 180-200 mAh/g; 3.6-3.7 V) offer highest power and energy densities at moderate lifespans but face safety concerns at high temperatures and are more expensive than NMC or LFP. For both NMC and NCA, current trends favor increasing Ni contents (≥90%) and the reduction of Co. Additional variants such as NMCA and LMFP[6] can be obtained by adding Mn to increase the operating potential and thus energy density (LFMP; voltage plateaus at 3.5-4.1 V) or improve the lifespan and reduce costs (NMCA).

[4] Typcially denoted as $LiNi_xMn_yCo_zO_2$ (x,y,z ≥ 0; x+y+z = 1) with NMC-811 ($Ni_{0.8}Mn_{0.1}Co_{0.1}$) as well-known variant.

[5] Typcially denoted as $LiNi_{0.8+x+y}Co_{0.15-x}Al_{0.05-y}O_2$ (0≤x<0.15; 0≤y<0.05)

[6] Typcially denoted as $LiMn_xFe_{1-x}PO_4$ (0<x≤0.75)

With respect to cell formats, three formats are most relevant for automotive LIB applications (Doppelbauer 2020; Hettesheimer et al. 2022; Link et al. 2023): (1) Pouch cells are noted for their lightweight, flexible designs and high energy-to-weight ratios but suffer from thermal management challenges and shorter lifespans and require external containment to mitigate issues such as swelling (when charged/discharged) and mechanical stress. (2) Prismatic hard-case cells, with moderate energy-to-weight ratios, facilitate simpler module designs owing to their solid housing, which also protects against physical damage and controls swelling. These cells can be larger, offering higher energy contents, although they are typically heavier and have lower heat dissipation efficiency, necessitating effective thermal control strategies. (3) Cylindrical cells are generally the cheapest (per kWh) and exhibit high cycle life, mechanical stability, and enhanced heat dissipation due to their high surface-to-volume ratio. However, their round shape results in poor space utilization within modules and limits design flexibility, and system integration can be complex since numerous small cells must be packaged, wired, and managed by the BMS.

Battery modeling: General

Battery models can be used for a detailed assessment of cell performance under different operating conditions. Most detailed models are typically parameterized for one specific cell, with more aggregated models (based on chemistry or format) or even generic battery models as typical derivations. Three main modeling approaches are typically categorized (Keil et al. 2012; Meng et al. 2018; Saldaña et al. 2019; Seaman et al. 2014; Wang et al. 2020):

1. *Electrochemical (multi-dimensional physico-chemical, or physics-based) models*: These material-level models aim to describe the battery structure and the physical or electrochemical processes inside the examined battery cell in high detail, allowing the reproduction of potential and diffusion gradients, particle concentrations, and temperature distributions at high spatial resolution. Thus, these models are the most detailed but suffer from high complexity owing to large parameter sets and complex sets of partial differential equations.
2. *Electrical models (mainly equivalent circuit model - ECM)*: These models aim to reproduce electrical behavior via simple components such as voltage sources, resistors, capacitors and inductors. Specific physical effects are then reproduced via tailored circuits of these components, leading to high flexibility and moderate accuracy but fast computation. Thus, ECMs are favored for system-level assessments and cosimulation with other systems and are most common in transport modeling. Further differentiation is possible in integral-order and fractional-order (frequency-dependent) models. ECMs are often coupled with empirical models to simulate aging effects.
3. *Mathematical (analytical, empirical or semi-empirical, data-driven or black-box) models:* These models are not based on actual electrochemical processes but consider the battery as a gray box (physics-inspired) or black-box, with linking input and output variables – such as current, voltage and SOC – using mathematical relationships based

on measurements. This approach leads to fast computation but limited interpretability of the model. Models range from the highly simplified Peuckert equation to stochastic battery models, empirical aging models, and neural networks.

This thesis will further limit to ECM-based battery models in combination with respective aging models that combine reasonable accuracy and good runtime for system-level assessments (Tomasov et al. 2019; Vermeer et al. 2022), also corresponding to the findings ot the literature review (refer to the previous section).

Battery modeling: Electrical

As there are numerous ECM variants, the following section introduces three typical models, including their principles and layout (see **Figure 3**):

(1) The ideal battery or so-called Rint model (*left*) is the simplest model, consisting of a voltage source ($\mathrm{U_{OCV}}$) that represents the cell's constant open circuit voltage (OCV) and a constant internal resistance ($\mathrm{R_0}$), which represents the total effective resistance within the battery (ohmic losses in the electrolyte plus others such as polarization resistance). $\mathrm{U_T}$ denotes the terminal voltage if the battery is charged or discharged, and $\mathrm{I_{cell}}$ denotes the cell current.

(2) First-order Thevenin models (*middle*) add a single RC-element, where $\mathrm{R_1}$ and $\mathrm{C_1}$ denote the RC-element components and $\mathrm{U_1}$ denotes the voltage across this element. This combination allows reproducing the instantaneous ohmic losses via $\mathrm{R_0}$ that lead to quick $\mathrm{U_T}$ drops, as well as gradual, short-term $\mathrm{U_T}$ dynamics via the lumped RC-element due to polarization effects during a change in current ($\mathrm{R_1}$) and transient responses after a change in current ($\mathrm{C_1}$). Second-order Thevenin models add another RC-element (with a larger time constant) to differentiate short- and long-term dynamics (Saldaña et al. 2019; Tamilselvi et al. 2021; Tomasov et al. 2019).

(3) The so-called Randle's circuit (*right*) consists of a Warburg impedance ($\mathrm{Z_W}$) within a RC-element ($\mathrm{R_{CT}}$ and $\mathrm{C_{DL}}$) and an optional second RC-element ($\mathrm{R_{SEI}}$ and $\mathrm{C_{SEI}}$). In contrast to the Thevenin model, single components are dedicated to reproducing specific, frequency-dependent electrochemical behaviors. On the one hand, these factors include the charge transfer resistance at the electrode-electrolyte interface ($\mathrm{R_{CT}}$) and the double-layer capacitance at the electrode-electrolyte interface ($\mathrm{C_{DL}}$). On the other hand, these are the resistive ($\mathrm{R_{SEI}}$) and capacitive ($\mathrm{C_{SEI}}$) effects of the solid electrolyte interphase (SEI). The Warburg impedance can be obtained via electrochemical impedance spectroscopy to model the frequency-dependent impedance due to ion diffusion. Typical visualizations include Bode plots (either the impedance`s amplitude or phase angle over frequency) and Nyquist plots (measured impedance visualized as a negative imaginary part over the real part for different frequencies). RC-elements that reproduce SEI effects are often replaced by so-called ZARC-elements that use a fixed resistance, and a constant phase element (CPE) as a generalized, frequency-dependent capacity (Keil et al. 2012; Saldaña et al. 2019).

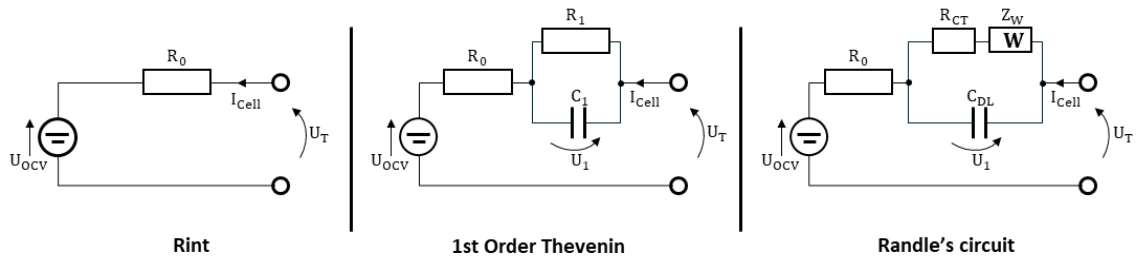

Figure 3: Electrical battery models. Overview of three equivalent circuit models

Each electric component of the ECM must be parameterized to match its dependency on conditions and stress factors such as temperature (simplified via the cell temperature T_{cell}), the cell current (I_{cell} – short for charge ($I_{cell,ch}$) or discharge($I_{cell,dch}$) cell current), the SOC, or the SOH. Typical methods involve (Keil et al. 2012): (1) *Electrochemical impedance spectroscopy* allows the characterization of individual effects on the frequency-dependent cell resistance, but it is expensive and time-consuming. (2) *Current pulse methods* that measure general voltage fluctuations due to current pulses with variable duration and frequency and allow approximation of the corresponding resistance values and time constants for short-term and long-term reactions. (3) *Constant current charge and discharge methods* allow the calculation of the overall resistance in relation to the SOC, the nonlinear relationship of U_{OCV} and the SOC via very low currents or approximating the Butler-Volmer characteristic by varying the current.

However, measuring these conditions and their mutual effects is usually limited by the available equipment, time, or costs (Vermeer et al. 2022). Thus, dependencies are usually modeled via empirical or semi-empircal models that use fitted analytical formulas on empirical data or scale findings from similar cells, still allowing for an intuitive feel to the effect of each stress factor. For example, this leads to the following generic relation for R_0 described by Equation (*2.1*):

$$R_0 = f(T_{cell}, I_{cell}, SOC, SOH) \tag{2.1}$$

Battery modeling: Thermal

Thermal models simulate the thermal behavior of a cell and its interactions with the battery housing, BTMS, and ambient temperature. Temperature is one of the most critical stress factors for LIB degradation since most reactions, parasitic and nonparasitic, are temperature related/activated. The literature identifies two main categories of modeling approaches (Vermeer et al. 2022), namely (1) complex *multi-dimensional models* and (2) simplified *lumped-capacitance models*, which reduce the battery to one single element and assume a uniform internal temperature distribution.

Battery modeling: Aging

Aging models reprodude the irreversible capacity loss (Q_{Loss}) and internal resistance increase (R_{inc}) due to aging effects caused by physical stress and chemical side reactions, where three interdependent degradation modes are prevalent. These are are triggered by multiple degradation mechanisms as visualized in **Figure 4** (Birkl et al. 2017; Edge et al. 2021; Han et al. 2019; Vermeer et al. 2022):

(1) The *Loss of Lithium Inventory (LLI)* represents the loss of active Li-ions that are no longer available for cycling[7], which leads to capacity loss and is caused by parasitic side reactions such as surface film formation and growth (mainly the SEI at graphite anodes), electrolyte decomposition (sometimes also denoted as the Loss of Electrolyte - LOE), and lithium plating.

(2) The *Loss of anode/cathode Active Material (LAM)* represents the loss or structural degradation of the available anode or cathode material, which leads to capacity and power loss, and is caused by cycling-induced particle cracking, material exfoliation, or electrode surface layer growth.

(3) The *Loss of conductivity (LC)* represents the degradation of electrical parts leading to power loss, caused by current collector corrosion, particle cracking, and binder decomposition.

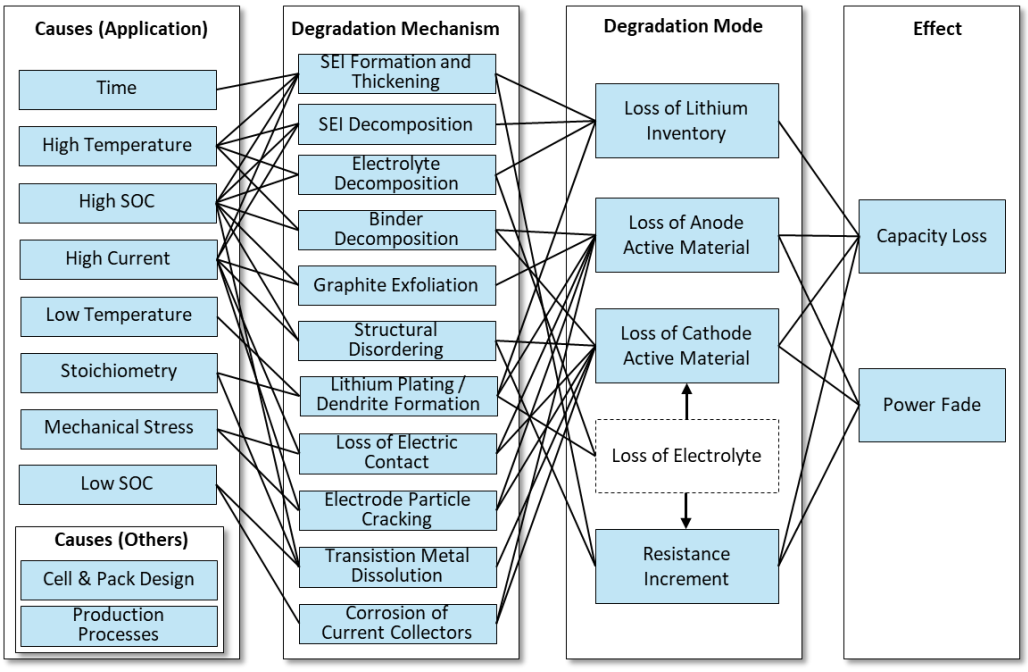

Note: Own illustration adjusted from Birkl et al. (2017) and Han et al. (2019)

Figure 4: Battery aging: Causes and effects of degradation mechanisms

[7] Deintercalation of lithium iions from the cathode and diffusion through the electrolyte and separator before intercalation at the anode (charging) and vice-versa (discharging).

The end-of-life (EOL) conditions for automotive applications are usually 70-80% of the remaining capacity (Han et al. 2019) or the internal resistance doubled its initial value (Ecker et al. 2012). Aging is associated with three typical phases of high aging at the beginning of life (Phase-I; mainly SEI formation during initial cycles after the production), a predictable and linear aging period while in operation (Phase-II), and accelerated, strongly nonlinear aging toward the end (Phase-III) (Han et al. 2019). LIB degradation modes can be classified into two types of aging, yet measuring and modeling their interdependent dynamics separately is complex and not trivial (Kairies et al. 2019; Vermeer et al. 2022):

(1) Calendar aging occurs even when a battery is not used, which is caused by side reactions due to the thermodynamic instability of the materials. Calendar aging is influenced by time, the SOC level during storage, and temperature. Typically, calendar aging increases with increasing SOC (low anode potential due to intercalated lithium ions increases the SEI growth) and higher temperatures due to increasing reaction rates. In terms of time dependence, effects are usually greater at the beginning (exponential in Phase-I) than later (linearized in Phase-II) so that models often use a power-law relationship (exponent values in the range of 0.5–0.9). The relationship between aging and temperature is commonly described by the Arrhenius law. Finally, modeling SOC dependency involves several approaches, ranging from linear to polynomial or exponential models (Schoch 2018; Vermeer et al. 2022). The following Equations (*2.2*) and (*2.3*) formulate this relationship for the capacity loss ($Q_{loss,cal}$) and internal resistance increase ($R_{inc,cal}$):

$$Q_{loss,cal} = f(SOC, T_{cell}) * t^{z_{Q,cal}} \quad (2.2)$$

$$R_{inc,cal} = f(SOC, T_{cell}) * t^{z_{R,cal}} \quad (2.3)$$

where $f(SOC, T_{cell})$ denotes either two separate functions or an integrated function describing the respective dependencies, t denotes time, and $z_{R,cal}$ and $z_{Q,cal}$ denote the respective power-law exponents.

(2) *Cyclic aging* results from charge/discharge cycles and is always superimposed by calendar aging. Cyclic aging is influenced by the energy throughput[8], SOC operating windows with the respective end voltages (charge and discharge), temperature, and charge and discharge currents (or C-rates). Typically, cyclic aging increases with lower DOD and increasing SOC windows, temperatures, and currents. In terms of energy throughput, models often use a power-law relationship (exponent values in the range of 0.5–1.0) such as time for calendar aging to describe the SEI growth (in Phase-II). Likewise, temperature dependence is commonly described by the Arrhenius law. The effects of C-rates often assume exponential dependence and are accompanied by temperature effects, particularly at high rates. In terms of the DOD, models commonly adopt Wöhler curves, meaning that the cycle life is modeled as a function of DOD and with a decreasing degradation rate as the DOD increases (power-law form); yet some models also assume a linear relationship. Note that the SOC effects are likely to have a large calendar

[8] Either expressed as net Ah delivered by the battery over all cycles or the number of FEC.

aging superposition with no clear model pattern (Schoch 2018; Vermeer et al. 2022). The following Equations (*2.4*) and (*2.5*) formulate this relationship for the capacity loss ($Q_{loss,cyc}$) and internal resistance increase ($R_{inc,cyc}$):

$$Q_{loss,cyc} = f(DOD, I_{cell}, \overline{SOC}, T_{cell}) * FEC^{z_{Q,cyc}} \quad (2.4)$$

$$R_{inc,cyc} = f(DOD, I_{cell}, \overline{SOC}, T_{cell}) * FEC^{z_{R,cyc}} \quad (2.5)$$

where $f(DOD, I_{Cell}, \overline{SOC}, T_{Cell})$ denotes either separate functions or an integrated function describing the respective dependencies, FEC denotes the energy throughput, $\overline{SOC}$ denotes the average operating window, and $z_{R,cyc}$ and $z_{Q,cyc}$ denote the respective power-law exponents.

Finally, most models combine the effects of calendar and cyclic aging, and the total capacity loss and internal resistance increase are calculated by addition, but sometimes also by multiplication, which also depends on the structure of the individual models. The additive case is described in Equations (*2.6*) and (*2.7*):

$$Q_{loss} = Q_{loss,cyc} + Q_{loss,cal} \quad (2.6)$$

$$R_{inc} = R_{inc,cyc} + R_{inc,cal} \quad (2.7)$$

Interim conclusion

The previous section outlined the basic concepts of LIBs and battery modeling necessary to accurately address battery characteristics in technical BET simulations. ECM-based battery models in combination with respective empirical models combine reasonable accuracy and good runtime and are most common in transport modeling. Effective battery sizing should account and compensate for aging effects, particularly increasing capacity losses, with key operating/stress factors involving temperature, cell current, and the SOC operating window.

To reflect electrical and aging battery characteristics in the BET simulation, this thesis adopts an ECM-based battery model and implements an appropriate battery sizing (see **Subchapter 4.3**).

2.4 Charging infrastructure for battery-electric trucks

This subchapter starts by introducing charger types and their typical locations, proceeds with summarizing modeling options, and concludes with the stated infrastructure needs of BETs.

Charger types and locations

The plug-in stationary charging infrastructure for BETs varies to meet operational needs such as fleet size, daily mileage, and type of operation. Typical charging options range from slow AC charging below 43 kW to DC fast charging. This thesis focuses on DC charging, where two

charging standards prevail in Europe: (1) The established Combined Charging System (CCS) operates at 200-1,000 V and can theoretically deliver up to 500 kW, with a peak power of 350 kW specified in the standard. Accordingly, typical charging levels are 50-100 kW for slow charging and around 300 kW for fast charging. (2) The emerging Megawatt Charging System (MCS), which is anticipated to be commercially available by 2025/26, operates at 200-1,250 V and can deliver up to 3,750 kW. However, in truck applications – currently characterized by 800 V onboard system architectures - the reachable peak power is likely to be capped at around 1 MW until the early 2030s.

Typical locations of these chargers vary, and three archetypal use cases can be identified (Berndard et al. 2022; Muratori et al. 2023), summarized by **Table 3**: (1) Depot charging is generally located at an operator's premises and is used primarily for overnight charging or when trucks idle over longer periods. (2) Destination charging is available at sites where trucks are loading or unloading, such as customer stores, warehouses, distribution centers, or intermodal hubs such as ports and rail freight terminals. Access to the charging infrastructure may be private or restricted in both cases. (3) Public charging infrastructure is located at publicly accessible locations, mainly along highways, so that trucks can charge anytime if needed, involving short daily driving breaks with high charging power (rather MCS) and longer nightly rest periods with low charging power (rather CCS).

Table 3: Charging infrastructure: Summary of charger types and locations

Charging use case	Nominal power level	Standard	Locations
Slow charging	50-150 kW	CCS	- Depots - Public charging stations
Fast charging	150-350 kW	CCS	- Depots - Destination locations - Public charging stations
Ultrafast charging	750-1,250 kW	MCS	- Public charging stations

Note: Extended from Berndard et al. (2022)

Theory on infrastructure modeling

Modeling charging infrastructure, as part of broader network planning and facility location issues, has been a subject of scientific study since the 1960s (Speth 2024) and often involves problems of the NP-hard class (Metais et al. 2021; Pishvaee et al. 2010), meaning that exact solutions are often impractical owing to the exponential increase in computational effort with problem size. Thus, this subchapter focuses on charging infrastructure for BETs, adopting the classification from Metais et al. (2021) and Deb et al. (2018) by distinguishing three primary approaches (see **Figure 5**): (1) node-based models, (2) path-based models, and (3) tour-based models. Each approach involves typical models and further subclassifications concerning the (I) problem formulations and (II) optimization goals are possible.

First, node-based models are a prevalent method in infrastructure modeling and allocate charging demand to specific locations (=nodes). The objective is to optimally place charging infrastructure with a specified service area at candidate nodes so that the whole network is covered. Renowned models include the Set Covering Location Model (SCLM), which minimizes the number of selected locations to cover all charging demand, and the Maximum Covering Location Model (MCLM), which is designed to maximize demand coverage with a fixed number of locations. The popular ρ-median model identifies p charging locations among all candidates by minimizing the weighted distance between nodes with charging demand and potential locations. This modeling typically uses registration figures, traffic data, or transport statistics (Metais et al. 2021; Pagany et al. 2019; Speth 2024).

Second, path-based approaches utilize flow-capturing logic to strategically place charging stations along network paths (origin node to destination node) with the highest vehicle flows, presenting a dynamic method of assessing charging demand compared with node-based strategies. This basic concept was initially introduced with the Flow Capturing Location Model (FCLM), fairly equivalent to a path-based MCLM. FCLMs focus on origin-destination (OD) pairs and aim to maximize the flow captured along the respective shortest network path, considering a path covered if at least one node along it is equipped with charging infrastructure. The later introduced Flow Refueling Location Model (FRLM) adds vehicle range limitations, so that vehicles may have to charge at more than one node to complete a path. Since this formulation requires testing every possible node combination for every path, several heuristics and reformulations occur to decrease computational demands for practical use in larger networks. This modeling typically uses traffic count data, which are particularly available for highway traffic (Metais et al. 2021; Pagany et al. 2019; Speth 2024).

Third, tour-based or activity-based models extend node-based and path-based models by considering entire trip schedules of selected vehicles over a certain period so that multiple origins, destinations, paths/trips, and idle times help to identify the most attractive charging infrastructure locations. Such models rely on large datasets such as GPS data or trip logbooks of large truck fleets, which is typically business-sensitive information. Thus, multi-agent models are frequently used to effectively simulate such data and analyze traffic dynamics per truck and then aggregate them to the fleet. Simulations are then calibrated with traffic count data or related transport statistics (Metais et al. 2021).

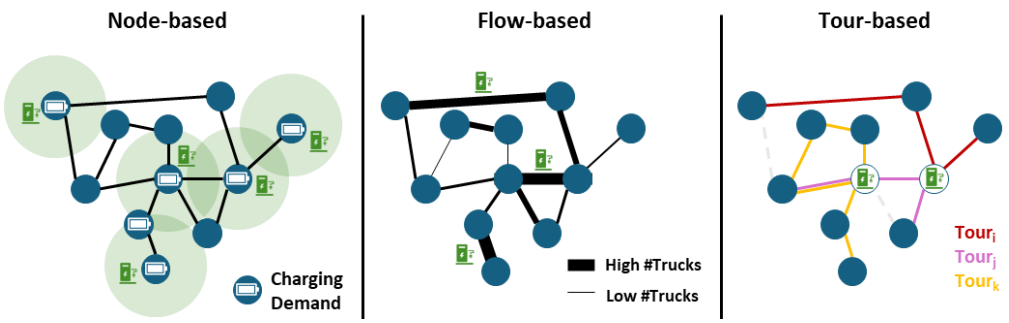

Note: Own illustration extended from Metais et al. (2021)

Figure 5: Charging infrastructure: Locations models

Each modeling approach enables diverse problem formulations and optimization objectives. For example, formulations can aim to either identify locations or size charging stations at chosen locations or both. Sizing problems can aim to determine either the number of required charging points or the required power levels or both. The optimization objectives vary from maximizing charged vehicles or charger utilization to minimizing infrastructure costs or the number of failed trips. Heuristic methods such as genetic algorithms, sampling techniques, or Particle Swarm Optimization are commonly used for finding sufficient solutions with reasonable efforts, whereas integer or mixed-integer optimization methods aim to identify optimal solutions. However, their suitability is highly dependent on the problem formulation, objectives, model constraints, and problem size (Metais et al. 2021; Pagany et al. 2019). Since most of these models are highly simplified, several extensions add further characteristics to ensure practical use (Pagany et al. 2019). This might involve temporal sequences (queuing models to simulate the arrival and waiting processes) to improve station sizing, adding capacity restrictions to avoid unrealistically large stations, incorporating uncertainty using stochastic demands or vehicle flows, or including geospatial analyses to determine suitable candidate locations by integrating real-world aspects such as grid availability, available space, or surrounding service facilities.

Infrastructure needs for battery-electric trucks

The literature review identified four core insights related to BET infrastructure needs, with a focus on Europe:

MCS charging enables long-haul transportation and is crucial for safeguarding tour completion. With reference to **Subchapter 2.1**, the study by Mareev et al. (2018) relied on 880 kW fast charging during driving breaks to conquer their approximately 700 km long tours with batteries around 600-900 kWh. Liimatainen et al. (2019) reported that even with up to 800 kWh batteries, full electrification of the Swiss and Finnish truck fleets fails if on-route fast charging is limited to 400 kW. Nykvist et al. (2021) reported that MCS substantially increases the techno-economic competitveness of BETs, as decreasing battery sizes reduce costs and payload deficits. Ragon et al. (2022a) reported that 30% of all long-haul tractors in Europe need more than 800 kWh electricity per day and therefore rely on MCS charging. Teichert et al. (2023) showed that an upgrade from 350 kW to 1,000 kW for charging during a driving break substantially improved the BET`s technical feasibility and profitability for all battery cells. Shoman et al. (2023) reported that even BETs with 750 kWh batteries (435 km of range) need fast charging (700-1,200 kW) to cover almost all European trips (99%). Zähringer et al. (2024) highlighted that dense charging infrastructure networks (every 50 km) with high power (700-1,500 kW) are required to safeguard the BET operations of currently available models (500 kWh). Speth et al. (2024) simulated 2,410 German driving profiles with BETs (450-700 km of range) and reported that even though only a few charging events require more than 350 kW, without their availability, electrifying long-haul operations will fail. Lange et al. (2024) reported that increasing the charging power from 600 kW to 1 MW increased the theoretical coverage of European long-haul traffic flows from 85-90% to above 97%, while fewer locations were needed.

Most charging demand will likely occur at private depots and at low power. Borlaug et al. (2021) argued that only a small fraction of the US truck fleet requires an operating range above 500 miles (805 km), with 70% operating within 100 miles (160 km). The additional observed shift from interregional and national long-haul transport toward decentralized hub-and-spoke logistics results in shorter and more predictable routes, further emphasizing that most trucks in short-haul operations will recharge during off-shift periods at depots. Basma et al. (2021b) assumed that, on the basis of daily mileage distributions, approximately 80% of the required daily electricity is charged at the depots. Ragon et al. (2022a) reported that 50% of all long-haul tractors in Europe have daily electricity needs below 680 kWh, indicating that operations are likely to rely on overnight charging at depots. Muratori et al. (2023) illustrated this charging paradigm with private depot charging below 150 kW as the foundation of the pyramid and on-route fast charging above 350 kW as the top. Speth et al. (2024) reported that most charging events (95% of night charging, 75% of day charging) theoretically require even less than 50 kW and occur on private or semi-public premises.

The deployment of public charging infrastructure will focus on main highways. Naturally, truck traffic focuses on major highways to reach destinations quickly, which is verifiable and quantifiable via truck traffic count data. The AFIR prescribes the deployment of charging infrastructure along major European highways, yet concrete locations must be identified by the Member States. Plötz et al. (2021) identified approximately 34,000 real truck stop locations based on processing and clustering GPS data from approximately 400,000 trucks, which were provided by truck manufacturers. These stop locations were concentrated around highly populated areas or industrial areas and followed main European roads. These patterns are similar in North America (Demissie et al. 2022; Dimatulac et al. 2023; Tong et al. 2021), China (Qian et al. 2024), and Australia (Whitehead et al. 2022).

Most likely, at least 3,000 public charging locations will be required by 2030 in Europe, which are generally equipped with more CCS chargers (80-90%) than MCS chargers (10-20%). The AFIR (see **Subchapter 2.1**) coverage approach with its distance-based intervals translates to about 300 required charging locations in Europe by 2025 and 3,000 locations by 2030 to establish an initial network. However, multiple studies have investigated potential locations for public charging infrastructure, suggesting even higher demand. Suzan et al. (2021) assessed infrastructure deployment along major highways and at urban centers using an updated European transport dataset and three BET diffusion scenarios. Their results suggest that 13,800 to 28,900 public overnight chargers (<150 kW) and 2,100 to 4,200 public high-power chargers (620-850 kW) as well as 3,400 to 7,100 destination chargers (350 kW, semi-public) at industry hubs are needed by 2030. These results imply an average ratio of 85% CCS charging points and 15% MCS charging points at public locations. The timestamp information in the evaluated GPS data by Plötz et al. (2021), which considers the distribution of arrival times and shorter MCS charging times, implies an average ratio of 90% CCS charging points and 10% MCS charging points at public locations.

Speth et al. (2022a) filtered European truck flow data[9] for long-haul to evaluate three long-haul infrastructure scenarios from a wide-meshed initial network by 2025 (100 km interval and 5% BET fleet) to either a densified network (60 km) or a retained wide-meshed network by 2030, both with an increased BET fleet (15%). Their MCS station dimensioning involved a queuing model, assuming peak hours handle 6% of daily charging events, with 5 min average waiting time, 30 min charge duration, and 25% public charging utilization. Their coverage approach suggests that 660 locations (both directions) with about 1,700 charging points (5%) to 3,700 charging points (15%) for the wide-meshed network and up to 1,486 locations and 4,800 charging points for the densified network are needed. On average, this translates to around 2-3 or 5-6 charging points per location, depending on the scenario. Ragon et al. (2022a) combined the same truck flow data[9] with a market diffusion model and five respective charging strategies that utilize slow (100 kW), fast (350 kW), and ultrafast (1,000 kW) charging based on a stochastic daily energy demand. Their results indicate that about 24,000 to 40,000 public charging points (60% slow, 23% fast, and 17% ultrafast) are needed by 2030 to satisfy the needs of the electric truck fleet, which are most likely located at around 5,000 dedicated parking areas. On average, this translates to around 4-8 charging points per location. Shoman et al. (2023) splitted the truck flow data[9] into trip chains to assess the number of public overnight chargers (50-100 kW) and MCS chargers (700-1,200 kW) via a queuing model. Their tour-based approach resulted in about 4,200 theoretical charging areas (25x25 km^2 squares) with an average distance of 25-35 km between charging locations and nearly 50,000 required charging points by 2030 (15% BET share), with a country-sensitive ratio of about 80% (CCS) to 20% (MCS) and around 12 charging points per area (note that several locations are feasible within an area). Lange et al. (2024) also filtered the truck flow data[9] for long-haul traffic but used real-world truck stop locations as potential candidates[10]. Their optimization approach aimed to maximize the share of electrified traffic by 2030 (15% BET share), included an annual capacity restriction to each location (< 100,000 events per year), and leveraged sampling techniques to reduce the problem size. Their results implied that approximately 1,000 optimally placed MCS charging locations (both traffic directions) can serve about 91% of BET long-haul traffic in 2030 and about 1,300 locations are sufficient to achieve the maximal coverage.

Electricity grid expansion and spatial constraints can become decisive bottlenecks for both public and private charging infrastructure. Particularly, power demand per location will be driven by fleet size and charger configuration (ratio of CCS-to-MCS), whereas the grid integration will highly depend on locally available capacities and national power grid architectures. Typically, building large charging hubs involves several steps, starting from site selection to permitting and planning, groundwork, local hardware installation, grid connection, and site commissioning.

[9] This European traffic flow dataset was published in Speth et al. (2022b). This dataset contains synthetic truck flows (trucks per day, OD pairs) between 1,675 European NUTS-3 regions and has an underlying road network that is close to the TEN-T network. Note that NUTS (Nomenclature of Territorial Units for Statistics) is a European geocode standard with four levels. NUTS-0: Country; NUTS-1: Major socio-economic regions; NUTS-2: Basic regions or provinces; NUTS-3: Small regions

[10] This dataset of real-world truck stop locations was published in Link et al. (2024a).

Regarding public charging infrastructure and power requirements, the AFIR mandates that by 2030, each charging pool on the TEN-T network must deliver between 1.5 MW (Comprehensive) and 3.6 MW (Core), with individual chargers offering at least 350 kW. Safe and Secure Truck Parking Areas (SSTPAs) must provide a minimum of 0.4 MW via four CCS chargers, while pools located at TEN-T urban nodes must deliver at least 1.8 MW through chargers of no less than 150 kW. In total, this results in a projected capacity of at least 8 GW across the TEN-T network by 2030, with Germany contributing around 0.9 GW. In contrast, Ragon et al. (2022a) advocate for a demand-oriented deployment strategy, emphasizing infrastructure targets based on traffic volumes across Member States. Their recommendation foresees gradually increasing charging pool capacities in relation to the traffic intensity, scaling from 1.4 MW to 3.0 MW, 6 MW, and up to 9 MW. In total, this results in a higher projected capacity of roughly 13 GW across the TEN-T network by 2030. For Germany, the planned truck fast-charging network includes 350 sites with approximately 1,800 MCS and 2,400 CCS charging points. Stated grid connection targets through 2035 prescribe an average of around 8 MW per location, with peaks up to 25.5 MW (lower quartile: 4.8 MW, upper quartile: 10.6 MW). In total, this results in a projected capacity of around 2.9 GW by 2035 (NOW GmbH 2024b).

Regarding depot infrastructure and power requirements, Borlaug et al. (2021) found that each BET contributes a peak load of 10-74 kW to the system, depending on the fleet and charging strategy. Similarly, Garrido et al. (2023) modeled home-base load profiles and found that each BET contributes a peak load of 17-47 kW. Walz et al. (2024) modeled different logistics centers with specific truck fleets and found that each BET contributes a peak load of 10-70 kW, depending on the centers and the charging strategies. All three studies converge on an average contributing peak load of 20-45 kW per BET, despite allowing for higher single charging powers per truck, which suggests low charging simultaneity due to varied trips and arrival patterns. However, in the case of large truck fleets, aggregated charging demand can easily lead to peaks in GW-scales in addition to the existing depot load, emphasizing the need for proactive grid planning. In addition, numerous individual depots call for customized solutions, complicating the standardization and scalability of large-scale deployment efforts. Battery-backed charging solutions, using buffer batteries for peak load balancing, or smart-charging strategies, such as the local PV integration for midday charging peaks or fleet-synchronized charging, might help to balance grid load and avoid excessive grid expansion in the short-term to long-term (Al-Hanahi et al. 2021; Borlaug et al. 2021).

Even with such strategies, however, the large-scale truck electrification will likely require new connections to the medium-voltage (MV) or high-voltage (HV) grid and the construction of new substations. This can involve substantial costs and long time scales, as indicated by Burges et al. (2021), Burges et al. (2022), Kippelt et al. (2022), or Berndard et al. (2021). Based on Burges et al. (2021), several grid configuration options for integrating truck charging hubs in Germany are outlined in NOW GmbH (2022). These configurations range from integration into an existing MV circuit (GC-1; typically below 8 kVA), to connection of a new MV cable to an existing MV busbar without substation modifications (GC-2; typically 8-20 kVA), expansion of the substation and a new MV cable (GC-3; typically 20-30 kVA), and the construction of a dedicated HV-MV substation with a direct connection to the HV grid (GC-4; typically above 30 kVA). Accordingly,

associated costs and timelines vary significantly by grid configuration, ranging from below €0.35 Mio. and a few months for GC-1 to up €20 Mio. and ten years for GC-4. Last, building large-scale charging locations can become challenging considering limited and costly space at both highways and within depots, while potentials layouts for large-scale public charging hubs are still under discussion (Plötz et al. 2024).

Interim conclusion

The previous section outlined modeling approaches and key findings on BET infrastructure needs, ranging from the role of MCS charging to depot charging, power requirements and potential numbers of public charging locations in Europe, and grid connection as potential bottleneck. Regarding modeling, tour-based approaches offer the most precise and specific simulation with combining strengths from node-based and path-based modeling. However, this approach relies on large datasets with precise geospatial information.

To ease the deployment of public truck charging facilities, this thesis implements a combined node-based and path-based approach in see **Subchapter 4.5**, which is inspired by AFIR regulation to enhance practical relevance. Thus, the analysis focuses on identifying real-world locations along highly populated areas, industrial zones, and highways along the TEN-T network.

2.5 Modeling vehicle activity and driving profiles

This subchapter introduces the basics of activity-based modeling and concepts for dealing with multivariate data that are required for the simulation of individual BET operating schedules.

Activity-based modeling

Modeling vehicle activities is a standard practice in transport system modeling (Ortúzar 2011). Real-world tour planning defines the commodities to be delivered, including their types, quantities, assigned trucks, delivery times, and the sequence of customer facilities along the route. However, this customer-sensitive information is typically confidential and not broadly available. Therefore, this thesis distinguishes two approaches to obtaining such activity plans.

First, macroscopic models simulate vehicle activities by translating supply-demand data or OD relations to trips or truck movements. Data-wise, specific OD relationships are available from transport statistics or created via discrete choice modeling (mode choice, route choice, or truck activity allocation) to simulate the decision-making process of individual truck owners and eventually obtain synthetic relationships based on a premise such as maximum likelihood or utility maximization. For example, Speth et al. (2022b) translated original OD relations[11]

[11] These OD traffic relations were published in the ETISplus project (Szimba et al. 2012).

(expressed as freight movement in tons per year) between 1,675 NUTS-3 regions into the number of trucks per year and obtained about 1.6 Mio. traffic flows on the underlying European highway network. Shoman et al. (2023) used these truck flows to create trips chains by splitting long paths into several consecutive trips, so that all trips happen within one week and comply with the European driving time regulation. Similiary, Menter et al. (2023) translated the original OD relations[11] into a trip-based OD schedule via similar procedures and limited to inner-German long-haul truck traffic. This schedule was then used as an input file for MATSim, which is a large-scale agent-based transport simulation, to simulate truck traffic on the German road network over one week.

Second, microscopic models leverage mobility statistics and empirical data to construct trip schedules, involving distributions of trip durations, trip lengths, departure times, or daily trip frequencies – and ideally underlying causalities and statistical correlations. Different approaches permit either random selection of existing data (discrete) or the generation of novel values (continuous). Fleet results are then obtained by executing such sampling processes and aggregating the results (Monte-Carlo approach). For example, the *emobpy* tool (Gaete-Morales et al. 2021) creates individual activity schedules (operationalized as time-series data) for battery-electric passenger cars. Hildermeier et al. (2020) determined the BET potential for European city logistics by sampling from real-world operational data and using Monte-Carlo modeling to determine the fleet daily energy demand. Baek et al. (2020) choose an optimally sized battery for a given truck based on its list of delivery tasks, which is determined via a respective scheduling algorithm. Teichert (2024) used real-world operational data to create synthetic trip schedules to optimize the BTMS design for BETs.

Mathematical concepts in dealing with multivariate data

Multivariate datasets contain multiple variables and the relationships between them are of central interest. Ignoring such dependencies and correlations can lead to biased estimates, loss of information, inaccurate predictions, or overestimation of variability (Tinsley et al. 2006). Several techniques can help to understand such relationships and reduce dimensionality involving *multivariate regression models*, *Principal Component Analysis* (PCA), *Analysis of Variance (ANOVA)*, or *Factor Analysis*. More complex methods also allow the generation of synthetic data that bears these relationships and closely aligns with the original dataset. Four established techniques are discussed below:

(1) Markov Chain Monte Carlo (MCMC): This concept involves a class of algorithms that construct a Markov chain that has the desired distribution as its equilibrium distribution so that model dependencies are captured indirectly. These algorithms are defined by a sequence of random variables where the next state depends only on the current state (Markov chain) and transition probabilities that define how to move from one state to another within that chain. After initializing with an arbitrary value, the transition involves testing a proposal distribution to generate a new candidate sample. If this candidate sample is rejected based on an acceptance criterion, this process repeats. In contrast, if this sample is accepted, an appropriate distribution

close to the desired distribution is found. This concept is widely used in Bayesian statistics for estimating posterior distributions (Gallagher et al. 2009).

(2) Copula Modeling: This concept allows modeling the joint distribution of multiple variables while explicitly separating the marginal distributions of each variable from their dependency structure (Nelsen 2006). This concept is common in finance, risk management, and econometrics (Hlawatsch et al. 2010). Formally, and following Sklar's Theorem, for a set of random variables $\mathrm{X}_1, \mathrm{X}_2, \dots, \mathrm{X}_\mathrm{N}$ with joint distribution $\mathrm{F}(\mathrm{x}_1, \mathrm{x}_2, \dots, \mathrm{x}_\mathrm{N})$, the copula C relates the joint distribution to the marginal distributions F_i as described in Equation (*2.8*) (Nelsen 2006):

$$\mathrm{F}(\mathrm{x}_1, \mathrm{x}_2, \dots, \mathrm{x}_\mathrm{N}) = \mathrm{C}\left(\mathrm{F}_1(\mathrm{x}_1), \mathrm{F}_2(\mathrm{x}_2), \dots, \mathrm{F}_\mathrm{N}(\mathrm{x}_\mathrm{N})\right) \tag{2.8}$$

Thus, each variable can follow its specific distribution, whereas the copula defines how these variables are correlated. Gaussian copulas are prevalent and assume that the joint distribution of variables is based on a multivariate normal distribution, which is ideally used to capture linear dependencies among the variables. Archimedean copulas (Clayton, Gumbel, or Frank copulas) are more accurate for modeling nonlinear dependencies and heavily skewed distributions. Thus, dependency structures can be explicitly controlled while handling arbitrary marginal distributions (Li et al. 2019; Nelsen 2006).

(3) Bayesian Networks (BNs): This rather graphical concept explicitly models a set of variables and their conditional dependencies via a directed acyclic graph, best suited for structured data with hierarchy levels, clear dependencies, and causal relations (Kaur et al. 2021; Margaritis 2003). While this representation is intuitive, graph construction can become complex with increasing dataset sizes. Given such a graph, a set of vertices represents random variables $(X_1, X_2, \dots, X_N)$ and the set of vertices represents conditional dependencies between specific vertices. The joint distribution of the variables is factored into conditional probabilities as described by Equation (*2.9*):

$$\mathrm{P}(\mathrm{X}_1, \mathrm{X}_2, \dots, \mathrm{X}_\mathrm{N}) = \prod_{i=1}^{\mathrm{N}} \mathrm{P}(\mathrm{X}_i | \ \mathrm{Parents}(\mathrm{X}_i)) \tag{2.9}$$

The sampling starts with the arbitrary marginal distributions of root vertices (without parents) and all vertices are sorted in topological order. This continues for each subsequent vertices, with its marginal distributions depending on the realized values of its parent vertices.

(4) Generative Adversarial Networks (GANs): This concept, which is also representative of other machine learning or data-driven techniques, is less interpretable and requires large datasets for training but is flexible and can be advisable if distributions are unknown, data are unstructured, or too complex for explicit modeling. This concept is common in image processing, computer vision, and speech synthesis. GANs consist of two neural networks: one tries to generate synthetic data that mimics real data (generator), whereas the other tries to distinguish between real data and synthetic data (discriminator). The training features an adversarial process in

which the generator tries to improve its synthetic data and trick the discriminator, whereas the discriminator tries to improve its ability to distinguish between real and synthetic data. Finally, the GAN generator has learned the desired distribution and can recreate representative samples (Aggarwal et al. 2021; Goodfellow et al. 2020).

Interim conclusion

The previous section outlined the basics of activity-based modeling and concepts for dealing with multivariate data. Regarding the latter, MCMC and GANs offer robust sampling methods from high-dimensional, complex probability distributions without the need for manual customization but have less traceability and can be either computationally intensive (MCMC) or require large training datasets (GANs). Bayesian networks, on the other hand, allow for the explicit incorporation of prior knowledge (causalities, constraints, or conditional probabilities) and the modeling of successive, hierarchical sampling processes. Copula models allow for flexible modeling with differing marginal distributions and are ideally suited for concurrent sampling processes.

To create truck-specific operating schedules, this thesis follows a microscopic approach using empirical truck driving data (see **Subchapter 4.1**). Consecutive trips within schedules are generated via Bayesian network logic, with conditional probability distributions per parameter, or Copula models. This approach allows capturing parameter dependencies and prior knowledge by intuitive and sequential model architectures.

3 Data

This chapter outlines five key data categories, detailing their background, preparation and filtering, and initial descriptive analysis with visualizations, and concludes with discussing related limitations.

3.1 Anonymized road carriage microdata

Overview

European road freight transport (ERFT) microdata are the most important data used in this thesis. Data collection relies on quarterly road freight surveys according to *Regulation (EU) 70/2012*. These surveys are continuously sent to private truck owners (web- or paper-based). The accompanying documentation and guidelines (see Eurostat 2008, 2016b) aim to standardize the survey process by national authorities, questionnaire designs and surveyed attributes, as well as the sampling process to ensure representativeness for the respective country. The key attributes recorded include truck-specific data and detailed journey logbooks with distance, date, payload, and origin-destination postal codes. These data are accessible as anonymised microdata files for scientific use. The anonymization process, described in Eurostat (2016a), involves removing specific identifiers such as reporting country, date information, and detailed truck information (type and axle configuration), and aggregating address data from postal codes to NUTS-2 regions. These anonymised microdata files provided by the European Commission span from 2011-2020 and cover all major EU-27 and EFTA member states[1] as well as the UK.

The data structure involves three levels (see **Figure 6**): truck records with vehicle-specific variables, journey records with trip-specific variables, and goods records for transported commodities on laden trips. A truck record may link to multiple trip records within a survey period (normally one week within the quarter[2]). Each trip record may be linked to multiple goods records, but each goods record is linked to a single journey. The datasets employ a grossing-up factor for scaling to fleet-representative statistics calculated by the national authorities and allow country comparisons despite individual sampling rates. Trip types distinguish between one-stop laden trips, laden trips with several stops (unspecified number), trips with complex collection/delivery structures and several stops (unspecified number), and one-stop unladen trips. Commodities are classified under NST-2007 (Level 1, 20 items).

[1] excluding Malta, Liechtenstein, and Island.

[2] Exceptions in Germany (half week: Either Sunday 10 pm to Wednesday 24 pm, or Thursday 0 am to Sunday 22 pm), Finland (2 days for national trucks (about 93% in 2011) and 1-2 weeks for trucks not registered in Finland (about 7%)), and the UK (one week for national registered trucks (>99%) and 1 day to 4 weeks for non-UK registered trucks(<1%)).

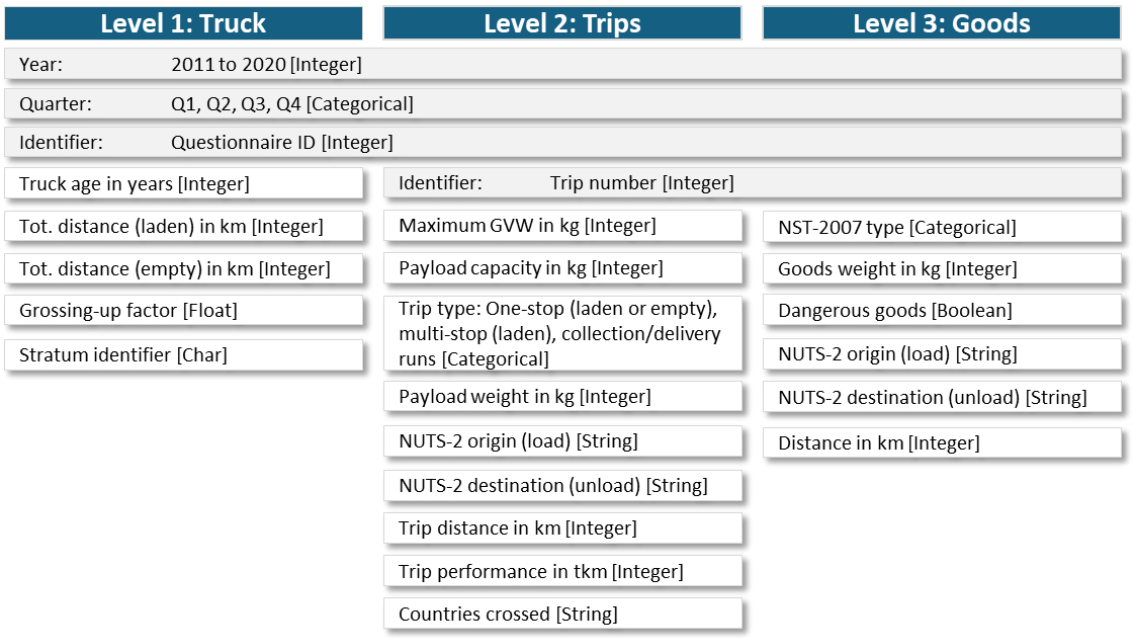

Note: Own illustration based on Eurostat (2016a)

Figure 6: ERFT microdata: Structure and parameters

The total sample involves 4,060,917 truck records, ranging from about 374,000 to 426,000 trucks per year. These truck records are coupled with 46,817,125 trip records (3,620,000 to 5,157,063 per year) and 33,570,228 goods records (2,994,774 to 3,488,401 per year). An annual breakdown is provided in **Table S6**. In addition, **Figure S1** provides an annual comparison to official Eurostat figures, which emphasizes its consistency and coverage across Europe.

Data processing

Processing involved the following assumptions and steps to ensure plausible and standardized datasets and remove inaccurate records:

- The home country of trucks is assumed to be the main country of operation, inferred from the most visited origins and destinations and, if inconclusive, the origin of the first trip. The accuracy of this approach is illustrated in **Figure S2**, which shows greater deviations in smaller EU Member States and those near Germany. Specifically, this method excludes so-called road cabotage effects, which are mainly seen in border regions and transit corridors, where trucks operate in host countries but are registered in other countries.
- Truck records with trips or home country labels outside the EU-27 or EFTA member states and the UK, such as the Western Balkans, Ukraine or Russia, were removed. This affects N=18,699 records (0.5%).
- Trucks were classified into 14 categories based on typical GVW limits within Europe and according to their reported mean GVW over the survey period. The accuracy of this

approach is illustrated in **Figure S3** and yields seven main N3 truck categories, allowing the deduction of truck or truck-trailer combinations in later modeling. Unclassified trucks or trucks with less than 3.5 tons (class N1) were subsequently removed, affecting N=261,112 records (6.5%).

- Truck records with missing journeys (no consecutive ascending journey numbers between the lowest and highest number) were removed. Otherwise, it is assumed that the list of journeys is complete. This affects N=91,345 records (2.3%).
- Truck records with incorrect OD sequences (last destination ≠ next origin) were removed to prevent that manual logbooks only list actual (laden) origin-destination relations but exclude (empty) interim trips. This affects N=662,408 records (16.5%). Note that empty return trips could have been added (direct commuting), but this was not done to avoid artificially influencing the dataset and favor one trip structure.
- Truck records for Germany and Finland were scaled to full weeks to have a standardized survey period (time unit: full week) across all countries. This was done by doubling (DE) or tripling (FI) the stated values, while correcting the grossing-up factor proportionately.
- Truck records that fell short of 100 km or exceeded 10,000 km per week[3] were removed to focus on active, regular operations. The lower limit affects N=246,096 records (6.1%) and the upper limit affects N=1,849 records (<0.1%).
- Truck records with excessive overloading (the actual cargo weight exceeded the stated capacity by more than 20%) were removed to account for moderate level overloading in later modeling, which is also observable from other data; however, excessively irregular operations or GVW errors were excluded. This affects N=9,241 records (0.2%).
- Origin and destination labels (NUTS-2 level) were updated to the NUTS-2021 version, which was necessary since four updates have been introduced over the survey period[4] so that certain regions or their nomenclature and composition could have changed.

Final sample

The filtered dataset (later denoted as $data_{ERFT}$) is summarized in **Table 4**, representing about 70% of the original records or around 2.8 million truck records, which still implies decent coverage and representativeness. Exclusions are primarily assigned to incorrect OD sequences, not classified truck classes, and insufficient weekly mileage. **Figure S4** visualizes the sample composition (2011-2020) and compares the coverage by country in relation to truck sales and stock figures, showing accurate proportions for most countries except Italy as well as logical peaks for the top seven European truck countries[5]. Further composition analyses suggest that temporal coverage per country is consistent, with no trend breaks or survey incidents between 2011 and 2020.

[3] This reflects an extraordinary working week (58 hours) in two-driver operations at an average speed of 85 km/h.

[4] Updates: NUTS-2006 (2008-2011); NUTS-2010 (2012-2014); NUTS-2013 (2015-2017); NUTS-2016 (2018-2020)

[5] Top 7: Germany, Poland, Spain, France, Netherlands, Italy, and the UK. Sale share: 75%; Stock share: 71%

Table 4: ERFT microdata: Scope of the final dataset.

Parameter	Original data	Processed data	Reduction
Number of trucks	4,060,917	2,828,764	-30.3%
Traveled distance (in km)	5,558,442,588	3,934,574,035	-29.2%
Number of trips	59,218,859	43,268,484	-26.9%
Transported goods (in tons)	513,666,573,000	362,086,964,100	-29.5%
Transport performance (in tkm)	63,830,479,470	44,256,354,158	-30.7%

For example, **Figure 7** visualizes the weekly mileage and average trip distance by truck classes among eleven countries as empirical cumulative density functions (ECDFs). Accordingly, smaller trucks (in blue tones) typically engage in more frequent but shorter trips than heavier trucks (in yellow tones), which cover longer individual tours and weekly distances. However, absolute values and skewed distributions reveal limited similarities and substantial differences in operational patterns both within countries across truck classes and between similar classes across countries.

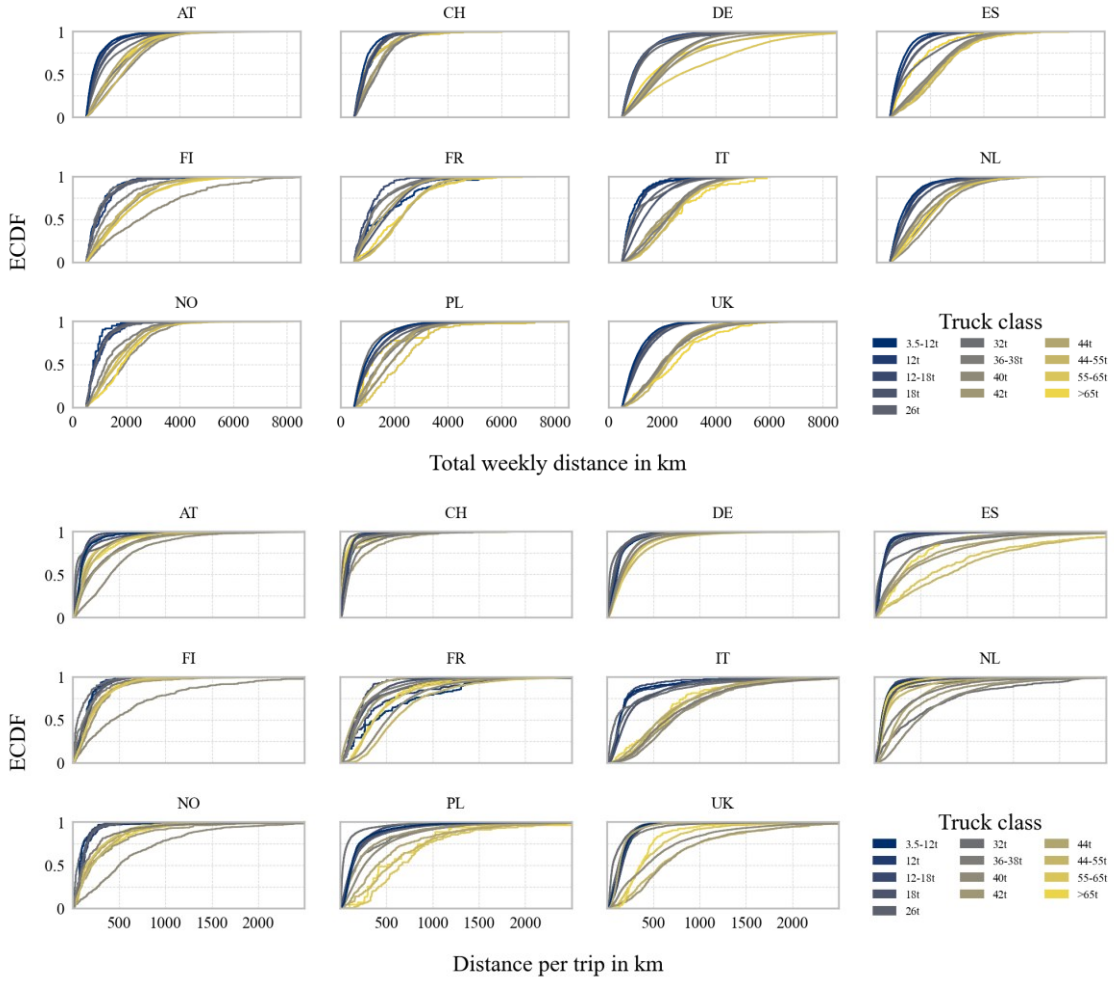

Figure 7: ERFT microdata: Weekly and per-trip distances by country.

Figure S5 illustrates the corresponding number of trips per week, showing that most trucks complete up to 25 trips per week, with analogous spreads and uncertainties among truck classes and countries. Additionally, most trucks operate between 60% and 90% of their maximum payload for at least one trip with high dependence on the NST type, whereas about 10-20% of all trucks complete at least one overloaded trip.

In summary, the filtered ERFT dataset provides a large and representative sample that allows analyzing major European truck markets based on a standardized, multi-year dataset. The observation period per truck is limited to one week, so that truck-specific weekly usage patterns and underlying trip variations and dependencies can be analyzed, involving trip distances, transported commodities, payloads, or trip origins and destinations (albeit with higher NUTS-2 resolution). However, truck-specific conclusions over several weeks are not possible. The information on truck age allows to map at least country-specific and class-specific trends in truck mileage with increasing service life. The anonymization process removed specific information such as the exact days and times of trips, thereby constraining insights into daily usage patterns.

3.2 Truck operating data

Overview

Real-world time series data gathered from various sources and companies constitute the second most important dataset in this thesis, with six distinguished data labels (Fleet 1, Fleet 2, Fleet 3, Fleet 4, DT-CARGO, and KiD).

The data collection is summarized in **Table S7**, which illustrates the heterogeneity concerning fleet composition and the number of trucks, collection methods, temporal coverage, and geographic coverage. Accordingly, samples range from just a few trucks in one fleet to several hundred trucks in the same or mixed fleets. Coverage ranges from single days to one month to longer periods of several months with operations mainly in Germany and Central Europe (Austria, Belgium, Czech Republic, France, Netherlands, and Switzerland) covering three general use cases (urban, regional, and long-haul). The data collection involves two spatial/temporal resolution classes from different sources: (1) Information is based on recorded trips via GPS data loggers. This approach yields precise time-based speed profiles, which might be connected to other information such as measured truck data, gradients or altitudes, certain events, or cargo loads. Single trips with distinct departure and arrival times can then be identified by extended idle times or changing vehicle states – such as ignition on/off – at plausible locations to avoid misdetection caused by congestion or traffic lights. (2) Information is based on manually or automatically created logbooks or tour schedules, which are collected via surveys or extracted from fleet management or tour planning software. This approach yields trip-based data with lower resolution and typical information such as departure and arrival times, address information, total distance traveled, average speeds based on driving times and distances, or cargo loads.

Data processing

All time series data are aggregated per day for all further evaluations to ensure equal resolution and to ease the connection to the weekly ERFT data. Accordingly, all trips per truck are sorted by their date information and then sequenced based on departure and arrival times. This allows the calculation of truck-specific daily information such as total mileage, average speed, number of trips, number of customer stops (or microtrips), daily driving time, first and successive departure times, or idle times between two consecutive tours. The daily operating time is calculated as the difference between the first departure time and the last arrival time. Further processing involved the following filtering steps to ensure plausible datasets and remove maneuvering events, which removed N=564 records:

- The daily average speed must fall between 5 km/h and 95 km/h.
- The daily mileage must be larger than 5 km.
- The total daily operating time must be greater than 10 min.
- The total operating time must be at least as long as the total driving time.

Final sample

The final dataset (later denoted as $data_{Tour}$) is summarized in **Table 5** and covers N=36,617 daily records by 1,900 trucks, which traveled over 10.6 million km.

Table 5: Tour data: Sample composition

Category	Distance in km	Share	Number of trucks	Share	Reference
Fleet 1	1,053,884	10%	224	12%	Scientific use files anonymized from project-related data
Fleet 2	129,322	1%	23	1%	
Fleet 3	2,151,772	20%	62	3%	
Fleet 4	5,584,875	53%	346	18%	
DT-CARGO	1,264,422	12%	53	3%	Balke et al. (2023)
KiD	453,625	4%	1,192	63%	Wermuth et al. (2012)
Total	**10,620,697**		**1,900**		

For example, **Figure 8** visualizes the total daily distance (incl. daily changeover), first departure time per day, and average daily driving speed as probability density functions (PDFs - left) and ECDFs (right), differentiated by the six categories. The average daily distances from a representative European fleet (Wentzel 2020) are given as a reference. The daily ranges vary strongly between the samples from short operations below 200 km to long-haul transports surpassing 1,000 km but likely cover a representative range of observable daily distances. Likewise, driving speeds and first departures cover a large data range, with most trucks operating between 40 and 70 km/h and starting their first tour in early mornings, usually between 4 and 7 AM and including tendencies to depart earlier for longer trips.

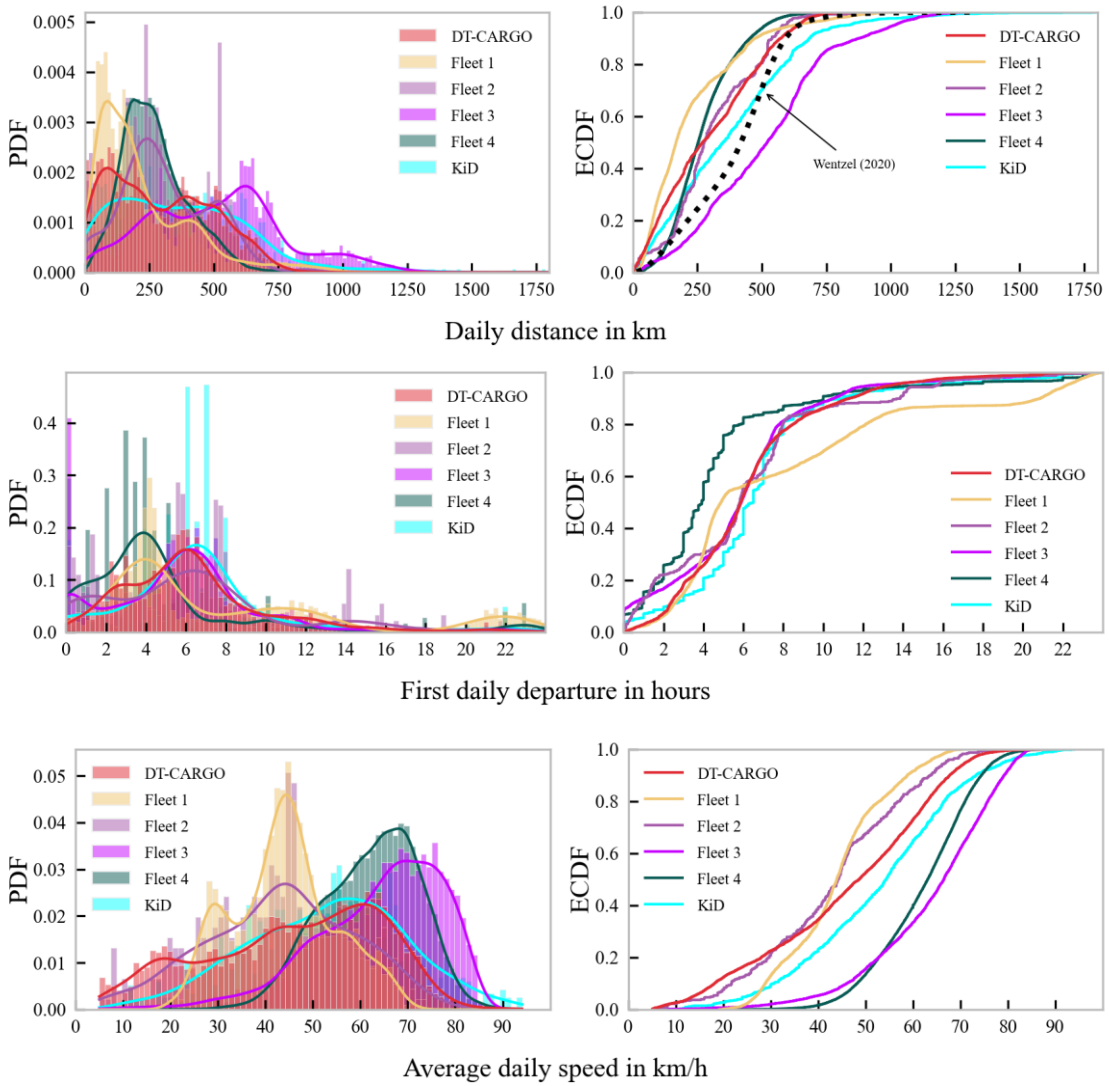

Figure 8: Tour data: Daily mileage, departure times and average daily speeds.

For example, **Figure 9** shows the variation in daily and weekly distances via different metrics. This involves the ratio between the observed maximum distances to the mean or median value per truck, as well as the coefficient of variation (CoV) and quartile coefficient of dispersion (QCD) to express the extent of variability in relation to the "average" day or week per truck. This implies, for example, that the maximum daily mileage can easily exceed the average daily mileage by a factor of 1.5-2.5 and even up to 3.5, which will likely affect the required BET battery sizes and thus technical feasibility of BETs. Although slightly smoothed compared with daily observations, the maximum weekly mileage can still exceed the average weekly mileage by a factor of 1.3-1.8 and even up to 2.5. The highest variability is observed for low to medium distance intervals in both cases. If the main corridor of 1,000 to 3,000 km per week is set in relation to 50-52 weeks per year, average mileages of approximately 50,000-150,000 km are obtained. This corresponds well with typical European mileages from other studies, implying certain representativeness and robustness.

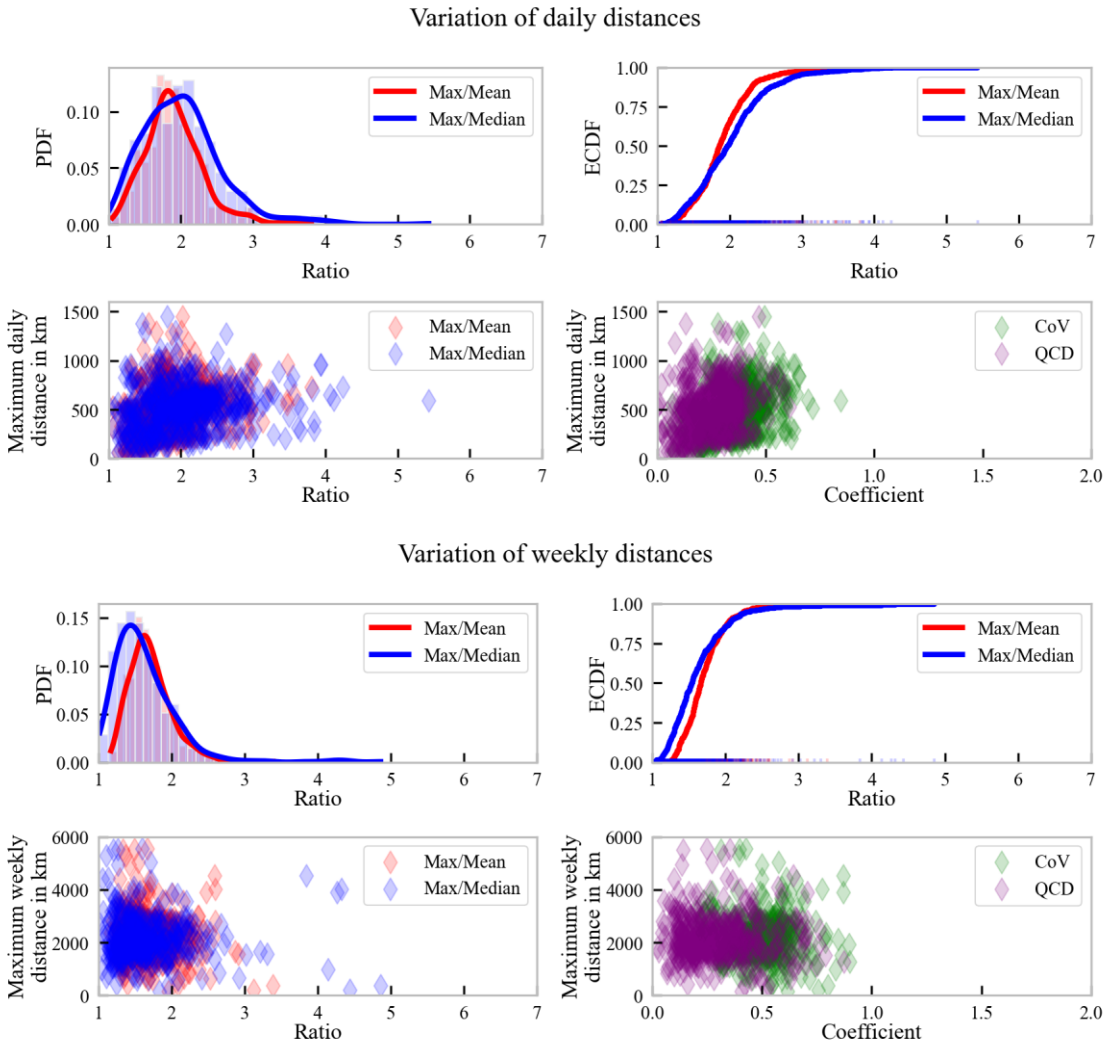

Figure 9: Tour data: Variations of daily and weekly distances.

In summary, the processed tour data allows the analysis of truck-specific daily usage patterns and variations over several weeks. Information, such as departure and arrival times, driving times, trip distances, or daily trip sequences, is limited to the trip level. The sample includes several hundred trucks from different fleets and industries and covers operations from UD to RD and LH transport. However, trucks operate predominantly in Germany and Central Europe.

3.3 Technical truck characteristics

Two data sources are differentiated for technical truck data, namely (1) official truck specifications from newly certified and registered trucks and (2) manufacturer truck datasheets.

First, reported truck specifications, as mandated by *Regulation (EU) 2018/956*, are analyzed to simulate truck characteristics accurately. The latest version of these data, later denoted as

$data_{EEA}$, was published on 22/03/2024 and is accessible via EEA (2024), covering 856,068 trucks between 2019-2022 and ten VECTO groups. Most of these trucks are equipped with conventional powertrains, mainly diesel (96.5%) or gas-powered (3.4%). The total dataset contains 460 parameters and includes official CO_2 certification figures based on the respective VECTO simulation runs with different payloads and driving cycles, while manufacturers must also report some technical characteristics about the respective trucks. The parameters of interest for vehicle simulations are the engine rated power (later denoted as P_{Rated}), air drag ranges as product of drag coefficient and truck frontal area (later denoted as A_{Drag}), tire rolling resistance coefficients (later denoted as c_{rr}), and DT chassis masses (later denoted as m_{DTCM}).

For example, **Figure 10** visualizes the data distribution for air drag, rated power, and DT curb mass per VECTO group as well as tire rolling resistance coefficients per axle and per tire configuration (single or twin tire). This expresses plausible value ranges and emphasizes the difficulties when selecting any single parameter value, even within the same VECTO group.

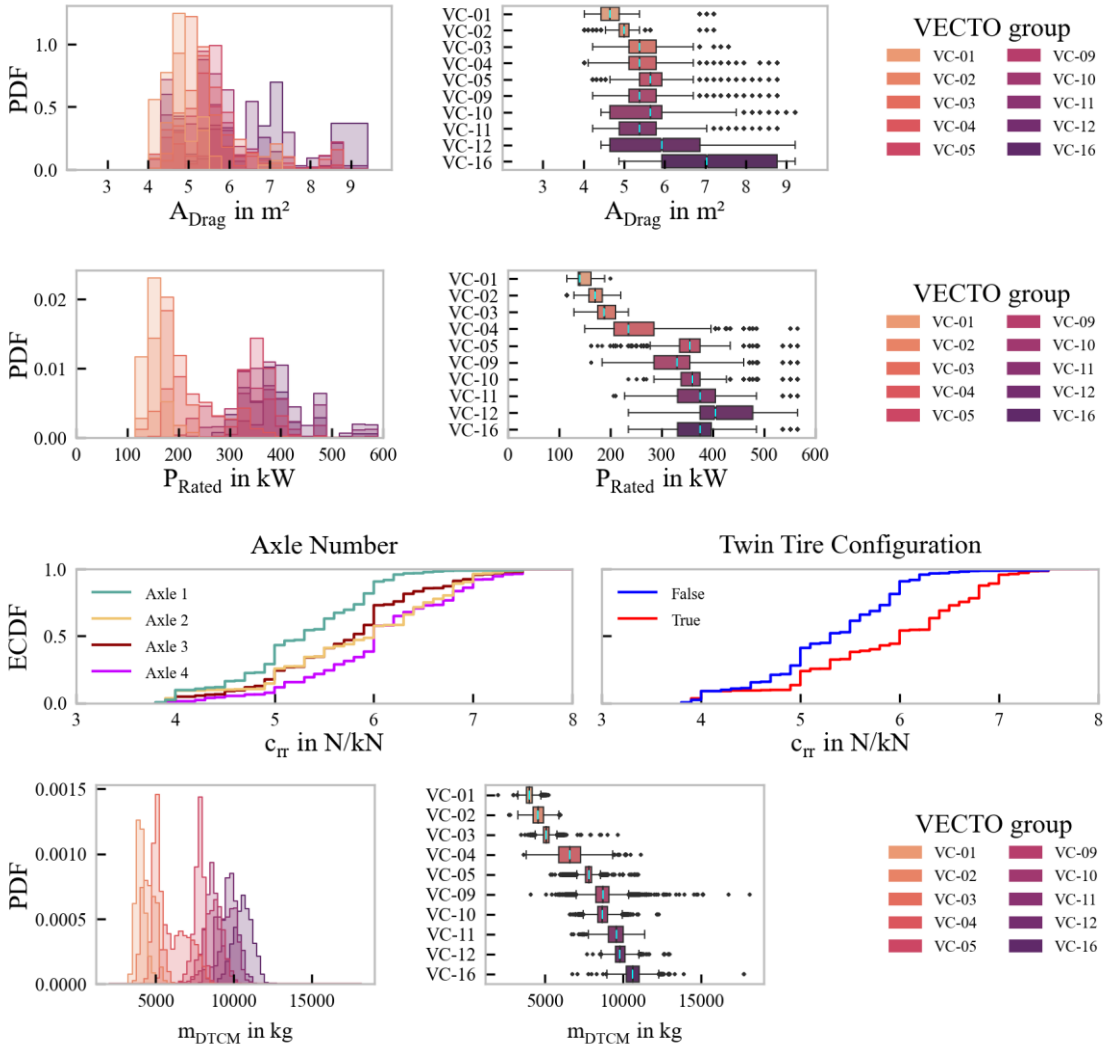

Figure 10: EEA data: Air drag, rated power, rolling resistance, and curb mass data.

Second, manufacturer datasheets are collected and digitized to estimate the potential installation space for batteries inside the truck chassis, which is later denoted as $data_{Datasheet}$. **Figure S6** shows an illustrative screenshot of such a datasheet. The parameters of interest are, among others, the total truck length (later denoted as l_{truck}), the wheelbase (later denoted as l_{wb}), and mass distributions among the front and rear axles, or maximum chassis loads (rigids only). This sample comprises 381 records and covers 80 different truck models, which are sold mainly by DAF, MAN and Volvo. **Table 6** summarizes the sample, differentiated by truck type and axle configuration.

Table 6: Truck data: Overview datasheets

Type	Number of axles	DAF	Daimler	IVECO	MAN	Renault	Volvo	Total
Rigid	2 (4x2, 4x4)	3	1	1	4		5	14
	3(6x2, 6x4)	2		1	4		7	14
	4 (8x2, 8x4)	6			2		5	13
Tractor	2 (4x2, 4x4)	4	1	1	3	1	5	15
	3 (6x2, 6x4, 6x6)	3	2	1	3	1	10	20
	4 (8x4)	3					1	4
Total		**21**	**4**	**4**	**16**	**2**	**33**	**80**

3.4 Diesel truck purchase and resale prices

The stated prices of new and used DTs are collected from three websites[6] and later evaluated to derive purchase costs for truck chassis (later denoted as $c_{Chassis}$), and truck resale values at the end of ownership (later denoted as RV_{Truck}).

Data collection occured in July 2023 and included a total of 7,147 tractors and 1,425 rigid trucks, all with EU-6 diesel engines. The key attributes included the manufacturer, country, application or body type (rigids only), engine rated power, vehicle mileage, axle configuration, date of first registration, and the stated sales price in EUR. There was no information about how often the truck had been resold. For rigid trucks, the price impact of any specialized body was summarized by a categorical variable (box body, chassis, or special). Approximately 40% of the records were incomplete and filtered out, predominantly with missing country information.

The final dataset (later denoted as $data_{Resale}$) comprises 4,471 tractors and 812 rigids, representing all major European truck manufacturers with balanced shares, ranging from 9.3% (Iveco) to 21% (DAF). However, with only five countries (BE, ES, FR, DE, NL) comprising 91% of the data, country-specific analysis and comparisons are limited. Specifically, **Figure 11** visualizes the separate impacts of mileage and vehicle age on the sales price, demonstrating that both

[6] Source 1: www.planet-trucks.com; Source 2: www.truckscout24.de; Source 3: www.mobile.de

parameters have a critical joint influence on the resale price. Additionally, distributions for truck mileage and age are visualized with reference corridors[7], which indicates that the sample should cover not only representative sales cycles but also extended parameter ranges for ages and mileages.

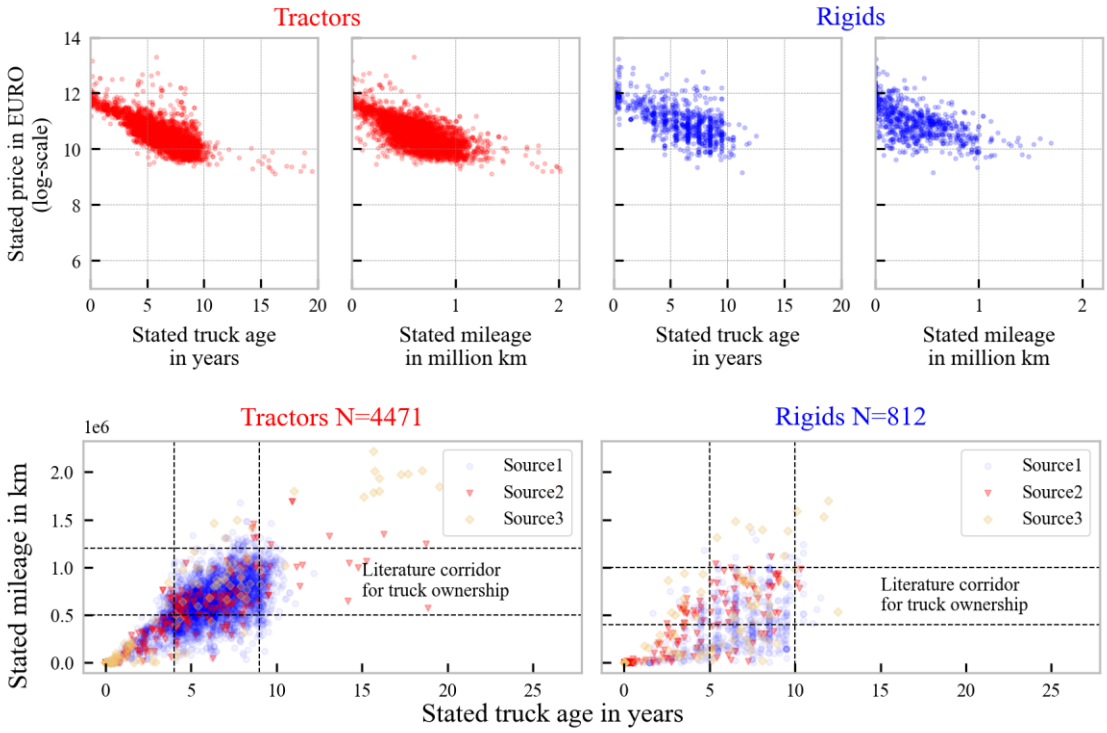

Figure 11: Resale data: Truck age and mileage distributions

3.5 Road network and infrastructure data

Real-world road network data and truck stop location data are used to accurately determine potential charging locations, which involve two main data sources.

First, the official TEN-T network was provided by the Directorate-General for Mobility and Transport (DG MOVE) as a shapefile (later denoted as $data_{TENT}$). Single roads are represented as so-called LineStrings objects that contain a series of connected GPS coordinates (latitude/longitude, WGS-84 format) in high spatial resolution. Roads are classified as either part of the TEN-T Core or the TEN-T Comprehensive network. **Figure 12** visualizes this network as a generic map including country borders (left) and as a close-up view of Baden-Württemberg (right), with **Figure S7** magnifying the European overview for better visibility.

[7] Literature corridor: Values for annual mileage, service life, and total mileage are collected from several studies, including Regulation (EU) 2019/1242, Noll et al. (2022), Seidenova et al. (2022), Seemungal et al. (2021), Basma et al. (2023), Meszler et al. (2018), and Tol et al. (2022).

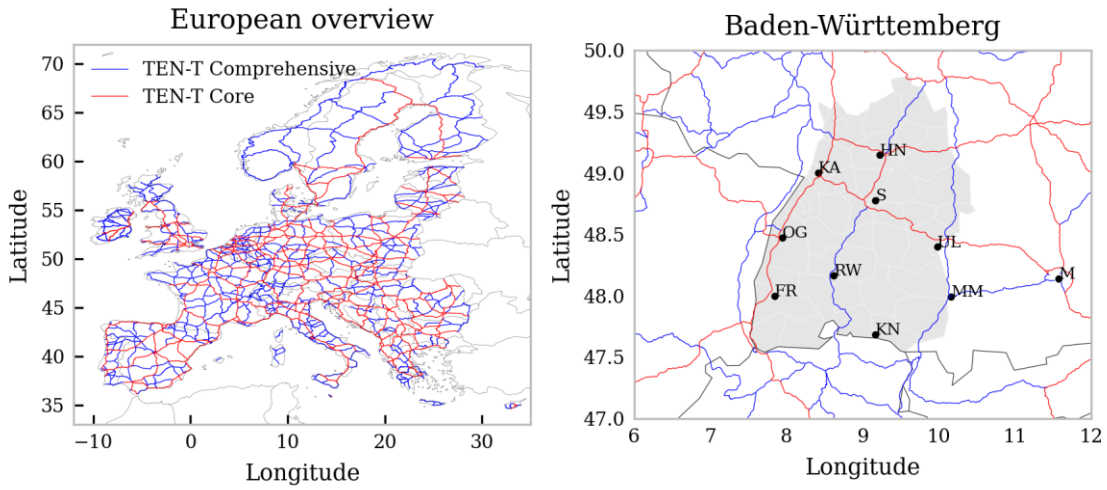

Figure 12: Charging infrastructure: Visualization of the TEN-T road network.

Second, an open-source dataset containing real-world public truck stop locations throughout Europe was developed during this thesis, later denoted $data_{TPL}$. The full documentation is published in Link et al. (2024a) and includes the data repository link. This dataset was systematically generated using OpenStreetMap (OSM) data and commercial truck routing software to identify truck stops, parking lots, rest areas, or truck fueling stations as predominant publically accessible truck parking facilities. Further refinement was achieved via the Mean-Shift algorithm, which is a density-based geospatial clustering technique, and yielded N=51,964 locations. Information from supplementary datasets was added to enhance the dataset and characterize locations. The published dataset was filtered to retain only publicly accessible and truck-certified parking and service facilities (medium and high confidence levels). This yielded N=19,713 designated truck parking sites. **Figure 13** visualizes these locations as a generic map including country borders (left) and as a close-up view of Baden-Württemberg (right), with **Figure S8** magnifying the European overview for better visibility.

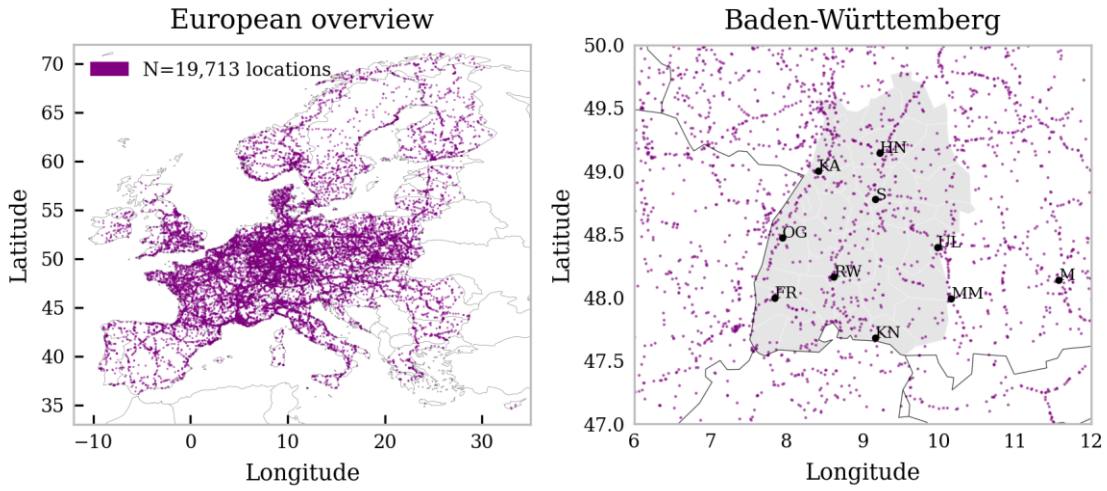

Figure 13: Charging infrastructure: Visualization of truck parking locations in Europe.

3.6 Summary and discussion

This previous chapter introduced four types of real-world data, ranging from truck driving data ($data_{ERFT}$ and $data_{Tour}$) to technical truck specifications ($data_{EEA}$ and $data_{Datasheet}$), price and sales information ($data_{Resale}$), and infrastructure data ($data_{TENT}$ and $data_{TPL}$). While these extensive datasets aim to ensure practical relevance and cover truck market heterogeneity, there are several limiations and shortcomings to each dataset.

The standardized survey-based ERFT data ($data_{ERFT}$) was available throughout Europe over ten years and covered several million DTs and several hundred million kilometers traveled so that all current truck operations are likely covered. However, truck-specific conclusions and modeling are limited to one week and the anonymization removed several key elements of the original survey, so that several assumptions and extensive data processing steps were required to utilize the data in the model. Plus, the geographical resolution is limited to NUTS-2 level, which is too inaccurate for a detailed geospatial localization of the subsequent driving profiles.

The tour-based data ($data_{Tour}$) were not standardized and covered just a few thousand DTs and several million kilometers, involving several collection techniques (surveys, software such as FMS and TPS, or GPS data loggers), varying observation periods, and different fleet sizes. Adding to this inherent heterogeneity, geographical coverage was highest for Germany and Central Europe, wheras most European countries are missing. Operational coverage was highest for UD and RD with daily returns to the depot, moderate for national LH with or without weekly returns to the depot, but lowest for international LH without confined operating territories. Truck departure and travel times fit well with findings from German traffic count data on federal highways and motorways[8], which typically coincides with main business hours and associated delivery/pickup windows. No checks were performed outside of Germany so that further studies might expand with country-specific tour data, scale to country-specific business hours, or validate against available traffic count data. However, rules on driving and working hours apply to all truck drivers throughout Europe and delivery/pickup windows should be similar so that a certain transferability to all European countries should be valid.

The truck market data ($data_{Resale}$) covered just a few thousand tractors and a few hundred rigid trucks with different body types, yet all with diesel powertrains. The resale corridors (age and mileage) correlate well with typical literature values (see **Figure 11**). However, some countries were missing or underrepresented while coverage was highest for Central Europe. Nonetheless, declining residual values with rising truck age and mileage should reflect market tendencies in every country and determining the first user resale age featured scaling with findings from $data_{ERFT}$ to reproduce country-specific age structures. However, the stated prices should be

[8] Morning peaks starting from 5-9 AM with a subsequent plateau until an afternoon peak at around 3-6 PM as visualized by Plötz et al. (2020).

considered as approximate upper limits since these do not account for the individual purchasing conditions of major customers with discounts and do not yet reflect price negotiations.

The sampled datasheet information ($data_{Datasheet}$) for truck specifications covered just 80 different DT models in standard configurations (engine, exterior, interior, cabin, etc.) yet involved all major European manufacturers, truck types (tractor and rigid), and axle configurations (2/3/4 axle configurations). However, the variation in truck designs beyond standard configurations is difficult to cover, so that future studies might survey truck specifications more systematically to assess vehicle installation spaces and weight distributions in greater detail.

The infrastructure data ($data_{TENT}$ and $data_{TPL}$) provide high spatial resolution and background information to each location, yet substantial uncertainty remains concerning site-specific constraints such as available area and grid connection, as also discussed in Link et al. (2024a).

To summarize this chapter, **Table 7** presents an overview of all datasets in relation to their usage at distinct step(s) in the model development.

Table 7: Data summary: Parameter overview

Data	Used for	Main parameters or insights
$data_{ERFT}$	Driving profile simulation	- Weekly operational patterns per truck - Differences among countries and truck classes - Mileage evolution by truck age
$data_{Tour}$	Driving profile simulation	- Truck-specific daily operational patterns - Speed and timestamp information - Mileage trends over several weeks
$data_{EEA}$	Truck energy simulation	- Truck parameters: P_{Rated}, A_{Drag}, c_{rr}, and m_{DTCM} - Official DT fuel consumption values for validation
	Cost model	Component specifications (P_{rated})
$data_{Datasheet}$	Battery packaging	Truck parameters: l_{truck}, l_{wb}, and vehicle mass distributions
$data_{Resale}$	Driving profile simulation	- Truck mileage at resale (1st user) - Truck age at resale (1st user)
	Cost model	- Truck chassis costs - Relative residual value
$data_{TENT}$	Infrastructure model	Road network of main European highways, where public charging infrastructure is most needed
$data_{TPL}$	Infrastructure model	Existing truck parking locations as candidate locations for charging infrastructure stations

4 Model development

This chapter describes the model development, with **Figure 14** detailing and visualizing the architecture and logical structure. The model is implemented in Python (version 3.7+) and configured to use only open-source packages/solvers. The implementation was done on a standard Lenovo notebook with i7-8565U @1.8 GHz (4/8 cores) and 16 GB RAM as well as a standard server with AMD EPYC 7742 @2.25 GHz (2/4 cores) and 120 GB RAM.

The logical structure is as follows. A series of multi-year operating schedules with hundreds of concatenated trips is generated via a novel probabilistic driving profile simulation. Each schedule represents one distinct truck sold in the selected country to a generic truck owner (agent-based approach) (see **Subchapter 4.1**). Energy needs are assigned to individual trips based on the truck characteristics and trip-specific information using the truck energy model (see **Subchapter 4.2**) and the battery model (see **Subchapter 4.3**). The latter also determines the required battery size based on energy consumption so that this schedule becomes technically feasible for a BET. The cost model then evaluates the TCO and compares this BET configuration versus a DT counterpart via different cost scenarios (see **Subchapter 4.4**). An add-on infrastructure model introduces respective charging costs, which are forwarded to the TCO analysis, and evaluates potential locations for public charging infrastructure in Europe (see **Subchapter 4.5**). This yields the techno-economic feasibility of BETs for individual truck owners in the selected countries, and recommendations for the deployment of charging infrastructure.

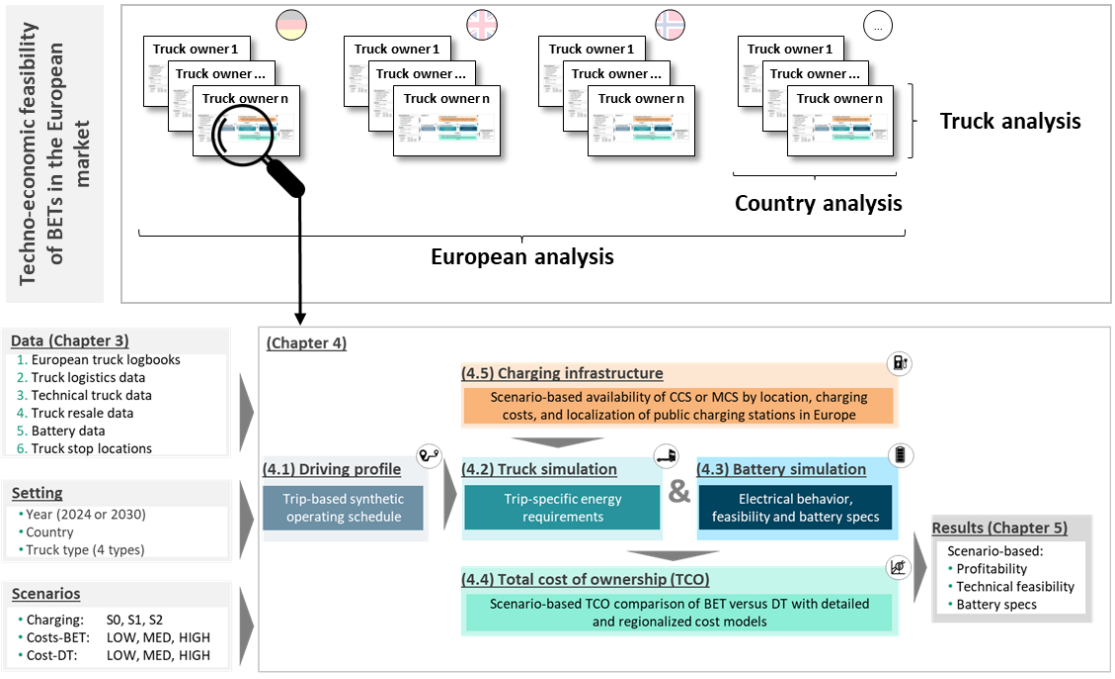

Figure 14: Model development: Overview and structure.

4.1 Probabilistic driving profile simulation

The generation of synthetic operating schedules uses a microscopic model leveraging $data_{ERFT}$, $data_{Tour}$, and $data_{Resale}$ and respective multivariate data sampling techniques. This approach was chosen to focus on single truck operating patterns with inherent variations. Accordingly, schedules are generated via respective conditional probability distributions.

This submodel consists of four main modules as visualized in **Figure 15**. For each specified truck, single operating weeks are generated (later referred to as the *Weekly Module*), with weeks consisting of at least one trip. All trips of a week are then allocated to weekdays and timestamps are generated to concatenate the trips accordingly (later referred to as the *Daily Module*). This process is repeated until the truck is sold, which then yields the targeted operating schedule. Finally, the OD-sequences are determined to locate trips starts and ends geographically.

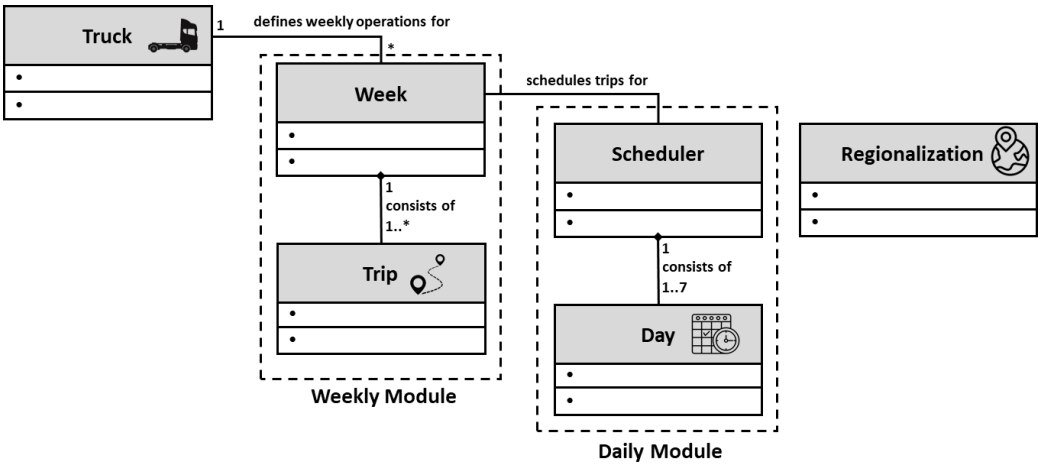

Figure 15: Driving profile simulation: Submodel structure

4.1.1 Initialization

The initialization defines, on the one hand, the simulation setup and, on the other hand, four fixed properties for each truck.

The setup defines how many trucks, which countries and which VECTO groups shall be simulated. This happens either manually for specific tests or proportionally based on historical market and sales figures (see **Table S1**, **Table S2, Table S3**). Since sales-weighted shares per VECTO group are only available at the European level, country-specific shares are calculated by offsetting this European share with the country-specific shares of potential truck classes (class 01 to 13) according to $data_{ERFT}$ by matching VECTO groups to potential ERFT truck classes based on logical matches, GVW limits, and potential trailer combinations. These shares are specified **Table S8**.

First and second, each truck is characterized by its home country and category. The truck categories follow the VECTO classification (see **Table S3**), since this scheme covers almost the entire European truck market and allows the deduction of truck type (rigids and tractors) and axle configuration.

Third and fourth, each truck is characterized by two end-of-ownership criteria (first-user life) based on either reaching a corresponding mileage or age. Values are sampled using a two-parameter Weibull distribution – a model that is frequently used in lifetime and reliability engineering. Weibull parameters are fitted based on $data_{Resale}$, with values normalized to $[0,1]$ using respective minimum/maximum values. Sampled values are then rescaled accordingly, with valid reselling windows limited to 2-20 years and 0.2-2.0 million kilometers. Equations (4.1) and (4.2) describe the PDF and CDF via shape parameter (α) and scale parameter (β):

$$f(x,\alpha,\beta) = \begin{cases} \frac{\alpha}{\beta} * \frac{x}{\beta}^{\alpha-1} * e^{-\frac{x^\alpha}{\beta}} & x > 0 \\ 0 & x \leq 0 \end{cases} \quad (4.1)$$

$$F(x,\alpha,\beta) = \begin{cases} 1 - e^{-\frac{x^\alpha}{\beta}} & x \geq 0 \\ 0 & x < 0 \end{cases} \quad (4.2)$$

A comparison between the fitted and the observed data for mileage and age, differentiated by tractors and rigid trucks, and parameter values are visualized in **Figure 16.**

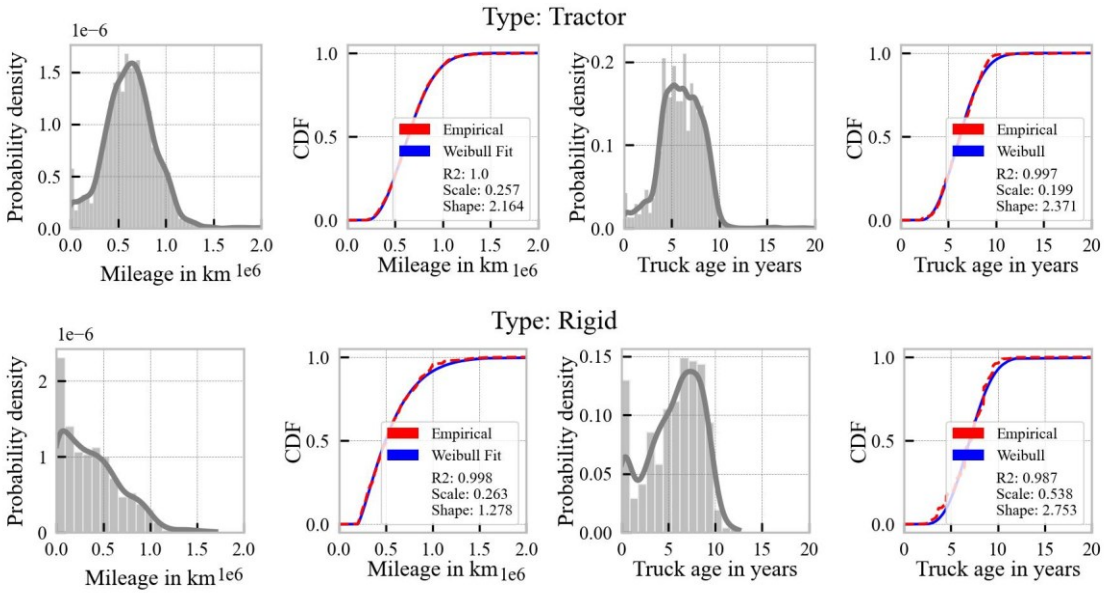

Figure 16: Driving profile simulation: Weibull model for first user life criteria

To account for different age structures and turnover times of truck fleets in Europe, country-specific scaling factors are used to adjust the truck age criteria based on $data_{ERFT}$. The values and ratios are specified in **Table S9**. Note that the mileage criteria remain unadjusted.

4.1.2 Weekly Module

The *Weekly Module* generates a list of weekly trips following Bayesian Network logic and using conditional probability distributions per parameter to either sample values (continuous variables) or to select values based on their likelihood (categorical variables). This approach allows capturing parameter dependencies and causal relations within one week and keep correlations beyond. One week is the reference unit following the observation period of $data_{ERFT}$.

Model structure and parameter dependencies

Parameter dependencies that define the Bayesian Network structure are identified combining linear regression and ANOVA as well as Generalized Linear Models (GLMs) and Wald tests to analyze and validate the influence of predictors on a dependent variable. Parameter dependencies are evaluated for significance and effect strength (predictor coefficients) using two sample sizes (N=10,000 or N=1,000,000). Table excerpts for main parameters are given in **Table S10**, **Table S11**, **Table S12**, **Table S13**, and **Table S14**. Generally, distance-related parameters strongly depend on the country, truck class, commodity group, and operation type. This is indicated by high regression coefficients, high F-statistics and very low p-values in ANOVA as well as high Chi-square statistics and very low p-values in GLM. Cargo-related parameters and trip structures depend mainly on the country, truck class, and commodity group. The transport performance is correlated to the weekly distance (by definition). Using these dependencies then allows filtering $data_{ERFT}$ to determine the respective conditional distributions per parameter.

The resulting logical structure per week is visualized in **Figure 17**, with specified truck characteristics and regulatory conditions as key inputs. The model starts with generating a country-specific total weekly mileage as the main parameter of interest. It proceeds with determining a suitable truck class for the specified weekly mileage and truck category. Similarly, it determines a probable commodity group (according to the NST-2007 classification) suitable for the specified weekly mileage and truck class. The targeted weekly transport performance (in tkm) and operation type are then determined based on the specified weekly mileage, truck class, and commodity type. The weekly operation type describes the possible area of operation, ranging from local (within the same NUTS-2 region) to regional (within the same NUTS-1 region), national (within the home country) and international (outside the home country). The maximum cargo load follows from the specified truck class and country-specific GVW limits. The number of weekly trips is then determined based on the specified mileage, truck class, commodity type, and operation type. This is followed by determining the probable type (single or multi-stop) for each trip and the overall number of laden and empty trips. The actual payloads for laden trips are then determined based on the specified truck class, commodity type, and maximum cargo load. Finally, the module calculates the optimal allocation between trips and calculated payloads to ideally match the targeted weekly transport performance.

For an initial orientation, according to $data_{ERFT}$ and $data_{Tour}$, weekly distances range between 1,000-4000 km in Europe, splitted into one or just a few trips and typically around 15-25 trips. However, there are substantial differences in these patterns among countries and truck classes.

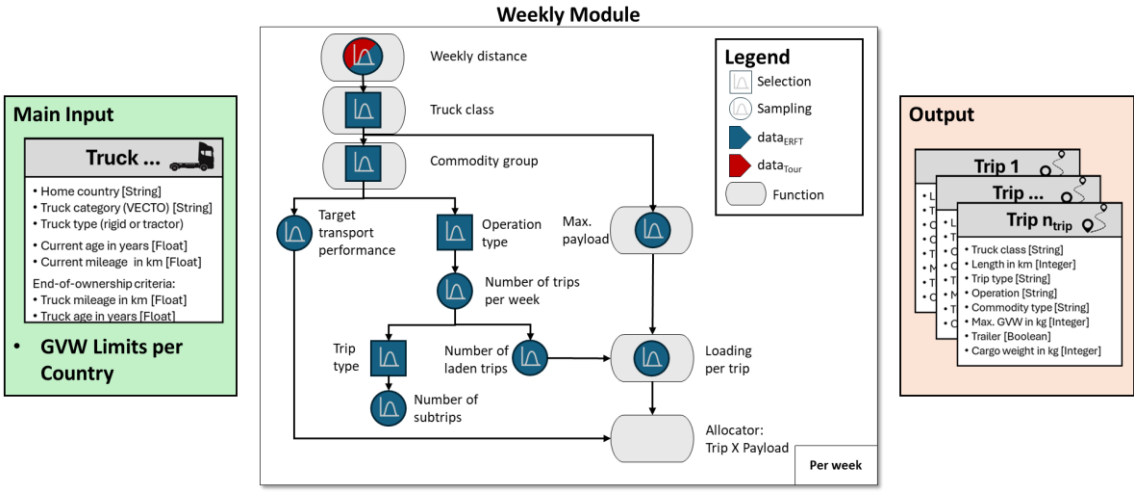

Figure 17: Weekly Module: Submodel structure

Conditional probability distributions

Three probability distributions are implemented to either sample values (continuous variables) or deduce corresponding realization probabilities (categorical variables). These are the Gamma (Γ) and Beta (B) distribution as parametric distributions, as well as the empirical PDF and CDF (denoted as E) if both parametric distributions cannot adequately reproduce the data. The motivation for using parametric distributions follows from ensuring robust and reliable probability distributions regardless of sample sizes in $\text{data}_{\text{ERFT}}$ (compare coverage in **Figure S4**).

Both Gamma $(0, \infty)$ and Beta distribution $(0,1)$ are right-skewed distribution. This skeweness means that most values are clustered around the left tail of the distribution, whereas the right tail of the distribution is longer. Both distributions are commonly used as prior distributions in Bayesian analysis and can adapt to various types of empirical distributions, from exponential to highly right skewed or more symmetric distributions via their shape/scale parameters. The gamma distribution is set as the default distribution.

For any model parameter, these parametric distributions are initiated by the calculated mean value (denoted as μ), standard deviation (denoted as σ), and minimum value of the respectively filtered $\text{data}_{\text{ERFT}}$ subset to determine the conditional probability distributions. This approach uses the mathematical relation to the shape (α), scale (β), and shift (γ) parameters of the Γ/B distribution, with Equation (*4.3*) describing the PDF of a Gamma distribution:

$$\mathrm{f}(\mathrm{x}, \alpha, \beta, \gamma) = \begin{cases} \dfrac{\beta^{-\alpha} * (\mathrm{x}-\gamma)^{\alpha-1} * \mathrm{e}^{-\frac{\mathrm{x}-\gamma}{\beta}}}{\Gamma(\alpha)} & \mathrm{x} \geq \gamma \\ 0 & \mathrm{x} < \gamma \end{cases} \tag{4.3}$$

$$\text{with } \alpha = \frac{\mu^2}{\sigma^2} \ (\alpha > 0) \text{ and } \beta = \frac{\mu}{\sigma^2} \ (\beta > 0) \text{ and } \gamma > 0$$

Equation (*4.4*) describes the PDF of a Beta distribution:

$$f(x,\alpha,\beta) = \frac{x^{\alpha-1} * (1-x)^{\beta-1}}{B(\alpha,\beta)} \text{ for } x \in [0,1]$$
$$\text{with } \alpha = \mu^2 * \left(\frac{1-\mu}{\sigma^2} - \frac{1}{\mu}\right), \alpha > 0 \qquad (4.4)$$
$$\text{and } \beta = \alpha * (\frac{1}{\mu} - 1), \qquad \beta > 0$$

The distribution parameters are precomputed and stored by filter condition to optimize runtime. Note that the following equations disregard the shift parameter (=minimum value) of the Gamma distribution to allow for a uniform notation. For Gamma distributions, an added upper bound (=observed maximum) limits extreme value problems and irregular values. In contrast, the Beta distribution inherently constrains a valid value range by normalization.

Example 1: Sampling weekly distances

Generating the total weekly distance features two modes to keep dependencies between consecutive weeks and to reflect reduced driving performance with increasing truck age.

First, the first weekly distance ($d_{week,1}$) has no preceding information, so that this value is sampled from a probability distribution $D_{wd} \in \{\Gamma, B, E\}$ specific to the home country (cty) and to the VECTO group as more information is not yet available. Each VECTO group is specified as a specific subset of potential truck classes (tc_{vg}) from all possible truck classes $TC_{all} \in \{TC_1, \dots, TC_{13}\}$. Additionally, $data_{ERFT}$ was filtered to include only new trucks (younger than three years). Equation (*4.5*) describes the sampling process:

$$p(d_{week,1} | \text{ cty}, TC_{VG}) = D_{wd}(\alpha(\mu,\sigma), \beta(\mu,\sigma))$$
$$\text{with } \mu = \mu(\text{cty}, TC_{VG}) \text{ and } \sigma = \sigma(\text{cty}, TC_{VG}) \qquad (4.5)$$
$$\text{so that } d_{week,1} \sim D_{wd}(\alpha(\mu,\sigma), \beta(\mu,\sigma))$$

Figure 18 visualizes the mean values and standard deviations among all countries and their VECTO groups and demonstrates the validity/accuracy of both parametric distributions by comparing the respective R2 and RMSE values, measured against the ECDF.

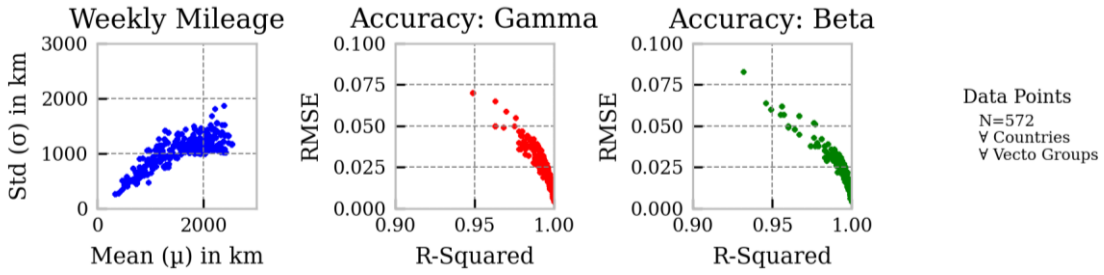

Figure 18: Weekly Module: Accuracy of determining the first weekly distance

Second, any subsequent weekly distance ($d_{week,i}$) builds on the preceding information, using the previous distances (d_{old}) and Markov-Chain logic. The relationship of historical to future weekly distances, reflected by probability distribution $D_{nw} \in \{\Gamma, B, E\}$, follows from $data_{Tour}$ (multi-week observation period for each truck). Equation (*4.6*) describes the sampling process:

$$\begin{gathered} p(d_{week,i} | \, d_{old}) = \; D_{nwd}(\alpha(\mu,\sigma), \beta(\mu,\sigma)) \\ \text{with } \; \mu = \; \mu(d_{old}) \text{ and } \sigma = \sigma(d_{old}) \text{ and if } i > 1 \\ \text{so that } d_{week,i} \sim D_{nwd}(\alpha(\mu,\sigma), \beta(\mu,\sigma)) \end{gathered} \tag{4.6}$$

Figure 19 visualizes the relationship between weekly distances of previous weeks to subsequent weeks for two aggregation steps, with the min-max range defined by the 99th percentile and functions fitted via log-log regression. The trends indicate that at low mileage (below 2,500 km) the probability of higher mileage in the following week increases and at higher mileage (above 3,000 km) the probability of a similar or even higher mileage decreases substantially. The figure also visualizes the restricted corridor for valid values defined by the min-max range.

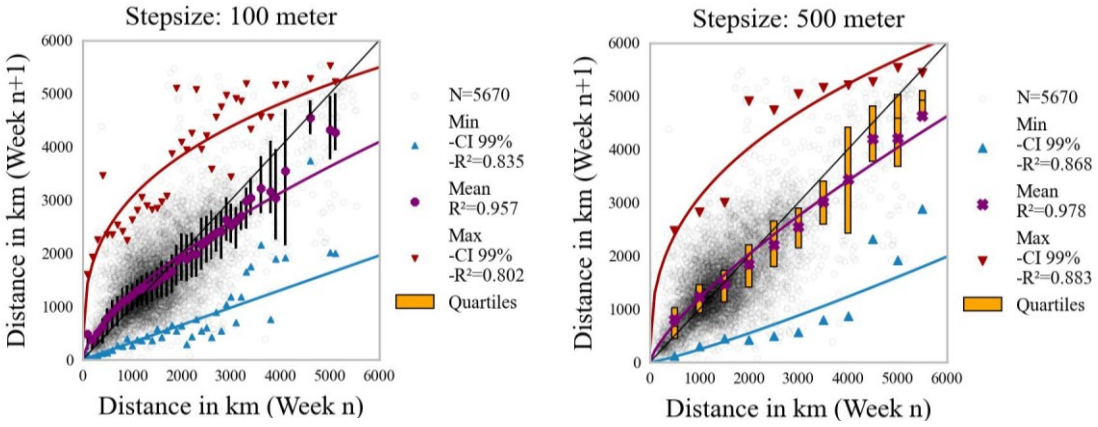

Figure 19: Weekly Module: Relationship of historical to future weekly distances

Previous distances (d_{old}) are estimated via two cases, both applying a correction factor (f_{corr_wd}) that captures the decline in mileage with age, specific to truck class (tc) and country (cty). This factor is derived from $data_{ERFT}$ by calculating the mean mileage by truck age in relation to the mileage of new trucks (younger than three years) and using a power-law relationship. **Figure S9** visualizes this relationship for selected countries. Although all countries and truck classes exhibit a decreasing mileage trend with age, the extent and speed of the decrease vary substantially, which motivates the decision for the chosen dependencies and the factor itself.

- Case 1: When the year changes, the previous distance is defined as the mean mileage of the previous year multiplied by the correction factor.
- Case 2: For every other week, the previous distance is modeled in relation to the direct predecessor (80%) and the mean mileage adjusted by the correction factor (20%). This split was determined by repeated testing to balance strong short-term dynamics and dependecies to the direct predecessor versus long-term smoothing to contain variability.

Example 2: Truck class selection

The weekly truck class is selected based on the most likely choice (maximum likelihood) using $\text{data}_{\text{ERFT}}$. The option of switching truck classes across different weeks aims to reflect operations using different trailers (tractors) or even operations without trailers (rigids).

The defined VECTO group pre-restrictes a specific subset of potential truck classes (TC_{VG}) from all possible truck classes $\text{TC}_{\text{All}} \in \{\text{tc}_1, \dots, \text{tc}_{14}\}$. The model calculates the probability that the weekly distance d_{week} belongs to all eligible truck classes using the respective probability distributions, which are specific to country (cty) using probability distribution $\text{D}_{\text{tc}} \in \{\Gamma, \text{B}, \text{E}\}$. For all eligible truck classes, this probability (describable as affiliation probability) is further multiplied by the relative share (s_{tc}: weighted truck count) of this truck class in the specific country. Finally, these adjusted probabilities (P_{norm}) are normalized to select the most likely truck class (denoted as tc^*). Equation (*4.7*) describes the selection process:

$$
\begin{gathered}
\text{tc}^* = \arg \max_{\text{tc}_x \in \text{TC}_{\text{VG}}} \text{P}_{\text{norm}}(\text{tc}_x|\text{cty}, \text{d}_{\text{week}}) \\
\text{with } \text{P}_{\text{norm}}(\text{tc}_x|\text{cty}, \text{d}_{\text{week}}) = \text{P}(\text{tc}_x|\text{cty}, \text{d}_{\text{week}}) * \text{s}_{\text{tc}}(\text{tc}_x), \forall\, \text{tc}_x \in \text{TC}_{\text{VG}} \\
\text{and } \text{P}(\text{tc}_x|\text{cty}, \text{d}_{\text{week}}) = \text{D}_{\text{tc}}\big(\alpha(\mu, \sigma), \beta(\mu, \sigma)\big) \\
\text{and } \mu = \mu(\text{cty}, \text{d}_{\text{week}}) \text{ and } \sigma = \sigma(\text{cty}, \text{d}_{\text{week}}) \\
\text{and } \sum_{\text{tc}_x \in \text{TC}_{\text{VG}}} \text{P}_{\text{norm}}(\text{TC}) = 1
\end{gathered}
\tag{4.7}
$$

Figure S10 visualizes the mean values and standard deviations among all countries and combinations of VECTO group and truck classes to demonstrate the validity/accuracy of both parametric distributions by comparing the respective R2 and RMSE values, measured against the ECDF.

Example 3: Commodity type selection

The weekly commodity type is selected based on the most likely choice (maximum likelihood) using $\text{data}_{\text{ERFT}}$, similiar to the truck class. Likewise, the option of switching commodity types across different weeks aims to reflect a certain flexibility. However, cargo transport is typically linked to specific trailer designs and truck body types, which restricts the possibility of transporting all types of goods. Types are defined according to the NST-2007 classification that differentiates 20 classes (denoted as NST_{All}). The model distinguishes between the first and all subsequent weeks.

(1) The first week with no preceding information so that the model calculates the probability that the weekly distance d_{week} belongs to the respective NST class, specific to country (cty) and truck class (tc) using a probability distribution $\text{D}_{\text{nst}} \in \{\Gamma, \text{B}, \text{E}\}$. This probability is further multiplied by the share s_{nst} (weighted tons) of any NST class in the specific country and truck class. Equation (*4.8*) describes the selection process:

$$
\begin{gathered}
\mathrm{nst}^{*} = \arg \max_{\mathrm{nst}_x \in \mathrm{NST_{All}}} \mathrm{P_{norm}}(\mathrm{nst}_x|\mathrm{cty}, \mathrm{tc}, \mathrm{d_{week}}) \\
\text{with } \mathrm{P_{norm}}(\mathrm{nst}_x|\mathrm{cty}, \mathrm{tc}, \mathrm{d_{week}}) = \mathrm{P}(\mathrm{nst}_x|\mathrm{cty}, \mathrm{tc}, \mathrm{d_{week}}) * \mathrm{s_{nst}}(\mathrm{nst}_x) \\
\forall\ \mathrm{nst}_x \in \mathrm{NST_{All}} \\
\text{and } \mathrm{P}(\mathrm{nst}_x|\mathrm{cty}, \mathrm{tc}, \mathrm{d_{week}}) = \mathrm{D_{nst}}\big(\alpha(\mu, \sigma), \beta(\mu, \sigma)\big) \\
\text{and } \mu = \mu(\mathrm{cty}, \mathrm{tc}, \mathrm{d_{week}}) \text{ and } \sigma = \sigma(\mathrm{cty}, \mathrm{tc}, \mathrm{d_{week}}) \\
\text{so that } \sum_{\mathrm{nst}_x \in \mathrm{NST_{All}}} \mathrm{P_{norm}}(\mathrm{NST}) = 1
\end{gathered}
\tag{4.8}
$$

(2) All subsequent weeks build on the preceding information, using the previous NST class ($\mathrm{nst_{old}}$) and a country-specific transition matrix ($\mathrm{M_{nst}}$) that reflects the conditional probability of transitioning from the previous NST class (rows) to another NST class (columns). This matrix is calculated from the transported tons per NST class for each truck, aggregated for the total fleet within a specific country, and normalized by row. Note that the probability of transporting the same NST class as in the previous week is typically the highest. Equation (*4.9*) describes the selection process:

$$
\begin{gathered}
\mathrm{nst}^{*} = \arg \max_{\mathrm{nst}_x \in \mathrm{NST_{All}}} \mathrm{P_{norm}}(\mathrm{nst}_x|\mathrm{cty}, \mathrm{tc}, \mathrm{d_{week}}), \mathrm{k} > 0 \\
\text{with } \mathrm{P_{norm}}(\mathrm{nst}_x|\mathrm{cty}, \mathrm{tc}, \mathrm{d_{week}}) = \mathrm{P}(\mathrm{nst}_x|\mathrm{cty}, \mathrm{tc}, \mathrm{d_{week}}) * \mathrm{s_{nst}}(\mathrm{nst}_x) \\
* \mathrm{M_{nst}}[\mathrm{nst_{old}}, \mathrm{nst}_x], \forall\ \mathrm{nst}_x \in \mathrm{NST_{All}} \\
\text{and } \mathrm{P}(\mathrm{nst}_x|\mathrm{cty}, \mathrm{tc}, \mathrm{d_{week}}) = \mathrm{D_{nst}}\big(\alpha(\mu, \sigma), \beta(\mu, \sigma)\big) \\
\text{and } \mu = \mu(\mathrm{cty}, \mathrm{tc}, \mathrm{d_{week}}) \text{ and } \sigma = \sigma(\mathrm{cty}, \mathrm{tc}, \mathrm{d_{week}}) \\
\text{so that } \sum_{\mathrm{nst}_x \in \mathrm{NST_{All}}} \mathrm{P_{norm}}(\mathrm{nst}_x) = 1
\end{gathered}
\tag{4.9}
$$

Example 4: Sampling the weekly number of trips

Trip lengths are sampled iteratively using a probability distribution $\mathrm{D_{trip}} \in \{\Gamma, \mathrm{B}, \mathrm{E}\}$ that generates individual trip distances specific to country (cty), truck class (tc), commodity type (nst), the weekly operation type (ops), and the weekly distance ($\mathrm{d_{week}}$). Note that the weekly distance is transformed into a categorical variable via a binning function ($\mathrm{f_{bin}}$), allowing to filter $\mathrm{data_{ERFT}}$ accordingly and derive the respective distributions. The pseudo-code for this sampling algorithm is provided in the Appendix (Equation *A.1*) and the logical structure is as follows:

Each sampling iteration yields a potential trip length, which are then summed. The sampling process stops once the predefined weekly distance is exceeded. The algorithm then minimizes the error by either removing the last trip and upscaling the remaining trips or downscaling all sampled trips so that the specified weekly distance is reached. This yields a list of trip distances $\{\mathrm{d_{trip},i}\}_{i=1}^{\mathrm{n_{trips}}}$, which add up to $\mathrm{d_{Week}}$ and with the weekly number of trips denoted as $\mathrm{n_{trips}}$ and individual trip distances denoted as $\mathrm{d_{trip}}$.

Other parameters

Sampling or selecting the other weekly parameters follow the same structure and notation as outlined in the four examples, considering the respective dependencies per parameter. The respective equations are provided in the Appendix.

- The weekly operation type (ops – see Equation *A.2*) follows from the most likely choice, derived by the probability that the weekly distance $\mathrm{d_{week}}$ belongs to the respective operation type (local, regional, national or international), specific to country (cty), truck class (tc), and commodity type (nst) using probability distribution $\mathrm{D_{ops}} \in \{\Gamma, \mathrm{B}, \mathrm{E}\}$.
- The targeted weekly transport performance ($\widehat{M}_{TKM}$ – Equation *A.3*) is sampled using probability distribution $\mathrm{D_{tkm}} \in \{\Gamma, \mathrm{B}, \mathrm{E}\}$, specific to country (cty), truck class (tc), commodity type (nst), and the weekly distance ($\mathrm{d_{week}}$).
- The maximum payload ($\mathrm{m_{PL,max}}$ – Equation *A.4*) is sampled using probability distribution $\mathrm{D_{mpl}} \in \{\Gamma, \mathrm{B}, \mathrm{E}\}$, specific to country (cty) and truck class (tc). Additionally, country-specific GVW limits are considered.
- Trip types are selected using probability distribution $\mathrm{D_{tt}} \in \{\Gamma, \mathrm{B}, \mathrm{E}\}$ among three generic types (single-stop, multi-stop, and collection/delivery runs), specific to country (cty), commodity type (nst), the weekly operation type (ops), and the number of trips ($\mathrm{n_{trips}}$). This yields a list of trip types $\left\{\mathrm{type_{trip},}_i\right\}_{i=1}^{\mathrm{n_{trips}}}$ for all weekly trips. This selection process is described in Equation (*A.5*). The allocation of trip lengths and trip types is random, with empty trips assumed to be single-stop trips.
- The number of subtrips per trip is sampled using probability distribution $\mathrm{D_{sub}} \in \{\Gamma, \mathrm{B}, \mathrm{E}\}$, specific to country (cty), truck class (tc), and commodity type (nst). This sampling process is described in Equation (*A.6*). This yields a list of subtrips $\left\{\mathrm{n_{subtrip},}_i\right\}_{i=1}^{\mathrm{n_{trips}}}$ for all weekly trips. Note that single-stop trips have no subtrips (by definition).
- The number of loaded trips ($\mathrm{n_{loaded}}$ – Equation *A.7*) is sampled using probability distribution $\mathrm{D_{load}} \in \{\Gamma, \mathrm{B}, \mathrm{E}\}$, specific to country (cty), commodity type (nst), and the number of trips ($\mathrm{n_{trips}}$). The number of empty trips ($\mathrm{n_{empty}}$) follows from the total number of weekly trips minus the number of loaded trips.
- The cargo load per trip is sampled using probability distribution $\mathrm{D_{cargo}} \in \{\Gamma, \mathrm{B}, \mathrm{E}\}$, specific to country (cty), truck class (tc), commodity type (nst), and the specified maximum payload ($\mathrm{m_{PL,max}}$). Specifically, the relative payload is sampled and then multiplied by the maximum payload. This sampling process is described in Equation (*A.8*) and yields a list of payloads $\left\{\mathrm{m_{tripPL},}_i\right\}_{i=1}^{\mathrm{n_{trips}}}$ among all weekly trips. Empty trips have no payload.

Allocator: Matching trip lengths and payload information

The combinatorial problem of finding the best allocation of trip lengths $\left\{\mathrm{d_{trip},}_i\right\}_{i=1}^{\mathrm{n_{trips}}}$ and payloads $\left\{\mathrm{m_{tripPL},}_i\right\}_{i=1}^{\mathrm{n_{trips}}}$ to match the target transport performance ($\widehat{M}_{TKM}$) is formalized as an optimization problem. Each trip out of the total number of weekly trips ($\mathrm{n_{trips}}$) must be paired

with exactly one payload and vice versa, while the objective function minimizes the absolute deviation between the achievable (sum product of trip lengths and payloads) and the target transport performance. Equation (*4.10*) describes the problem:

$$\text{Minimize} \left| \sum_{i=1}^{n_{trips}} \sum_{j=1}^{n_{trips}} x_{ij} * \left(d_{trip,i} * m_{tripPL,j}\right) - \widehat{M}_{TKM} \right|$$

$$\text{s.t.} \quad \sum_{i=1}^{n_{trips}} x_{ij} = 1, \forall i \in \{1, \dots, n_{trips}\} \tag{4.10}$$

$$\sum_{j=1}^{n_{trips}} x_{ij} = 1, \forall j \in \{1, \dots, n_{trips}\}$$

$$x_{ij} \in \{0,1\}, \forall i, j \in \{1, \dots, n_{trips}\}$$

While this formulation could be solved as an integer programming problem, its efficient solvability decreases strongly with a larger number of trips. Thus, a heuristic is applied that tests up to N=500 random combinations of trip lengths and payloads, as well as the minimum and maximum combinations by sorting the payloads and trip lengths accordingly.

Interim summary

The *Weekly Module* generates the total weekly distance, which is distributed across a corresponding number of trips with individual trip lengths. Furthermore, it is determined which vehicle combination the truck is moving in (= truck class), and which goods (= commodity type) are transported in which regional coverage (= operation type). Each trip is characterized by its payload, from empty to an allocated cargo weight, and by its type (single-stop or multi-stop). The corresponding number of subtrips is available for loaded trips with more than one stop.

4.1.3 Daily Module

The *Daily Module* uses Bayesian Network logic and conditional probability distributions, and the main data source is $data_{Tour}$. Resulting schedules reflect all minute-by-minute operations of the truck within a single week. This involves driving times, taking breaks or rest periods, time spent at customer locations during intermediate stops, loading and unloading of cargo, idling between tours, or inactivity between consecutive days. A schedule is valid only if all trips start and end within the same week. Otherwise, the *Weekly Module* will repeat until a valid one is created.

Model structure

The *Daily Module* takes the generated list of weekly trips and tries to allocate trips to days, adds timestamp information using respective probability distributions (depending on daily mileage) and finally creates a time-based schedule by concatenating the individual trips based on durations, timestamps, and a common trip logic. **Figure 20** visualizes this model structure.

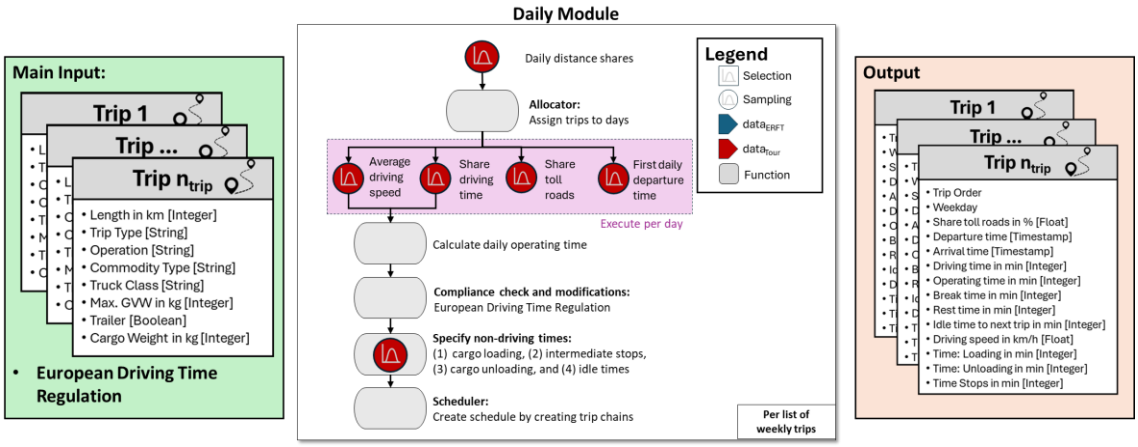

Figure 20: Daily Module: Submodel structure

The common trip logic and resulting trip chains are schematically illustrated in **Figure 21**. Trips start with loading processes (t_{load}) at the defined departure time (t_{DEP}). After that, the truck takes off and the driving time (t_{drive}) starts. Intermediate stops with the respective durations (t_{stop}) may split the total driving time for multi-stop trips. A 45-minute break after 4.5 hours (t_{break}) and a 10-hour break after 9 hours of driving (t_{rest}) may further divide the total driving time to comply with the European Driving Time Regulation. Each trip ends with unloading (t_{unload}) at the destination or depot, which then defines the arrival time (t_{ARR}). The total operating time per trip (t_{tot}) is defined as the sum of all individual times or difference between the arrival time and departure time, respectively. A consecutive trip starts after a possible idle time (t_{idle}), which then defines the departure time of the consecutive trip. The first trip of a new day starts either at its defined departure time, which then results in a nightly idle time, or after a short idle time after the previous trip finished, depending on the concatenated timestamps and trips potentially lasting more than one day (due to break and rest periods).

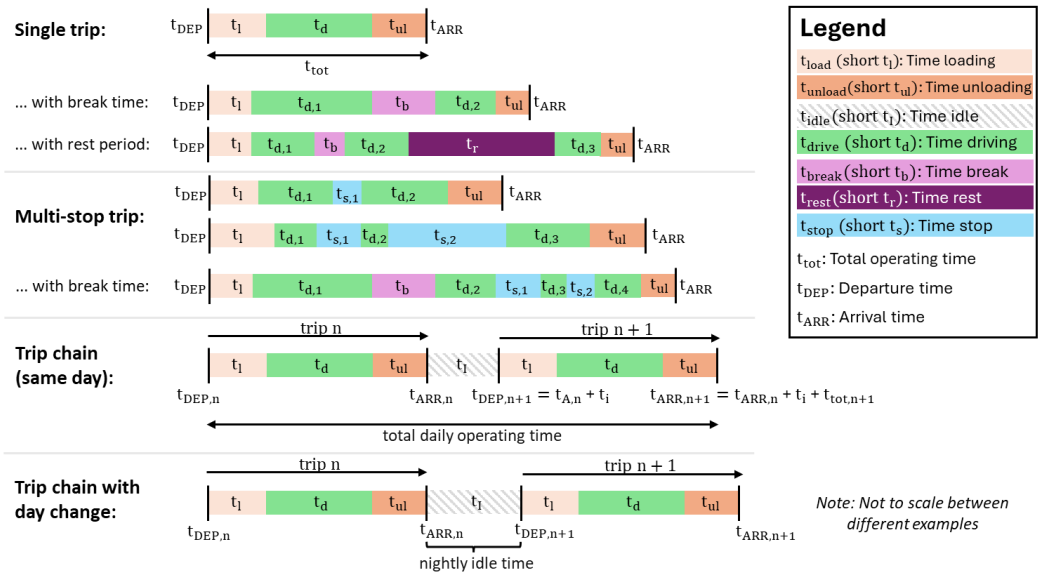

Figure 21: Daily Module: Trip logic

Example 1: Daily distance shares and allocating trips to days

Trips are matched to days via two steps, starting with iteratively sampling target distances per day and then using binsort logic. This procedure is schematically illustrated in **Figure 22**. The pseudo-code for this logic is provided in the Appendix (Equation *A.9*).

First, the algorithm generates daily shares ($s_{\mathrm{day},i}$) via a distribution $D_{\mathrm{dd}} \in \{\Gamma, B, E\}$ specific to the total weekly distance d_{week} until the full weekly distance is distributed among a maximum of seven days (Monday to Sunday). **Figure S12** visualizes the relationship among the weekly distance and single distances per day for two aggregation steps, with the min-max range defined by the 99$^{\mathrm{th}}$ percentile and functions fitted via linear or log-log regression. Accordingly, sampled daily shares likely concentrate on five to six working days. If less than seven days are needed, the remainder of the week is padded with zeros. The normalized shares are then multiplied by the total weekly distance to obtain a daily target distance ($\hat{d}_{\mathrm{day}}$) for each day. An additional rearrangement of these shares ensures that larger distances are rather allocated to the beginning of the week and smaller distances toward the end of the week. This logic aims to maximize transport intensity on weekdays and avoids excessive driving on weekends, with generally lower business activity and partial driving bans. This yields a sorted list of daily target distances $\{\hat{d}_{\mathrm{day},i}\}_{i=1}^{7}$.

Second, the algorithm allocates the given list of trips $\{d_{\mathrm{trip},i}\}_{i=1}^{n_{\mathrm{trips}}}$ to different days based on these target distances. The binsort logic minimizes the excess distance for each day relative to its specified target, prioritizes days with the largest remaining distance, and prefers earlier weekdays versus later ones. Days with a target distance of zero are excluded from the allocation. This involves sorting the set of weekly trips in descending order and distributing the unladen trips first and then all laden trips, which promotes fair distributions of laden and unladen trips. Per day, the generated set of daily trips is then shuffled to randomize the trip order, subject to the additional constraint that laden and unladen trips alternate wherever possible. Thus, the final mileage per day $\{d_{\mathrm{day},i}\}_{i=1}^{7}$ depends on the trip structure (number and individual lengths) and follows from the sum of all trip distances per day. Accordingly, some days may have a target distance, but no trips are assigned to them.

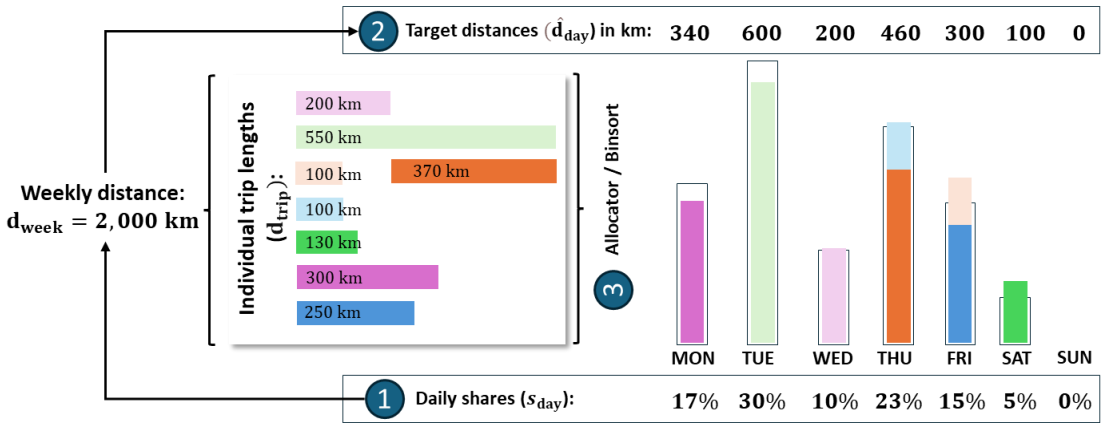

Figure 22: Daily Module: Trip to day allocation

Example 2: Daily parameters depending on the daily mileage

The following daily parameters are determined in dependence to the daily mileage using the respective conditional probability distribution. Per day (i), this concerns the average driving speed (v_i), the ratio between the driving time and the total operating time ($r_{driving,i}$), the share of daily driving on toll roads ($z_{tollRoad,i}$), and the first daily departure time ($t_{DEP,i}$). The relationship between the daily mileage and the corresponding parameter follows from $data_{Tour}$, with daily distances transformed to a categorical variable via a respective binning function (f_{bin}). The respective generic equations are provided in the Appendix (Equation *A.10*).

For example, **Figure 23** visualizes the relationship among daily mileage to the average speed as a density plot with four distance bins. The positive correlation seems logical, with a wide range of possible speeds at low daily mileages and a narrowing range with increasing mileage towards 60-90 km/h. Note that the official maximum speed for trucks in Europe is generally 80 km/h, with country-specific derogations.

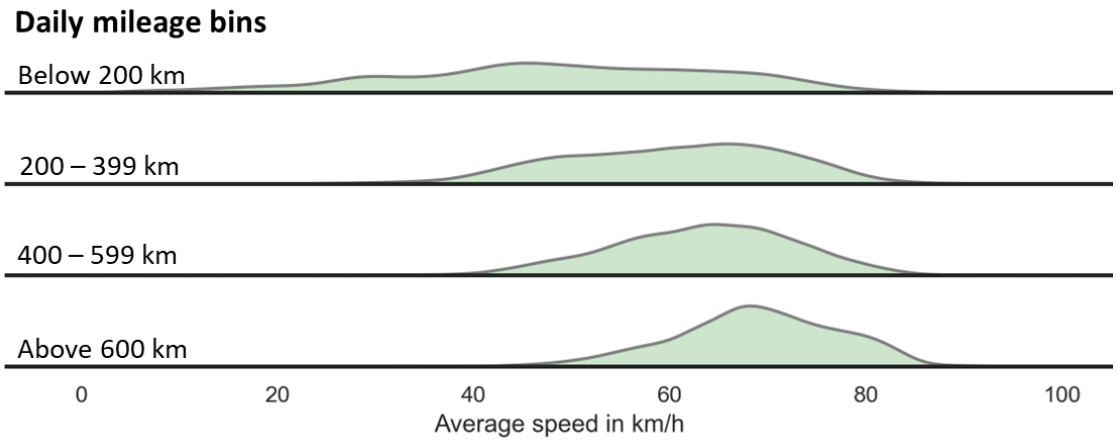

Figure 23: Daily Module: Daily distance versus average driving speed

Further visualizations for these daily parameters are provided in the Appendix, all showing the causal dependence on the daily mileage and corresponding feasible (and mostly narrowing) parameter ranges, which motivates the implementation. Specifically, this involves **Figure S13** (average speed), **Figure S14** (ratio of driving to operating time), **Figure S15** (first daily departure time), and **Figure S16** (share of daily driving on toll roads). These visualizations show the respective data distributions, the min-max range defined by the 99th percentile, and respective functions fitted via regression.

Timestamp calculations and compliance check

Concerning driving times, the total daily driving time ($t_{drive,day}$) follows from the daily mileage and the average daily driving speed. Likewise, the driving time per trip ($t_{drive,trip}$) follows from the trip-specific mileage and the average daily driving speed.

To ensure compliance with the European driving time regulation, excessive driving times per trip are split. This particularly involves daily rest periods of 10 h after 9 h of driving and driving breaks of 45 min after 4.5 h of driving, which might cause trips to last more than one day. While one-driver operations are the default, two-driver operations are enabled if required to complete this trip within one week without exceeding the allowed weekly driving time per driver. The total break time per trip ($t_{break,trip}$) follows from adding up all breaks and rest periods.

Concerning operating times, the total operating time per trip ($t_{tot,trip}$) follows either from the ratio of driving time to operating time and the respective driving time per trip, or the trip-specific driving time plus the trip-specific total break time plus 30 min. Typically, the higher the mileage is, the higher the share of driving time on the total time (compare **Figure S14**). The total operating time per day ($t_{tot,day}$) follows from adding up the operating times per trip.

The remaining time per trip ($t_{others,trip}$), generally defined as the difference of $t_{drive,trip}$ plus $t_{break,trip}$ and $t_{tot,trip}$, accounts for the time that is spent with four non-driving operations: loading ($t_{load,trip}$), unloading ($t_{unload,trip}$), customer stops ($t_{stop,trip}$), and idling before the next trips starts ($t_{idle,trip}$). For each process, this involves sampling a time using the respective probability distribution (not conditional – visualized in **Figure S17**). Finally, the sum of these randomly generated times is scaled so that it equals the remaining time.

- *Loading* is assumed to be at least 10 min (also interpretable as a setup time) with peaks in the probability distribution at 30 min and 60 min, and up to around two hours.
- *Unloading* is assumed to be at least 5 min (also interpretable as a shutdown time) with a plateau the probability distribution at around 10-25 min, and up to around one hour.
- *Customer stops* are assumed to be at least 5 min with peaks in the probability distribution at 15 min and 35 min. For multi-stop trips, the total driving time is randomly split and distributed among all stops. Likewise, the total time for stops at the customer's premises is randomly allocated, as no information on individual stop lengths was available.
- *Idling* before the next trips starts is assumed to be at least 15 min (peak in the probability distribution) but might take up to around three hours.

Interim summary

The *Daily Module* allocates trips to days throughout the week, generates timestamps for trip-related processes, and creates a temporal operational schedule across one week by concatenating all trips based on their timestamps.

4.1.4 Regionalization

The last module adds the origin and destination information per trip based on the most likely choice (maximum likelihood). This module is configured as post-processing since the total schedule (i.e., the sequence of all trips) is required. Respective probabilities involve the attractiveness of NUTS-2 regions per country (truck and cargo intensity), observed trip distances between any NUTS-2 OD tuple, and – if feasible – the defined weekly operation type (ops) to further restrict potential OD combinations.

The module differentiates between the origin of the first tour (no predecessor) and all subsequent OD tuples. The sequence of trips implies that the destination of the preceding trip defines the origin of the next trip.

The first origin, broadly restricted by the defined home country, is localized using a combined probability that involves three pieces of information (see **Figure 24**). First, all trips from $\mathrm{data}_{\mathrm{ERFT}}$ are grouped by their NUTS-2 origin to determine the total transported cargo weight (weighted sum) and the total number of trucks (weighted sum of unique truck IDs), differentiated by country (cty) and commodity type (nst). Both metrics are normalized to determine the commodity-specific importance for each NUTS-2 region within a country, with the importance interpretable as either a truck or cargo intensity. Second, all trip lengths from $\mathrm{data}_{\mathrm{ERFT}}$ are grouped by their NUTS-2 origin and NST-type. This allows to determine the probability that the distance of the first trip $\mathrm{d}_{\mathrm{trip},1}$ belongs to a NUTS-2 region, with the NST-type used as an additional filter. With using the distance of the first trip, the home country information, and the NST-type, the first NUTS-2 origin follows from multiplying the truck intensity, the cargo intensity, and the calculated probability for all NUTS-2 regions in the home country and selecting the most likely option. Note that the respective product must be normalized per country (sum up to 1).

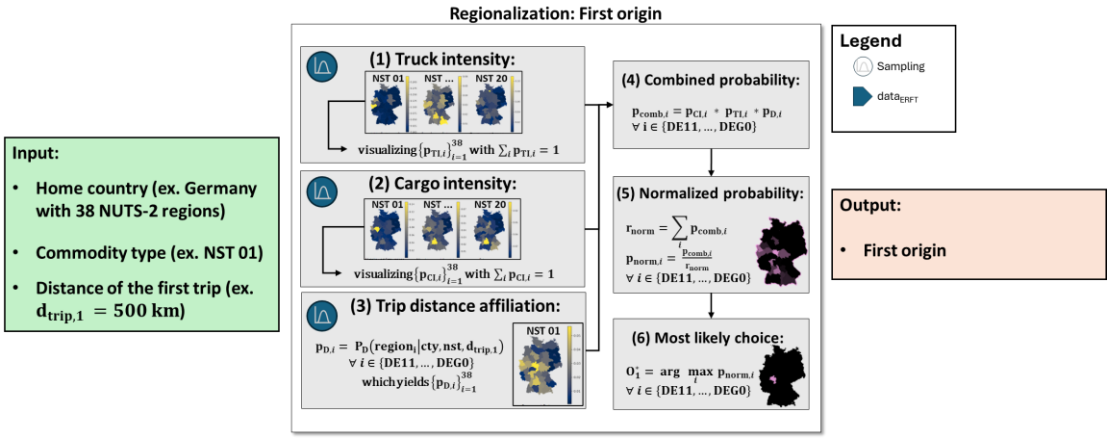

Figure 24: Regionalization: First trip origin

All destinations are localized via a combined probability that involves three level of information, similar to the previous logic. First, this involves the NST-specific truck and cargo intensity (see previous paragraph). Second, the probability of any reachable destination from the current NUTS-2 origin is calculated. The initial set of potential destinations is defined by all observed destinations (in $data_{ERFT}$) from the given NUTS-2 origin. This set is further restricted by taking the minimum and maximum observed trip distances between OD tuples as a reference. Accordingly, a destination is only reachable if the respective trip distance is between the minimum and maximum values. This set of reachable destinations is filtered with the defined weekly operation type, which results in a set of reachable-scheduled destinations. Specifically, local operations require that the start and destination have the same NUTS-2 region. Regional operations require the same NUTS-1 region. National operations require the same NUTS-0 region, which is equal to all operation occuring in the home country. International operations mean that current origin and/or next destination are outside the home country. For this set of reachable-scheduled destinations, the probability that the respective trip length belongs to this OD tuple is calculated. If no destination remains after the weekly operation filter, it is gradually expanded from limited (local) to unlimited (international) until there are remaining destinations. If no destination remains after the minimum/maximum filter (typically for very small trips), local operations are assumed. In both cases, the determined operation type in the weekly schedule is adjusted accordingly. Among all options (=potential destinations), these three values are multiplied, then normalized among the options and then the most likely NUTS-2 destination is selected.

To summarize, the applied probability-based regionalization considers both the importance of individual regions within a country in terms of trucks and cargo activity and ensures the practical feasibility of selected OD chains.

4.1.5 Summary

The previous chapter introduced a novel methodology to generate synthetic operating schedules using multivariate data sampling techniques and respective probability distributions.

This enables simulating any truck activity over its first user service life, with schedules reflecting all trip-related operations in minute-by-minute resolution. These activities involve driving times, taking breaks or rest periods at extended trips, time spent at customer locations (intermediate stops for microtrips), times for loading and unloading cargo, idling between tours, or inactiveness between consecutive days.

Figure 25 visualizes the operating schedule as an activity diagram for a German long-haul tractor (VECTO-5), which is sold after around 7.5 years and 830,000 km. The annual mileage is predominantly well over 100,000 km, fluctuates up to 150,000 km, and drops in the seventh year to around 80,000 km. In the last half year, the truck still drives around 40,000 km. The different zoom levels indicate the level of detail and reflect the trip logic (compare ***Figure 21***). Operation patterns occasionally show very long trips that require a rest period and frequent use of the 45-minute break. However, these long trips occur (with decreasing frequency) over the entire service life. Most trips have one stop, yet there are multi-stop trips (15%) with predominantly 2-4 intermediate stops. Typically, there are 1-5 consecutive trips per day, which occasionally reduce nightly inactivity.

This novel methodology is applied and tested for a sample of 15 European countries and N=18,954 trucks. The total simulated mileage equals around 10.21 billion kilometers (unscaled[1]) and the total average annual mileage equals around 1.86 billion kilometers per year (unscaled[2]). Note that the total annual mileage in Europe ranks at 160-180 billion kilometers per year (compare **Figure S1**). More specifically, this driving performance is distributed among 5.9 million truck weeks[3] and about 77 million individual trips[4], and the trucks are distributed across the following European countries: Austria (AT; N=408), Belgium (BE; N=608), Switzerland (CH; N=404), the Czech Republic (CZ; N=400), Germany (DE; N=4,760), Denmark (DK; N=404), Spain (ES; N=1,802), Finland (FI; N=196), France (FR; N=3,008), Italy (IT; N=1,656), the Netherlands (NL; N=972), Norway (NO; N=972), Poland (PL; N=744), Sweden (SE; N=400), and the UK (UK; N=1,864). Further details on the sample with corresponding visualizations follow in **Section 5.1**.

[1] If the grossing-up factor of $data_{ERFT}$ (mean value per country) is employed, this equals 109.4 billion km.

[2] If the grossing-up factor of $data_{ERFT}$ (mean value per country) is employed, this equals 19.61 billion km per year.

[3] Number of simulated weeks: 5,908,063

[4] Number of simulated trips: 77,420,819

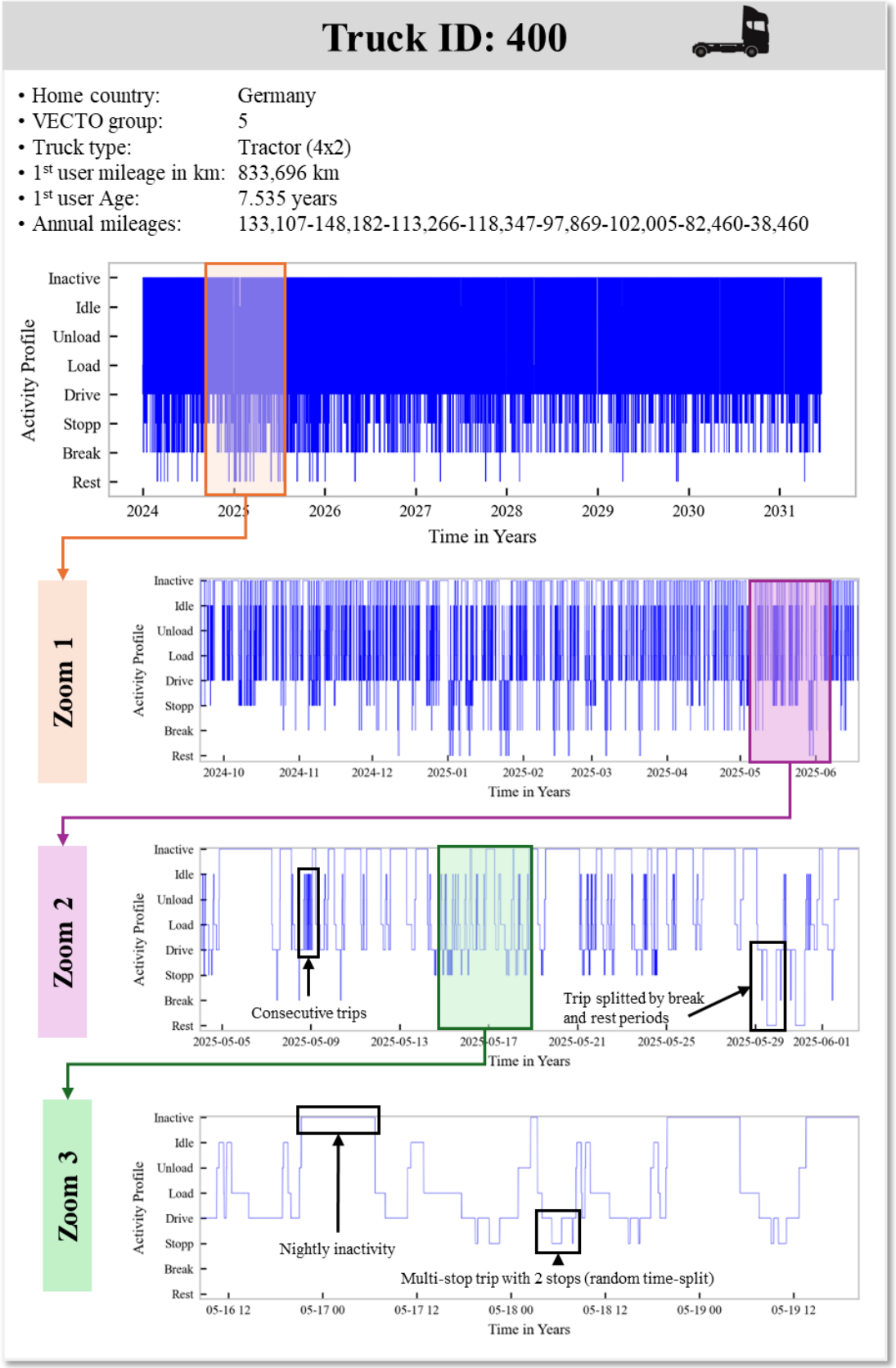

Figure 25: Driving profile simulation: Exemplary operational schedule (activity plot)

4.2 Truck energy simulation

The truck energy simulation consists of four submodules and two steps, differentiates DT and BET powertrains, and determines the energy consumption for each trip in the defined operating schedule. In the first step, the detailed approach considers the defined truck characteristics, regional and seasonal information, truck and payload weight, and trip information (duration, speed, and distance) while employing the VECTO mission profiles as basic truck speed cycles. In the second step, actual energy consumption values per trip are determined via look-up and interpolation from pre-calculated simulation runs to enhance runtime over millions of trips. This two-step approach aims to facilitate a fast yet accurate estimation of energy consumption, incorporating trip-specific variations that affect energy consumption, and enables a consistent and comparable assessment among DTs and BETs.

4.2.1 Longitudinal-dynamics model

The vehicle model simulates the energy consumption using a distance-based longitudinal-dynamics model that is close to the VECTO implementation and a point-mass representation of the truck-trailer combination, which is visualized by **Figure S18**. Thus, lateral forces are neglected, and vertical dynamics are limited to the elevation profile since their influence on truck energy consumption is negligible. The following section extends Teichert et al. (2023) and a list of key parameter values with references is provided in **Table S15**.

The three main VECTO mission profiles, namely urban delivery (UD), regional delivery (RD), and long-haul (LH) are used as reference cycles so that trip dynamics are covered and more accurate modeling (as opposed to just average trip speeds) is enabled. These mission profiles define the target speed, road gradient and duration of stops along a route (100 km) yet exclude braking or acceleration phases, both strongly influenced by drivers and the truck specifications. **Figure S19** visualizes these profiles (speed, road gradient, and elevation profile)[5].

Braking behavior is modeled in the simulation by inserting constant deceleration phases preceding distance segments where a target speed reduction is specified. Equation (*4.11*) describes this procedure, where $\mathrm{v}_{\mathrm{target,k}}$ denotes the modified target speed at a distance step with index k, $\mathrm{v}_{\mathrm{cycle},k}$ is the actual target speed, $\mathrm{k}_{\mathrm{dec}}$ is the distance step index at which the target speed reduction occurs, $\mathrm{a}_{\mathrm{dec}}$ is the deceleration, and $s_k$is the distance along the route.

$$\mathrm{v}_{\mathrm{target},k} = \sqrt{\mathrm{v}^2_{\mathrm{cycle},k=\mathrm{k}_{\mathrm{dec}}} + 2 * \mathrm{a}_{\mathrm{dec}} * (s_{k=\mathrm{k}_{\mathrm{dec}}} - \mathrm{s}_k)} \tag{4.11}$$

[5] The UD cycle is designed to simulate typical urban delivery conditions, including high start-stop frequency and low top speeds, and has an average speed of about 25 km/h. The RD cycle is designed to simulate mixed driving speeds, including frequent stops and starts, and has an average speed of about 60 km/h. The LH cycle is designed to simulate continuous highway driving and has an average speed of about 78 km/h.

Acceleration behavior modeled in the simulation via a forward approach using step index j. The start conditions are given by Equation (*4.12*), where t denotes driving time and v denotes the vehicle speed.

$$\begin{aligned} s_{j=1} &= 0 \\ v_{j=1} &= 0 \\ t_{j=1} &= 0 \end{aligned} \tag{4.12}$$

The model initially evaluates each distance step to determine whether a stop event occurs. If true, an additional data point is added according to Equation (*4.13*), where t_{stop} denotes the stop duration defined by the mission profile and where P_{mot} denotes the applied motor power.

$$\left.\begin{aligned} s_{j+1} &= s_j \\ t_{j+1} &= t_j + t_{stop,k} \\ v_{j+1} &= 0 \\ P_{mot,j} &= 0 \\ j &= j + 1 \end{aligned}\right\} \text{if } t_{stop,k} > 0 \tag{4.13}$$

Driving resistances are calculated via Equation (*4.14*), where m_{Total} denotes the total vehicle mass, g is the gravitational constant, c_{rr} denotes the rolling resistance coefficient, α denotes the road gradient, ρ is the density of air, and A_{Drag} denotes the drag area. This leads to the following representation of the rolling (F_{roll}), aerodynamic (F_{drag}), and gradient resistance (F_{grad}):

$$\begin{aligned} F_{roll,j} &= m_{Total} * g * c_{rr} * \cos(\alpha_k) \\ F_{Drag,j} &= \frac{1}{2} * \rho * A_{Drag,j} * v_j^2 \\ F_{Grad,j} &= m_{Total} * g * \sin(\alpha_k) \end{aligned} \tag{4.14}$$

The following simulation parameters are adjusted to current operating conditions as summarized by Equation (*4.15*). Specific formulas or visualizations are listed in the Appendix.

The quasi-static implementation for c_{rr} (see Equation *A.11*) considers weight differences (such as fully loaded versus empty tours) and the ambient temperature (T_{amb}). This implementation considers that c_{rr} generally increases with higher tire load (increased deformation and larger contact patch areas) and lower temperatures (increased stiffness and higher hysteresis losses).

The quasi-static implementation for ρ (see Equation *A.12*) considers and the ambient temperature (T_{amb}) by accounting for increasing air density at lower temperatures, and thus increasing aerodynamic resistance, via the empirical Magnus formula.

The dynamic implementation for A_{Drag} adopts the speed-dependent VECTO correction formula to account for crosswind influence, which is found to be greater at low speeds and decreases at speeds greater than 60 km/h. The implementation is given by Kies (2018) and **Figure S20** visualizes the respective correction factor (denoted via f_{drag}).

$$\begin{aligned} c_{rr} &= f(m, T_{amb}) \\ \rho &= f(T_{amb}) \\ A_{Drag,j} &= A_{Drag} * f_{drag}(v_{j-1}) \end{aligned} \tag{4.15}$$

The acceleration is calculated using the acceleration required to reach the target speed (a_{target}), the maximum achievable acceleration limited by the motor power (a_{mot}) and an absolute acceleration limit ($a_{acc,max}$) that is set to 1.0 m/s². This procedure is described in Equation (*4.16*), where Δs denotes the distance step length, P_{rated} denotes the rated motor power, η_j denotes the current drivetrain efficiency, J_{wheels} denotes the total inertia of all tires, and r_{dyn} denotes the dynamic tire radius:

$$\begin{aligned} a_{target,j} &= \frac{1}{2 * \Delta s} * (v_{target,k+1}^2 - {v_j}^2) \\ a_{mot,j} &= \frac{1}{m_{Total} + \frac{J_{wheels}}{r_{dyn}^2}} * \left(\frac{P_{rated} * \eta_j}{v_j} - F_{drag,j} - F_{roll,j} - F_{grad,j}\right) \\ a_j &= \min\left(a_{target,j}, a_{mot,j}, a_{acc,driverMax}\right) \end{aligned} \tag{4.16}$$

The drivetrain efficiency (η_j) per simulation step follows from component-specific losses, with individual losses per component modeled as a function of the relative tractive power (λ_{trac}) of the previous simulation step (see Equation *4.17*). The diesel drivetrain efficiency (η_{DDT}) depends on losses by the transmission (subscript TM) and the axle gear plus wheel bearings (subscript AX). The electric drivetrain efficiency (η_{EDT}) further depends on losses by the electric motor and power electronics (subscript EM)[6]. Specifically per component, this 1D-relation to the relative tractive power is pre-calculated from 2D efficiency maps (torque and rotational speed) over the mission profiles, derived other studies or tools, and – if applicable – calibrated with values from FASTSim (Brooker et al. 2015), which is a comparable and fast simulation tool[7].

$$\eta_j = \begin{cases} \eta_{DDT,j} = \eta_{TM,j} * \eta_{AX,j} = f_{TM}\left(\frac{P_{mot,j-1}}{P_{rated}}\right) * f_{AX}\left(\frac{P_{mot,j-1}}{P_{rated}}\right) \\ \eta_{EDT,j} = \eta_{EM,j} * \eta_{TM,j} * \eta_{AX,j} = f_{EM}\left(\left|\frac{P_{mot,j-1}}{P_{rated}}\right|\right) * f_{TM}\left(\left|\frac{P_{mot,j-1}}{P_{rated}}\right|\right) * f_{AX}\left(\left|\frac{P_{mot,j-1}}{P_{rated}}\right|\right) \end{cases} \tag{4.17}$$

Figure 26 visualizes the implemented component-specific efficiency maps in relation to the relative tractive power. The efficiency of the diesel engine (subscript ICE) is introduced in the following paragraph, alongside battery charge and discharge losses (subscript BAT).

[6] Configuration: PMSM with a central e-axle

[7] List of references: EM: Basma et al. (2021a), Wolff et al. (2021), Brooker et al. (2015); Diesel ICE: Brooker et al. (2015), EEA (2024); TM: VECTO (2025), Tansini et al. (2019); AX: VECTO (2025), Tansini et al. (2019).

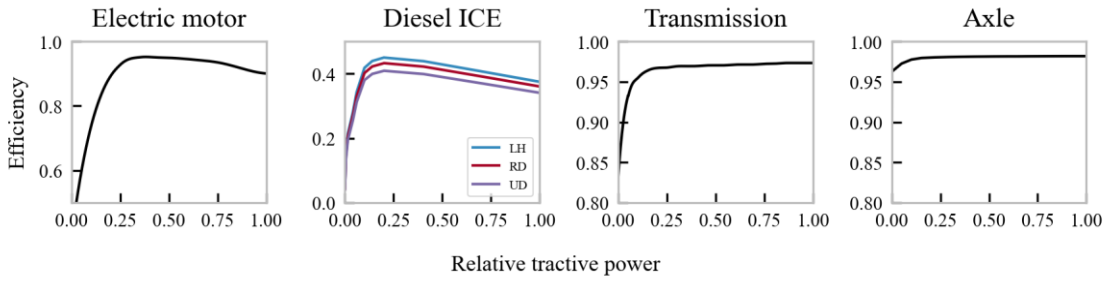

Figure 26: Truck simulation: 1D component efficiency maps

Based on the determined acceleration a_j, the truck status is upated according to Equation (*4.18*). This process is repeated until the mission profile has been completed.

$$
\begin{aligned}
v_{j+1} &= \sqrt{v_j^2 + 2 * a_j * \Delta s} \\
t_{j+1} &= t_j + \frac{2 * \Delta s}{v_j + v_{j+1}} \\
s_{j+1} &= s_j + \Delta s \\
F_{tot,j} &= \left(m_{Total} + \frac{J_{wheels}}{r_{dyn}^2} \right) * a_j + F_{drag,j} + F_{roll,j} + F_{grad,j} \\
P_{mot,j} &= F_{tot,j} * v_j * \eta_j^{-sgn(F_{tot,j})}
\end{aligned}
\tag{4.18}
$$

Diesel truck: Power profile and energy consumption

The actual power profile of DTs (P_{ICE} in Watts) only relies on mechanical braking so that the engine brake (or motoring) is neglected. The average energy consumption per kilometer ($\bar{ec}_{DT}$ in kWh per km) over the VECTO mission profile can then be calculated according to Equation (*4.19*), where η_{ICE} denotes the diesel engine efficiency as a function of the relative tractive power and different VECTO cycles (see **Figure 26**), P_{aux} denotes the auxiliary power (see next subchapter), and n is the number of simulation steps. With using the respective energy density of diesel[8], this energy consumption can also be expressed in liters per km.

$$
\begin{aligned}
P_{ICE,j} &= \max(P_{mot,j}, 0) \; \forall \, j \\
\bar{ec}_{DT} &= \frac{1}{3600 * s_{j=n}} * \left(\sum_{j=1}^{n-1} \frac{(P_{aux} + P_{ICE,j}) * (t_{j+1} - t_j)}{\eta_{ICE,j}} \right) \\
\eta_{ICE,j} &= f_{ICE} \left(\frac{P_{ICE,j-1}}{P_{rated}} \right)
\end{aligned}
\tag{4.19}
$$

[8] energy density: 9.7 kWh per liter

Battery-electric truck: Power profile and energy consumption

The power drawn from or supplied to the battery (P_{BAT} in Watts) is calculated according to Equation (*4.20*), where recuperation is limited to the rated motor power and the remaining power is converted into heat by the mechanical brakes. This procedure is repeated for every step in the driving cycle. The time-integrated power profile is checked and, if more energy is recuperated than consumed, the power supplied to the battery is set to zero.

$$P_{bat,j} = \max\left(P_{mot,j}, -P_{rated}\right) \forall j \tag{4.20}$$

The average energy consumption per kilometer ($\overline{ec}_{BET}$ in kWh per km) over the VECTO mission profile can then be calculated using Equation (*4.21*), where η_{BAT} denotes the dynamic battery charge/discharge efficiency (see *next **Chapter 4.3**),* P_{aux} denotes the auxiliary power (see next subchapter), E_{bat} denotes the total battery capacity, and n is the number of simulation steps.

$$\overline{ec}_{BET} = \frac{1}{3600 * s_{j=n}} * \left(\sum_{j=1}^{n-1} \frac{(P_{aux} + P_{bat,j}) * (t_{j+1} - t_j)}{\eta_{BAT,j}} \right)$$
$$\text{with } \eta_{BAT,j} = f_{BAT}\left(\frac{P_{bat,j}}{E_{bat}}, T_{amb}, SOC_j\right) \tag{4.21}$$

Pre-calculation to obtain trip-specific energy consumption values

Determing the actual energy consumption per trip i of the operating schedule ($ec_{BET,i}$ or $ec_{DT,i}$) involves all trip-specific information and follows from look-up tables and interpolation via pre-calculated simulation runs, summarized via $f_{EC,BET}(v_{av}, m_{Total}, S_{Truck}, T_{amb})$ and $f_{EC,DT}(v_{av}, m_{Total}, S_{Truck}, T_{amb})$. Accordingly, this approach includes the average driving speed (denoted via v_{av}), total vehicle mass (denoted via m_{Total}), the ambient temperature (denoted via T_{amb}) and general truck specifications including trailer presence (denoted via S_{Truck}) as the main factors affecting the energy consumption. Specifically, the simulation runs involve the following variations to determine pre-calculated $\overline{ec}_{BET}$ and $\overline{ec}_{DT}$ values:

- Different truck specifications involve truck type variations (tractors and rigids), different axle configurations (two- and three-axle), and operations with or without trailers. Technical specifications (i.e., P_{rated}, A_{Drag}, c_{rr} and m_{DTCM}) are varied based on $data_{EEA}$.
- Different total vehicle masses follow via payload variations from empty to fully laden, operations with or without trailers and their curb weight, truck curb mass variations (via m_{DTCM}), and battery capacity variations (BETs only).
- Different speed and trip dynamics follow from using the three VECTO mission profiles (UD, RD, LH), further extended by applying variable scaling factors to the defined target speeds to increase coverage of average driving speeds.
- Different ambient temperatures involve varations from -20 to 40°C.

4.2.2 Ambient temperature

The actual ambient temperature of trip i follows from historical monthly temperature profiles (median values) that are defined per NUTS-2 region and using the regionalized operational schedule. For each trip, the temperature of its origin region is assigned. This approach, however, neglects daily temperature fluctuations and changes towards the destination region.

The historical temperature data is derived from ECA&D (2024), which contains daily temperature profiles for several thousand stations that are spread across Europe. The temperature profiles are aggregated per NUTS-2 region and month by calculating the respective median value. If no temperature information is available for a NUTS-2 region, the national temperature is used.

For example, **Figure 27** visualizes such monthly temperature profiles for selected countries (N=12) and their respective NUTS-2 regions (N=185). Country-specific patterns and peak temperature variations may be more pronounced depending on the country's characteristics (i.e., geographical location, topography, and size).

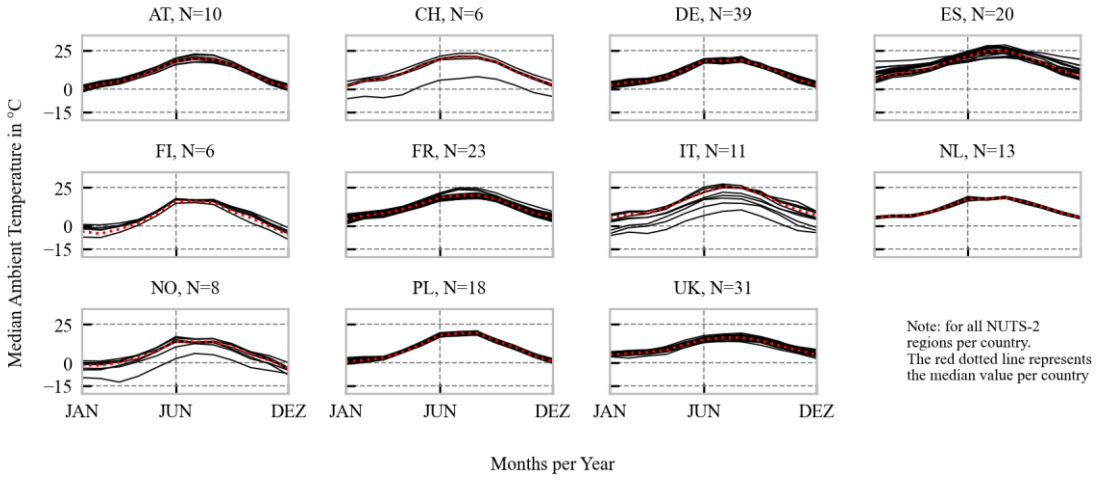

Figure 27: Truck simulation: Monthly temperature profiles per country

4.2.2 Total vehicle mass

For DTs, the total vehicle mass of DTs ($m_{Total,DT}$) follows from the chassis curb mass of the truck in read-to-drive configuration (m_{DTCM} from $data_{EEA}$), which includes a driver`s weight (75 kg) and diesel fuel (500 L), and the specified payload weight ($m_{payload}$). An additional body weight must be added to the chassis curb mass of rigid trucks. Additionally, the weight of the trailer (rigids) or semi-trailer (tractors), denoted as $m_{trailer}$, must be included. Thus, the total vehicle mass is calculated according to Equation (*4.22*):

$$m_{Total} = m_{truck} + m_{payload} + m_{trailer} \quad (4.22)$$

For BETs, the total vehicle mass ($m_{Total,BET}$) follows by assuming a conversion design of DTs to BETs and allowing an additional GVW bonus of two tons (see **Subchapter 2.1**). Accordingly, the truck weight is calculated via the chassis curb mass of the DT couterpart, minus the weight of the DT powertrain components and fuel (denoted as m_{DPT}) plus the weight of the e-axle[9] (m_{eAx}) and battery (m_{bat}), where m_{DPT} uses the power-to-weight ratio of the engine (3.3 kg/kW) and the energy density of diesel (0.846 kg/l). Thus, the total vehicle mass is calculated according to Equation (*4.23*):

$$\begin{aligned} m_{Total,BET} &= m_{BET} + m_{payload} + m_{trailer} \\ m_{BET} &= m_{DTCM} - m_{DPT} + m_{eAx} + m_{bat} \\ m_{DPT} &= P_{rated} * 3.3 + V_{diesel} * 0.846 \end{aligned} \tag{4.23}$$

4.2.3 Auxiliary power demand

The total auxiliary power demand (P_{aux}), which is assumed to be constant over the mission profile, consists of one general element and two temperature-affected elements that differentiate between BETs and DTs.

First, P_B denotes the power demand by general electrical consumers (onboard electronics, exterior lighting, and cabin interior) and add-on units such as steering and pneumatics. This power requirement is assumed to be constant and independent of the powertrain at 1,800 W (Heidt et al. 2019; Tansini et al. 2019; Zhao et al. 2013).

Second, P_{HVAC} denotes the electrical power demand by the HVAC (Heating, Ventilation and Air Conditioning) system of the driver cabin, which depends on the ambient temperature (T_{amb}) and average driving speed over the mission profile (v_{av}). This involves calculating the electrical power to cool/heat the cabin to a comfortable temperature in relation to speed-dependent losses. The details are described in the Appendix (see Equation *A.13*). To summarize, the implementation builds on Magnino et al. (2024), who reported that heat losses (expressed as heat transfer coefficients multiplied by the cabin areas) increase with higher speeds, with lower values for day cabins (50-155 W/K) than for sleeper cabins (65-201 W/K). The implementation assumes a modern HVAC design with heat pumps and electric resistance heater – following Steinstraeter et al. (2022) and Yang et al. (2022) – and identical components in BETs and DTs. However, a certain proportion of waste heat utilization by DTs is accounted, which results in reduced heating power. Using respective temperature-dependent COP (Coefficient of Performance) values for cooling ($COP_{HVAC,C}$) and heating ($COP_{HVAC,H}$), the required heating/cooling energy is translated into an electrical power.

[9] Typical weight estimates range at 450-800 kg (Mareev et al. 2018; Wolff et al. 2021).

Figure 28 visualizes the HVAC power demand as 2D heatmaps for different cabin types and DTs versus BETs, with varying the average driving speed and ambient temperature. The effect of the waste heat recovery for DTs is visible as well as higher energy requirements for heating than cooling, typically caused by lower COP values. As a reference, the electrical power at 25°C (standard temperature) is 230-280 Watts, which equals the VECTO default (VECTO 2025).

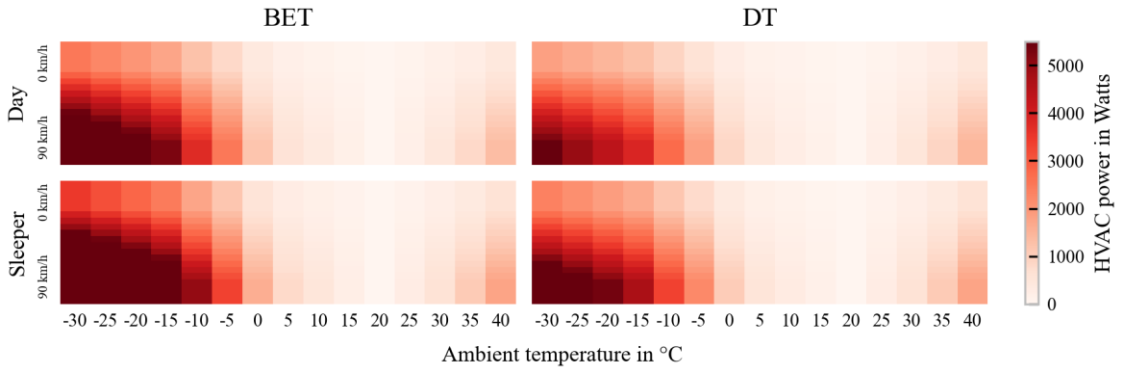

Figure 28: Truck simulation: HVAC power demand

Third, P_{BTMS} denotes the electrical power demand of the battery thermal management system (BTMS) to cool/heat the battery subject to the ambient temperature (T_{amb}) and battery capacity (E_{bat}). The details are described in the Appendix (Equations *A.14-A.16*). To summarize, the implementation calculates the maximum electrical power of the BTMS in relation to the battery size and then uses a non-linear temperature dependence to translate this maximum electrical power to an average electrical power over the whole trip. This temperature dependence is adopted from Tol et al. (2022). **Figure 29** visualizes the average electrical power demand of the BTMS for different battery sizes as a function of the ambient temperature. The effect of larger batteries and lower temperatures, which lead to higher power requirements, is noticeable, as is a plateau with no power demand at around 10-20°C.

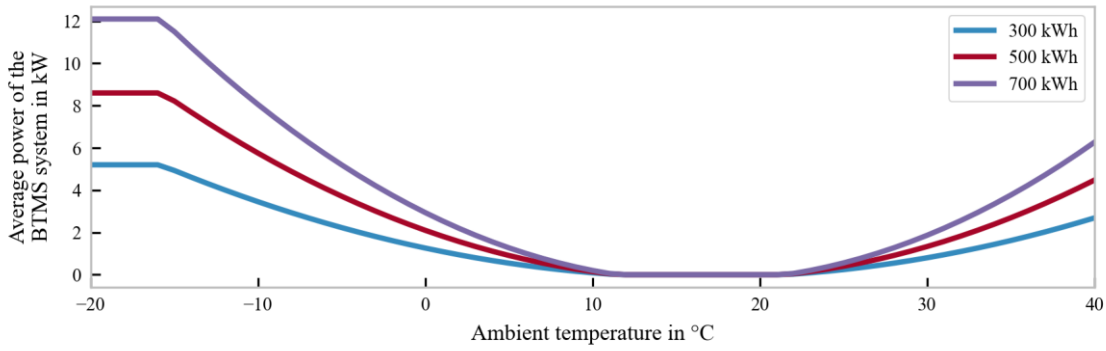

Figure 29: Truck simulation: Average BTMS power demand

To summarize, the total auxiliary power demand of either DTs ($P_{aux,DT}$) or BETs ($P_{aux,BET}$) follows from Equation (*4.24*), comprising the electrical power of general electrical consumers (BET and

DT), the HVAC system (BET and DT), and the BTMS system (BETs only), where T_{amb} denotes the ambient temperature, v_{av} denotes the average driving speed over the mission profile, and E_{bat} denotes the battery capacity:

$$\begin{gathered} P_{aux,DT} = P_B + P_{HVAC,DT} \\ \text{with } P_{HVAC,DT} = f_{HVAC,DT}(T_{amb}, v_{av}) \\ P_{aux,BET} = P_B + P_{HVAC,BET} + P_{BTMS} \\ \text{with } P_{HVAC,BET} = f_{HVAC,BET}(T_{amb}, v_{av}) \\ \text{and } P_{BTMS} = f_{BTMS}(T_{amb}, E_{bat}) \end{gathered} \tag{4.24}$$

4.2.4 Validation for diesel trucks

To validate the implementation and check plausibility for DTs, simulated energy consumption values are compared versus the reported VECTO fuel consumption values by the manufacturers (see $data_{EEA}$). Simulated BET consumption values are discussed at the end of the next subchapter.

Table S16 summarizes the comparisons for different mission profiles (UD, RD, LH, CO) to test the sensitivity toward speed and trip dynamics, for different payload weights to test the sensitivity toward mass and payload, and for different VECTO groups to test the sensitivity toward truck types (rigid vs. tractor and axle configuration). Using Monte-Carlo simulation (N=500) per setting, the simulation is executed with VECTO standard conditions (T_{amb}=25°C) and technical truck characteristics (P_{rated}, A_{Drag}, c_{rr} , and m_{DTCM}) are varied simultaneously using respective PERT distributions[10] (see parameter ranges in **Figure 10**). The variable ratio of cabin types (day or sleeper cabin) follows also from $data_{EEA}$. The stated values represent the mean value and the standard deviation. The comparison indicates that tendencies and effect strenghts obtained by varying the mission profiles, payload weights, and VECTO groups correspond to the reported values, and simulated values are highly consistent with usual deviations below 5%. The largest deviations are observable for the UD cycle, probably caused by the static efficiency maps without transient/dynamic effects.

4.3 Battery simulation

The battery simulation consists of three submodules that implement the battery`s charge/discharge efficiency as an additional element to the truck energy simulation, size the battery and include aging effects, and install the battery within the available chassis space.

[10] The PERT distribution is a special case of the beta distribution, widely used in risk analysis to represent the uncertainty of individual values, and initiated by a minimum, maximum and most likely (here: mean) value.

4.3.1 Electrical model

The electrical model simulates the charge/discharge efficiency of a battery via a R_{int} model, where the internal resistance depends on the temperature and SOC level. As described in Equation (*4.25*), this efficiency is calculated by expressing the open circuit voltage (U_{ocv}) by the nominal cell voltage (U_{nom}) and using the internal resistance measured for a certain temperature (20°C), SOC level (50%) and pulse duration (1s), denoted as $R_{ref,0}$. The average cell current is expressed via the cell capacity (Q_{cell}) and the respective C-rate that follows from the power drawn or supplied to the battery (P_{bat}) and the total battery capacity (E_{bat}):

$$\eta_{BAT} = f_{BAT}(P_{bat}, T_{amb}, SOC) = \frac{1}{1 + \frac{R_{ref} * Q_{cell}}{U_{nom}} * \frac{P_{bat}}{E_{bat}}} \qquad (4.25)$$

$$\text{with } R_{ref} = R_{ref,0} * f_{BAT,IR}(T_{amb}, SOC)$$

The values for U_{nom}, $R_{ref,0}$, and Q_{cell} are taken from three recent automotive-grade battery cells with different chemistries and cell formats, as summarized in **Table 8**. The actual internal resistance, denoted as R_{ref}, follows from dependence on the temperature and SoC-level, both derived from the respective sources. Other influencing parameters such as the current intensity and pulse duration are neglected. The details are described in Equation (*A.17*).

Table 8: Battery model: Technical battery characteristics.

Name	Type	U_{nom}	$R_{ref,0}$	Q_{cell}	Source
VW ID.3 (2021)	Pouch NMC	4.2 V	1.857 mΩ	79.06 Ah	Wassiliadis et al. (2022) Günter et al. (2022)
Tesla Model 3 LR (2022)	Prismatic LFP	3.2 V	0.79 mΩ	164.83 Ah	Stock et al. (2023) Rosenberger et al. (2024)
Tesla Model Y (2022)	Cylindrical (4680) NMC	4.25 V	5.5 mΩ	22.41 Ah	Ank et al. (2023)

4.3.2 Battery sizing

The battery sizing algorithm determines the required gross battery size based on the highest amount of energy required (E_{req}), which follows from the operating schedule, and aging-infused oversizing.

First, the highest amount of energy required may be derived per trip, per section of the trip interrupted with stops or break periods, per day, or over the whole operational schedule. Accordingly, this value has a large overlap with the available charging infrastructure and power.

Second, the oversizing accounts for aging-related deterioration of the battery, which might require higher battery capacities to endure over the whole operational schedule without replacement. The model adopts the implementation by Karlsson et al. (2023a), which concentrates on cyclic aging and uses the relationship between the number of possible FECs and the average SOC window (power-law function), with an increasing SOC window reducing the number of feasible cycles and vice versa. The total number of FECs (FEC_{req}) follows from the operating schedule by calculating the total energy throughput via energy consumption and mileage information and by adopting the highest amount of energy required to size the battery. The power-law functions, differentiated for NMC and LFP, are visualized in **Figure 30**.

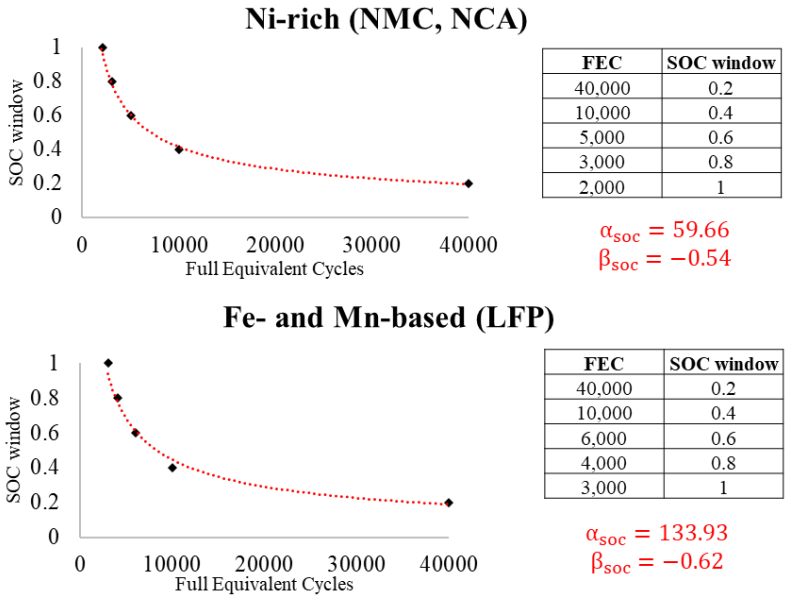

Figure 30: Battery model: Power-law relationship among FEC and SoC

Equation (*4.26*) summarizes the battery sizing, where z_{usable} denotes the share of usable energy (92% - Wassiliadis et al. 2022) to determine the gross capacity, r_{soc} defines the required SOC window, and the power-law function coefficients are denoted as α_{soc} and β_{soc}:

$$E_{bat} = \frac{E_{req}}{z_{usable} * r_{soc}} \quad \text{where } r_{soc} = f_{sizing}(FEC_{req}) = \min(1, \alpha_{soc} * FEC_{req}^{\beta_{soc}}) \tag{4.26}$$

Note that the maximum feasible battery capacity (see next subchapter) limits the installable battery capacity. Thus, the final gross battery capacity must always be equal to or smaller than the maximum feasible battery capacity. If not, the operational schedule cannot be electrified.

4.3.3 Battery packaging

The specified installation space for the battery system follows from the assumed DT-to-BET conversion design, similar to determining truck weights. Accordingly, truck shapes as well as non-powertrain related components and structures such as the driver cabin, chassis, and nondriven axles remain unchanged.

The available installation space is determined by removing all ICE-specific components (engine, diesel tank, transmission, cardan shaft, exhaust and emission control systems) so that large areas under the cabin, outside the chassis between the axles and within the chassis become available. The wide range of truck configurations is simplified by determing this space specific to the truck type (tractor vs. rigid) and number of axles (two, three and four), with the wheelbase as the independent sizing parameter. This builds on the detailed assessment by Bstieler (2021), who developed a package model of a 4×2 diesel tractor with a wheelbase of 3600 mm. The specified installation spaces are then transferred using information of $data_{Datasheet}$. Smaller, irregular areas and the area around the axles are excluded to leave space for the suspension and the e-axle.

Figure 31 visualizes the available installation space for different truck types and axle configurations, which are split into three large areas: V_{cabin} (purple), V_{Tank1} and V_{Tank2} (green), and V_{Frame} (orange).

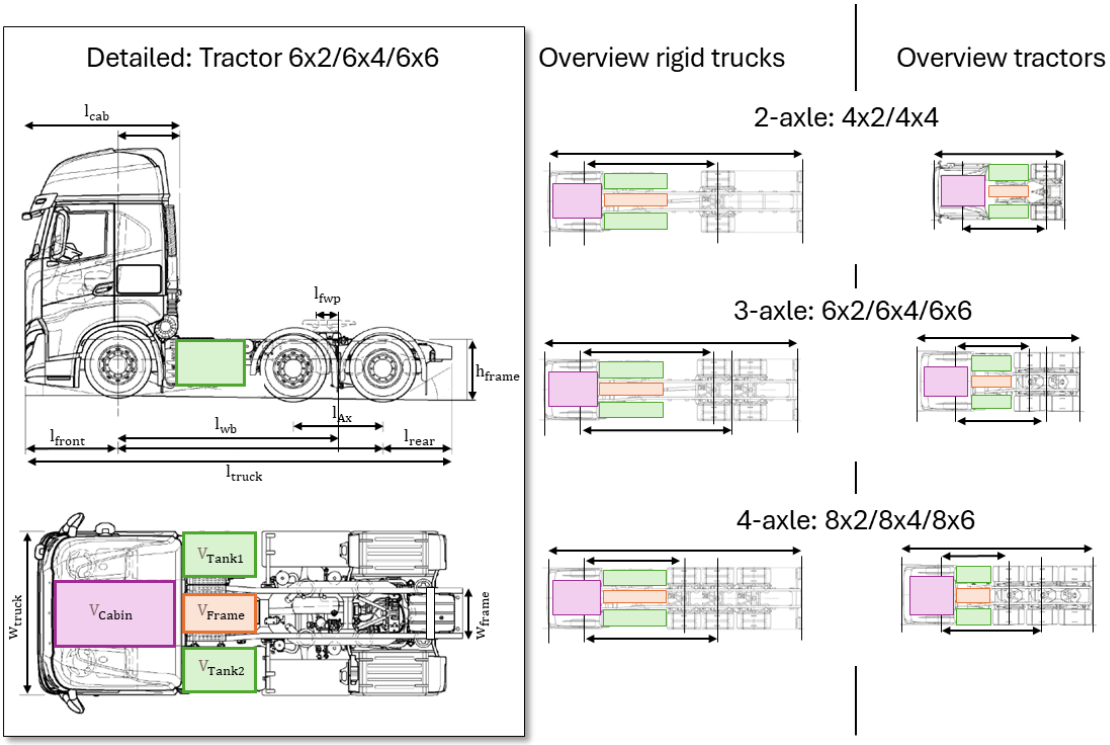

Figure 31: Battery model: Truck packaging model

Equation (*4.27*) quantifies the available installation spaces (in mm³) as functions of the wheelbase ($\mathrm{l_{wb}}$) minus the wheel radius plus housing (r_{wheel}), with dimensions adopted from Bstieler (2021):

$$\begin{aligned} \mathrm{V_{cabin}} &= 1400 * 780 * 920 \\ \mathrm{V_{Tank1}} &= (\mathrm{l_{wb}} - 2 * \mathrm{r_{wheel}}) * 700 * 650 \\ \mathrm{V_{Tank2}} &= (\mathrm{l_{wb}} - 2 * \mathrm{r_{wheel}}) * 700 * 650 \\ \mathrm{V_{Frame}} &= 0.8 * (\mathrm{l_{wb}} - 2 * \mathrm{r_{wheel}}) * 590 * 500 \end{aligned} \tag{4.27}$$

The packaging algorithm uses these four installation spaces to package the battery system while checking the total truck mass, GVW limits including the 2-ton bonus, and compliance with the European axle load limits. This uses the calculated weight distribution of the empty DT chassis (per $\mathrm{data_{Datasheet}}$ minus the weight of all removed ICE components and their mass centroids) and adds the weight of the e-axle weight. This yields a BET weight distribution without the battery system. Next, the algorithm fills the available installation space with batteries, starting with the area under the cabin and moving from the truck front to the rear. The new BET weight distribution and the achievable payload are calculated iteratively by assuming a symmetrical mass centroid of the battery systems and testing different length specifications.

The packaging simulation differentiates truck types (tractor vs. rigid) and axle configurations (denoted as 2A, 3A, and 4A), uses different battery system specifications, and compares the payload capabilities with those of the DT counterpart while varying the DT mass (chassis curb masses and powertrain mass) to account for different truck specifications. Battery specifications involve generic combinations of specific energy (ϵ_{grav} in Wh/kg) and energy density (ϵ_{vol} in Wh/L) for different chemistries, as summarized in **Figure 32** with several reference systems. Eventually, this yields the maximum feasible battery capacity per battery specification as a function of the achievable payload, truck type, and axle configuration.

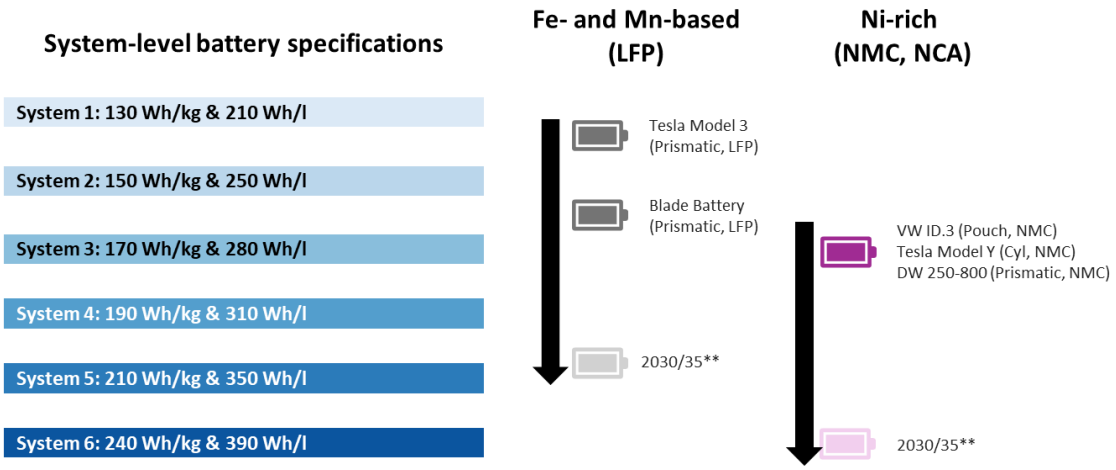

**: Determined from Mauler et al. (2022), Hettesheimer et al. (2022), and Hasselwander et al. (2023)

Figure 32: Battery model: Battery system specifications

4.3.4 Validation for battery-electric trucks

To validate the implementation and check plausibility for BETs, simulated BET energy consumption values are compared versus reported energy consumption values by manufacturers (see **Table 1**) and other studies. For example, BET 4x2 tractors are typically reported with values ranging from 1.1-1.5 kWh/km[11], which corresponds to the simulated values. More specifically, **Figure S22** visualizes the power drawn/supplied to the battery and the corresponding SOC for different VECTO mission profiles to prove the sensitivity toward trip dynamics and recuperation. An extended examination (see **Figure S23**) visualizes various SOC profiles among different battery capacities and ambient temperatures to prove their sensitivity toward battery mass and temperature. **Figure S24** visualizes the average consumption versus the ambient temperatures against different settings (auxiliary power demand and battery cells) via Monte-Carlo simulation (N=500) to prove sensitivity toward varying technical truck characteristics.

4.4 Economic model

For each truck and its specific operational schedule, the profitability of a BET compared to a DT is determined via TCO comparison, following the implementations by Noll et al. (2022) and Teichert et al. (2023). TCO calculation follows a scenario-based scheme by varying individual costs in three variations: *LOW*, *MEDIUM*, and *HIGH*. Equation (*4.28*) summarizes the TCO framework:

$$
\begin{aligned}
\mathrm{TCO} &= \frac{\mathrm{C_{capex}} * \mathrm{CRF} + \sum_{t=1}^{\mathrm{t_{tot}}} \frac{\mathrm{C_{opex},t}}{(1+\mathrm{r})^{t}}}{\mathrm{d_{tot}}} \\
\mathrm{CRF} &= \frac{\mathrm{r} \cdot (1+\mathrm{r})^{\mathrm{t_{tot}}}}{(1+\mathrm{r})^{\mathrm{t_{tot}}} - 1} \\
\mathrm{C_{capex}} &= \mathrm{C_{truck}} - \frac{\mathrm{RV}}{(1+\mathrm{r})^{\mathrm{t_{tot}}}} \\
\mathrm{C_{opex},t} &= \mathrm{C_{toll},t} + \mathrm{C_{energy},t} + \mathrm{C_{ms},t} + \mathrm{C_{in}}\,, \qquad t \in \{1, \dots, \mathrm{t_{tot}}\}
\end{aligned}
\tag{4.28}
$$

where costs per kilometer (in $\mathrm{EUR_{2020}}$ per km) include capital expenditures (CAPEX – denoted as $\mathrm{C_{capex}}$) and annual operational expenditures (OPEX – denoted as $\mathrm{C_{opex}}$) in relation to the total kilometers traveled (denoted as $\mathrm{d_{tot}}$). The latter equals the total mileage of the first user at the end of the ownership (denoted as $\mathrm{t_{tot}}$ in years). CRF denotes the capital recovery factor with an interest rate (denoted as r) to determine the net present value of future cash flows. CAPEX

[11] Sources: Basma et al. (2021a); Volvo Trucks (2022); Mauler et al. (2022); Teichert et al. (2023); Daimler Trucks (2024).

involves the purchase of the truck at the specified retail price (denoted as C_{truck}) and its final resale value (denoted as RV). OPEX involve costs for tolls (C_{toll}), energy (C_{energy}), maintenance and service (C_{ms}), and insurance fees (C_{in}). Insurance fees are assumed to be 3% of the specified retail price (Plötz et al. 2023a). Driver wages are omitted owing to the assumed one-by-one replacement, which results in (almost) identical operational schedules and working hours. Country-specific annual registration taxes are omitted, as these payments are typically limited to a few hundred Euros per truck and year.

4.4.1 Truck purchase costs

The cost-based retail prices for DTs and BETs (see Equation *4.29*) are calculated via specific component costs, a retail price equivalent (RPE) factor and costs for a generic truck chassis. This scheme follows Link et al. (2024c). Accordingly, chassis costs summarize the frame, axles, suspension, wheels, steering, and cabin equipment. The RPE factors adds a broader spectrum of costs beyond component expenditures, such as research and development, marketing and sales, overheads, warranty, and profit margins, typically related to technology maturity (Basma et al. 2021b; Rogozhin et al. 2010).

$$\begin{aligned} C_{truck,DT} &= RPE_{MT} \cdot [c_{chassis} + P_{rated} \cdot (c_{ICE} + c_{EAT})] \\ C_{truck,BET} &= RPE_{ET} \cdot [c_{chassis} + P_{rated} \cdot (c_{EM} + c_{HV}) + E_{Bat} \cdot c_{Bat}] \end{aligned} \quad (4.29)$$

with the following notation and values (defined in **Table S17**) for future cost developments of price-setting ZETs components, centred on batteries and the electric drivetrain, adopted from Link et al. (2024c) , derived via meta-forecasting from more than 200 sources:

RPE_{MT}, RPE_{ET}	RPE factor for mature (MT - 1.27) and emerging (ET - 1.42) technologies
$c_{chassis}$	Truck chassis costs in EUR_{2020}
P_{rated}	Rated motor power in kW
c_{EM}	Electric motor costs in EUR_{2020} per kW
c_{HV}	HV system costs in EUR_{2020} per kW
E_{Bat}	Gross battery capacity in kWh
c_{Bat}	Battery system costs in EUR_{2020} per kWh
c_{ICE}	Diesel ICE system costs in EUR_{2020} per kW
c_{EAT}	Emission aftertreatments costs in EUR_{2020} per kW

Generic truck chassis costs, differentiated by truck type and axle configuration, follow from $data_{Resale}$ via two steps. First, stated DT resale prices were calculated to their original retail prices (new trucks with zero mileage and years) via regression analysis (see next section) and assuming an average rated power (mean value per $data_{EEA}$). Second, truck chassis costs were re-calculated using Equation (*4.29*). The determined chassis costs (mean values across all trucks) are summarized in **Table S18** (rigid trucks) and **Table S19** (tractors).

4.4.2 Residual value

Truck resale values for DTs and BETs (excluding the battery) are calculated via a combined aging formula based on total mileage and truck age, determined for DTs using $data_{Resale}$, and assuming the same relative residual value development for DTs and BETs.

Using the stated prices of new and used DTs from $data_{Resale}$, the regression formula given by Equation (*4.30*) allows to derive an appropriate cost model. This models stated prices (p_{stated}) as a function of the truck age (t_{stated}), truck mileage (d_{stated}), axle configuration (ax), rated motor power (P_{Rated}), and body type, with the respective regression coefficients ($\beta_0, \beta_1, \beta_2, \beta_3, \beta_4, \beta_5$) differentiaed for rigids (subscript ri) and tractors (subscript tr). Axle configuration and body type are implemented as categorical variables. The regression summary and coefficient values are provided in **Table S20**, showing reasonable accuracy ($R^2 \approx 0.75$) for both truck types.

$$p_{stated,ri} = e^{\beta_{ri,0}} * e^{\beta_{ri,1} * t_{stated}} * e^{\beta_{ri,2} * d_{stated}} * e^{\beta_{ri,3} * P_{Rated}} * e^{\beta_{ri,4} * ax} * e^{\beta_{ri,5} * bt}$$
$$p_{stated,tr} = e^{\beta_{tr,0}} * e^{\beta_{tr,1} * t_{stated}} * e^{\beta_{tr,2} * d_{stated}} * e^{\beta_{tr,3} * P_{Rated}} * e^{\beta_{tr,4} * ax} \quad (4.30)$$

The actual resale value (RV) then follows from the relative residual value (denoted as r_{resale}) and the original retail price, as given by Equation (*4.31*). For BETs, the residual value of the battery is added (see next paragraph). Note that relative residual values follow solely from the total mileage and truck age, while the other regression parameters refine the curve.

$$RV_{DT} = C_{truck,DT} * r_{resale}$$
$$RV_{BET} = C_{truck,BET} * r_{resale} + RV_{bat} \quad (4.31)$$
$$r_{resale} = f_{resale}(t_{tot}, d_{tot}) = e^{\beta_{x,1} * t_{tot}} * e^{\beta_{x,2} * d_{tot}} \text{ with } x \in \{tr, ri\}$$

The residual battery value at the end of the ownership is assumed to be proportional to the remaining battery life (z_{SOH}) as given by Equation (*4.32*), where $p_{bat,scr}$ denotes the battery value for second-use applications or scrappage (15% - Burke et al. 2019):

$$RV_{bat} = \left(p_{bat,scr} + \left(1 - p_{bat,scr}\right) * z_{SOH}\right) * E_{Bat} \cdot c_{Bat} \quad (4.32)$$

The remaining battery life depends on either the remaining cycle life or calendar life, as given by Equation (*4.33*), where FEC_{cyc} denotes the certified number of full cycles for an 80% SOC operating window (see **Figure 30**), FEC_{bat} denotes the actual number of full cycles, t_{cal} denotes the certified battery age, and t_{own} denotes the battery age at the end of the ownership. The certified battery age is set at 13 years for Ni-rich chemistries and 15 years for Fe- and Mn-based chemistries (Hesse et al. 2017). A linear relation is assumed for both aging effects during the utilization phase so that exponents $z_{cyc,RV}$ and $z_{cal,RV}$ are set to one.

$$z_{SOH} = \min\left(\left(\frac{FEC_{cyc} - FEC_{bat}}{FEC_{cyc}}\right)^{z_{cyc,RV}}, \left(\frac{t_{cal} - t_{own}}{t_{cal}}\right)^{z_{cal,RV}}\right) \quad (4.33)$$

4.4.3 Maintenance costs

Maintenance and service costs comprise all monetary spending for maintenance, tires, repair and inspections of the truck. These costs are operationalized as specific costs per kilometer (c_{ms}) so that costs per year (t) are calculated via Equation (*4.34*). The costs are assumed to be constant over the service life. However, note that maintenance costs typically increase with rising mileage and expiring maintenance contracts. The scheme differentiates DTs (100%) and BETs (60-85%), since regular oil changes and AdBlue refilling are not applicable, and components are typically considered less maintenance-intensive owing to lower mechanical complexity than DTs. The values, including a summary of the literature, are defined in the Appendix (see **Table S21**).

$$\begin{aligned} C_{ms,DT,t} &= d_{annual,t} * c_{ms,DT}, \quad t \in \{1, \dots, t_{tot}\} \\ C_{ms,BET,t} &= d_{annual,t} * c_{ms,BET}, \quad t \in \{1, \dots, t_{tot}\} \end{aligned} \quad (4.34)$$

4.4.4 Road tolls

Distanced-based tolling is assumed to be adopted in all European countries. An average toll rate is assumed for those countries without present distance-based toll schemes. As introduced in **Subchapter 2.1**, the updated Eurovignette directive requires all member states to harmonize their toll schemes or update concession agreements to include CO_2-based tolling, air pollution charges, and distance-based tolling (at least) on all segments of the TEN-T Core network within the 2020s. **Table S22** summarizes the adopted toll rates for DTs. For BETs, the *MEDIUM* and *HIGH* scenario grant a 50% toll reduction, and the *LOW* scenario grants a 75% reduction, all deduced from the scheme by the Eurovignette directive (Directive (EU) 2022/362).

The actual mileage traveled on toll roads is modeled as a fraction of the total mileage and can be calculated from trip specifc shares, which are defined in the operational schedule. Given the NUTS-2 resolution of trip OD relations that limits knowledge on borders crossed for international trips, the total distance per trip is attributed to the origin country. Thus, annual toll costs are calculated by Equation (*4.35*), where N_t denotes the total number of trips per year (t), d_{trip} denotes the trip distance, r_{toll} denotes the toll road share per trip, and $c_{toll,c,wc}$ denotes the toll rate in the respective origin country (cty) and the respective truck weight class (wc).

$$\begin{aligned} C_{toll,DT,t} &= \sum_{n=1}^{N_t} d_{trip,n} * r_{toll,n} * c_{toll,DT,cty,wc}, \quad t \in \{1, \dots, t_{tot}\} \\ C_{toll,BET,t} &= \sum_{n=1}^{N_t} d_{trip,n} * r_{toll,n} * c_{toll,BET,cty,wc}, \quad t \in \{1, \dots, t_{tot}\} \end{aligned} \quad (4.35)$$

4.4.5 Energy costs

The costs for diesel and charging are calculated via cost-based pricing schemes using country-specific historic baselines, probabilistic modeling, and five-year increments. The probabilistic model uses PERT distributions that are defined by the corresponding minimum, mean, and maximum values. **Figure S25** visualizes historical ranges of differential prices among diesel and electricity, according to the scheme below, to simplify country-specific characterization and comparison. The applied scheme aims to include country-specific differences (such as taxes), keep historical price tendencies, and derive reasonable cost scenarios.

Diesel costs

Diesel costs are calculated via five elements, with only the first being country-specific and the others being standardized across Europe. First, historical prices of conventional diesel are taken from Eurostat and adjusted for inflation (EUR_{2020}) to determine a country-specific minimum, mean and maximum value. These historical prices are available on a weekly basis and cover around 19 years[12]. **Table S23** summarizes different metrices for these historical prices. Second, a standardized European cost index is incorporated to consider future cost trends of conventional diesel. Third, cost developments for synthetic diesel and increasing blend ratios are included, each with its own PERT distribution. Fourth, cost developments for biogenic diesel and increasing blend ratios are included, each with its own PERT distribution. Fifth, a common European CO_2 price[13] is included so that the prices of conventional diesel increase. According to Gnann et al. (2023), this CO_2 price might increase from €25 per ton in 2021, to €115 per ton by 2030, and €300 per ton from 2040 onward. Combining these five elements per five-year increment, at-the-pump diesel costs (including taxes without VAT) are defined as the mixed costs of conventional diesel plus CO_2 price and the index trend, synthetic diesel and biogenic diesel in the corresponding ratio. Linear interpolation is used between these reference years. **Table S24** summarizes the parameters for future diesel cost development.

The corresponding scenario values are determined via a Monte-Carlo simulation (N=500). Per country and per five-year increment, values of the lower quartile (25% quantile) are assigned to the *LOW* scenario, median values are assigned to the *MEDIUM* scenario, and values of the upper quartile (75% quantile) are assigned to the *HIGH* scenario.

Figure 33 visualizes the diesel fuel costs in the *MEDIUM* scenario among all countries, with slightly rising costs to an average of around 1.5 EUR_{2020} per liter by 2030 to approximately 2.0 EUR_{2020} per liter by 2035, and long-term costs of approximately 2.1-2.5 EUR_{2020} per liter among all countries.

[12] Reported values range from 01/03/2005 to 11/18/2024 and accessible via the Weekly Oil Bulletin.

[13] in future effective under the EU Emissions Trading System II (EU ETS 2)

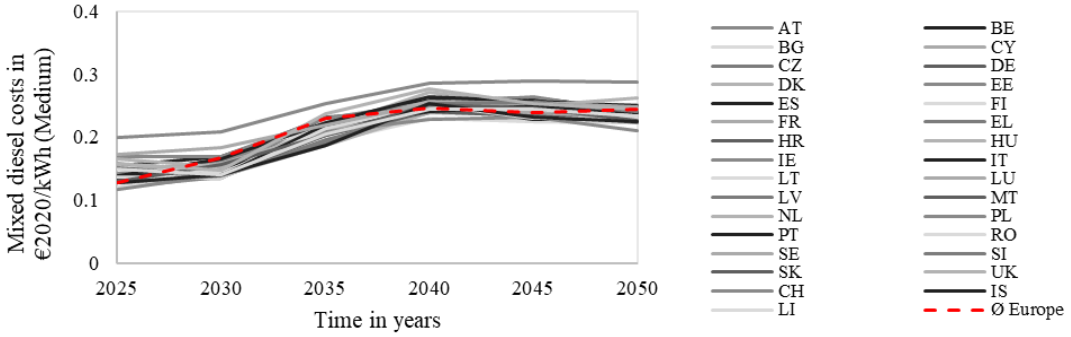

Note: Overlapping color scheme - only to visualize trends and scales.

Figure 33: Cost model: Diesel fuel costs (MEDIUM scenario)

Accordingly, the annual energy costs for DTs are calculated by Equation (*4.36*), where N_t denotes the total number of trips per year (t), d_{trip} denotes the trip distance in km, ec_{DT} denotes the trip-specific energy consumption according to the operating schedule, and c_{diesel} denotes the at-the-pump diesel costs in the corresponding year. It is assumed that DTs always refuel in their home country.

$$C_{energy,t} = \sum_{n=1}^{N_t} d_{trip,n} * ec_{DT,n} * c_{diesel,t}, \qquad t \in \{1, \dots, t_{tot}\} \tag{4.36}$$

Charging costs

Charging costs are calculated following the implementation by Basma et al. (2021b) and Noll et al. (2022) in splitting charging costs into electricity and infrastructure components.

Electricity costs are calculated via three elements, with only the first being country-specific and the others being standardized across Europe. First, historical electricity prices are taken from Eurostat[14] and adjusted for inflation (EUR_{2020}) to determine a country-specific minimum, mean and maximum value. These historical prices are available per half year, covering 2007-2024, and differentiate annual consumption ranges, so-called bands (denoted as IA to IG). These bands incorporate consumption-dependent costs from whole-sales prices to network costs, fees, and taxes that typically lead to lower specific prices for larger electricity consumers. This differentation is used to separate electricity costs for truck owners at their private depots (low consumption) and large CPOs with numerous public charging stations (high total consumption). Additionally, the share of generation and network costs on the total costs is evaluated. Second, a standardized European cost index is incorporated to consider future trends for energy generation and supply, with higher shares of renewable energies likely leading to lower costs. Third, a standardized European cost index is incorporated to consider future trends for increasing network costs and charges due to general electricity grid expansion. Combining these

[14] Available via data code 10.2908/nrg_pc_205_c (Electricity prices components for non-household consumers)

three elements per five-year increment, band-specific electricity costs (including taxes without VATs) then follow from the historical electricity costs and indexed trends for lower generation costs yet higher network costs in the respective share. Linear interpolation is used between these reference years. **Table S25** summarizes the parameters for future electricity cost development.

The corresponding scenario values are determined via a Monte Carlo simulation (N=500) and using the two lowest bands (IA and IB[15]) for the electricity costs of private depots and all bands (IA to IG) for the electricity costs of public charging. Per country and per five-year increment, values of the lower quartile (25% quantile) are assigned to the *LOW* scenario, median values are assigned to the *MEDIUM* scenario, and values of the upper quartile (75% quantile) are assigned to the *HIGH* scenario.

Figure 34 visualizes the electricity costs (denoted as c_{elec}) in the *MEDIUM* scenario among all countries and differentiated by depots and public charging. On average, the modeled difference of electricity costs between depot and public charging is around 0.06 EUR_{2020} per kWh.

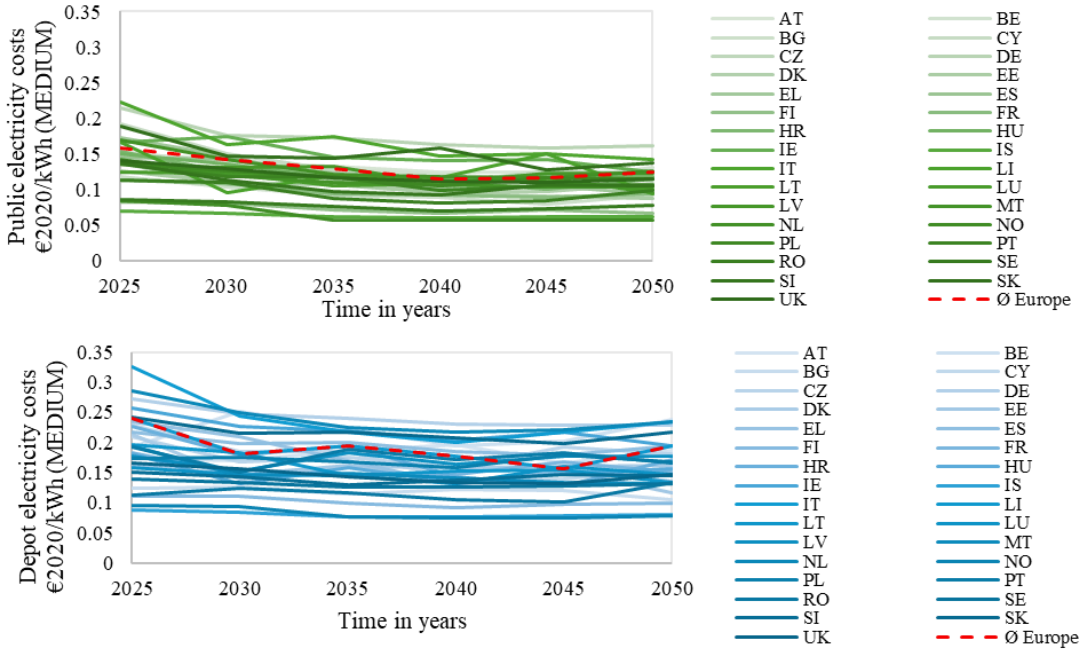

Note: Overlapping color scheme - only to visualize trends and scales.

Figure 34: Cost model: Electricity costs (MEDIUM scenario)

Additional costs for charging infrastructure and local grid expansions are discussed in the next chapter, with additional infrastructure costs for private depots denoted as $c_{infra,depot}$ and $c_{infra,public}$ for public charging stations. Accordingly, final charging costs per year (t) at depots ($c_{charging,depot}$) or public locations ($c_{charging,public}$) are calculated via Equation (*4.37*), where

[15] Annual consumption per Eurostat band: IA below 20 MWh per year and IB 20-500 MWh per year

$c_{elec,depot}$ denotes the final electricity costs for truck owners at their depots, $c_{elec,public}$ denotes the final electricity costs for CPOs at their public charging locations, and p_{cpo} denotes an additional CPO profit margin (10%). The annual costs for public charging are capped at €0.399 per kWh, which corresponds to the current price quoted by Milence for public charging in their basic tariff (Milence 2024).

$$\begin{gathered} c_{charging,depot,t} = c_{elec,depot,t} + c_{infra,depot,t} \\ c_{charging,public,t} = \left(c_{elec,public,t} + c_{infra,public,t}\right) * (1 + p_{cpo}) \\ t \in \{1, \dots, t_{own}\} \end{gathered} \tag{4.37}$$

The annual energy costs for BETs are then calculated by Equation (*4.38*), where N_t denotes the total number of trips per year (t), d_{trip} denotes the trip distance, $ec_{BET,n}$ denotes the trip-specific energy consumption according to the operating schedule, and $c_{charging,mixed}$ denotes mixed charging costs per trip. For the latter, $z_{sc,n}$ denotes the trip-specific ratio of depot-charged vs. public-charged energy to the corresponding costs of the year, with the ratio defined by the operational schedule.

$$\begin{gathered} C_{energy,t} = \sum_{n=1}^{N_t} d_{trip,n} * ec_{BET,n} * c_{charging,mixed,t,n} \\ c_{charging,mixed,t,n} = z_{sc,n} * c_{charging,depot,t} + \left(1 - z_{sc,n}\right) * c_{charging,public,t} \end{gathered} \tag{4.38}$$

4.4.6 Summary

The economic model determines the profitability of a BET compared to a DT for the given operational schedule via TCO, which covers CAPEX and OPEX to purchase and operate the truck. Different cost scenarios are implemented to test sensitivity and robustness, which affect mainly truck purchase costs, tolling scheme, maintenance costs, and energy costs. Toll rates and energy costs are regionalized per country. **Table 9** summarizes the scenarios:

Table 9: Cost model: Overview cost scenarios

Cost parameter	**Details**	**Cost scenario**		
		LOW	**MEDIUM**	**HIGH**
Truck purchase costs	Battery, Diesel engine, Emission aftertreatment, Electric motor, Power Electronics	DT: *LOW* BET: *LOW*	DT: *MEDIUM* BET: *MEDIUM*	DT: *HIGH* BET: *HIGH*
Energy costs (per country)		Diesel: *LOW* Charging: *LOW*	Diesel: *MEDIUM* Charging: *MEDIUM*	Diesel: *HIGH* Charging: *HIGH*
Tolling scheme (per country)		DT: 100% BET: 50%	DT: 100% BET: 75%	DT: 100% BET: 75%
Maintenance costs		DT: *LOW* BET: *LOW*	DT: *MEDIUM* BET: *MEDIUM*	DT: *HIGH* BET: *HIGH*

4.5 Infrastructure model

4.5.1 Charging infrastructure costs

The total costs for charging infrastructure are calculated via cost-based schemes and comprise two components (i.e., infrastructure and electricity grid). Both costs are assumed to represent the European average, so there are no country-specific differences.

The infrastructure costs are calculated based on the levelized cost of charging, which cover CAPEX and OPEX to install and operate the infrastructure in relation to the total energy throughput (Basma et al. 2021b; Noll et al. 2022). Depots are likely to rely mainly on CCS chargers, whereas large public charging stations are likely to have CCS and MCS chargers (see **Subchapter 2.4**). For any location, the number of charging stations in relation to the total energy throughput, and charger utilization heavily affects the final costs per kWh. Following Plötz et al. (2023a), the potential minimum, mean, and maximum costs are determined in five-year increments, all of which assume decreasing equipment costs and increasing utilization with different time delays. This yields respective input values for the PERT distribution to derive depot infrastructure ($c_{\mathrm{charger,depot}}$) and public infrastructure costs ($c_{\mathrm{charger,public}}$) per year ($t$). Further information is provided in **Table S26**.

Additional costs for local grid connection and expansion of substations are added based on Burges et al. (2021), Kippelt et al. (2022), and Plötz et al. (2023a). The potential minimum, mean, and maximum costs differ between private depots and public charging stations. This yields respective input values for the PERT distribution to derive respective grid expansion costs for depots ($c_{\mathrm{grid,depot}}$) and for public charging stations ($c_{\mathrm{grid,public}}$) per year (t). Further information is provided in **Table S27**.

The total infrastructure costs for private depots ($c_{\mathrm{infra,depot}}$) and public charging stations ($c_{\mathrm{infra,public}}$) per year ($t$) are then calculated by Equation (4.39).

$$\begin{aligned} c_{\mathrm{infra,depot},t} &= c_{\mathrm{charger,depot},t} + c_{\mathrm{grid,depot},t}, t \in \{1, \dots, t_{\mathrm{own}}\} \\ c_{\mathrm{infra,public},t} &= c_{\mathrm{charger,public},t} + c_{\mathrm{grid,public},t}, t \in \{1, \dots, t_{\mathrm{own}}\} \end{aligned} \quad (4.39)$$

The corresponding scenario values for $c_{\mathrm{infra,depot}}$ and $c_{\mathrm{infra,public}}$ follow by using a Monte Carlo simulation (N=500) and the respective PERT distributions. Per five-year increment, values of the lower quartile are assigned to the *LOW* scenario, median values are assigned to the *MEDIUM* scenario, and values of the upper quartile are assigned to the *HIGH* scenario.

Final charging costs

Figure 35 visualizes the depot and public charging costs in the medium scenario, indicating that both could settle at similar levels in the long term (see also **Figure S26**). Concerning public charging, average charging costs clearly decrease from around 0.54 EUR_{2020} per kWh by 2025 to

0.36 EUR_{2020} per kWh by 2030, and long-term costs coverge toward 0.20-0.25 EUR_{2020} per kWh. The corresponding price cap (Milence: 39.9 ct/kWh) is effective in many countries throughout the 2020s. Concerning depot charging, average costs show, on average, a minor decrease from around 0.33 EUR_{2020} per kWh by 2025 to 0.26 EUR_{2020} per kWh by 2030 and average costs coverge towards 0.20-0.25 EUR_{2020} per kWh. The total infrastructure cost component (i.e., surcharge) accounts for around 6-9 ct/kWh.

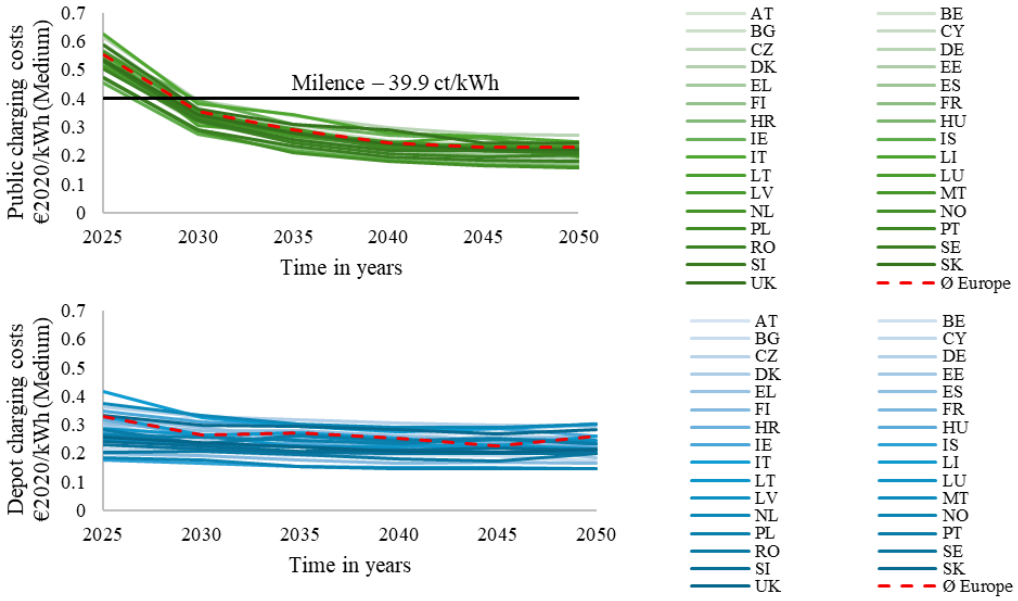

Note: Overlapping color scheme - only to visualize trends and scales.

Figure 35: Cost model: Charging costs (medium scenario)

4.5.2 Charging locations

Determining attractive charging locations is conceived as an add-on module using $data_{TPL}$ and extending Link et al. (2024a) (see **Subchapter 3.5**). This involves five steps as illustrated schematically in **Figure S27**.

First, $data_{TPL}$ is re-processed using additional data sources to ensure sufficient coverage and increase credibility, with details documented in Link et al. (2025a). In addition to the published data (medium and high confidence, N=19,713), the unpublished data (low confidence, N=32,251) are included. This yields N=51,964 possible locations. These locations are matched against the top 10% truck stop locations per country according to the data published by Plötz et al. (2021) to ensure that largest truck stop locations are covered. These locations are also matched against designated Safe and Secure Truck Parking Areas (SSTPAs) as defined by the European Commission to ensure that important highway rest areas are covered. Both steps use geospatial matching based on the latitude/longitude information. If no match is confirmed within a one-kilometer radius, locations are added. If there is a match, the credibility of the nearest is location is increased. Compared with the initially published dataset, this yields

N=22,647 locations with high and medium confidence and N=52,771 locations in total. Furthermore, added information also concerns nearby electric infrastructure (chargers or substations – see also Auer et al. 2022), nearby freight hubs such as ports or airports, or the proximity to TEN-T urban nodes.

Second, locations are refiltered and sorted according to their attractiveness. Per location, its attractiveness comprises the number of stops per year according to Plötz et al. (2021), nearby truck flow information according to Speth et al. (2022b), the adjusted confidence label, SSTPA information, the distance to the TEN-T network and urban nodes, and the availability of electric infrastructure (i.e., the presence of existing car charging hubs and the proximity to the next transformer). The following description illustrates the mechanism: *Prefer locations that are close to the TEN-T network or TEN-T urban nodes, labelled as SSTPA and have high truck activity (stops and flows) with high confidence that locations are suitable and accessible for trucks, ideally with existing electric infrastructure and high total area.* Note that sorting is enabled by converting different scales (categorical and ordinal) into a metric scale and calculating corresponding scores. Given these scores, locations are sorted per country due to the different scale of truck flows and the number of truck stops. To ensure scalability and condense the dataset, a subset of candidate locations is constructed by keeping only the most attractive location within a five-kilometer radius via a MeanShift algorithm, inspired by Lange et al. (2024). This yields N=13,323 candidate locations along the TEN-T network.

Third, circular buffer zones are placed around the candidate locations to account for their service areas along the TEN-T network. According to the AFIR requirements, these buffer zones could be 60 km (r=30 km) or 100 km (r=50 km). It is assumed that all road segments within the buffer zones can be served from this candidate location, and that one location serves both directions of travel. All metric distance operations use EPSG:3035 as the reference coordinate system.

Fourth, TEN-T road segments are matched with the corresponding truck flow information (Speth et al. 2022b) and sorted accordingly. Furthermore, all road segments are trimmed to a maximum length and splitted accordingly to ensure a homogeneous network and to avoid distortions caused by very long segments. The original file contains about 3,500 sections to display the whole network (about 137,000 km) and about 3,000 sections without the Balkan countries.

Fifth, a greedy heuristic is applied that aims to cover the busiest TEN-T network segments with the most attractive candidate locations. The road segments are labeled as fully covered if at least 90% of the total length is covered. A candidate location covers a road segment partially, if at least 33% the total length is covered. The partially covered segments are then split into covered and uncovered sections. A new location is added to the solution, if it covers a new segment/section of the road network. This process is repeated until either all TEN-T road segments are covered, or all candidate locations have been iterated.

4.6 Summary and discussion

The previous chapter introduced five consecutive submodels to assess the techno-economic feasibility of BETs for the European truck market through simulation and scenario analysis. While this combined framework facilitates truck-level feasibility assessments of BETs and recommendations for charging infrastructure, each submodel has limitations that need to be discussed.

The primary conceptual limitation, affecting all submodels, is the assumed one-to-one replacement of DTs with BETs, implying identical driving behavior, operational schedules, or general truck characteristics. This assumption is discussed alongside the results in **Chapter 5.5**.

(1) Concerning operating schedules, the novel probabilistic driving profile simulation uses specific probability distributions to capture the nonlinear propagation and simultaneous interaction of major parameters, in contrast to deterministic models that rely on single estimate inputs. However, the reliability and accuracy of results still depend on the quality of the data input (mainly $data_{ERFT}$ and $data_{Tour}$) and the selected model architecture and parameterization.

The model aims to reproduce realistic truck operating behaviours in selected European member states, but user-specific variations could be too high. For example, trucks with very similar to identical daily shuttle trips throughout their service life are likely not reproduced by the model. This overestimated variability can likely complicate the switch from DTs to BETs. This model effect originates from its probabilistic modeling, the Bayesian Network architecture with very few predefined parameters, and prediction of multi-year schedules from a few daily to weekly observations with limited information on truck-specific changes over multiple years. To solve this issue, future model updates might implement distinct case definitions (e.g., regional food retail depots) as model parameters, which then limit probabilistic choices, use generally more predefined paramters, or crop parameter distributions accordingly. While this could improve interpretability and partially reduce variability, there are no standardized definitions for such use cases and implications for whole markets are likely to become more complicated. Furthermore, while manipulation or even fixing may be intuitive for some parameters, for others it is arbitrary and likely to require (country-specific) manual adjustments, thus artificially and a-priori limiting the solution space.

The geographical resolution of operating schedules is limited to the NUTS-2 level of the origin and destination per trip. Tracing trucks along their trips and accurately localizing interim charging stops during driving breaks is not implemented. The NUTS-2 level follows from the resolution of $data_{ERFT}$, where the anonymization process removed postal codes and aggregated the address information to NUTS-2 regions. This level was available to determine likely OD paths based on connected traffic flows and given distances between all regions. While transport statistics are also available at NUTS-3 level, distance information is missing so that the practical feasibility of an OD path between two NUTS-3 regions cannot be ensured. Future studies could determine such feasible distances via truck routing softwares by calculating real-world distances between NUTS-3 regions (e.g., based on regional centroids or city coordinates as respective references. However, there is uncertainty related to the start and finish of trips. Plus,

note that even the size and geographical expansion of NUTS-3 regions largely differs across Europe, with more granular resolution for countries like Germany and large territories in Sweden or Finland. Thus, reaching a higher spatio-temporal resolution likely requires the application of a large-scale transport simulation. Agent-based transport simulations, such as MATSim, might then create synthetic BET populations and simulate their mobility patterns using the generated operating schedules. However, a European-wide truck simulation over several years will likely require extensive computational resources and is likely impractical to accomplish with reasonable effort[16] so that certain trade-offs among high temporal versus geographical resolution for tracing activities or truck conditions are likely to persist.

(2) Concerning the truck energy simulation, the developed model integrates the most critical factors affecting energy consumption but relies on standard mission profiles and uses pre-calculated energy consumption values to determine trip-specific energy needs.

The truck energy model focuses on longitudinal vehicle dynamics and uses certain submodels to adjust parameters specific to the simulation setting. These submodels have been adopted from different studies and rely on empirical relations or simplified gray-box models to approximate the associated effect. Future studies might extend the truck energy simulation with further submodels or evaluate the impact of further optimization to reduce energy consumption, such as road load reduction technologies or more advanced recuperation strategies.

The total DT energy consumption was compared against reported certification ($data_{EEA}$). Validation for BET energy consumption was limited to comparison with other studies. However, both showed good correlations with existing studies and plausible model reactions.

Determining the energy consumption relied on using the VECTO mission profiles since specific speed profiles were not available and precise elevation profiles would have required a higher geographical resolution. Concerning elevation as another critical factor on energy consumption, future studies might use one of the following approaches to further regionalize the model accuracy (e.g., flat terrain in the Netherlands vs. mountainous conditions in Austria): (1) An empirical country-specific correction factor; (2) scale the VECTO by the route-specific net elevation change between the origin and destination regions; or (3) consider the cumulative elevation ascent and descent from the trip origin to its destination. However, both latter approaches require route-specific knowledge, which is not available (NUTS-2 trip resolution).

Cargo-related additional power demand from accessory units is neglected as no data was available to calibrate the model. However, future studies might include the intermittent power requirements of pneumatic or hydraulic systems or additional power for cargo cooling/heating in relation to the NST-2007 group, as demonstrated by Link et al. (2021) for refrigerated food transport.

Median monthly temperature profiles are derived for each NUTS-2 region and country via historical values, with specific values assigned to each trip based on its origin and date

[16] Note that Menter et al. (2023) simulated one week of inner-German long-haul truck traffic using MATSim to simulate the charging demand along highways, which required 64 virtual processors (3.69 GHz) and 100 GB of RAM.

information. However, this approach smooths temporal and daily variability, omitting intraday fluctuations and extreme temperature events, so that the temperature impact on energy consumption (and the battery) is likely underrepresented. Future studies could implement daily profiles or consider more extreme temperatures (instead of median values).

The final energy consumption per trip follows from using pre- calculated energy values to enhance the runtime over millions of trips. This approach uses the average driving speed, total vehicle mass, ambient temperature, and truck characteristics. However, this neglects dynamic power profiles with pulses and variations over the mission profile. Future studies might select random sections of a VECTO mission profile (all 100 km long) and crop these sections to match the given trip distance and then scale the speed profile to match the respective target speed of the trip. This would include dynamic load pulses and power variations over the mission profile but increase runtime.

(3) Concerning the battery model, this thesis adopts a simplified internal resistance model to reproduce the electrical behavior while considering temperature and SOC dependence and calculate the charge/discharge efficiency in relation to the C-rate. This approach relies on three recent automotive-grade cells with different cell chemistries (NMC vs. LFP) and cell formats (pouch vs. cylindrical vs. prismatic). However, future studies might extend the electrical model to include more dependencies or update the aging submodel with latest findings.

Battery modeling focuses on the system-level capabilities but falls short of modeling single cell characteristics or cell-to-system effects. Such a cell-based approach was demonstrated by Teichert et al. (2023) for over 160 commercial battery cells, serving as a high-level cell selection filter to identify the most suitable battery cells, which can subsequently be tested and analyzed in greater detail. However, scaling cell-level parameters to the system-level, such as gravimetric and volumetric energy densities, highly depends on the specific cell (size, format and chemistry) so that generic cell-to-system scaling parameters from empirical data were used. Accordingly, this thesis focused directly directly on analyzing plausible system-level characteristics.

Battery aging, featuring cyclic and calendar effects, is complex and depends upon the combined effect of many dynamic influences throughout battery life. Typically, datasheet specifications rely on accelerated aging tests that seem to inadequately reflect real-world aging under dynamic conditions and higher idle times that allow for recovery. Exemplary, Geslin et al. (2024) and Wassiliadis et al. (2022) reported that varying charge/discharge profiles substantially increased the battery life beyond stated warranty information from such accelerated aging tests. This thesis incorporates battery aging by means of dimensioning, with a focus on cyclic aging and deducing an SOC operating window based on the expected FEC over the service life.

The battery packaging assumes an arbitrary battery split in predefined installation zones. However, an actual battery system will be constrained by the dimensions and design of the battery modules and packs. In contrast to this arbitrary split, predefined modules – potentially inspired by existing automotive or other standardized modules – could be assembled in the installation zones. However, this approach is likely very sensitive and can cause excessively large unutilized spaces, while cell-to-pack and cell-to-system integration concepts will likely enable battery systems that are tailored to the available space. Nevertheless, derived capacities match

current and expected models (refer to **Table 1** and the Cleanroom Talks by the NOW GmbH 2024a).

The battery model is implemented for state-of-the-art LIBs but could be expanded to alternative battery chemistries in future studies. Accordingly, alternatives such as sodium-ion batteries – with current characteristics similar to LFP batteries yet lower energy density – might be simulated as low-cost battery chemistry for short-distance trucks up to around 400 kWh.

(4) Concerning the economic assessment, the implemented TCO comparison follows an established methodology but inherently simplifies real-world pricing or individual cost structures and contracts. Plus, TCO eveluations are subject to several uncertainties, assumptions, and generalizations – particularly with projections toward 2030 and beyond.

The TCO model uses a cost-based calculation scheme to determine the CAPEX and OPEX parameters. However, this approach fails to include actual market price mechanisms and pricing strategies so that future prices for trucks or energy carriers are highly uncertain. Plus, this generic approach fails to include individual, user-specific conditions that should rather be examined via isolated case studies, such as demonstrated by Link et al. (2021) or Karlsson et al. (2023a). Such case studies then enable customized recommendations by including individual interest and financing costs as well as actual truck purchase costs, local electricity prices, available power supply, or space availability at the depot for charging infrastructure.

Incentives and purchase subsidies, which apply in some European countries, are neglected in the TCO calculation. These relative or fixed subsidies may compensate for additional purchase costs of BETs compared to DTs (at least partially), so that their implementation should improve the profitability of BETs, especially relevant in early market phases. However, the duration and stability of such subsidies remain uncertain. Thus, future studies could implement current schemes, following Noll et al. (2022), Basma et al. (2021b), or Tol et al. (2022).

Residual values are highly uncertain and empirical data on BET is not yet available. Thus, the implementation assumes the same relative residual value development of DTs and BETs, with a separate residual value of the battery (SOH-dependent) that is at least 15%. Future studies could incorporate this uncertainty by pessimistically omitting all residual values in the cost scenarios to safeguard financing, which would have a higher impact on the BET profitabilty.

Truck purchase costs rely on specific component costs that are adopted from Link et al. (2024c). Their meta-forecasting used more than 200 sources (from near-market to scientific) and analysed floor costs, growth rates and learning rates to reach certain cost levels. With respect to battery system costs, costs are reported to decrease toward 150 EUR_{2020} per kWh by the late 2020s and approach 100 EUR_{2020} per kWh toward post-2035. Yet, real-world costs might be lower and decrease substantially quicker, with industry players – such as BloombergNEF (2024) – already reporting average pack prices of around 115 USD_{2024} per kWh. However, tailored truck battery systems could also be more expensive than average systems (due to higher standards and requirements). Apart from costs, supply and availability of batteries, especially in Europe, are likely no obstacle for BET diffusion, as analyzed by Link et al. (2025b).

Country-specific energy costs (diesel and electricity) are determined via historical prices and their fluctuations, with future costs projected based on these historical trends and a common

European scheme with indexed cost trends. However, actual market price mechanisms based on supply and demand are neglected. Diesel costs increase in all scenarios due to increasing CO_2 taxation along with increasing blends of synthetic and biogenic diesel to comply with stated European climate neutrality targets. In contrast, electricity costs across all scenarios either remain constant or slightly decrease. The final charging costs follow from electricity costs and adding standardized extra costs for charging infrastructure and possible grid expansions. However, both can vary strongly depending on the country and local configuration of the public charging park or depot and existing equipment. Future studies could examine depot-related aspects in case studies in cooperation with companies, whereas detailed examinations for public charging parks will require detailed spatio-temporal load profiles and onsite information.

Country-specific road tolls are standardized by modeling as distance-based tolls in compliance with the future Eurovignette Directive. However, current toll regulations vary and involve time-based or distance-based tolls as well as national schemes or region-dependent tolling systems with concessions, whereas countries like Finland currently even have no tolls.

(5) Concerning the infrastructure assessment, the identification of locations and their attractiveness has several uncertainties and shortcomings. However, the approach is traceable and generates reproducible results for large-scale networks and thousands of candidate locations, with parameters and their sorting allowing for an intuitive feeling.

The attractiveness relies on different input datasets, with varying information quality across countries and partially only sufficiently precise[17], and a coverage heuristic to identify a subset of most attractive locations among candidates to cover the network. However, specific demand per location as well as sizing (i.e., the number of charging stations), local power requirements, or local energy throughput remain unknown. This would necessitate the application of queuing models, detailed data on the spatio-temporal distribution of public charging events, and vehicle-specific charging demands.

The current model assumes no capacity constraints at locations. Introducing such constraints would likely increases the total number of required locations, as highlighted by Speth et al. (2025). Future studies might update the algorithm so that each location can only serve a maximum annual truck volume (e.g., 100,000 trucks as adopted by Lange et al. 2024). This would necessitate more nearby locations along the same road segment to maintain coverage where traffic exceeds this threshold. However, setting such a limit is challenging, as it is likely specific per location (e.g., available local space) and it requires detailed information on arrival times as well as local BET diffusion and flows.

The Greedy heuristic cannot guarantee an optimal set of locations, for which other modeling techniques and algorithms would be required. However, optimization approaches might take several days to weeks to identify locations in such large-scale, real-world networks. And while the location attractiveness follows from onsite information and an intuitive best practice, the relevant parameters could also differ by country or region.

[17] This includes indicators such as the presence of existing car charging hubs or proximity to the nearest transformer, which serve as proxies for the local electrical infrastructure. However, critical information—such as the available grid capacity at each site—is unavailable.

5 Results

The following chapter presents the main results of this thesis. **Subchapter 5.1** introduces the scenario setting. **Subchapter 5.2** highlights the technical feasibility, particularly concerning installable versus required battery sizes, trip-level to day-level energy requirements, and the effects of intermediate charging using different scenarios. **Subchapter 5.3** supplements the TCO comparison of BETs and DTs among the selected countries. **Subchapter 5.4** demonstrates the Greedy Algorithm and implications for most attractive charging locations along the TEN-T network. Finally, **Subchapter 5.5** concludes with a discussion of the results.

5.1 Scenario introduction

The model application is tested for a sample of N=18,954 trucks, distributed across 15 countries four truck classes (see **Subchapter 4.1.5**). Assessing the technical feasibility of BETs uses different metrices and threshold values, as defined in the respective section. The TCO results evaluate two truck purchase dates (2024 versus 2030) each differentiated by three cost scenarios (*LOW*, *MEDIUM*, and *HIGH*). As a reminder, the total simulated mileage equals around 10.21 billion kilometers, distributed across 5.9 million weeks and 77 million individual trips.

The country selection covers the most important European truck markets as well as countries with special effects such as their geographical location and expansion, the presence of key European freight hubs, and the EMS allowance. Specifically, the countries involved are Austria (AT), Belgium (BE), Switzerland (CH), the Czech Republic (CZ), Germany (DE), Denmark (DK), Spain (ES), Finland (FI), France (FR), Italy (IT), the Netherlands (NL), Norway (NO), Poland (PL), Sweden (SE), and the UK (UK). Overall, these 15 countries account for 88% of new truck sales (cf. **Table S1**)and 82% of the truck stock (cf. **Table S2**) in Europe.

The truck class selection covers the four most important groups, namely VC-04 and VC-09, which represent two- and three-axle rigid trucks respectively, and VC-05 and VC-10, which represent two- and three-axle tractors respectively. Overall, these four groups constitute about 80% of all truck CO_2 emissions and about 85% of all heavy truck sales (cf. **Table S3**).

Simulated annual mileages

Figure 36 visualizes the annual mileage by country (upper) and by VECTO group (lower). The median annual mileage for new trucks[1] is 110,000 km per year and the interquartile range (IQR) is 93,000-124,000 km per year. The lower 5% of new trucks drive less than 65,000 km per year, and the upper 5% more than 140,000 km. In contrast, old trucks operate at around 80,000 km

[1] New trucks are defined as less than three years old, otherwise classified as old trucks.

per year (IQR: 58,000-88,000 km), whereas only the lower 5% drive less than 40,000 km. A breakdown by VECTO group indicates that the simulated annual mileage for rigid trucks is around 80,000 km, with a median value of 74,000 km for VC-04 (IQR: 57,000-95,000 km) and 82,000 km for VC-09 (62,000-107,000 km). For tractors, the annual mileage is around 100,000 km for VC-05 (IQR: 85,000-118,000 km) and around 105,000 km for VC-10 (90,000-120,000 km).

To summarize, simulated annual mileages seem to cover European mileages with reasonable accuracy, reproduce country-specific characteristics (cf. **Figure 7**), and capture recognized patterns between truck classes and types correctly[2].

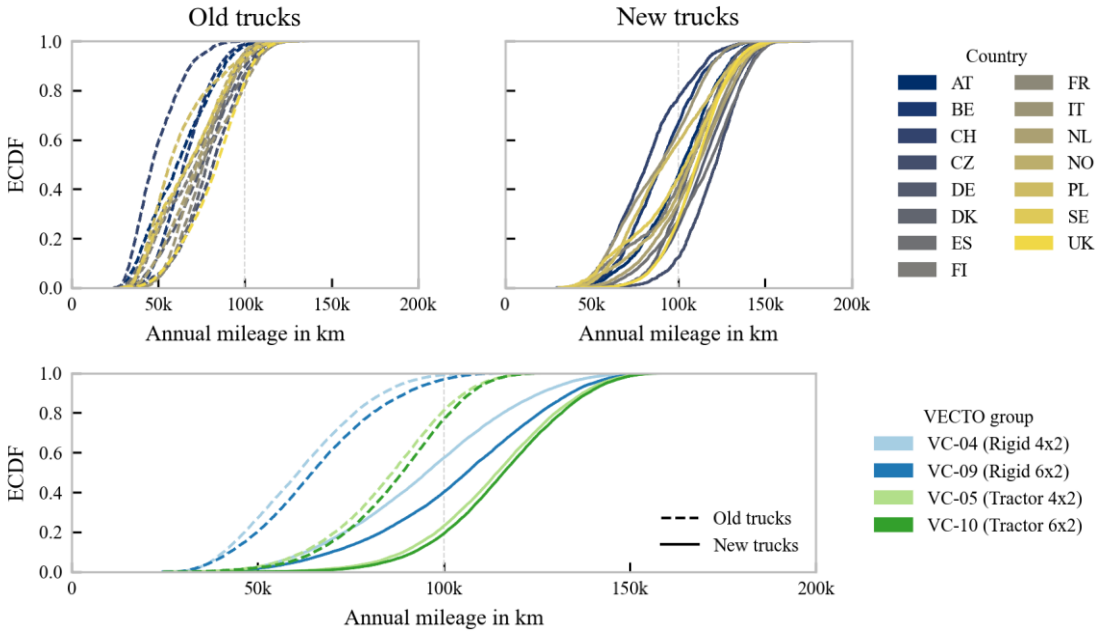

Figure 36: Results: Simulated annual mileage distributions

Simulated daily mileages

Figure 37 visualizes daily mileage distributions by country (upper) and by VECTO group (lower), including three reference distributions from other studies (cf. **Figure 8**). Note that simulated daily mileages might include a change of day. Among all simulated trucks, average daily mileage is around 250-350 km (median values) and the IQR is around 200-450 km, with new trucks having higher daily mileage values than older ones (cf. **Figure S28**). The simulated daily mileage seems to align with the references by reasonable accuracy. Yet, the reference distributions have pronounced probability peaks at around 400-600 km per day and mileages above 600 km are limited (<10%). In contrast, the simulated distributions are smoother with longer distribution

[2] The European approval process defines annual mileages of 60,000 km for urban delivery, 68,000-78,000 km for regional delivery, and 98,000-116,000 km for long-haul. The breakdown by VECTO group is as follows: 60,000-98,000 km for VC-04 (rigid); 78,000-116,000 km for VC-05 (rigid); 73,000-108,000 km for VC-09 (tractor); 68,000-107,000 km for VC-10 (tractor). Also compare the literature corridor for truck age and mileage, visualized in **Figure 11**.

tails (higher skeweness resulting from the continuous modeling with Gamma/Beta distributions) so that daily driving events above 600 km are more likely (up to 20%) and depending on the country. Patterns among truck classes and types are similar to annual mileage patterns (cf. **Figure 36**), yet less pronounced.

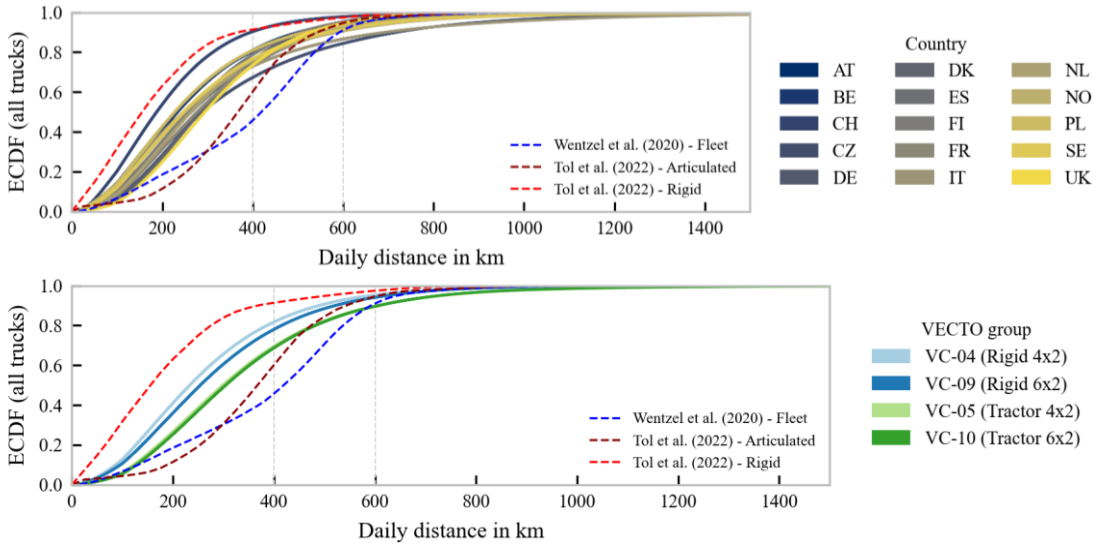

Figure 37: Results: Simulated daily mileage distributions

Simulated number of daily trips

Figure 38 visualizes the corresponding number of daily trips by country (upper) and by VECTO group (lower). Accordingly, trucks perform mostly 1-2 trips per day, sometimes 3-5 and rarely more than that. The overall mean value is around 2.22 trips per day, with more pronounced country-specific differences than differences by truck type and class. Mean values range from 1.30 (IT) to 3.06 (CH) by country, or from 2.23 (VC-04) to 2.47 (VC-09) by VECTO group.

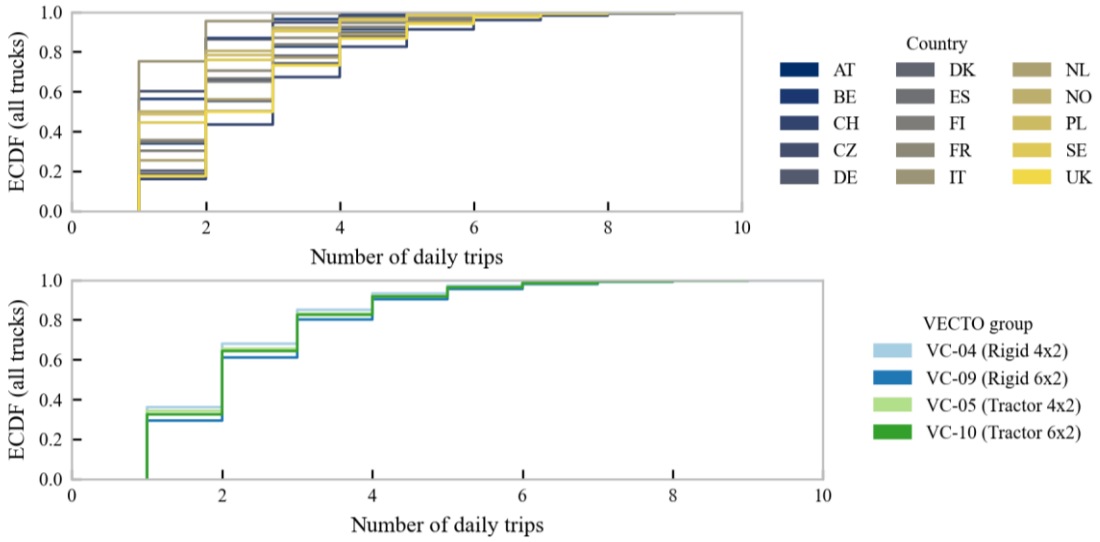

Figure 38: Results: Simulated number of daily trips

5.2 Technical feasibility of battery-electric trucks

Assessing technical feasibility uses different metrices and threshold values, ranging from one-by-one replacement to allowing minor deviations. This approach picks up on the findings by Link et al. (2021) and Tol et al. (2022) (cf. **Subchapter 2.2**), stating that the technical feasibility of BETs is often negated by just a few extralong trips or extreme days, even though the remaining schedule would have been feasible[3]. This implementation shall avoid distorted findings caused by the assumed one-by-one replacement.

The following section discusses energy needs and battery capacities in several steps - from broad to detailed - starting with installable battery capacities and proceeding with the required energy level per day and per trip. This section concludes by discussing energy needs and battery capacities that follow from the distinct operating schedules and related SOC-profiles, thus including the presence of charging events during non-driving operations.

5.2.1 Installable battery capacities

Figure 39 (tractors) and **Figure 40** (rigids) visualize installable battery capacities versus the achievable payload for various battery pack specifications (cf. **Figure 32**), with ranges resulting from different DT configurations. The four-axle truck configurations are visualized in **Figure S29**.

For two-axle BET tractors (VC-05), current Fe-based batteries (LFP and LMFP) manage up to around 600-650 kWh without payload losses compared with DTs, which reach around 25 tons. This range also follows from stated manufacturer specifications (cf. **Table 1**). Larger batteries then involve notable payload losses of up to 3 tons (12%). However, around 90% of maximum payload capacity should still be sufficient to cover most operations for almost all NST-types except for a few heavy commodities and overloaded trips (70-90% of operations, cf. **Figure S5**). Future chemistry advances by 2030 might allow for up to around 800 kWh. In contrast, current Ni-rich chemistries can already manage up to around 700-750 kWh and future advances by 2030 might allow for up to around 900 kWh without payload losses.

Ranges and patterns are similar for three-axle BET tractors (VC-10) that can operate in intermodal transport (GVW up to 44 tons), yet payload losses for larger batteries are more pronounced and maximum battery capacities are lower due to the reduced installation space.

Compared with rigids, battery capacities are rather limited by the installation space than by weight. A detailed assessment of the fifth wheel load of tractors (see **Figure S30**) shows that this load is substantially reduced despite similar total payload ranges, which implies less flexibility of the BETs and imposes stricter requirements on the trailer load distribution.

[3] Note that, such few extralong trips or extreme days could also lead to substantially larger required batteries compared to requirements by the remaining schedule. This massive overdimensioning then impairs profitability.

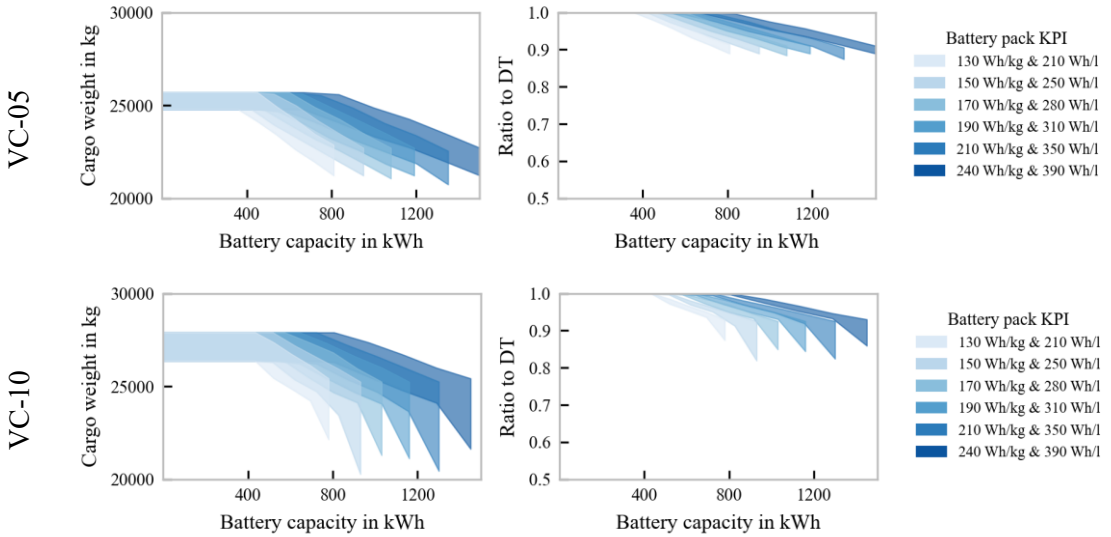

Figure 39: Results: Installable battery capacities (tractors)

For two-axle BET rigids (VC-04), current Fe-based batteries (LFP and LMFP) manage up to around 500-550 kWh without payload losses compared to DTs, which reach around 10-12 tons. Larger batteries then involve notable payload losses since the available installation space is hardly limited. The battery capacity ranges without payload losses for three-axle BET vehicles (VC-09) are comparable to those of tractors, since the additional axle reduces axle weight restrictions.

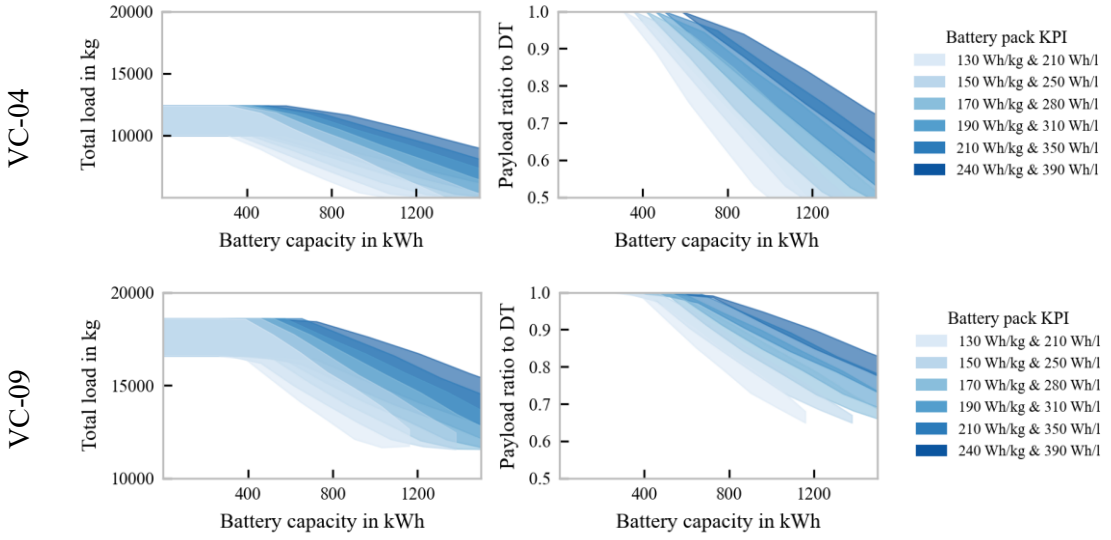

Figure 40: Results: Installable battery capacities (rigids)

5.2.2 Simulated energy consumption

Figure 41 visualizes the simulated energy consumption as a 2D probability density with a breakdown by country (upper) and VECTO group (lower). Specifically, the simulated mean

energy consumption among all trips per truck is compared with very high consumption values (90th percentile) and high consumption values (upper quartile) to determine a range of reasonable yet expectable consumption values. Even higher consumption values are effectively omitted in this consideration. In addition, **Table S28** summarizes country-specific values and **Table S29** presents values per VECTO group.

The simulated energy consumption averages between around 1.12 to 1.34 kWh/km among all countries. For rigids, the average consumption values are at 1.12 kWh/km for VC-04 and 1.22 kWh/km for VC-09. For tractors, average consumption values are at 1.26 kWh/km for both VECTO groups. The energy consumption spread for rigids is higher than that for tractors because of greater operational flexibility, involving operations with or without an articulated trailer (higher curb mass and air drag) and associated higher payload fluctuations. This effect is particularly evident in countries with EMS allowances such as Belgium, Finland, Denmark, Sweden, or Norway. Plus, general higher consumption due to lower temperatures is particularly evident in the Scandinavian countries.

High consumption values exceed mean values by around 27% on average (range: 15-34%). Very high consumption values average at around 1.87 kWh/km (range: 1.57-2.36 kWh/km), which corresponds to a 50% increase compared to the mean consumption. Thus, these scales and comparative figures highlight potential pitfalls of relying on average BET consumption values compared to trip-specific values.

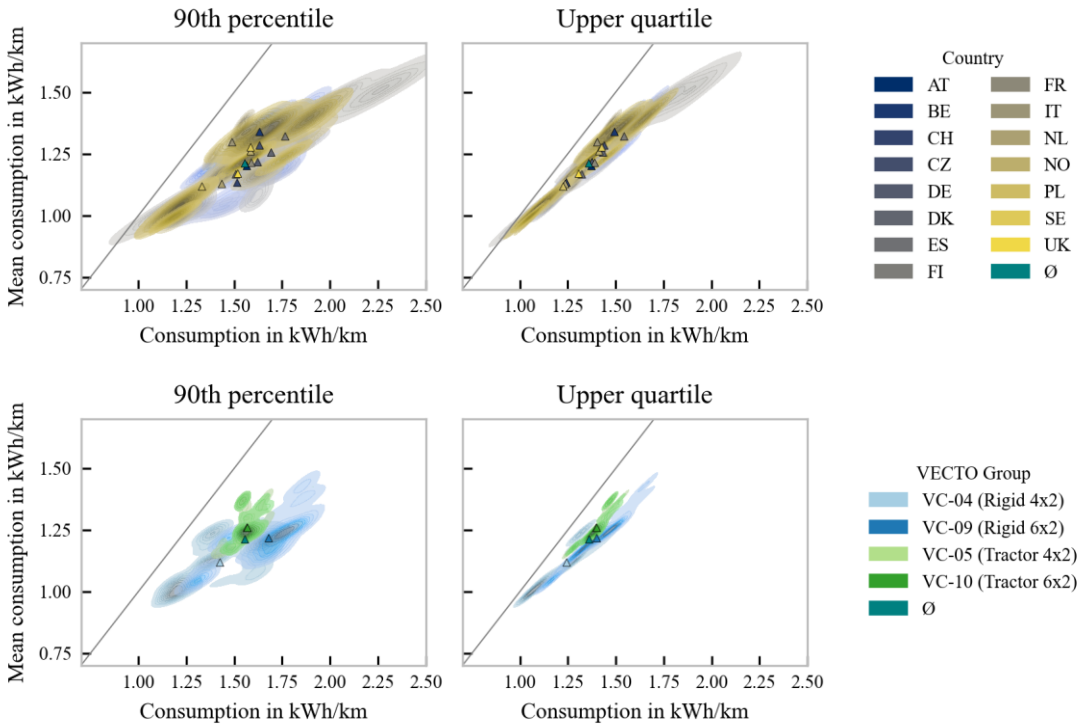

Figure 41: Results: Variation of specific energy consumption per truck

5.2.3 Daily energy requirements

Figure 42 visualizes daily energy requirements as a 2D probability density by country (upper) and VECTO group (lower). Specifically, the mean daily energy requirements per truck are compared to extended daily energy requirements. This involves defining three threshold values to quantify the effect of a few extreme days: (1) the overall maximum; (2) the upper 1% (99th percentile); (3) and the upper 5% (95th percentile). **Table S30** summarizes country-specific values.

The simulated daily energy requirements average between 200 and 600 kWh among all countries with local peaks at around 180-250 kWh, 400-450 kWh, and 510-570 kWh. For rigids, average daily energy requirements are 340 kWh for VC-04 and 400 kWh for VC-09, with higher spreads than for tractors (see previous section). For tractors, average daily energy requirements are at 460 kWh for both VECTO groups, attributed to higher daily mileages (cf. **Figure 37**).

If the maximum daily energy is used as a reference, the average daily energy requirement is exceeded by a factor of 3 to 5. If the upper 1% is used as a reference, this factor shrinks to around 2.7 (mean value; range: 2.4-3.0). If the upper 5% is used as a reference, this factor shrinks to around 2.1 (mean value; range: 1.88-2.19). In practical terms, the latter case means that if the average daily energy requirement was used for battery sizing, one additional battery charge would be required to accomplish this profile. If the highest daily energy requirements were used for battery sizing, the resulting batteries would often exceed the available installation space (cf. **Subchapter 5.2.1**) but would not be needed in day-to-day operations. This strongly limits the technical feasibility of BETs.

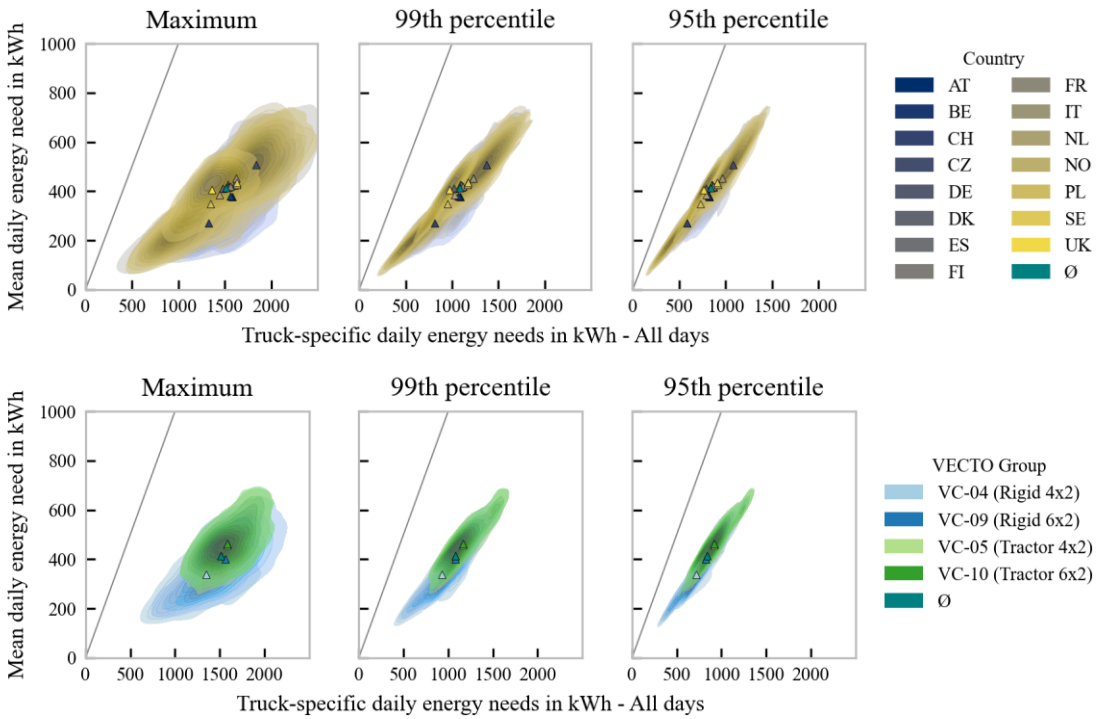

Figure 42: Results: Variation of daily energy requirements (all days)

These patterns are similar if the daily energy requirements are limited to days in single-shift operations (refer to **Figure S31**). Accordingly, daily energy requirements decrease slightly. If the upper 1% is used as a reference, the average daily energy requirement is exceeded by a factor of around 2.20 (mean value; range: 2.01-2.69). If the upper 5% is used as a reference, this factor shrinks to around 1.89 (mean value; range: 1.74-2.04).

5.2.4 Trip energy requirements

Trip-specific energy requirements are evaluated per entire trip, which may last several days, and per trip segment. A segment represents either the entire trip - if there are no interruptions by driving breaks, rest periods, or intermediate stops - or corresponding trip sections to determine the minimum amount of energy required to accomplish sections without an additional stop. Specifically, extended energy requirements for each truck are compared, which are defined by three threshold values to quantify the effect of a few extreme trips or trip sections: (1) the overall maximum; (2) the upper 1% (99th percentile); and (3) the upper 5% (95th percentile).

Trip-specific analysis among all trips versus single-day trips[4]

Figure 43 visualizes trip-specific energy requirements for each truck among all trips (upper) and single day trips (lower) via ECDF plots, differentiated by country.

Energy requirements among all trips have an extreme spread, also between countries, which is mainly caused by the relevance of (international) long-haul trips. For example, there is an accentuated difference for the UK (predominantly national long-haul) compared to Belgium and the Netherlands with their large overseas ports from where goods are delivered to all of Europe. These trips might last for several days and several thousand kilometers, so that total energy requirements consequently add up to several thousand kWh. However, these trips are interrupted by mandatory driving breaks and mandatory rest periods, which creates an opportunity for charging. The required energy decreases rapidly if most extreme trips are ignored, with energy requirements of up to 1,200-2,500 kWh (upper 20% of the upper 1%) and 700-1,800 kWh (upper 20% of the upper 5%).

Energy requirements among single-day trips show similar paterns but have proportionally reduced spreads. However, most extreme trips still require well above 1,000 kWh, where again mandatory driving breaks might create an opportunity for charging. Similarly, the required energy decreases rapidly if most extreme single day trips are ignored, with energy requirement of up to 850-1,400 kWh (upper 20% of the top 1%) and 630-950 kWh (upper 20% of the top 5%).

[4] Single-day trips are defined as trips that start and end on the same day.

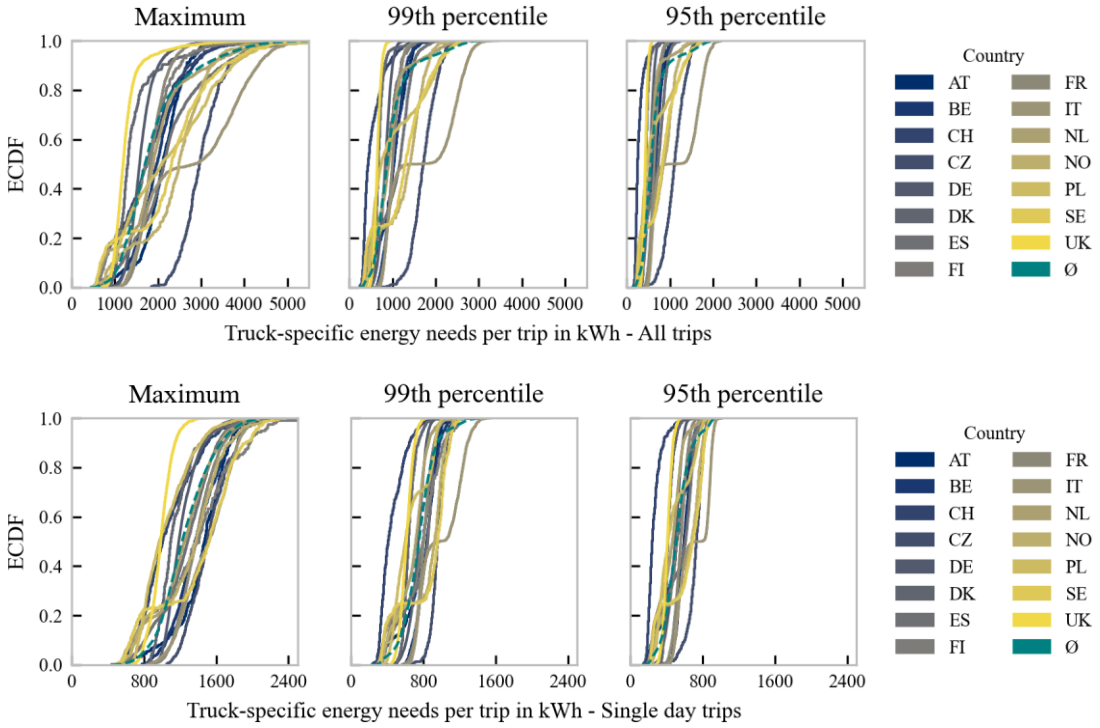

Figure 43: Results: Truck-specific maximum energy requirements per trip by country

Figure S32 presents the breakdown by VECTO group, showing similar patterns and only minor differences. **Figure S33** supplements the breakdown by country via 2D density distributions by comparing mean energy requirements per trip versus the respective threshold.

Trip-section analysis

Figure 44 visualizes truck-specific energy requirements per trip section by country (upper) and VECTO group (lower) via ECDF plots. Accordingly, the average maximum energy needs per trip section are around 570 kWh (median value; IQR: 550-600 kWh) but extreme sections might require up to 800 kWh. If the upper 1% is used as a reference, this range decreases to 440-520 kWh but extreme sections might still require up to 700 kWh. If the upper 5% is used as a reference, this range decreases to 340-430 kWh but extreme sections might still require around 590 kWh. However, these energy requirements per trip section are within the range of available and announced BETs (cf. **Table 1**) as well as installable battery capacities (cf. **Subchapter 5.2.1**)[5].

The breakdown by VECTO groups indicates a pronounced bimodality for rigid trucks, where the first peak represents trucks that operate exclusively without a trailer. Apart from this pattern, energy requirements are similar among the truck classes and types, which is likely caused by the mandatory driving break after 4.5 hours of driving.

[5] Note that recalculating the gross battery capacity from such (net) energy requirements requires further factors such as the share of usable energy and restrictions on the SOC window or DOD limits, respectively.

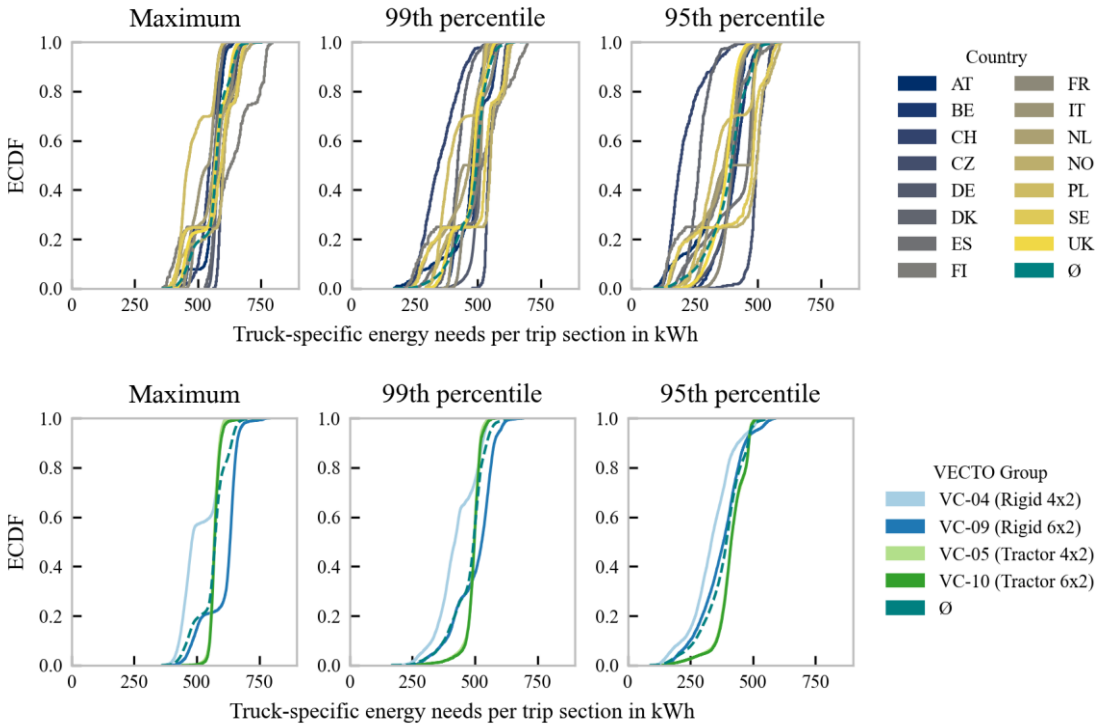

Figure 44: Results: Truck-specific maximum energy requirements per trip section

5.2.5 Electrifying schedules and SOC profiles

SOC-based considerations utilize the truck-specific operational schedule and evaluate the technical feasibility for (1) different battery configurations, (2) charging scenarios, and (3) feasibility conditions, with the implemented algorithm aiming to maximize the SOC. The SOC profile then follows from the cumulative energy balance in relation to the battery capacity, where energy drawn from the battery (driving events) has a negative effect and energy supplied to the battery (charging events) has a positive effect. For clarification, **Figure S34** visualizes the SOC profile of the corresponding operating schedule at different zoom levels (cf. activity plot shown in **Figure 25**).

(1) Battery configurations differentiate NMC and LFP, each with higher energy densities for a 2030 analysis. This chemistry choice impacts the maximum installable battery capacity without payload losses (refer to **Subchapter 5.2.1**), the battery sizing, the fast-charging capability, and the DOD limit. For both NMC and LFP, the battery sizing uses the energy requirement per trip section (upper 1%) to derive the required minimum battery capacity. Concerning NMC, the implementation allows for a maximum charging rate of 2C, a maximum capacity of 750 kWh in 2024 (2030: 900 kWh), and the DOD limit is defined at 0.05. Concerning LFP, the implementation allows for a maximum charging rate of 2.25C, a maximum capacity of 650 kWh in 2024 (2030: 800 kWh), and the DOD limit is defined at 0.01. To determine the feasible minimum battery capacity, the algorithm gradually increases the battery capacity from 300 kWh to the maximum

battery capacity in increments of 25 kWh until the operating schedule becomes feasible and the required minimum battery capacity is maintained.

(2) Charging is generally allowed during breaks, rest periods, and idle times between trips and may be granted during long intermediate stops of more than 30 minutes. The truck parking time must exceed 15 min in any case. It is assumed that 65% to 80% of the parking time is available for charging. The charging power is defined as a variable parameter that is determined ex-post based on the amount of energy recharged and the charging time. Two cases are distinguished, which limit the available charging power in addition to the C-rate limit of the battery. If *MCS-charging* is available, the average maximum charging power is set at 850 kW. If only *CCS-charging* is available, the average maximum charging power is set at 450 kW. The actual charging power is then categorized according to the following scheme, where the upper limits of the class are as follows: CCS-50kW; CCS-150kW; CCS-350kW; CCS-450kW; and MCS. This categorization enables an assessment of which technology is required in what quantities, such as number of events or total charged energy. Based on the operating schedule, charging events are further labeled as public, if occuring during breaks and rest periods, or private. The latter summarizes depot and destination charging while idling between tours or being inactive overnight or during intermediate stops.

The utilization of *CCS-charging* and *MCS-charging* is evaluated for three scenarios (cf. **Figure 14**), as summarized by **Figure 45**. The *unlimited scenario* allows the maximum charging power at all locations. The *limPrivate scenario* limits the maximum power for private charging to 150 kW to evaluate options with limited private charging facilities, which are caused, for example, by low residual grid connections. The *onlyPrivate scenario* disables public charging so that charging is only allowed at private locations (with up to 150 kW) to evaluate options without public charging infrastructure. Between 2024 and 2030, only the maximum installable battery capacity is varied.

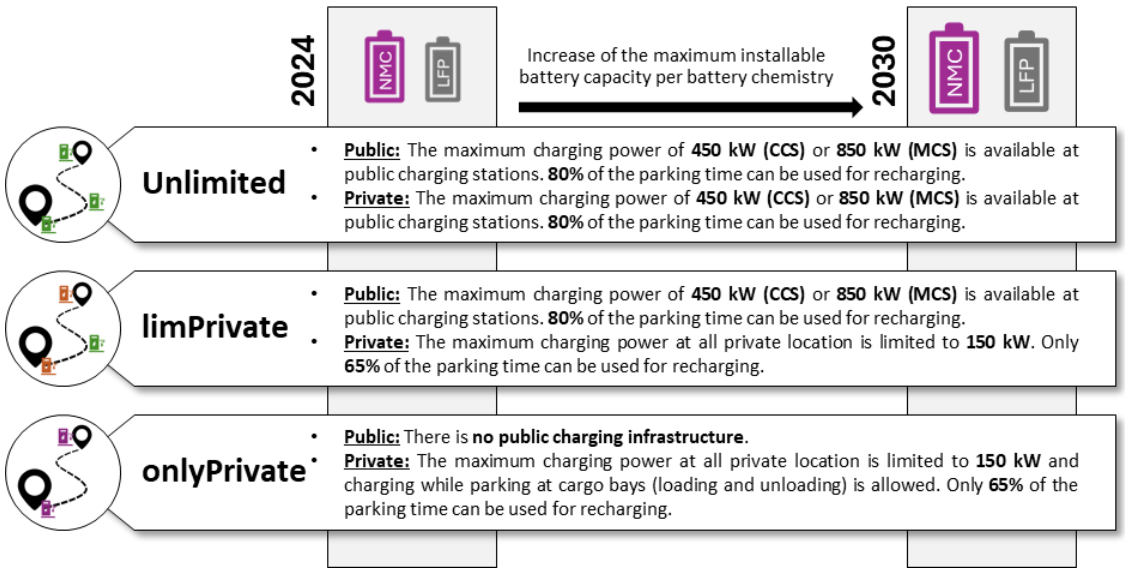

Figure 45: Results: Scenarios to evaluate the technical BET feasibility per schedule

(3) Feasibility conditions are implemented to handle and quantify the effect of extralong trips or extreme days efficiently and partly mitigate the effect of the assumed one-by-one replacement. Specifically, it is assumed that the DOD limit of the BET may be violated for a limited number of events as follows: 100 times (*100-cuts*), 50 times (*50-cuts*), 10 times (*10-cuts*), or zero times (*0-cuts*). The practical interpretation of these feasibility conditions is that short additional charging stops would be required to avoid these violations. Note that this approach was chosen, since operating schedules typically involve several thousand trips and a forward simulation that would shift and adjust all timestamps in the operating profile proved to require too much runtime.

Scenario: unlimited – Technical feasibility and utilized battery capacities

Figure 46 visualizes technical feasibility heatmaps for the *unlimited scenario* by 2024 (upper) and 2030 (lower). Each subplot represents the proportion of feasible schedules subject to the charging case (left: *CCS-charging*, right: *MCS-charging*), battery chemistry (upper: LFP, lower: NMC) and feasibility condition (x-axis).

By 2024, even the CCS-scenario allows to electrify most operating schedules (86-94%) in the most relaxed condition (*100-cuts*). However, if the operating schedule must be strictly observed and the DOD limits must not be cut (*0-cuts)*, the technical feasibility decreases to between 11% (LFP) and 16% (NMC). With only minimal relaxations (*10-cuts*), around 30% (LFP) to 46% (NMC) of the schedules can be electrified. With minor relaxations (*50-cuts*), however, the feasibility rises to between 71% (LFP) and 85% (NMC). The introduction of MCS substantially increases feasibility, with three out of four conditions reaching at least 89% and up to almost 100%. Yet, the high sensitivity remains when zero DOD cuts are allowed (*0-cuts)*, with feasibility decreasing to between 39% (LFP) and 56% (NMC).

By 2030, the greater maximum battery capacity allows for increased technical feasibility in all aspects. However, strict conditions (*0-cuts*) still limit the technical feasibility to between 26% (LFP) and 40% (NMC) for *CCS-charging*, while the introduction of *MCS-charging* increases feasibility to between 72% (LFP) and 81% (NMC). Already minimal relaxations (*10-cuts*) will allow for near-complete electrification of all schedules (99%) by both cell chemistries, if MCS is available. And without MCS, around three quarters (71-83%) of all schedules can be electrified.

The results for both years show that the sensitivity toward the feasibility condition is generally higher for LFP than for NMC. This follows since stricter conditions cannot be compensated with larger batteries because of the lower maximum battery capacity for LFP compared to NMC. Yet, the introduction of MCS narrows the gap between both chemistries, so that NMC and LFP can reach similar feasibility levels. The next section will show utilized battery capacities among the scenarios.

In addition, ***Figure S35*** extends these heatmaps for 2024 and 2030 by presenting country-specific sensitivities and ratios among six selected candidates (DE, ES, FR, IT, NL, UK). Specifically, feasibility challenges are highest in Italy and Spain, followed by Germany and France, while challenges remain comparatively lower in the UK and the Netherlands.

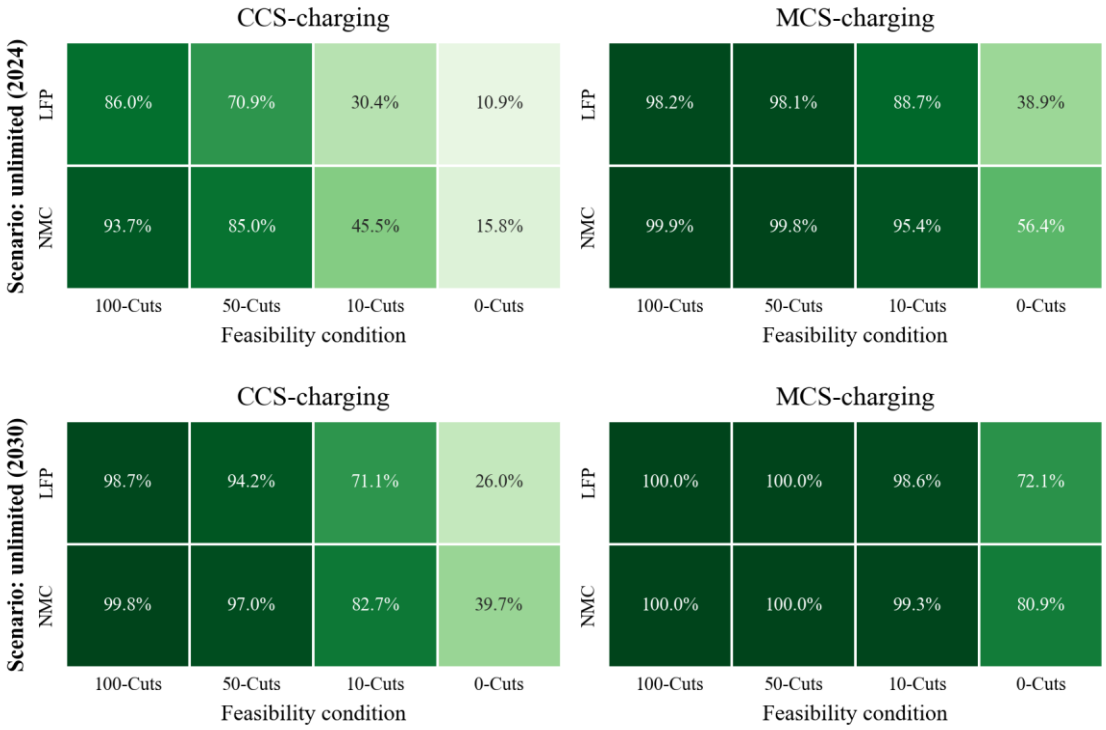

Figure 46: Results: Technical feasibility heatmaps for the unlimited scenario

Figure 47 visualizes the utilized gross battery capacity for the *unlimited scenario* by 2024 (upper) and 2030 (lower) as density distribution plots, subject to the charging case (left: *CCS-charging*, right: *MCS-charging*), battery chemistry (upper: LFP, lower: NMC) and color-coded feasibility condition. Note that the hard cuts represent the corresponding maximum battery size per chemistry and year. Three trends are observed:

(1) *Larger batteries can compensate for stricter feasibility conditions*: This is visualized by stricter conditions (darker colors) having broader and more right-leaning distributions, particularly for the *0-cuts* condition. On average, battery capacites must be increased by around 100 kWh (range: 28-189 kWh) to ensure feasibility for *0-cuts* compared to *100-cuts*.

(2) *The introduction of MCS leads to smaller batteries compared to relying on CCS:* This is visualized by MCS scenarios having more distinct peaks and left-leaning distributions with less frequent usage of the maximum battery capacity. Average battery capacites may be reduced by around 40 kWh and up to 125 kWh, corresponding to -6% to -17% respectively.

(3) *The required battery capacities range mainly from 500 to 700 kWh, with less frequent need for 850 to 900 kWh*: This is visualized by distinct distribution peaks, particularly for relaxed feasibility conditions. Average utilized battery capacities increase toward 2030, along with higher feasibility of the schedules. This increase ranges from 76-117 kWh for LFP and 61-94 kWh for NMC batteries, with higher increases attributed to *CCS-charging*.

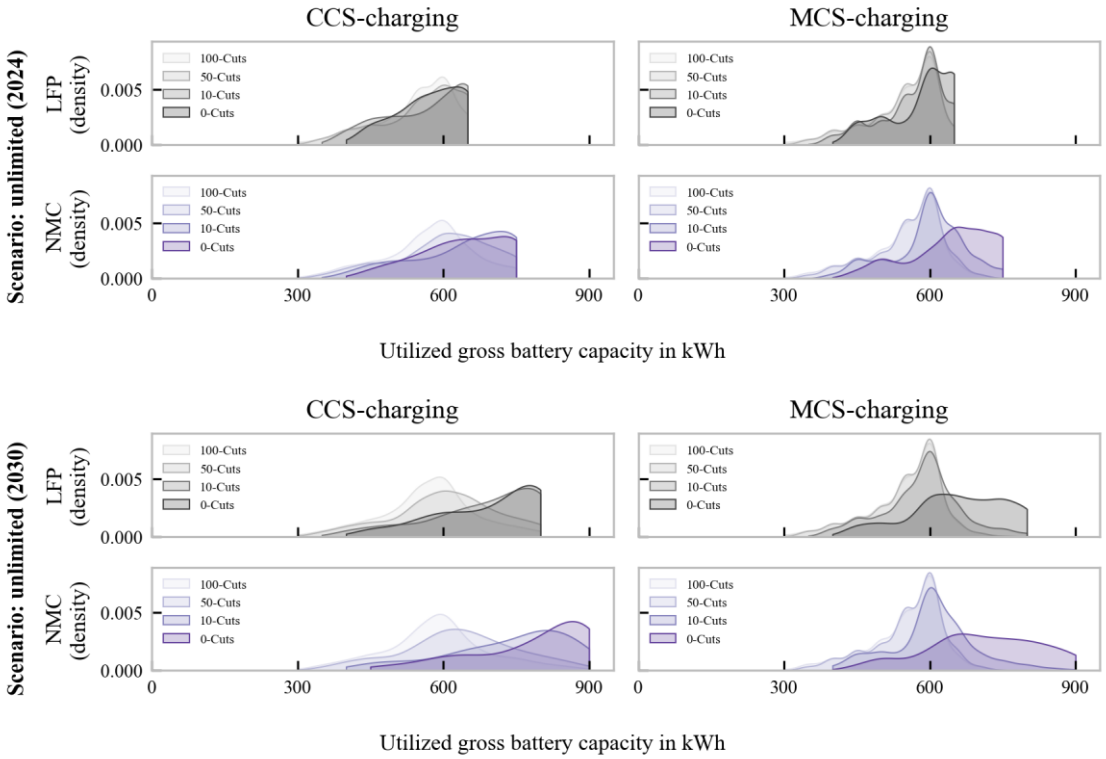

Figure 47: Results: Utilized battery capacities for the unlimited scenario

To supplement the battery assessment, **Figure S36** visualizes the resulting FEC for the unlimited scenario by 2024 (upper) and 2030 (lower) as density distribution plots (analogous structure to **Figure 47**). Batteries typically lasted around 500 to 2500 FEC at the end of their first-user life, with the majority falling within 1000-1500 FEC and generally less FEC for stricter feasibility conditions due to the compensation effect.

Scenario: unlimited – Relevance of charging locations and power

Figure 48 visualizes the share of charged energy at private locations for the *unlimited scenario* by 2024 (upper) and 2030 (lower) via 2D probability densities. Specifically, these plots are subject to four combinations of charging case and feasibilty condition (columns), battery chemistry (upper: LFP, lower: NMC) and the average annual mileage (x-axis). Note that private locations encompass charging at depots and at destinations.

Charging at private locations represents the largest share, usually well over three-quarters even for very high annual mileage and combination. There are no substantial differences related to battery chemistry or year, and the sensitivity of this share compared to the annual mileage is slightly negative, which is reasonable due to the higher proportion of national/international long-haul.

Concerning the charging technology, the relevance of private charging is slightly higher for *CCS-charging* than for *MCS-charging.* Specifically, the average share stands at 87% (range of means:

83-92%) for *CCS-charging* compared to 79% (range of means: 75-86%) for *MCS-charging*. Accordingly, the average increase stands at 6.9% (range of means: 4.7-9.4%).

Concerning the feasibility conditions, the relevance of private charging increases when comparing *100-cuts* and *0-cuts*. Specifically, if *100-cuts* are allowed, the average share of charged energy at private locations stands at 81% (range of means: 77-87%) and, if *0-cuts* are allowed, this share stands at 85% (range of means: 81-91%). Accordingly, the average increase stands at 4.2% (range of means: 2.4-6.0%). This increase results from numerous trucks with high mileage operating in mulit-shift operations or completing several back-to-back trips, so that high charging power is required at depots/destination locations or in their immediate vicinity.

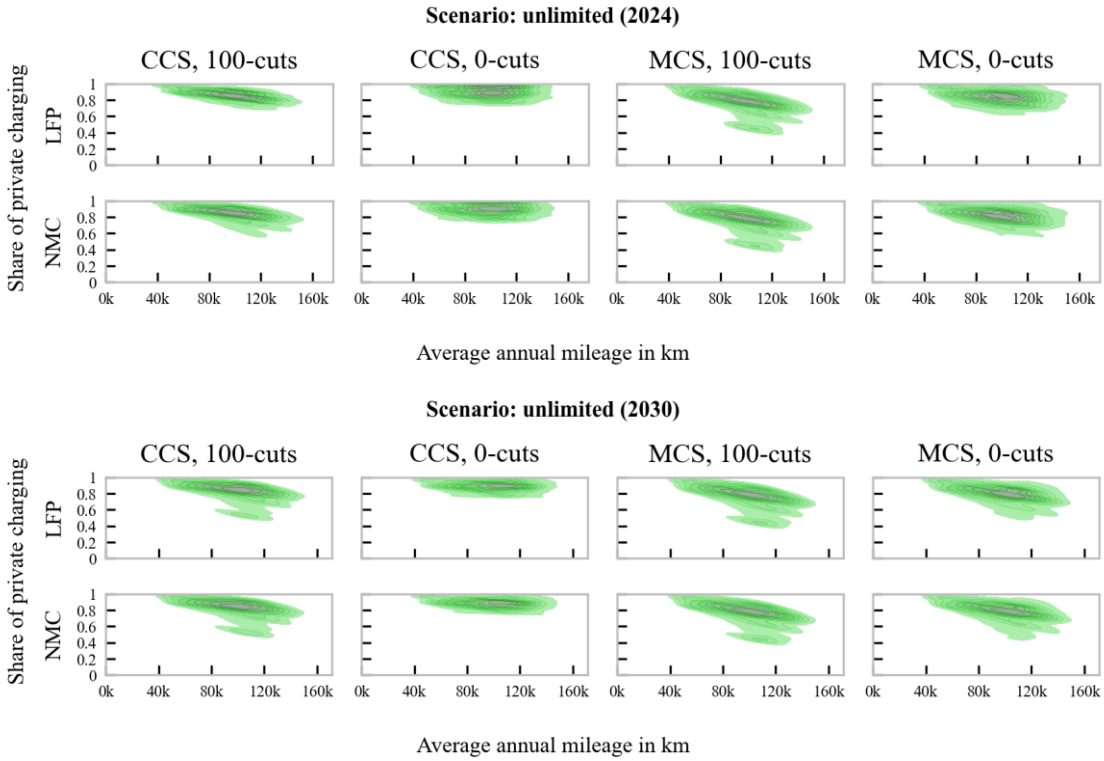

Figure 48: Results: Relevance of charging at private locations for the unlimited scenario

Figure 48 visualizes the share of utilized charging power levels for the *unlimited scenario* by 2024 (upper) and 2030 (lower) via 2D probability densities. Specifically, these plots are subject to the five power levels (columns), charging case (upper: *CCS-charging*, lower: *MCS-charging*) and the average annual mileage (x-axis).

Charging at 50 kW usually accounts for around half of the total charged energy (45%-75%) in both cases and years and shows little sensitivity to annual mileage. The share of charging with 150 kW to 350 kW is in a similar range, each at around 10-20%. If *MCS-charging* is available, the relevance of 50 kW charging decreases slightly with higher mileage and the share of MCS-charged energy increases accordingly, which averages around 20-25% and spans from 10% to 30%, thereby taking over almost all shares of the CCS charging with 450 kW.

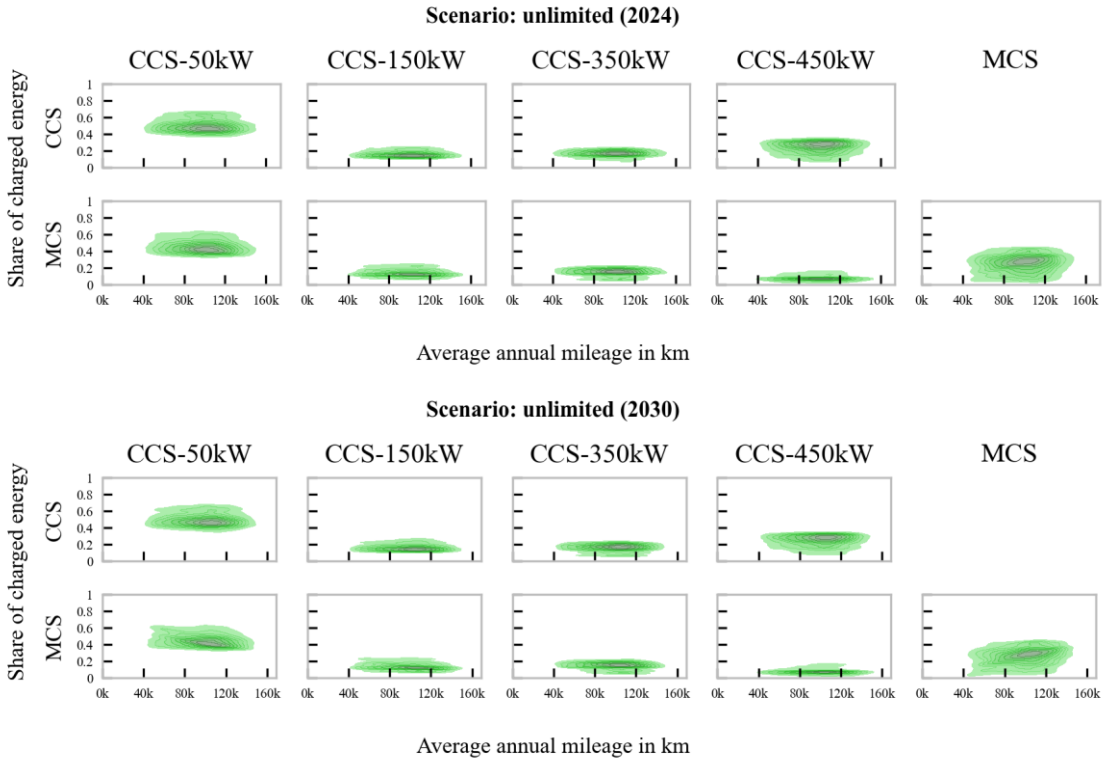

Note: Overlay of battery chemistry (LFP and NMC) and feasibility condition (*100-cuts* and *0-cuts*)

Figure 49: Results: Relevance of charging power for the unlimited scenario

Scenario: limPrivate

Figure 50 visualizes analogous heatmaps of technical feasibility for the limPrivate scenario by 2024 (upper) and 2030 (lower). Corresponding figures for a country-specific heatmaps by 2024 (see **Figure S37**), the utilized battery capacity (see **Figure S38**), shares by charging location (see **Figure S39**), and charging power (see **Figure S40**) are available in the Appendix.

Concerning technical feasibility, strict conditions (*0-cuts*) limit feasibility to below 5% by 2024 and to below 10% by 2030. The substantial decrease compared to the *unlimited scenario* highlights the need for high charging power at private locations. In the most relaxed consideration (*100-cuts*), however, even *CCS-charging* allows electrifying a medium share of schedules (33-49%) by 2024 and a high share of schedules by 2030 (73-86%). If *MCS-charging* is available, technical feasibility increases to 56-81% by 2024, while allowing to electrify almost all schedules (95-99%) by 2030. Compared to the *unlimited scenario*, the difference between *CCS-charging* and *MCS-charging* is more pronounced. This also applies to NMC versus LFP batteries, with NMC allowing for higher electrification due to superior compensation with larger battery capacities, so that utilized battery capacities are shifted to the right, particularly in 2030. Specifically, average battery capacities by 2030 are increased by around 40-60 kWh for LFP and 50-75 kWh for NMC, with higher values attributed to *CCS-charging*. This combined observation implies that the relevance of MCS and larger batteries is increasing if private charging is limited.

Concerning location and power, patterns and ranges are similar compared to the *unlimited scenario.* However, the relevance of charging at private locations slightly increases, particularly with higher charging power (150 kW; up to 40%). The relevance of charging with 50 kW remains more stable at around 50% (range: 40-60%), while the relevance of *MCS-charging* is slightly decreasing, with average values of around 12-20%.

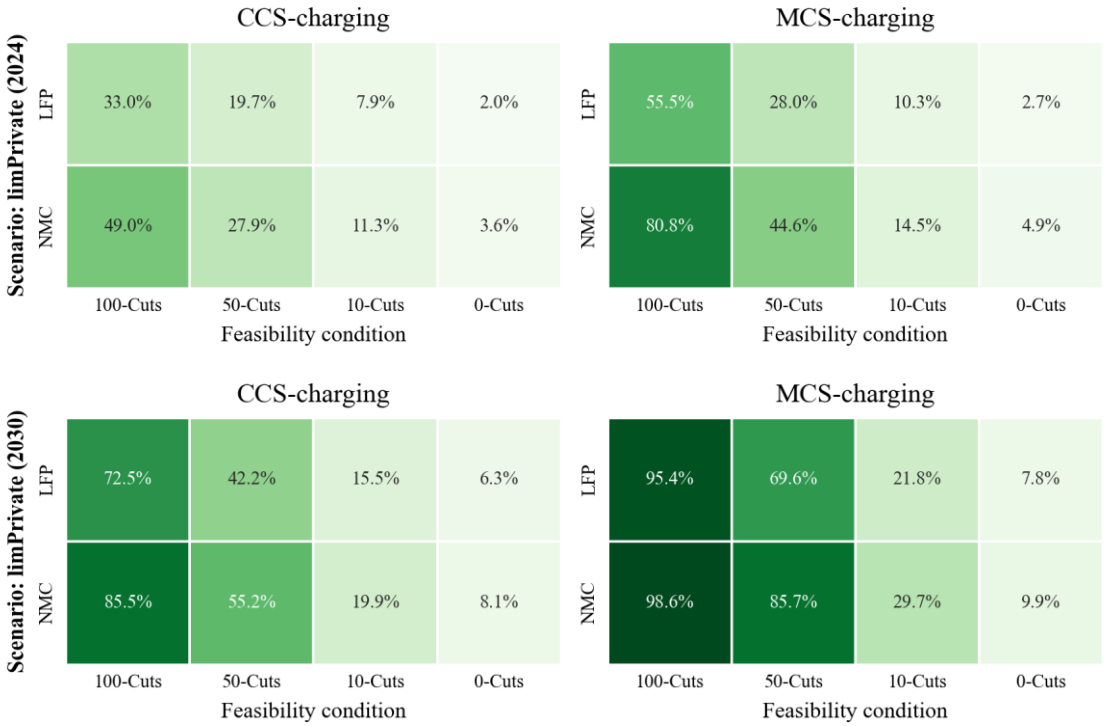

Figure 50: Results: Technical feasibility heatmaps for the limPrivate scenario

Scenario: onlyPrivate

Figure 51 visualizes analogous heatmaps of technical feasibility for the limPrivate scenario by 2024 (upper) and 2030 (lower). Corresponding figures for the utilized battery capacity (see **Figure S41**) and charging power (see **Figure S42**) are available in the Appendix. Note that *MCS-charging* is omitted by the scenario design.

Concerning technical feasibility, strict conditions (*0-cuts*) limit feasibility to around 2% even by 2030. The substantial decrease compared to the other scenario higlights the need for public charging, particularly with the assumed one-by-one replacement. In the most relaxed consideration (*100-cuts*), however, even *CCS-charging* allows electrifying a small share of schedules (12-18%) by 2024 and a medium share of schedules by 2030 (26-32%). Similar to the *limPrivate scenario*, NMC allows to electrify more schedules due to superior compensation with larger battery capacities toward the maximum. Specifically, average battery capacities by 2030 are increased by around 70 kWh for LFP and 85-110 kWh for NMC, with higher values attributed to *CCS-charging*. Concerning charging power, the relevance of charging at private locations with either 50 kW or 150 kW is roughly similar (both approximately 50%).

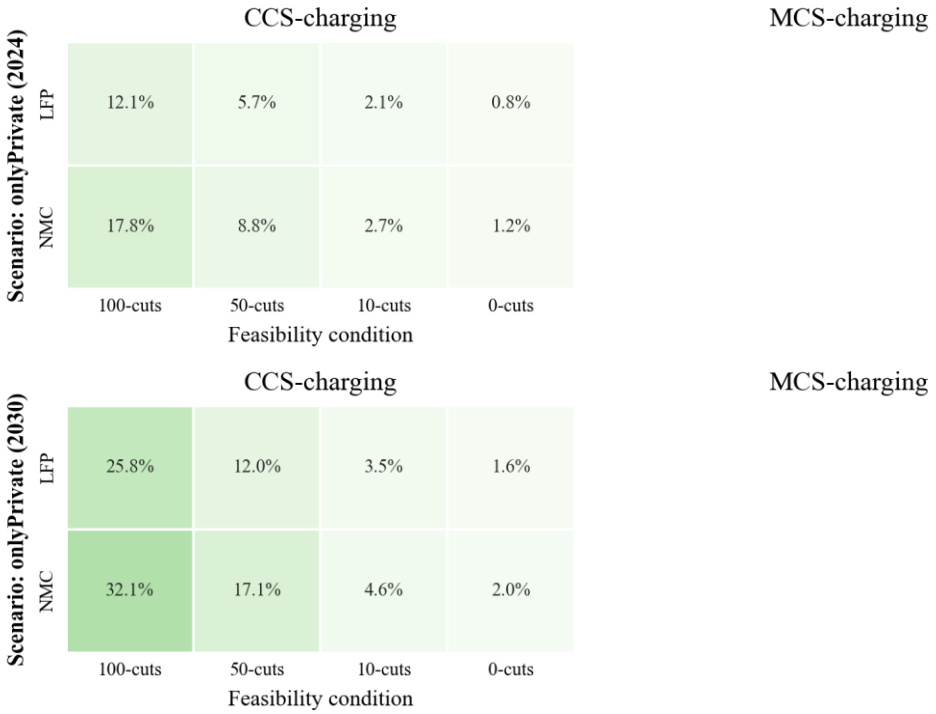

Figure 51: Results: Technical feasibility heatmaps for the onlyPrivate scenario

5.2.6 Interim summary

The previous section examined the technical feasibility of BETs. Initially, the maximum battery capacity was determined based on the available installation space in the truck chassis. The required battery capacities per schedule were subsequently examined versus the energy requirements via various metrics and charging infrastructure scenarios to highlight the wide range of options and associated pitfalls.

The results indicate that battery capacities of up to 650 kWh (LFP) and 750 kWh (NMC) are currently feasible without payload limitations, thanks to the two tons GVW bonus granted in Europe. Yet, BETs are likely to exhibit greater restrictions on cargo distribution to comply with axle load restrictions. The energy requirements vary by country and truck type, but particularly depend on the reference unit (day, trip, or trip segments). For all instances, relying solely on average values can be misleading and may not accurately reflect the true, variable energy requirements, which ultimately define the actual technical feasibility. However, when very extreme values are excluded, more consistent patterns emerge, and the most likely energy requirements converge toward similar ranges. Specifically, the mean daily energy requirements range from 200 to 600 kWh, with more intense days (95th percentile) calling for twice the amount of energy. Extreme trips might call for up to 800 kWh per section, whose end should allow for opportunity charging. However, 600 to 700 kWh (95th and 99th percentile) should be enough to secure almost all trips.

The SOC-based considerations indicate that electrifiying almost all operating schedules is feasible, particularly by 2030. The introduction of *MCS-charging* facilitates electrification with smaller batteries, safeguards many trips, and can significantly increase electrification compared to relying on *CCS-charging,* with even smaller batteries. However, if one-to-one replacement remains the norm so that operating schedules must be strictly observed, the technical feasibility of BETs will remain restricted. Should fast-charging infrastructure at private locations prove to be a limiting factor in the short- and long-term, larger batteries can partially offset this constraint and still enable large-scale to almost full electrification, with an advantage of NMC over LFP batteries. However, if there is no public charging infrastructure, the technical feasibility of BETs will remain low but still up to a third.

5.3 Profitability of battery-electric trucks

The profitability of a BET compared to a DT is assessed via a TCO analysis for each truck and its specific operating schedule. Battery capacities, derived from SOC-based considerations, are mainly between 450–750 kWh (2024) or 450–900 kWh (2030), with pronounced peaks around 550–750 kWh. As introduced in **Subchapter 4.4**, two dates of purchase (2024 and 2030) and three cost scenarios (*LOW*, *MEDIUM*, *HIGH*) are analyzed, affecting key factors such as truck purchase costs, tolling scheme, maintenance costs, and energy costs.

5.3.1 General TCO results

Figure 52 visualizes the TCO analysis in a 3x3 matrix across the cost scenarios for 2024 (blue) and 2030 (red), where BET costs are varied vertically (y-axis), and DT costs are varied horizontally (x-axis). Each point represents a specific truck and its kilometer-specific TCO as BET or DT.

By 2024, the comparative TCO advantages of BETs are highly sensitive to the cost scenario. Concerning the *MEDIUM-MEDIUM* scenario, BETs achieve parity or cost advantages versus DTs in around 30% of all schedules, with average costs of around 1.09 EUR_{2020} per km (IQR: 0.98-1.19 EUR_{2020} per km). In extreme comparisons (*LOW-HIGH* and *HIGH-LOW*), the respective technology in the *LOW* scenario clearly dominates the other. Under a *HIGH-HIGH* cost scenario for both technologies, BETs are favorable for only a fraction of the schedules (1.1%), with DTs remaining dominant. Under a *LOW-LOW* cost scenario for both technologies, there is almost a 50:50 split, with BETs as favorable technology for a notable share of the schedules (45%).

By 2030, BETs account for notable shares or even dominate, except for *HIGH* cost scenarios (left column). Concerning the *HIGH* cost scenarios, BETs are favorable for only a fraction of the schedules (below 3%), unless DT costs are high too (*HIGH-HIGH*: 33%). Concerning the other cost scenarios, BETs account for at least 40% (*LOW-MEDIUM*), with BETs as favorable and dominant technology (at least 88%) in the remaining five scenarios.

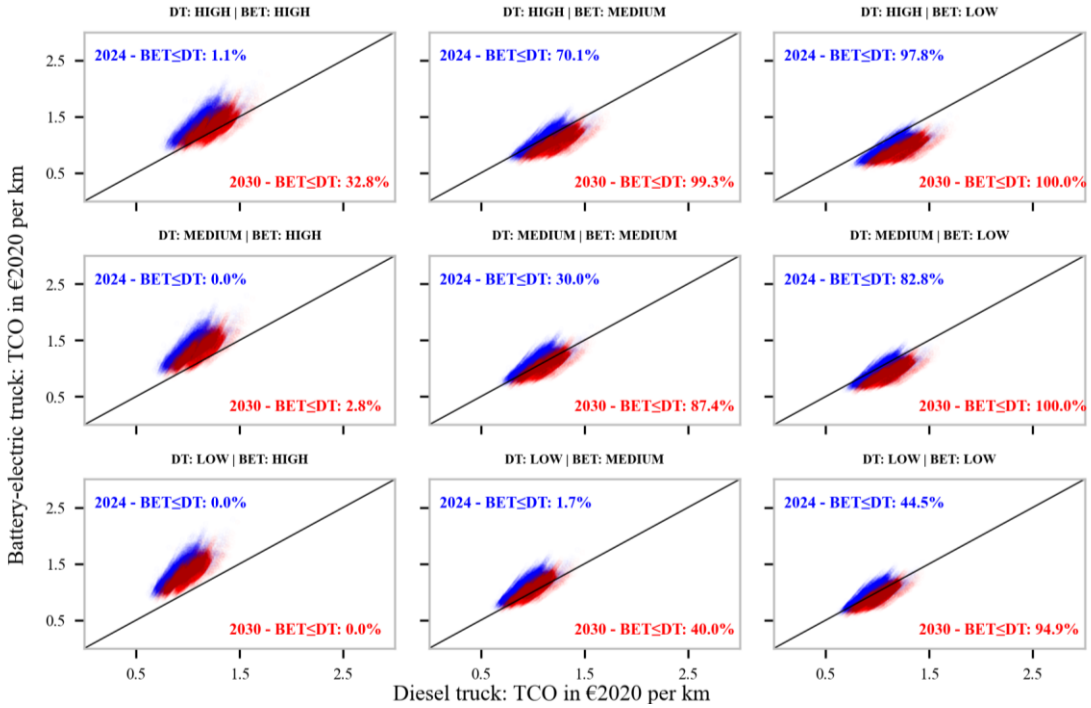

Figure 52: Results: TCO comparison for 2024 and 2030

5.3.2 Mileage dependency and break-even

Figure 53 visualizes the TCO difference of BETs versus DTs across the total first-user mileage in an analog 3x3 matrix across the cost scenarios for 2024 (blue) and 2030 (red). The reference lines – determined via LOWESS regression and extrapolated via suitable splines – assist in estimating the average European break-even mileage (within or beyond the sample).

By 2024, the break-even mileages and favorable BET operating windows are highly sensitive to the cost scenario. In scenarios with high BET advantage[6] (cf. **Figure 52**), break-even mileages range from 150,000 to 300,000 km. For scenarios with moderate relevance[7], break-even mileages rise to around 650,000–850,000 km. For the remaining scenarios where BETs are marginal or absent, break-even mileage requires at least around one million km.

By 2030, the break-even mileages are shifting towards lower values. In scenarios with high BET advantage[8] (cf. **Figure 52**), break-even mileages range from a few ten thousand kilometres to around 100,000 km. For scenarios with moderate relevance[9], break-even mileage rises to around 600,000 km. For the remaining scenarios where BETs are marginal or absent, break-even mileage still requires abov 950,000 km.

[6] 2024 (blue): *HIGH-MEDIUM (70%)*, *HIGH-LOW (98%)*, *MEDIUM-LOW (83%).*
[7] 2024 (blue): *MEDIUM-MEDIUM (30%) LOW-LOW (45%).*
[8] 2030 (red): *HIGH-MEDIUM (99%)*, *HIGH-LOW (100%)*, *MEDIUM-LOW (100%), MEDIUM-MEDIUM (88%), LOW-LOW (95%).*
[9] 2030 (red): *HIGH-HIGH (33%)*, *LOW-MEDIUM (40%)*.

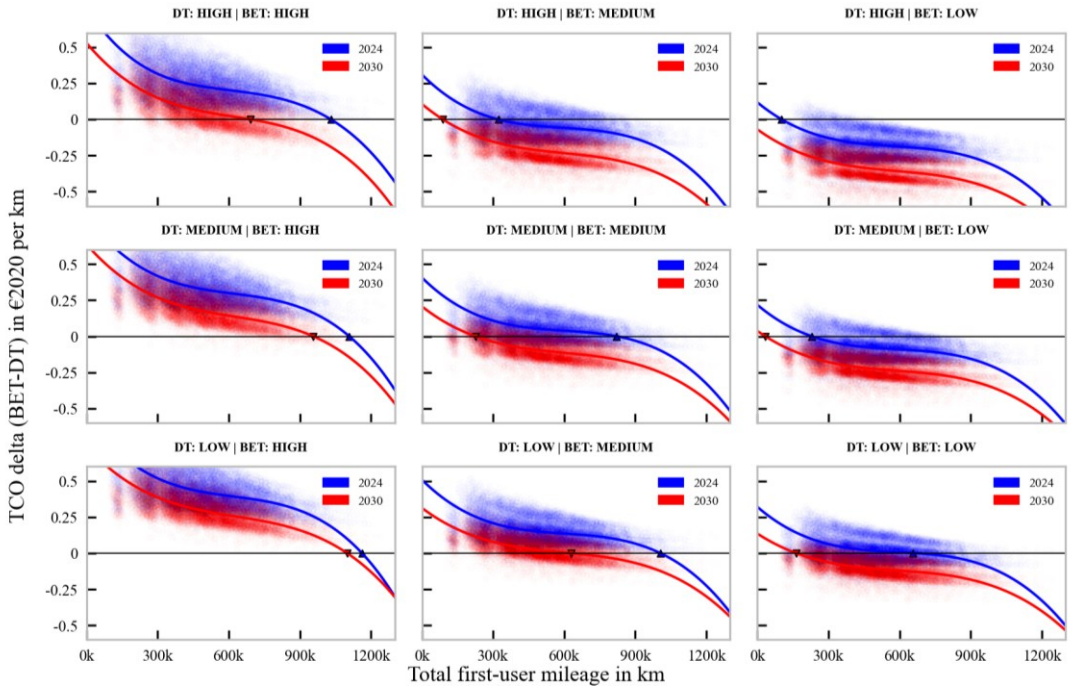

Figure 53: Results: Mileage dependency of the TCO differency by 2024 and 2030

5.3.3 Comparisons among battery chemistries

Figure 54 visualizes the relevance of LFP batteries (gray) versus NMC batteries (purple) in an analog 3x3 matrix across the cost scenarios for 2024 (left) and 2030 (right). The bars reflect the share of trucks (cf. **Figure 52**) where BETs achieve TCO parity or advantages.

By 2024, NMC achieves notable shares as it allows for larger battery capacities, averaging around 33% (range: 17-50%). In specific scenarios with high BET advantage (right column), NMC shares range from 23% to 34%. By 2030, the relevance of NMC is marginal, with LFP batteries dominating the market by accounting for over 95%.

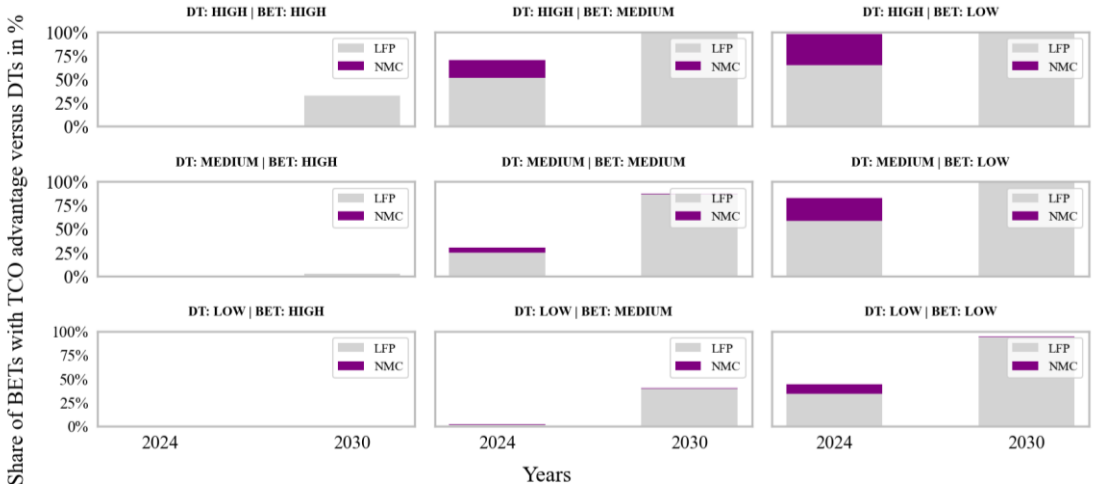

Figure 54: Results: Relevance of NMC and LFP by 2024 and 2030

5.3.4 Comparisons among countries

Figure 55 supplements the breakdown by country (y-axis) for 2024 (upper) and 2030 (lower) in an analog 3x3 matrix across the cost scenarios, with green bars indicating the relative share of BETs with TCO parity or advantage.

In general, country-specific findings are highly sensitive to the cost scenario, both by 2024 and 2030. In scenarios with high BET advantage (cf. **Figure 52**), BET prospects consistently improve across all countries, even up to full electrification. For scenarios with moderate relevance, BET prospects are more limited and regional differences become more apparent. For the remaining scenarios where BETs are marginal or absent, only a few isolated cases exhibit notable TCO prospects at the country level. However, based on the red-green distribution across scenarios and years – particularly in middle and right panels – three distinct country clusters emerge, which are highly correlated to differential costs of electricity and diesel (cf. **Figure S25**).

(1) *Top-performing* countries with most favorable TCO prospects (rather green-dominant) appear to be smaller markets such as Sweden (SE), Finland (FI), and Switzerland (CH), and closely followed by the United Kingdom (UK) and Belgium (BE).

(2) *Challenging* countries with higher economic hurdles (rather red-dominant) appear to be larger markets such as Italy (IT) and Austria (AT). Poland (PL), Germany (DE) and Spain (ES) may also be included in this category, albeit with better prospects compared to the other two countries. Overall, BET prospects appear to be most restricted in Italy, where relatively low DT toll rates and medium costs for diesel fuel add up to comparatively high electricity costs.

(3) The remainder of the European market – still involving smaller and major markets – may be classified as *average-performing* countries, showing partially green- or red-dominant mixes as well as similar patterns and TCO prospects across the scenarios and years.

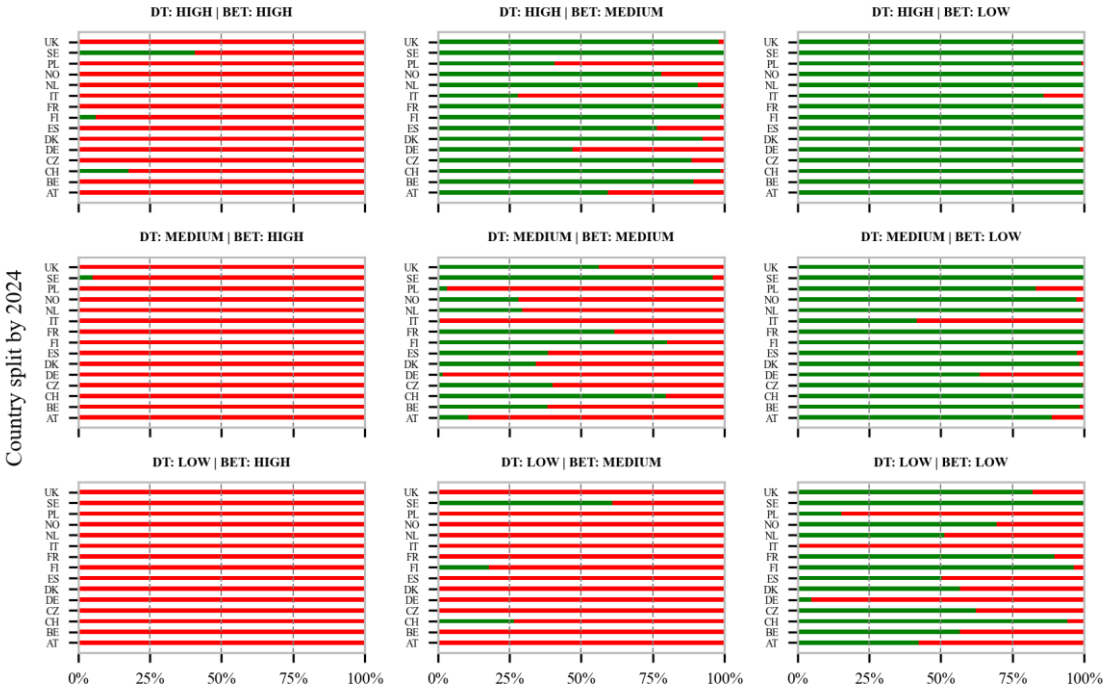

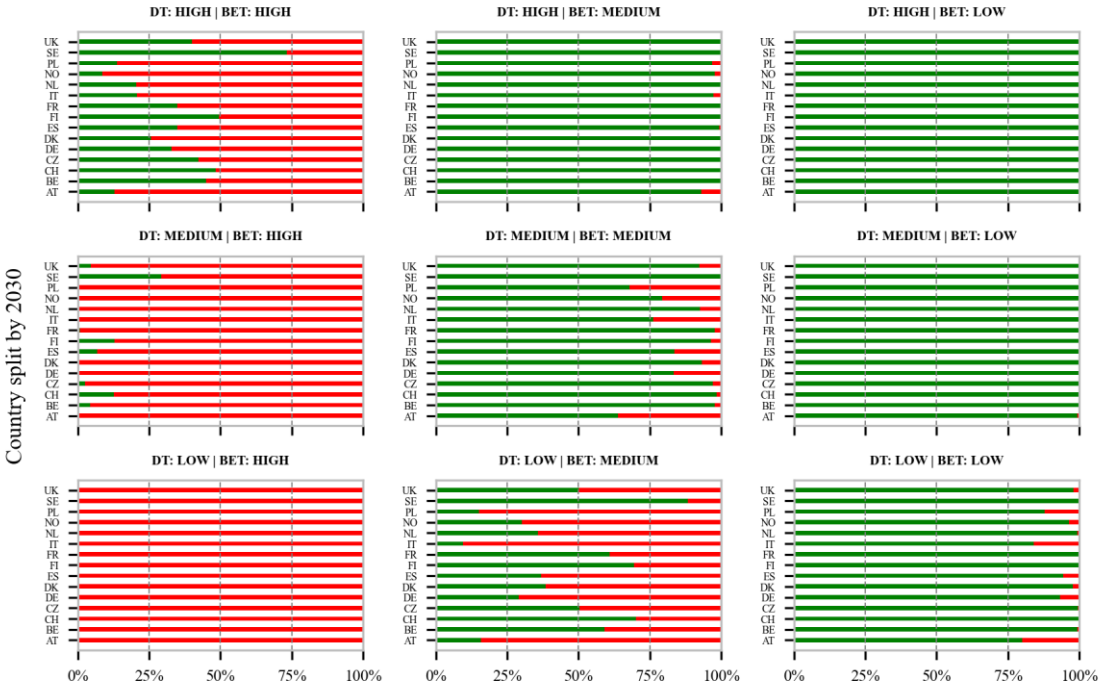

Figure 55: Results: 2024 TCO attractiveness by country for 2024 and 2030

5.3.5 Sensitivity toward battery capacity and costs of public charging

Figure 56 indicates the TCO sensitivity by 2024 in an analog 3x3 matrix across the cost scenarios, if battery capacities (x-axis) or the costs for public charging (y-axis) are varied by ±20%. Note that the figure only contains the results for LFP batteries by 2024 (gray colormap) and that there is an overlaying effect related to technical feasibility.

Comparing the shares of BETs with TCO parity or advantage indicates a greater sensitivity toward public charging costs than battery capacity, and most patterns are observable in middle (medium BET costs) and right panels (low BET costs). Specifically, variations in battery capacity (horizontally) yield changes of only a few percentage points, whereas variations in charging costs (vertically) can alter outcomes by as much as 30%.

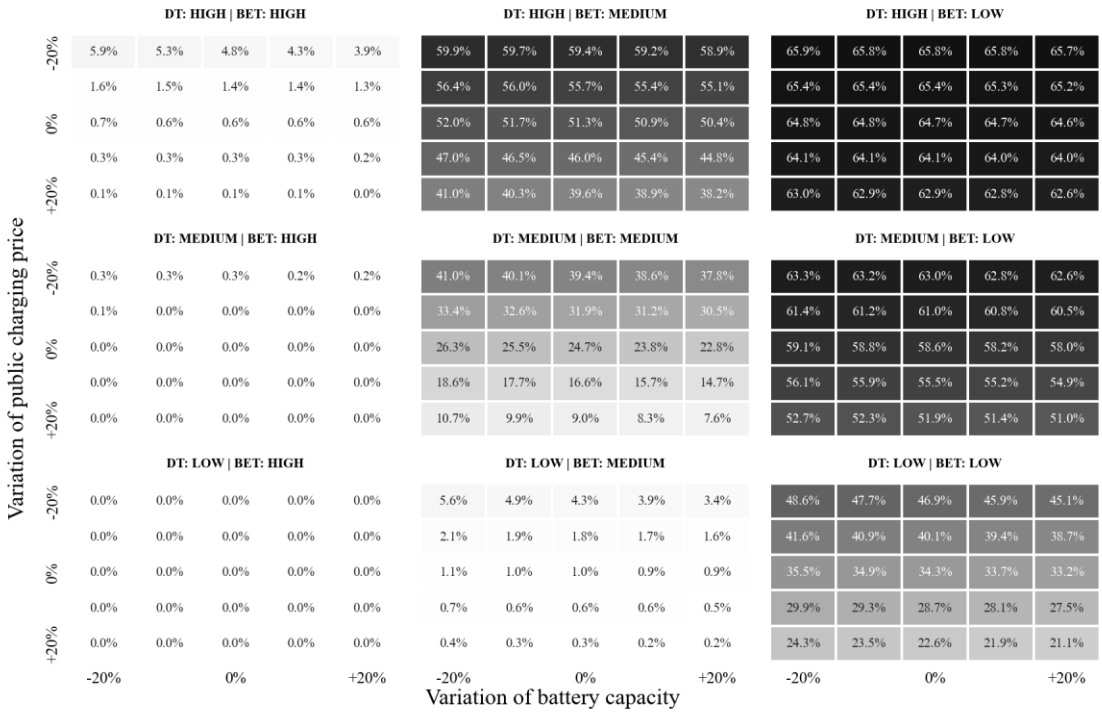

Note: The ratios and values from **Figure 52** or **Figure 54** would result from using the 0%–0% sensitivity across each panel, followed by incorporating the corresponding share of NMC batteries.

Figure 56: Results: 2030 TCO scenario comparison – specific costs

5.3.5 Interim summary

The previous section analyzed the profitability of a BET in comparison to a DT via TCO assessments for each truck along with its distinct operating schedule.

Across scenarios and years, three country clusters for economic prospects of BETs emerged: *top-performing*, *average-performing*, and *challenging*.

By 2024, the results strongly depend on the contrasting cost scenario, country, and total mileage. In general, BETs are nearing profitability in many countries and applications, so BETs can already comprise notable shares and compete at a similar or even lower TCO than DTs. However, DTs remain cost-competitive in most segments and usually comprise even higher shares than BETs. Accordingly, the required break-even mileages are rather in the medium-to-high range. Both NMC and LFP chemistries are relevant, with market shares roughly split one-third (NMC) to two-thirds (LFP). Higher sensitivity to costs of public charing than battery capacity implies that if costs for charging are high or uncertain, it is adviseable to choose larger batteries rather than relying on charging to avoid jeopardizing profitability.

By 2030, BETs are cheaper to operate than DTs for most operating schedules and less sensitive to the contrasting cost scenario, insofar as toll advantages are effective, diesel costs are increasing and charging costs are decreasing. Average European break-even mileages decline to a few tens or hundreds of thousands of kilometers. The results imply that LFP becomes the dominant battery chemistry, with NMC playing a subordinate role.

5.4 Infrastructure locations along the TEN-T network

5.4.1 Medium-dense network

Figure 57 visualizes the application of the greedy algorithm to the TEN-T network for a medium-dense (r=30 km) network of charging locations[10]. For TEN-T road sections, a maximum length of either 10 km or 5 km is applied, which results in around 14,800 (10 km) to 27,500 (5 km) individual road sections. The left panel visualizes all charging locations across Europe as purple x-markers. The right-hand panel supplementes a detailed view for Spain (ES) and Portugal (PT) either without (upper) or with the corresponding circular buffer (lower).

The medium-dense network comprises N_{30km}=2,343 locations to cover 97.99% of the TEN-T network (5 km segments)[11]. Depending on the attractiveness and spatial distribution of the locations, as well as the local TEN-T network density, overlaps between the buffer zones are smaller or larger. The panels also indicate that the locations are not uniformly spaced; instead, inter-site distances vary, with some locations positioned more closely together and others more widely dispersed.

The medium-dense network leaves a few road segments uncovered, mainly attributed to a lack of locations in the original dataset or deviations in the TEN-T dataset (as of 2021). Particularly in Spain, this concerns the route from Puertollano/Ciudad Real to Mérida, where the actual highway (E-903) remains uncovered as it is specified incorrectly.

[10]This network is inspired by the AFIR (TEN-T Core) and the densified 2030 network by Speth et al. (2022a).

[11]For 10 km segments, there are N_{30km}=2,313 locations to cover 98.05% of the TEN-T network.

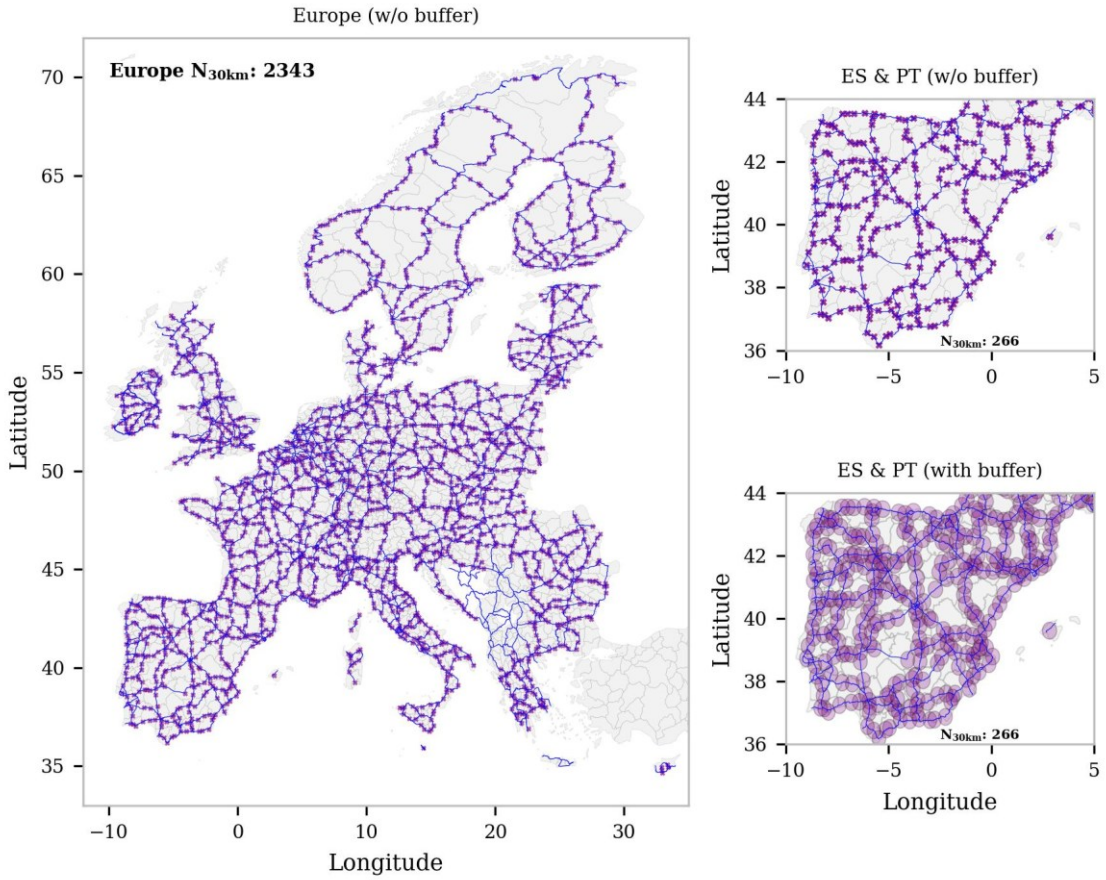

Figure 57: Results: Medium-dense charging network (30 km)

5.4.2 High-dense and wide-meshed networks

Other networks are visualized in the Appendix, similar to the previous figure. Specifically, this involves a high-dense (r=15 km)[12] network (see **Figure S43**) and a wide-meshed (r=50 km)[13] network (see **Figure S44**). In addition, **Figure S45** visualizes the computational time of the algorithm for different settings, demonstrating that an entire European network can be evaluated in a few minutes, with sensitivity toward buffer size and network resolution.

In general, the wide-meshed network comprises N_{50km}=1,415 locations to cover 99.01% of the TEN-T network (5 km segments). The high-dense network comprises N_{15km}=4,943 locations to cover 92.73% of the TEN-T network (5 km segments). The lower coverage of the high-dense network is attributable to the smaller buffer zone around locations. Country-specific location splits for all networks are provided in **Table S31**.

[12]Inspired by Shoman et al. (2023), who reported locations are required every 25-35 km.

[13]Inspired by the AFIR (TEN-T Compr.) and networks by Speth et al. (2022a) and Zähringer et al. (2024).

Across all networks, the lack of candidate locations becomes especially evident in less densely populated regions. Specifically, there are very few locations to cover roads in the northern Scandinavian regions, resulting in lower coverage of the European roads E-10, E-45, and E-75 that are located across Norway, Sweden and Finland.

5.4.3 Validation of the German networks

The derived networks are validated against the planned fast-charging network for trucks in Germany, which was released by the National Centre for Charging Infrastructure (NLL) and the Federal Ministry for Digital and Transport (BMDV). The current release comprises around 350 locations along the federal motorways (TEN-T highways and others), of which 220 are located at managed and 130 at unmanaged service areas. To improve comparability, nearby locations – such as locations on opposite sides of the road – are clustered using the MeanShift algorithm (r=5 km), resulting in N_{NLL}=248 clustered locations. In contrast, the original German dataset of truck parking locations contains N_{DE}=2,218 locations as potential candidates.

The derived networks involve $N_{DE,50km}$=134 (wide-meshed), $N_{DE,30km}$ =222 (medium-dense), and $N_{DE,15km}$ =507 (high-dense) selected locations across Germany. The map-based comparison is visualized in **Figure 58**, while **Figure S46** supplements the evaluation of the proximity to the nearest NLL locations via the aerial distance. Accordingly, the medium-dense network matches around 40% of the locations. The match varies from 25% (wide-meshed) to 75% (high-dense) network, and extreme mismatches arise from locations away from the TEN-T network.

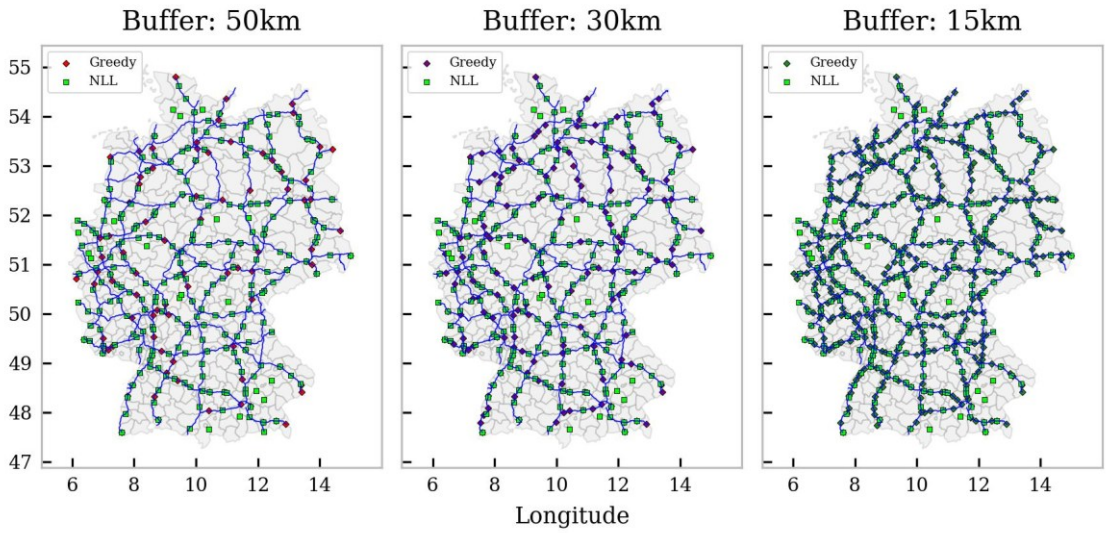

Figure 58: Results: Validation of the German charging network

5.4.4 Interim summary

The presented approach benefits from its traceability, practical feasibility, and speed. The number of locations in Europe ranges from N_{50km}=1,415 (wide-meshed), to N_{30km}=2,343 (medium-dense), and N_{15km}=4,943 (high-dense). These figures are consistent with other studies (cf. **Subchapter 2.4**). The reasonable consistency compared to planned truck fast-charging network in Germany indicates the basic feasibility and validity of the approach, and the high achievable level of coverage implies an adequate completeness of the underlying dataset.

5.5 Discussion

The previous chapter evaluated the technical feasibility and profitability of BETs in the European market through simulation and scenario analysis, and derived recommendations for charging infrastructure deployment. The integrated framework comprises five consecutive submodels and relies on multiple real-world datasets. Beyond data-related constraints (see **Subchapter 3.6**) and model-specific limitations (see **Subchapter 4.6**), the resulting findings and implications are subject to additional limitations and uncertainties that warrant discussion.

The techno-economic feasibility of BETs was evaluated with a sample of N=18,954 trucks, distributed across 15 key European countries (representing 88% of sales and 82% of stock) and four major truck classes (accounting for 80% of truck-related CO_2 emissions and 85% of heavy-duty sales). The analysis revealed both similarities and variations across countries and truck classes. However, note that many national peculiarities (such as locally differentiated axle load limits, weight limits, length restrictions, or weekend driving restrictions) were omitted. The total simulated mileage amounts to approximately 10.21 billion kilometers, or 1.86 billion kilometers annually (cf. **Subchapter 4.1.5**), so that this sample represents only a fraction of the European market. Thus, future studies might consider expanding coverage to additional countries (and in greater detail), truck classes, and larger sample sizes to improve accuracy and robustness.

In general, the findings on the relevance of charging infrastructure – both in terms of location and power levels – and battery chemistry advantages align with current literature, but there are differences.

LFP batteries seem most promising for almost all applications, especially if MCS charging becomes broadly available toward 2030 (cf. **Subchapter 2.2**). However, if high-power depot charging infrastructure is restricted, public fast charging remains limited or fleet operators continue striving for ever larger batteries, NMC batteries are favorable and allow for higher electrification. Given the prevailing uncertainties related to these aspects, the diversification of strategies pursued by truck manufacturers (cf. **Table 1**) appears reasonable.

The importance of slow charging (up to 50 kW) at private locations (especially overnight) is consistent with the literature (cf. **Subchapter 2.4**). However, the importance of fast charging up to MCS – for example in comparison to the results of Speth et al. (2024), which are based on daily profiles – is substantially increased owing to the more complex driving profiles lasting

several weeks/years. This emphasis the critical role of high-power charging infrastructure in facilitating large-scale electrification, while also implying that current simplified estimates may underestimate the demand for high-power charging infrastructure, particularly in the near term.

This thesis focused on the evaluation of BETs (first-user) and stationary plug-in charging, since this technological pathway is currently regarded as the most promising and very likely primary solution for most applications in Europe (Craglia 2022; Link et al. 2024b). However, there are alternative truck technologies that might help to cut emissions faster and decarbonize certain niche applications. Yet, the technological readiness and availability of FCETs, catenary electric systems, and renewable fuels is currently limited (Gnann et al. 2025). Hydrogen and renewable liquid fuels (biogenic and synthetic) are likely to also face scarcity and high prices (Ueckerdt et al. 2024). However, future studies might consider expanding to these alternatives too.

Electrified trailers (equipped with their own battery and e-axle) might accelerate truck decarbonization in general and increase BET ranges. While the same total weight and axle load restrictions apply, truck-related space restrictions are mitigated. However, these independent trailers currently require separate charging, which increases the demand for charging points.

Plug-in hybrid or extended-range hybrid trucks (equipped with a fuel-based range extender) might enable predominantly electric operation in urban or regular service while maintaining long-range capability without the need for frequent charging or compromising payload capacity. Plus, both technologies might partially mitigate constraints related to charging infrastructure and grid capacity. However, the synergetic interaction between the technologies must be optimized, and both technologies must be integrated within the limited truck space and accounted for in terms of cost and maintenance. While concepts and pre-series models exist (Scania.com 2025), neither concept is currently in the focus of European manufacturers.

Battery swapping represents an alternative to stationary plug-in charging, offering the potential for reduced vehicle downtime, lower purchase costs through battery-as-a-service models, mitigation of grid constraints, and improved battery lifecycle management. However, challenges remain, including the need for standardization across manufacturers, battery ownership concerns, on-site battery inventory and logistics management, and extensive station deployment. While battery swapping is actively pursued in China (electrive.com 2025), it is currently irrelevant in the European context.

Focusing on the first-user life might also overlook critical aspects of the entire service life through scrappage. While residual values of trucks and batteries are covered, future studies might consider expanding to the entire service life. However, this would require the consideration of cross-country trading schemes for used trucks within Europe and beyond. This aspect might increase uncertainty about residual values due to varying BET suitability across regions, but it also highlights the need for broad BET flexibility, particularly in the near term.

Central to all the results and findings are the assumed DT-BET analogy and one-by-one replacement of DTs with BETs, which highly influence the battery sizing, charging strategies, and

infrastructure requirements. This mainly concerns (1) the truck operating characteristics, (2) the battery installation space, and (3) the technical truck specifications.

(1) One-by-one replacement was adopted to ease the BET transition and emphasize practical flexibility without payload restrictions or additional stops, responding to current concerns of fleet operators and truck owners. However, adapted schedules with a few deviations – such as extra charging stops – can facilitate technical feasibility and safeguard a few extra-long tours or days. BET-optimized routing and trip replanning could further adjust current operational schedules to increase electrification and safe costs, as showcased by Engholm et al. (2025). Indeed, large amount of empirical data from China, published by Zhao et al. (2024), suggest that only 30% of the purchased BETs have replaced their DT predecessors one-by-one and instead operate in specialized operations. In contrast to the restrictive setting on payload and additional stops, both aspects could also be priced in via revenue losses or driver wages to reflect a rational utility-based purchase decision. However, this neglects driver comfort and non-salary related contentment while revenue losses might be difficult to price in, as not every transport process (single, bulk, or standing orders) can be skipped or billed proportionally.

The variance of DT operations – from day-to-day to week-to-week and beyond – substantially impacts the feasibility of BETs. However, the extent to which such variations could be reduced in the future remains questionable. This mainly concerns trip distances, successive trips, and cargo weights. For example, extralong daily or weekly distances exceed their respective average values by a factor of 1.5-2.5 (daily) or 1.3-1.8 (weekly). Most trips in Europe are constrained by volume rather than weight, with most trucks operating between 60% and 90% of their maximum capacity (see **Figure S5**). However, such weight statistics fail to trace the payload requirements over the entire service life, where the probability that trips require the maximum payload increases so that any restriction could be more critical. However, all these variations are based on DT tour data, which are neither limited by range nor weight and can be used interchangeably for any trip. Thus, fleet operators have limited incentives to optimize operational schedules. In contrast, optimized routing and trip planning for BET fleets with varying battery sizes might allow operators to select the best-suited truck for each trip, leading to less trip-related or daily variations per truck.

Recent logistics trends – such as growing e-commerce, regionalized supply chains, driver shortage, low driver retention, and changing trade flows – may shift transport from interregional and national long-haul trips toward decentralized hub-and-spoke distribution models and shorter supply chains with increased return-to-depot shuttle trips (Borlaug et al. 2021). These aspects should simplify overnight charging opportunities, reduce variations and increase predictability, which is all expected to ease the switch from DTs to BETs (Karlsson et al. 2023b). In contrast, autonomous trucking has the potential to seriously alter operational patterns, driving durations, and parking behavior, thereby influencing battery sizing, charging strategies, and infrastructure requirements.

(2) The battery packaging used predefined installation spaces subject to current DT specifications without massive design changes and compliance with current legal restrictions. Thus, potential installation zones are restricted such that accommodating larger batteries is challenging because of weight (primarily rigids) and volume (primarily tractors) constraints

without losing payload. New installation zones – such as those behind the driver cabin – have already been explored by some manufacturers. However, these can limit usability as overall length restrictions apply or special semitrailers are then needed. A purpose-built BET chassis could also create further installation spaces.
(3) The technical truck specifications of BETs were transferred from DTs. However, these specifications may differ, especially toward 2030 when the truck efficiency will be improved via road load reduction technologies (e.g., lower air drag and chassis curb mass). Plus, current BET powertrains are equipped with higher power than DTs, both in continuous power (to help compensate for the higher weight) and in peak power (about a factor of 1.5), which can particularly increase recuperation and thus lower energy consumption.

Building on this research and modeling, future work could examine the interaction of batteries and charging infrastructure in greater detail.

The SOC-based consideration follows a strategy that guarantees feasibility by maximizing the SOC (by suitable combinations of battery size and charging infrastructure) to ensure high reliability and availability of the BET. However, future studies could evaluate further objectives, such as minimizing total costs, maximizing the share of private charging, minimizing the required battery capacity, or minimizing the amount of energy charged. The latter might use model predictive control or backward iteration. All these varied objectives can seriously alter battery sizing, charging strategies, and infrastructure requirements.

Other approaches, such as system dynamics, might be used to better assess reactions among the players. Optimization problems could be used with single or multiple objectives such as maximizing the number of electrified schedules, the total BET sales revenue, and total revenue from fast charging. These objectives could depend on correspoding global decision variables, such as an optimal battery price or optimal fast charging price, and represent the fleet-level as well as different stakeholders that may have conflicting priorities. For example, policymakers may prioritize maximizing electrification to accelerate the decarbonization, where each truck owner may react to global prices by choosing a battery capacity to minimize TCO. Truck manufacturers may prioritize maximizing revenue from BET and battery sales. CPOs may prioritize maximizing revenue from their charging locations. To illustrate the interaction, lowering battery prices likely increase electrification but could increase (higher total battery sales) or decrease (lower revenue per battery) the total revenue of truck manufacturers, and vise versa. Likewise, increasing fast charging prices might improve revenue for CPOs but reduce electrification or causes truck owners to choose larger battery sizes to avoid public charging, and vice versa.

6 Summary and conclusion

Low-carbon road freight transport is pivotal in mitigating global warming, yet electrifying heavy-duty trucks is challenging due to high technical requirements and cost competitiveness. Battery electric trucks are very likely the most promising pathway and primary technology for decarbonizing the European truck fleet (EU-27, EFTA, and the UK), with an increasing number of studies confirming their technical feasibility and profitability in almost all applications. However, no truck is similar to another, nor are its operations. This truck market heterogeneity and variety of operations complicate generalized findings that rely on single day assessments and archetypal utilization patterns so that truck owners continue to cite concern toward BET prospects for their specific usage.

This thesis assesses the techno-economic feasibility of BETs for the European truck market around 2025 to 2030 via simulation and scenario-based evaluation to resolve potential shortcomings related to this heterogeneity and variety of truck operations. Accordingly, the results support truck owners, engineers, and policymakers by clarifying truck operations and requirements, analyzing techno-economic trade-offs for truck purchase, evaluating battery designs based on European operations, and guiding the strategic deployment of charging infrastructure across Europe. To this end, five consecutive models are developed, each of which is based on an extensive set of real-world data to ensure practical relevance and cover truck market heterogeneity.

(1) The novel probabilistic driving profile simulation allows to derive operational schedules via multivariate data sampling techniques, Bayesian Network logic, and respective multivariate probability distributions. This allows to simulate the acticity of any truck over its first user service life, with schedules reflecting all trip-related operations in minute-by-minute resolution. These activities involve driving times, taking breaks or rest periods at long trips, time spent at customer locations (intermediate stops), times for loading and unloading of cargo, idling between tours, or inactivity between consecutive days. Differences such as trip distances and patterns or transported cargo types and payload weights are distinguished for each country and different truck classes, from medium to heavy and ultra-heavy. This relies on two main datasets: Weekly trip data comprise about 3 milion trucks and cover all major European member states (EU-27, EFTA, and the UK) over ten years. Multiweek operating data with detailed daily timestamps comprise about 2,000 trucks that traveled over 10 million kilometers in Central Europe.

(2) The truck energy simulation determines the energy consumption for each trip in the defined operating schedule by considering the defined truck characteristics, regional information such as ambient temperature, payload weight, and trip information (duration, speed, and distance). Specifically, the model initially simulates the energy consumption (BET and DT) using a distance-based longitudinal-dynamics model and complementary submodels to integrate ambient conditions and energy demand from auxiliary units, with standard European mission profiles as

a reference. Final values per trip are then determined from pre-calculated simulation runs via look-up tables and interpolation to enhance runtime. This two-step approach aims to facilitate a fast yet accurate estimation of energy consumption and enables a consistent and comparable assessment among DTs and BETs. Technical truck data rely on recent diesel truck specifications by over 800,000 trucks from European certification, covering ten different truck classes in several configurations and all European manufacturers.

(3) The battery model focuses on the electrical performance of the battery system in interaction with the truck energy model, considering temperature and SOC dependence and calculating the charge/discharge efficiency in relation to the C-rate. This involves three automotive-grade battery cells with two different cell chemistries and three cell formats. The battery sizing anticipates aging effects by means of overdimensioning to ensure the technical feasibility of each schedule and its specific energy requirements, with a focus on cyclic aging and deducing an SOC operating window based on the number of expected FEC. Plus, SOC-based feasibility considerations involve three scenarios (*unlimited*, *limDepot*, and *privateOnly*) to evaluate the electrification potential via the interaction of battery sizing and charging strategy. The battery packaging uses the available installation space in the truck chassis to install batteries and determine chemistry-specific maximum capacities, subject to weight constraints and axle load limits. The technical data rely on datasheet information from 80 truck models with 380 configurations by different truck types and manufactures.

(4) The cost model evaluates the profitability of battery-electric trucks versus their diesel counterpart using total cost of ownership (TCO) calculations, which cover all relevant costs over the vehicle service life from vehicle purchase until resale and differentiate between capital and operational expenditures. Two dates of purchase (2024 and 2030) are analyzed via three cost scenarios (*LOW*, *MEDIUM* and *HIGH*), which affect mainly the levels and evolution for truck purchase costs, tolling scheme, maintenance costs, and energy costs. Regionalization relies on country-specific road tolls as well as country-specific energy costs for diesel and electricity, which are projected based on historical price information and via a probabilistic model. The most likely costs for central powertrain components are determined via meta-forecasting using over 200 original sources. Truck residual values rely on stated prices from over 5,000 real-world diesel trucks, covering all European manufacturers and several countries.

(5) The add-on infrastructure model focuses on charging locations and costs. Charging infrastructure costs are calculated based on the levelized cost of charging and forwarded to the cost model to determine charging costs. The location model refines a previously published dataset of real-world truck stop locations and finally determines N=13,323 candidate locations via filtering and geospatial clustering. The attractiveness of each location involves several criteria, such as proximity to the TEN-T network and urban nodes, amenities and service level on site, local truck flows and parking frequency, and existing electric infrastructure. Using an adopted Greedy algorithm and specific buffer zones around locations, the most attractive locations are selected to establish a public charging network that covers the whole TEN-T network with as few locations as possible.

The most relevant findings and recommendations are as follows:

Variations in the operational schedule – from trip to trip, day to day, and week to week – often lead to a few extralong or heavy-loaded operations that substantially impact the technical feasibility of battery-electric trucks and complicate the replacement of diesel trucks. Typically, extralong trips or extreme days can exceed the average performance by a factor of 1.5-2.5 and even up to 3.5. The maximum weekly mileage can still exceed the average weekly mileage by a factor of 1.3-1.8 and even up to 2.5. In contrast, increasing tour predictability and return-to-depot concepts paired with lower variability are expected to substantially ease this replacement. However, the extent to which such variations could be reduced in the future remains questionable.

Country-specific conditions substantially impact the techno-economic feasibility of battery-electric trucks, leading to considerable differences among European countries. Technical feasibility, energy consumption, and battery sizing are affected by the truck type and trailer configuration, distances traveled per trip and the total mileage, trip speed patterns, cargo types and weights, and ambient temperatures. Consequently, the technical feasibility is particularly hampered in Nordic countries with extraheavy truck configurations. The differential costs between charging and diesel as well as toll regulations have the strongest impact on profitability.

Battery capacities of up to 650 kWh (LFP) and 750 kWh (NMC) can be installed in current diesel truck chassis without payload limitations. Limited packaging space, total weight and axle load limits restrict tractors so that batteries need to have both high volumetric and gravimetric energy densities. Rigid trucks usually have more packaging space available. BETs can also comply with axle load and total weight limits, thanks to the GVW bonus of two tons granted in Europe, but exhibit a higher restriction on cargo distribution, which is likely limiting their flexibility. Chemistry advances might facilitate up to around 800 kWh (LFP) and 900 kWh (NMC) by 2030, which corresponds to a range of about 1,000 km, in line with manufacturers' expectations.

Energy requirements vary, but electrifying most operations is feasible with 500-700 kWh of battery capacity, which is available as of today. Energy requirements particularly depend on the reference (per day, trip, or trip segment), where relying solely on average values can be misleading and may not accurately reflect the actual, variable energy requirements. However, daily energy requirements average around 200 to 600 kWh, with more intense operations calling for twice the amount of energy, which then requires intermediate charging. Similar conclusions have been drawn in other studies based on simplified assumptions, which implies this detailed and schedule-based approach is generally not needed.

The introduction of MCS facilitates electrification with smaller batteries and can significantly increase electrification compared with relying on CCS charging. While private slow-charging infrastructure constitutes the backbone for BET operations (50-75%), many consecutive trips call for high-power charging at depots or nearby. The relevance of MCS-charged energy increases with driving performance to around 15% to 25%. Should fast-charging infrastructure at private locations prove to be a limiting factor in the short and long term, larger batteries can partially

offset this constraint and still enable large-scale to almost full electrification, depending on schedule adjustments. However, public charging infrastructure will be required to safeguard European truck operations and reach electrification rates greater than one third.

Minor deviations from current schedules drastically increase electrification and reduce the required battery capacities by up to 150 kWh. Typically, a few additional stops are sufficient to make all operations over the entire service life feasible. However, if one-to-one replacement remains the norm so that operating schedules must be strictly observed, the technical feasibility of BETs will likely remain limited, and larger batteries will be required.

If the charging costs are uncertain but likely high, it is adviseable to choose larger battery capacities rather than relying on more frequent charging. Typically, the TCO is more sensitive to charging costs than battery costs, so that this strategy, if the payload allows, should avoid jeopardizing profitability, which could then benefit Ni-rich battery chemistries.

LFP batteries seem most promising for almost all applications due to their aging resistance, larger SOC operating window, and better tolerance to high C-rates. With MCS charging available during driving breaks or consecutive trips, LFP batteries overcompensate for the higher gravimetric energy density of NMC batteries and facilitate similar electrification rates with smaller battery capacities. However, if high-power depot charging is restricted, public fast charging remains limited, trucks are heavily loaded, or fleet operators continue striving for larger batteries to increase flexibility or avoid reliance on public charging infrastructure, NMC batteries are potentially favorable and allow for higher electrification. However, reaching low battery system costs toward 100 $€_{2020}$ per kWh seems more likely for LFP than NMC, as it does not require critical raw materials such as nickel and cobalt.

The novel driving profile and power profile generation allows to derive truck-specific operational schedules and trace their activity in a minute-by-minute resolution. While this thesis focused on truck and batteries, future studies could analyze the grid impact, analyze load shift potentials, or evaluate the prospects of bidirectional charging and vehicle-to-grid applications (system-level perspective). A refined examination could also adjust the probabilistic driving profile simulation by modifying parameter dependencies and distributions to reflect case studies (individual perspective).

Despite several individual models, the large number of real-world datasets, and stochastic modeling approaches with broad ranges of parameter values, the results seem robust and plausible yet are still subject to uncertainty, data bias, and the scenario assumptions. Specifically, this concerns the assumed analogy to diesel trucks, where future studies might explore the effects of adjustments for battery-electric trucks, such as optimized routing or replanning of tours. Plus, future studies might extend this thesis by exploiting other charging strategies or optimization problems for specific cases to examine the interaction of battery and charging in greater detail.

Appendices

A1: Supplemental information to Chapter 2

Table S1: Sales figures for medium and heavy-commerical trucks in Europe

Country	Short	2020	2021	2022	2023	Average Share
Austria	**AT**	5,676	6,680	7,079	8,008	1.9%
Belgium	**BE**	7,516	8,181	8,566	10058	2.4%
Bulgaria	**BG**	2,055	3,073	3,705	4,197	0.9%
Croatia	**HR**	895	1,284	1,508	2,048	0.4%
Cyprus	**CY**	85	83	94	159	0.0%
Czech Republic	**CZ**	7,355	8,679	8,971	10,408	2.5%
Denmark	**DK**	3,724	4,384	4,872	4,973	1.3%
Estonia	**EE**	493	772	940	872	0.2%
Finland	**FI**	3,430	3,536	3,339	3,942	1.0%
France	**FR**	42,699	45,030	44,567	49,613	13.0%
Germany	**DE**	74,779	78,981	76,218	94,820	23.1%
Greece	**EL**	561	568	676	726	0.2%
Hungary	**HU**	3,275	4,476	5,707	6,359	1.4%
Ireland	**IE**	1,936	2,271	2,203	2,654	0.6%
Italy	**IT**	20,276	24,762	25,688	28,628	7.0%
Latvia	**LV**	716	1,379	1,672	1,868	0.4%
Lithuania	**LT**	4,188	7,982	9,941	10,662	2.3%
Luxembourg	**LU**	991	1,054	1,425	1,832	0.4%
Malta	**MT**	N/A	N/A	N/A	N/A	N/A
Netherlands	**NL**	10,527	11,742	13,291	16,139	3.6%
Poland	**PL**	20,672	32,684	34,876	35,472	8.7%
Portugal	**PT**	3,585	4,264	4,707	6,922	1.4%
Romania	**RO**	4,112	6,389	7,115	8,489	1.8%
Slovakia	**SK**	1,943	2,868	3,160	3,939	0.8%
Slovenia	**SI**	1,380	1,925	2,306	2,526	0.6%
Spain	**ES**	19,245	20,805	23,462	28,685	6.5%
Sweden	**SE**	5,502	5,910	6,024	7,184	1.7%
United Kingdom	**UK**	40,164	42,372	45,859	53,271	12.9%
Iceland	**IS**	203	275	287	423	0.1%
Liechtenstein	**LI**	N/A	N/A	N/A	N/A	N/A
Norway	**NO**	5,993	6,035	5,603	6,490	1.7%
Switzerland	**CH**	3,579	3,565	3,716	4,482	1.1%
Total		**297,555**	**342,009**	**357,577**	**415,849**	

Note: Based on ACEA press releases (2021-2024) for new commercial vehicle registrations.

Table S2: Stock figures for medium and heavy-commerical trucks in Europe

Country	NUTS	2019	2020	2021	2022	Average Share
Austria	**AT**	73,336	73,378	74,473	75,171	1.0%
Belgium	**BE**	139,136	138,415	137,152	137,467	1.9%
Bulgaria	**BG**	124,937	127,895	130,076	132,576	1.8%
Croatia	**HR**	47,536	48,621	51,072	52,581	0.7%
Cyprus	**CY**	13,016	13,329	13,710	13,825	0.2%
Czech Republic	**CZ**	186,881	185,602	186,905	187,035	2.6%
Denmark	**DK**	42,586	42,266	43,227	43,483	0.6%
Estonia	**EE**	39,848	40,106	41,014	41,156	0.6%
Finland	**FI**	95,141	94,691	94,771	92,633	1.3%
France	**FR**	609,822	607,789	616,886	620,593	8.5%
Germany	**DE**	951,481	952,285	964,696	990,403	13.3%
Greece	**EL**	226,913	225,216	225,571	224,719	3.1%
Hungary	**HU**	96,109	94,306	95,964	96,272	1.3%
Ireland	**IE**	48,311	47,273	48,158	48,875	0.7%
Italy	**IT**	946,393	949,967	960,284	969,488	13.2%
Latvia	**LV**	33,739	33,116	33,144	33,367	0.5%
Lithuania	**LT**	67,111	69,780	73,019	80,424	1.0%
Luxembourg	**LU**	12,300	13,784	13,966	14,266	0.2%
Malta	**MT**	6,941	7,105	7,226	7,365	0.1%
Netherlands	**NL**	160,608	157,638	158,108	161,829	2.2%
Poland	**PL**	1,150,493	1,184,677	1,234,074	1,276,594	16.5%
Portugal	**PT**	132,500	134,000	135,000	135,800	1.8%
Romania	**RO**	296,489	346,911	348,517	366,693	4.5%
Slovakia	**SK**	81,083	78,959	83,341	82,867	1.1%
Slovenia	**SI**	37,285	37,674	37,951	38,463	0.5%
Spain	**ES**	607,020	566,362	571,867	581,631	8.1%
Sweden	**SE**	84,153	84,333	85,554	86,060	1.2%
Iceland	**IS**	7,954	8,011	8,254	8,502	0.1%
Liechtenstein	**LI**	N/A	N/A	N/A	N/A	N/A
Norway	**NO**	86,069	87,638	87,791	86,105	1.2%
Switzerland	**CH**	59,634	61,231	61,410	60,207	0.8%
United Kingdom	**UK**	607,998	727,913	740,568	758,841	9.5%
Total		**7,072,823**	**7,240,271**	**7,363,749**	**7,505,291**	

Note: Based on ACEA Vehicle in Use Reports (2021-2024) and Eurostat figures (https://doi.org/10.2908/TRAN_R_VEHST).

Table S3: Truck market segmentation according to the European CO2 regulation

Class	VECTO group	VECTO subgroup	Axle configuration	Body type	GVW (t)	Regulated	Sales share
N2	**Light trucks**		4x2	Rigid	3.5–5	-	4.00%
	Medium trucks				5–7.4	Yes	4.92%
	1	**1**		Rigid or tractor	7.5–10	Yes	1.47%
	2	**2**			>10–12	Yes	3.78%
N3	**3**	**3**	4x2	Rigid or tractor	>12–16	Yes	3.82%
	4	**4-UD**		Rigid	>16	Yes**	0.35%
		4-RD				Yes**	7.09%
		4-LH				Yes**	1.71%
	5	**5-RD**		Tractor		Yes**	0.60%
		5-LH				Yes**	46.73%
	6	**6**	4x4	Rigid	7.5–16	-	1.10%
	7	**7**			>16	-	0.92%
	8	**8**		Tractor		-	0.76%
	9	**9-RD**	6x2	Rigid	all weights	Yes**	5.47%
		9-LH				Yes**	7.00%
	10	**10-RD**		Tractor		Yes**	0.02%
		10-LH				Yes**	2.57%
	11	**11**	6x4	Rigid		Yes	1.75%
	12	**12**		Tractor		Yes	0.52%
	13	**13**	6x6	Rigid		-	0.48%
	14	**14**		Tractor		-	0.02%
	15	**15**	8x2	Rigid		-	0.53%
	16	**16**	8x4			Yes	3.49%
	17	**17**	8x6/8			-	0.39%
	Others		All others	Rigid or tractor		Yes	0.50%

Note: Sales shares depending on 2019/2023 values based on Ragon et al. (2022a)
** Covered in the original CO2 regulation with reference year 2019.

Table S4: General maximum permissible weights and axle limits in Europe

Country	Axle limit		Rigids		Road trains		Articulated trucks	EMS
	Non	Driven	2 axles	3 axles	4 axles	5+ axles	5+ axles	
AT	10	11.5	18	26	36	40/44		
BE	10	12	19	26	39	44		
BG	10	11.5	18	26	36	40		
CH	10	11.5	18	26	36	40		
CY	10	11,5	18	25	36	40	40/44	
CZ	10	11.5	18	26	32	48		
DE	10	11.5	18/19	26/27	36	40/44		
DK	10	11.5	18	24/26	38	44/50/56		**Yes**
EE	10	11.5	18	26	35/36	40/44		
EL	7/10	13	19	26	33/38/40	40/42	40/42/44	
ES	10	11.5	18	25/26	36/38	40	40/42/44	
FI	10	11.5	18	28	36	44/56/60/64-68/69-76		**Yes**
FR	12/13	12/13	19	26	32/38	40/44		
HR	10	11.5	18	25/26	36	40	40/44	
HU	10	11.5	18/20	25/26	36/38	40	40/42/44	
IE	10	10.5/11.5	18	26	36	42	40/44/46	
IS	10	11.5	18	26	36	40	44	
IT	12	12	18	26	40	44		
LI	10	11.5	18	26	36	40		
LT	10	11.5	18	25/26/27	36	40/42	40/44	
LU	10	11.5/12	19	26	44	44		
LV	10	11.5	18	25/26	36	40	40/42/44	
MT	10	11.5	18	25	36	40	40/44	
NL	10	11.5	21.5	21.5-30.5	40	50		**Yes**
NO	10	11.5	19	26	39	46-50		**Yes**
PL	10	11.5	18	26	36	40		
PT	10	12	19	26	37/38	44	44/60	**Yes**
RO	10	11.5	18	25/26	36	40	40/42/44	
SE	10	11.5	18	25/28	38	40	44	**Yes**
SI	10	11.5	18	25/26	36	40	40/44	
SK	10	11.5	18	26	40	40		
UK	10	11.5	18	26	36	40/44		

Note: The permissible maximum weight varies according to different conditions: The distance between the axles, number of driven axles, type of suspension, tire configuration (twin- or single tires), the vehicle is operating in national or international traffic, performing intermodal transport operations, road types, regions within one country, or type of goods. A more differentiated country overview is available via the International Transport Forum website: https://www.itf-oecd.org/weights-and-dimensions

Table S5: General maximum permissible dimensions in Europe

Country	Lorry or Trailer	Road Train	Articulated Truck	EMS
AT	12	18.75	16.50	
BE	12	18.75	16.50	
BG	12	18.75	16.50	
CH	12	18.75	16.50	
CZ	12	18.75	16.50	
DE	12	18.75	16.50	
DK	12	18.75	16.50	
EE	12	18.75	16.50	**Yes – 25.25m**
EL	12	18.75	16.50	
ES	12	18.75	16.50	
FI	18	34.50	23	
FR	12	18.75	16.50	**Yes – 25.25m**
HR	12	18.75	16.50	
HU	12	18.75	16.50	
IE	12	18.75	16.50	
IT	12	18.75	16.50	
LI	12	18.75	16.50	
LT	12	18.75	16.50	
LU	12	18.75	16.50	
LV	12	18.75	16.50	
MT	12	18.75	16.50	
NL	12	18.75	16.50	
NO	12	19.50	17.50	
PL	12	18.75	16.50	**Yes – 25.25m**
PT	12	18.75	16.50	**Yes – 25.25m**
RO	12	18.75	16.50	
SE	24	24	24	**Yes – 25.25m**
SI	12	18.75	16.50	
SK	12	18.75	16.50	**Yes – 25.25m**
UK	12	18.75	16.50	

Note: A more complex country overview is available via the International Transport Forum website: https://www.itf-oecd.org/weights-and-dimensions

A2: Supplemental information to Chapter 3

Appendix to Section 3.1

Table S6: ERFT microdata: Annual split

Year	# Truck records	#Trip records	#Goods records
2011	426,115	5,157,063	3,471,240
2012	407,029	4,845,083	3,285,850
2013	409,931	4,783,748	3,388,582
2014	418,521	4,907,588	3,488,401
2015	412,213	4,801,319	3,440,641
2016	411,940	4,725,653	3,416,381
2017	404,337	4,701,676	3,394,289
2018	394,808	4,648,105	3,333,913
2019	401,649	4,626,890	3,356,157
2020	374,374	3,620,000	2,994,774
Total	**4,060,917**	**46,817,125**	**33,570,228**

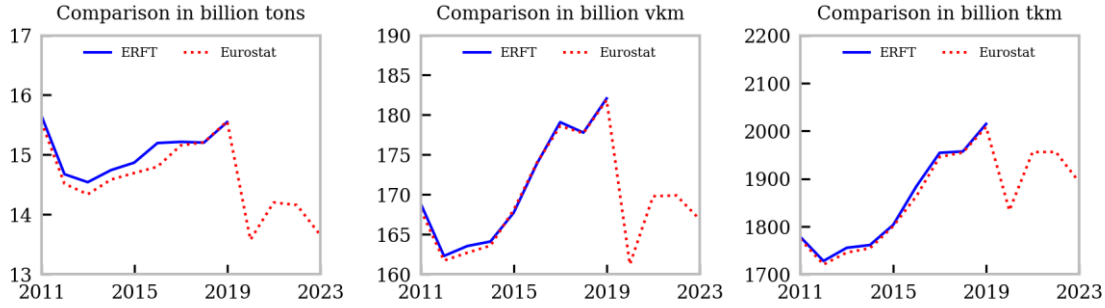

Note: Eurostat data taken from the *road_go_ta_tott* dataset (DOI: 10.2908/ROAD_GO_TQ_TOTT), comprising the EU-27 and EFTA member states and the UK (until 2019).

Figure S1: ERFT microdata: Validation with Eurostat statistics

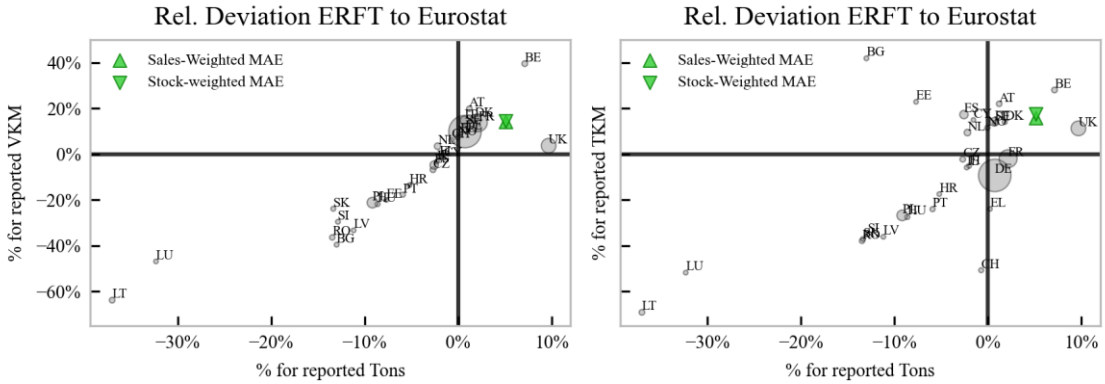

Note: Markersize correlated to the sales share per country. MAE as abbreviation for Mean Absolute Error

Figure S2: ERFT microdata: Accuracy of the country labelling approach

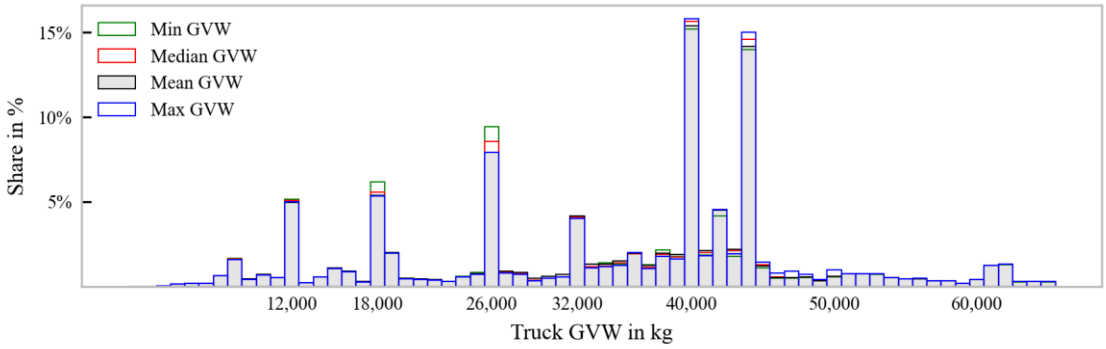

Seven main truck categories (Class-N3):

(1) Rigid trucks with a GVW of 18/19 tons (2-axle configuration)
(2) Rigid trucks with a GVW of 26/27 tons (3-axle configuration)
(3) Rigid trucks with a GVW of 32 tons (4-axle configuration)
(4) Tractor-trailer and rigid-trailer combinations at 36/38 tons (four axles)
(5) Tractor-trailer and rigid-trailer combinations at 40 tons (five+ axles)
(6) Rigid-trailer and tractor-trailer combinations at 42/44 tons in intermodal operations (5 or more axles)
(7) EMS-like combinations with a total GVW of 50 tons or 60/65 tons (8 or more axles)

Figure S3: ERFT microdata: Accuracy of the GVW truck class labels

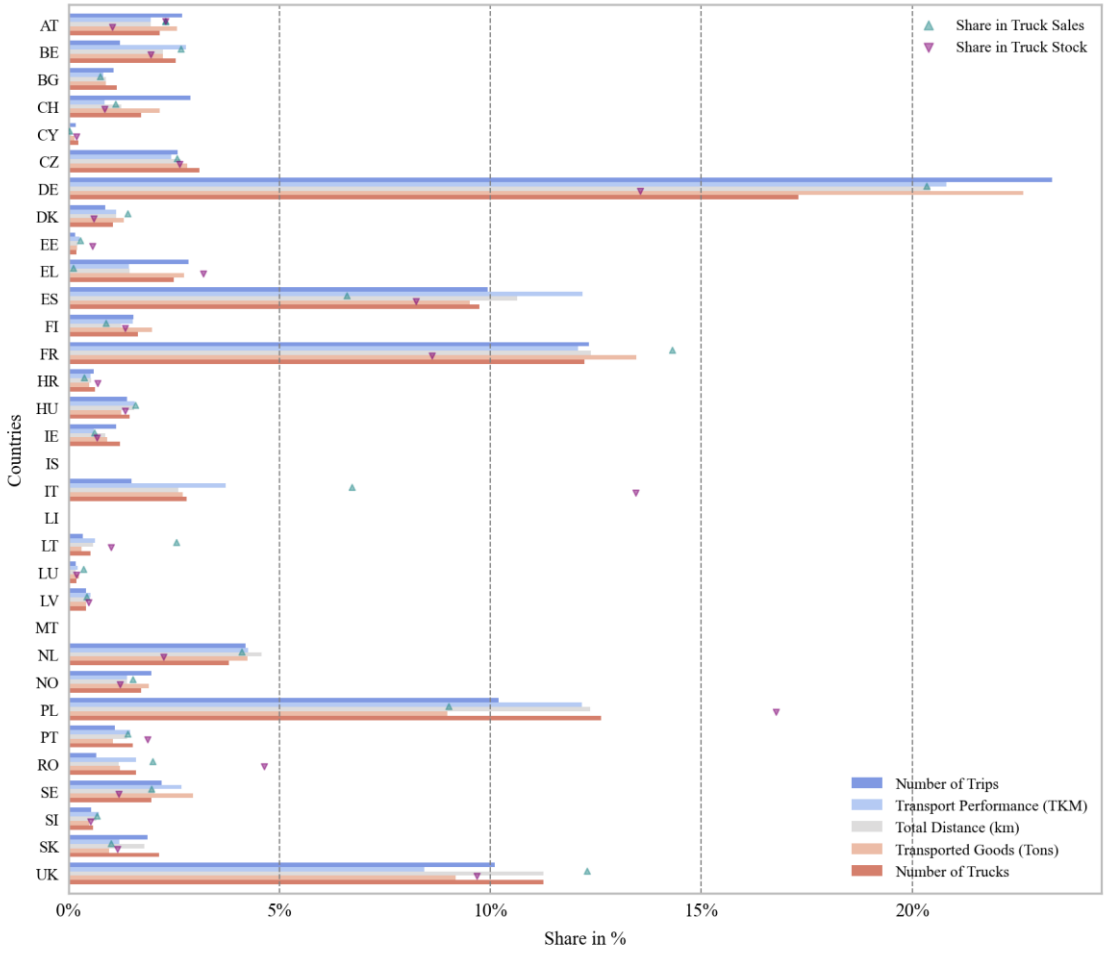

Figure S4: ERFT microdata: Composition and coverage by country

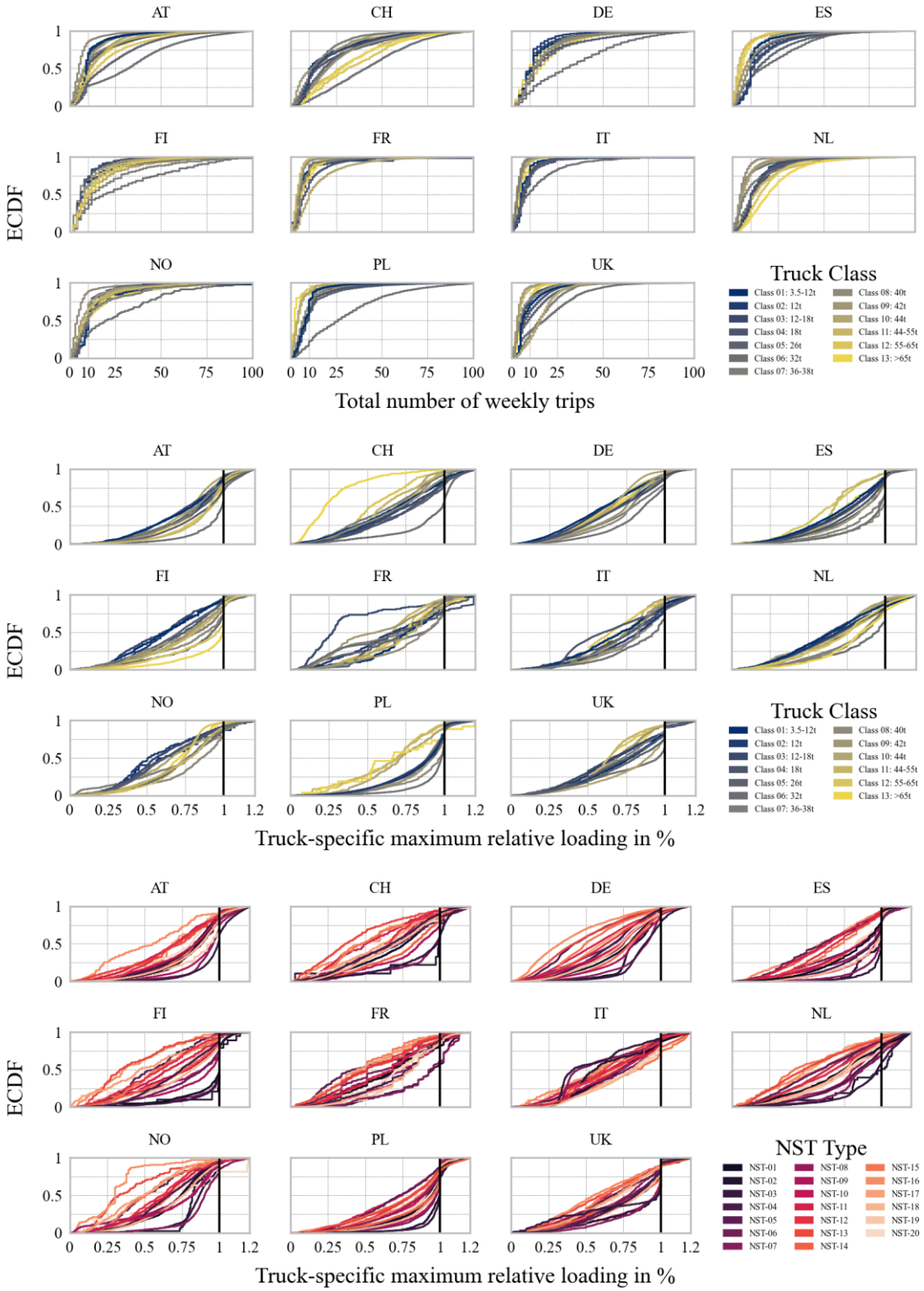

Figure S5: ERFT microdata: Distribution of weekly trips and payload statistics

Appendix to Section 3.2

Table S7: Tour data: Data collection and overview

Label	Fleet	Data source	#Trucks	Year	Temporal coverage	Geographic coverage	Tour types
Fleet 1	SINGLE	TPS schedules	224	2021	1 month	Germany	UD, RD
Fleet 2	SINGLE	FMS trip reports	9	2023	1 month	Germany	MIXED
	SINGLE	FMS trip reports	14	2023	1 month	Germany	MIXED
Fleet 3	SINGLE	FMS trip reports	10	2020	12 months	Central Europe	MIXED
	SINGLE	FMS trip reports	5	2019/20	6 months	Central Europe	RD, LH
	SINGLE	FMS trip reports	5	2019/20	13 months	Central Europe	LH
	MIXED	Data logger time-series	4	2020-2022	<16 months	Central Europe	RD, LH
	MIXED	FMS trip reports	38	2022	2 months	Central Europe	RD, LH
DT-CARGO [1]	MIXED	Data logger time-series	53	2021/22	7 months	Central Europe	Mixed
KiD [2]	MIXED	Survey-based logbook	1,192	2009/10	Days	Germany	Mixed
Fleet 4	SINGLE	TPS schedules	346	2023	3 months	Germany	UD, RD

Abbreviations: TPS (Tour Planning Software), FMS (Fleet Management Software),
UD (Urban Delivery), RD (Regional Delivery), LH (Long-Haul)

[1] Reference: Balke et al. (2023)

[2] Reference: Wermuth et al. (2012)

Appendix to Section 3.3

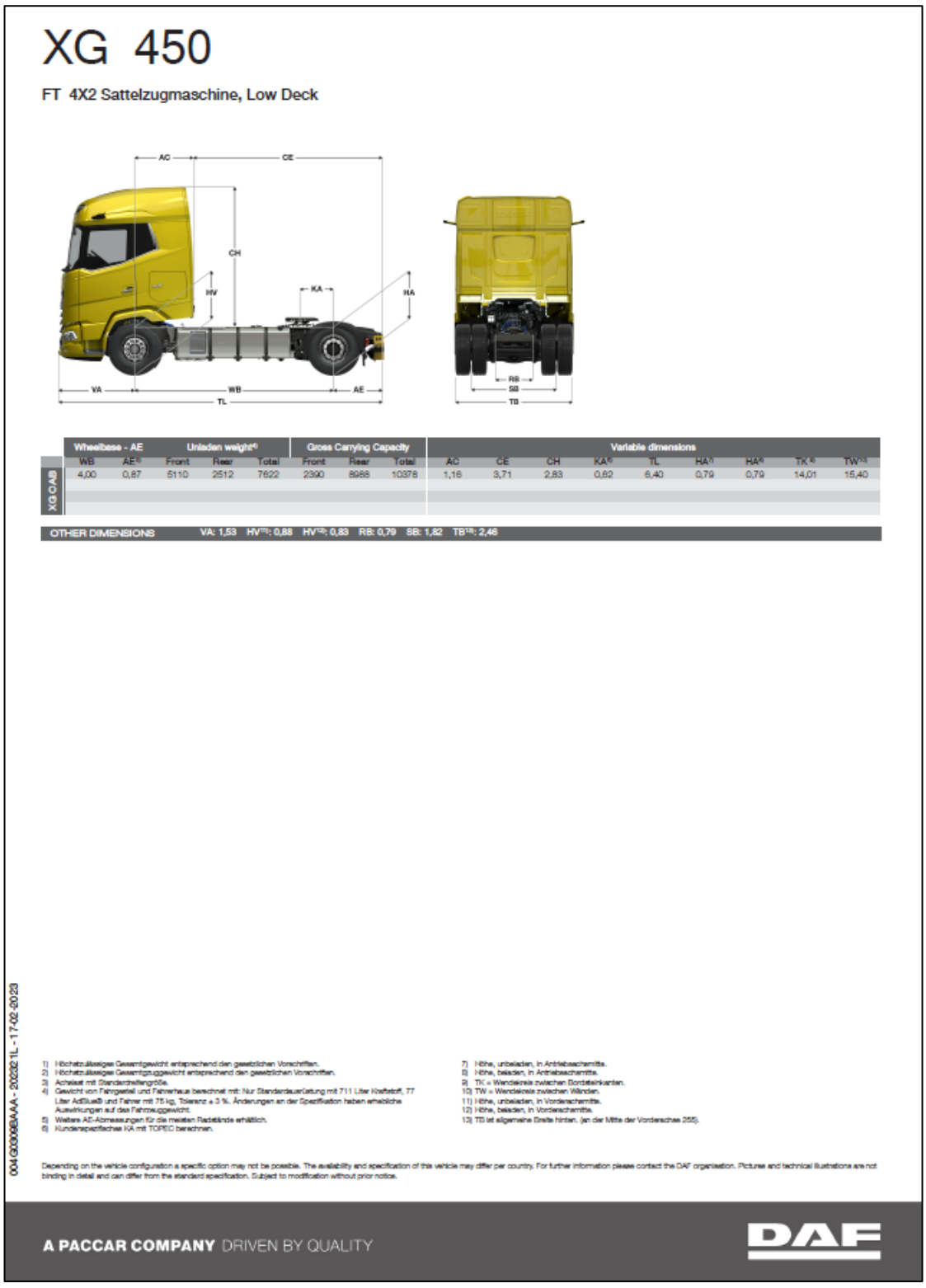

XG 450

FT 4X2 Sattelzugmaschine, Low Deck

	Wheelbase - AE		Unladen weight[4]			Gross Carrying Capacity			Variable dimensions								
	WB	AE[5]	Front	Rear	Total	Front	Rear	Total	AC	CE	CH	KA[6]	TL	HA[7]	HA[8]	TK[9]	TW[10]
XG CAB	4,00	0,87	5110	2512	7622	2390	8988	10378	1,16	3,71	2,83	0,62	8,40	0,79	0,79	14,01	15,40

OTHER DIMENSIONS VA: 1,53 HV[11]: 0,88 HV[12]: 0,83 RB: 0,79 SB: 1,82 TB[13]: 2,46

1) Höchstzulässiges Gesamtgewicht entsprechend den gesetzlichen Vorschriften.
2) Höchstzulässiges Gesamtzuggewicht entsprechend den gesetzlichen Vorschriften.
3) Achslast mit Standardreifengröße.
4) Gewicht von Fahrgestell und Fahrerhaus berechnet mit: Nur Standardausrüstung mit 711 Liter Kraftstoff, 77 Liter AdBlue® und Fahrer mit 75 kg, Toleranz ± 3 %. Änderungen an der Spezifikation haben erhebliche Auswirkungen auf das Fahrzeuggewicht.
5) Weitere AE-Abmessungen für die meisten Radstände erhältlich.
6) Kundenspezifisches KA mit TOPEC berechnen.
7) Höhe, unbeladen, in Antriebsachsmitte.
8) Höhe, beladen, in Antriebsachsmitte.
9) TK = Wendekreis zwischen Bordsteinkanten.
10) TW = Wendekreis zwischen Wänden.
11) Höhe, unbeladen, in Vorderachsmitte.
12) Höhe, beladen, in Vorderachsmitte.
13) TB ist allgemeine Breite hinten. (an der Mitte der Vorderachse 255).

004G0309BAAA - 202321L - 17-02-2023

Depending on the vehicle configuration a specific option may not be possible. The availability and specification of this vehicle may differ per country. For further information please contact the DAF organisation. Pictures and technical illustrations are not binding in detail and can differ from the standard specification. Subject to modification without prior notice.

A PACCAR COMPANY DRIVEN BY QUALITY

DAF

Datasheet ID: 004G0309BAAA - 202321L - 17-02-2023)
Available at: https://www.daftrucks.de/de-de/lkw/produktspezifikationsblatter

Figure S6: Truck data: Manufacturer datasheet (screenshot)

Appendix to Section 3.5

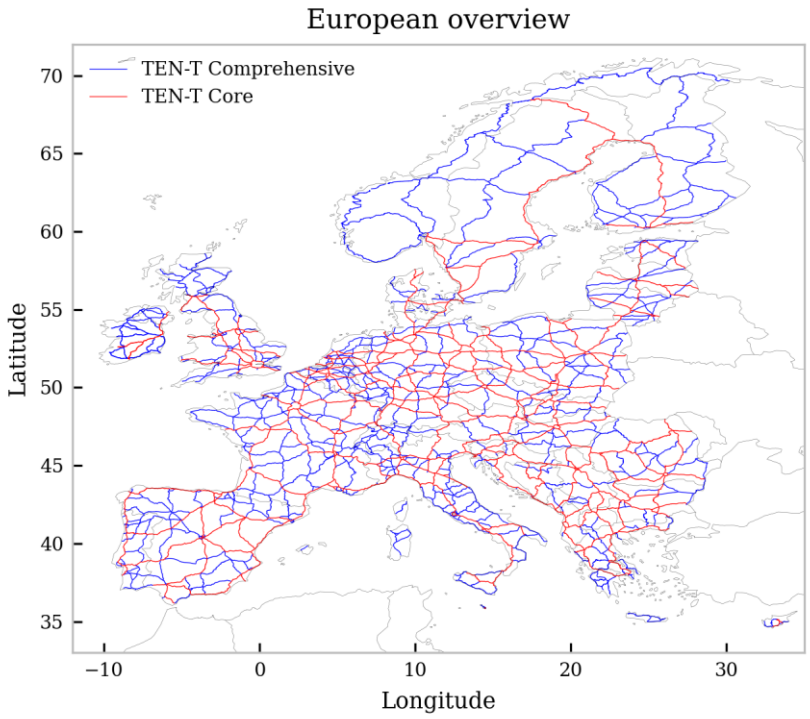

Figure S7: Charging infrastructure: Visualization of the TEN-T road network

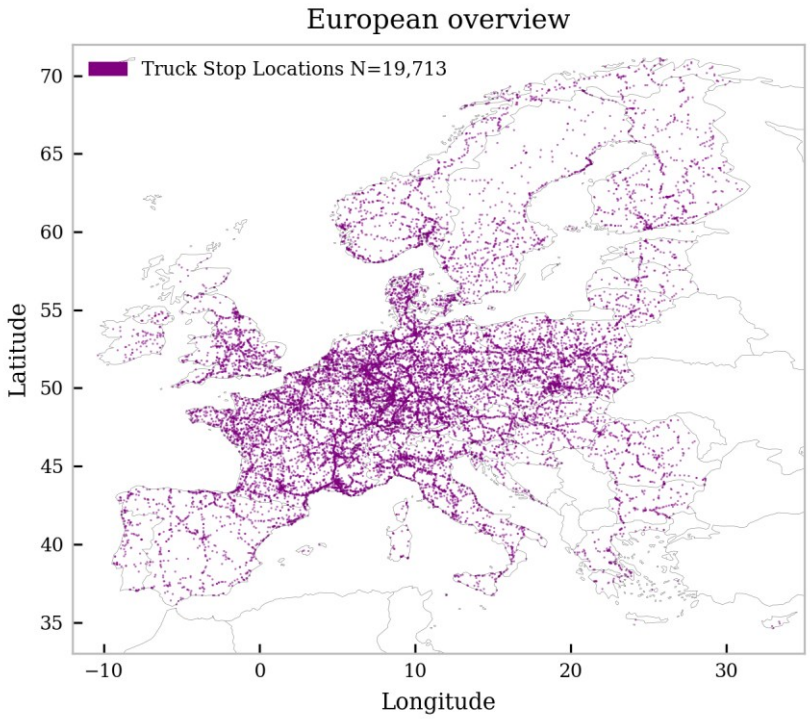

Figure S8: Charging infrastructure: Visualization of truck parking locations in Europe

A3: Supplemental information to Chapter 4

Appendix to Section 4.1

Table S8: Driving profile simulation: Sales shares per VECTO group

Country	VECTO Group																	
	0	1	2	3	4	5	6	7	8	9	10	11	12	13	14	15	16	17
AT	3.6	0.6	2.5	3.5	7.8	41.2	1.7	0.3	0.2	25.1	2.9	2.0	0.6	0.5	0.0	0.9	5.8	0.6
BE	3.2	0.5	2.9	2.0	28.4	40.1	1.4	0.5	0.3	13.7	2.1	1.4	0.4	0.4	0.0	0.3	2.3	0.3
BG	1.8	0.3	0.6	4.6	12.6	53.3	1.5	0.8	0.6	14.0	3.2	2.2	0.6	0.6	0.0	0.4	2.4	0.3
CH	7.9	1.3	1.7	3.8	3.9	53.1	1.6	0.9	0.7	10.1	3.3	2.2	0.7	0.6	0.0	1.0	6.4	0.7
CY	11.2	1.9	3.6	5.4	16.5	31.4	2.6	0.6	0.5	12.1	1.6	1.1	0.3	0.3	0.0	1.3	8.8	1.0
CZ	8.3	1.3	5.2	2.8	5.9	50.8	2.3	0.6	0.4	13.8	3.6	2.4	0.7	0.7	0.0	0.1	0.8	0.1
DE	1.9	0.3	5.3	3.5	6.5	55.4	2.5	0.9	0.6	12.4	2.7	1.8	0.5	0.5	0.0	0.6	3.9	0.4
DK	1.3	0.2	2.3	1.7	6.8	41.5	1.1	0.4	0.2	26.4	4.0	2.7	0.8	0.7	0.0	1.2	7.8	0.9
EE	1.8	0.3	0.7	0.8	2.5	27.4	0.5	0.1	0.1	46.5	9.2	6.2	1.9	1.7	0.1	0.0	0.2	0.0
EL	8.9	1.5	3.2	7.0	12.6	40.7	2.9	0.8	0.6	10.1	2.2	1.5	0.4	0.4	0.0	0.9	5.7	0.6
ES	3.2	0.5	2.4	2.2	6.2	65.7	1.3	1.3	1.0	6.3	3.4	2.3	0.7	0.6	0.0	0.4	2.3	0.3
FI	16.8	2.1	1.6	2.9	6.3	12.4	1.3	0.1	0.1	39.7	6.8	4.6	1.4	1.3	0.1	0.3	2.1	0.2
FR	0.2	0.0	0.3	1.1	7.5	66.3	0.4	0.3	0.2	15.0	3.6	2.4	0.7	0.7	0.0	0.2	1.1	0.1
HR	7.0	1.2	4.1	5.7	8.0	41.9	2.8	0.1	0.1	20.7	3.4	2.3	0.7	0.6	0.0	0.2	1.1	0.1
HU	1.8	0.2	2.7	2.9	12.4	51.0	1.6	0.9	0.3	8.6	1.5	1.0	0.3	0.3	0.0	1.8	11.5	1.3
IE	45.9	7.4	2.1	3.1	4.5	22.1	1.5	0.2	0.1	9.2	1.9	1.3	0.4	0.3	0.0	0.0	0.1	0.0
IS	N/A	N/A	N/A	N/A	N/A	N/A	N/A	N/A	N/A	N/A	N/A	N/A	N/A	N/A	N/A	N/A	N/A	N/A
IT	2.7	0.4	3.2	3.0	48.0	16.6	1.8	0.3	0.2	18.6	0.9	0.6	0.2	0.2	0.0	0.4	2.7	0.3
LI	0.0	0.0	0.0	0.6	4.1	76.2	0.2	1.0	0.7	6.0	3.8	2.5	0.8	0.7	0.0	0.4	2.6	0.3
LT	2.1	0.3	3.7	2.1	7.1	64.8	1.7	1.2	0.9	7.8	3.3	2.2	0.7	0.6	0.0	0.2	1.1	0.1
LU	0.4	0.1	5.2	1.2	3.9	57.1	1.8	0.3	0.2	16.3	3.2	2.2	0.6	0.6	0.0	0.8	5.5	0.6
LV	1.3	0.2	1.2	1.1	8.1	67.5	0.6	1.0	0.8	9.6	3.8	2.6	0.8	0.7	0.0	0.1	0.6	0.1
MT	N/A	N/A	N/A	N/A	N/A	N/A	N/A	N/A	N/A	N/A	N/A	N/A	N/A	N/A	N/A	N/A	N/A	N/A
NL	3.7	0.6	3.2	1.1	5.2	21.6	1.2	0.3	0.2	43.4	9.2	6.2	1.8	1.7	0.1	0.1	0.4	0.0
NO	0.9	0.1	1.6	3.4	13.1	37.0	1.4	0.1	0.1	30.6	4.5	3.0	0.9	0.8	0.0	0.3	1.9	0.2
PL	7.8	1.3	5.7	1.8	4.1	57.0	2.2	1.1	0.9	8.9	3.1	2.1	0.6	0.6	0.0	0.4	2.4	0.3
PT	8.8	1.4	1.2	3.2	8.0	51.3	1.3	1.0	0.5	5.5	2.0	1.4	0.4	0.4	0.0	1.6	10.8	1.2
RO	2.0	0.3	1.2	1.2	29.9	43.8	0.7	0.5	0.3	11.6	2.5	1.7	0.5	0.5	0.0	0.4	2.5	0.3
SE	0.7	0.1	2.6	3.9	8.5	13.9	1.9	0.2	0.1	47.9	8.2	5.5	1.6	1.5	0.1	0.4	2.6	0.3
SI	2.9	0.5	1.6	2.6	7.6	59.0	1.2	0.6	0.3	15.1	3.5	2.3	0.7	0.6	0.0	0.2	1.0	0.1
SK	57.8	0.8	2.5	1.1	2.2	25.5	1.0	0.3	0.2	4.3	1.4	0.9	0.3	0.3	0.0	0.2	1.1	0.1
UK	13.6	2.3	2.0	2.4	12.3	36.0	1.3	0.1	0.1	17.2	1.9	1.3	0.4	0.3	0.0	1.1	7.0	0.8
Total	**8.9**	**1.5**	**3.8**	**3.8**	**9.2**	**47.3**	**1.1**	**0.9**	**0.8**	**12.5**	**2.6**	**1.8**	**0.5**	**0.5**	**0.0**	**0.5**	**3.5**	**0.4**

Note: All values as percentages

Table S9: Driving profile simulation: Country-specific truck ages

	Age			Ratio			
Country	Mean (UW)	Mean(W)	Q75	Mean (UW)	Mean (W)	Q75	Ø
AT	5.99	5.99	9.00	1.05	1.13	0.97	1.05
BE	5.71	6.71	8.00	1.00	1.00	1.09	1.03
BG	12.03	11.60	16.00	2.11	2.00	1.88	2.00
CH	5.77	5.78	8.00	1.01	1.00	0.94	0.98
CY	12.73	8.93	16.00	2.24	2.00	1.44	1.89
CZ	9.57	9.83	14.00	1.68	1.75	1.59	1.67
DE	4.29	4.44	6.00	0.75	0.75	0.72	0.74
DK	4.28	4.74	6.00	0.75	0.75	0.77	0.76
EE	8.91	8.80	13.00	1.56	1.63	1.42	1.54
EL	12.44	11.83	16.00	2.18	2.00	1.91	2.03
ES	8.73	8.55	13.00	1.53	1.63	1.38	1.51
FI	7.02	8.44	10.00	1.23	1.25	1.37	1.28
FR	4.38	5.52	6.00	0.77	0.75	0.89	0.80
HR	9.45	9.23	14.00	1.66	1.75	1.49	1.63
HU	9.27	9.09	14.00	1.63	1.75	1.47	1.62
IE	10.22	10.58	16.00	1.79	2.00	1.71	1.84
IS	N/A	N/A	N/A	N/A	N/A	N/A	N/A
IT	5.67	5.98	8.00	1.00	1.00	0.97	0.99
LI	4.77	4.52	7.00	0.84	0.88	0.73	0.81
LT	9.83	9.50	14.00	1.73	1.75	1.54	1.67
LU	5.83	5.58	8.00	1.02	1.00	0.90	0.98
LV	9.19	9.62	13.00	1.61	1.63	1.56	1.60
MT	N/A	N/A	7.00	N/A	N/A	N/A	N/A
NL	5.36	5.68	6.00	0.94	0.88	0.92	0.91
NO	4.24	5.82	11.00	0.75	0.75	0.94	0.81
PL	7.75	9.90	15.00	1.36	1.38	1.60	1.45
PT	10.46	9.95	12.00	1.84	1.88	1.61	1.77
RO	8.40	8.48	7.00	1.48	1.50	1.37	1.45
SE	4.78	5.33	11.00	0.84	0.88	0.86	0.86
SI	7.70	7.55	13.00	1.35	1.38	1.22	1.32
SK	8.49	7.71	7.00	1.49	1.63	1.25	1.45
UK	5.22	5.50	9.00	0.92	0.88	0.89	0.89
Europe	**6.09**	**6.96**	**6.96**	**1.07**	**1.13**	**1.13**	**1.11**

Table-specific abbreviations: Q75 (75% quantile, upper quartile); W (weighted); UW (unweighted)

Table S10: Driving profile simulation: Parameter dependency (weekly distance)

N=10,000	Linear Regression (Ordinary Least Squares - OLS) and ANOVA						Wald test with GLM	
	Regr. coefficient	Degrees of freedom	Sum of squares	Mean square	F-statistic	P-value	Chi-square statistic	P-value
Intercept	1525.0	-	-	-	-	-	30.2	3.81E-08
Country (C)	1532.7	29	5.94E+08	2.05E+07	24.2	3.38E-124	672.8	4.79E-123
Truck Class (C)	897.2	14	1.80E+09	1.28E+08	151.5	0	447.0	1.54E-86
NST-2007 (C)	883.6	19	6.70E+08	3.53E+07	41.6	2.55E-149	221.4	1.77E-36
Operations (C)	1520.3	3	2.40E+09	7.99E+08	942.8	0	2828.3	0
Residual	-	9934	8.42E+09	8.47E+05			-	-
N=1,000,000								
Intercept	1830.9	-	-	-	-	-	5041.9	0
Country (C)	1360.6	29	5.13E+10	1.77E+09	2109.0	0	54,651.7	0
Truck Class (C)	775.0	14	1.86E+11	1.33E+10	15865.1	0	48,954.5	0
NST-2007 (C)	825.3	19	6.25E+10	3.29E+09	3917.8	0	21,384.4	0
Operations (C)	1461.4	3	2.22E+11	7.41E+10	88313.3	0	264,940.0	0
Residual	-	999,934	8.39E+11	8.39E+05				-

Notes:

- Regression coefficient for categorical (C) variables are given as delta between maximum and mininum value.
- Random sample with N=10,000 and N=1,000,000 taken from $\text{data}_{\text{ERFT.}}$
- Reg. model: $\text{Weekly Distance} \sim \text{C(Country)} + \text{C(Truck Class)} + \text{C}(\text{NST}_{2007}) + \text{C(Ops)}$
- GLM: Generalized Linear Model with Gaussian error distribution models
- R^2 OLS ≈ 0.38; R^2 GLM ≈ 0.46

Table S11: Driving profile simulation: Parameter dependency (weekly trips)

N=10,000	Linear Regression (Ordinary Least Squares - OLS) and ANOVA						Wald test with GLM	
	Regr. coefficient	Degrees of freedom	Sum of squares	Mean square	F-statistic	P-value	Chi-square statistic	P-value
Intercept								
Country (C)	17.6	30	2.45E+06	8.17E+04	252.7	0	436.5	1.10E-73
Truck Class (C)	12.4	14	1.22E+05	8.73E+03	27.0	1.37E-70	171.7	3.05E-29
NST-2007 (C)	25.5	19	3.69E+05	1.94E+04	60.1	2.00E-217	859.0	6.07E-170
Operations (C)	13.5	3	1.32E+05	4.41E+04	136.5	1.19E-86	489.2	1.02E-105
Distance (C)	8.1	5	3.55E+04	7.10E+03	21.9	6.24E-22	109.7	4.69E-22
Residual	-	9929	3.21E+06	3.23E+02			-	-
N=1,000,000								
Intercept								
Country (C)	15.6	30	2.51E+08	8.37E+06	25127.0	0	35,831.3	0
Truck Class (C)	12.0	14	1.17E+07	8.36E+05	2508.7	0	14,957.9	0
NST-2007 (C)	25.2	19	3.94E+07	2.07E+06	6220.6	0	86,939.9	0
Operations (C)	14.8	3	1.46E+07	4.86E+06	14575.4	0	57,188.2	0
Distance (C)	9.1	5	5.23E+06	1.05E+06	3141.0	0	15,705.1	0
Residual	-	999,929	3.33E+08	3.33E+02				-

Notes:

- Regression coefficient for categorical (C) variables are given as delta between maximum and mininum value.
- Random sample with N=10,000 and N=1,000,000 taken from $\text{data}_{\text{ERFT.}}$
- Reg. model: $\text{Weekly Trips} \sim \text{C(Country)} + \text{C(Truck Class)} + \text{C}(\text{NST}_{2007}) + \text{C(Ops)} + \text{C}(\text{Weekly Distance Bins}_{1000})$
- GLM: Generalized Linear Model with Gaussian error distribution models
- R^2 OLS ≈ 0.25; R^2 GLM ≈ 0.39

Table S12: Driving profile simulation: Parameter dependency (weekly tkm)

N=10,000	Linear Regression (Ordinary Least Squares - OLS) and ANOVA						Wald test with GLM	
	Regr. coefficient	Degrees of freedom	Sum of squares	Mean square	F-statistic	P-value	Chi-square statistic	P-value
Intercept								
Country (C)	14,313.7	29	2.94E+12	1.02E+11	895.5	0	520.6	1.65E-91
Truck Class (C)	11,583.3	14	7.98E+11	5.70E+10	502.6	0	699.0	4.16E-140
NST-2007 (C)	10,361.9	19	1.00E+11	5.29E+09	46.6	6.91E-168	191.6	1.60E-30
Operations (C)	541.5	3	5.05E+11	1.68E+11	1486.0	0	145.2	2.85E-31
Distance	12.18	1	1.22E+12	1.22E+12	10,785.7	0	10792.0	0
#Trips	-28.14	1	3.14E+09	3.14E+09	27.7	1.43E-07	27.7	1.40E-07
Residual	-	9872	1.12E+12	1.13E+08			-	-
N=1,000,000								
Intercept								
Country (C)	14,976.5	30	2.96E+14	9.85E+12	8.35E+04	0	42,324.5	0
Truck Class (C)	13,169.7	14	7.98E+13	5.70E+12	4.83E+04	0	73,001.8	0
NST-2007 (C)	8709.3	19	9.96E+12	5.24E+11	4.44E+03	0	15,996.9	0
Operations (C)	701.2	3	5.08E+13	1.69E+13	1.44E+05	0	13,218.9	0
Distance	12.36	1	1.26E+14	1.26E+14	1.06E+06	0	1.06E+06	0
#Trips	-33.2	1	3.66E+11	3.66E+11	3.10E+03	0	3101.6	0
Residual	-	993,879	1.17E+14	1.18E+08			-	-

Notes:

- Regression coefficients for categorical (C) variables are given as delta between maximum and mininum value.
- Reg. Model: Weekly $\mathrm{TKM} \sim \mathrm{C(Country)} + \mathrm{C(Truck\ Class)} + \mathrm{C(NST_{2007})} + \mathrm{C(Ops)} + \mathrm{Distance_W} + \mathrm{\#Trips_W}$
- Generalized Linear Model with Gaussian error distribution models; R^2 OLS ≈ 0.7; R^2 GLM ≈ 0.9

Table S13: Driving profile simulation: Parameter dependency (payload per trip)

N=10,000	Linear Regression (Ordinary Least Squares - OLS) and ANOVA						Wald test with GLM	
	Regr. coefficient	Degrees of freedom	Sum of squares	Mean square	F-statistic	P-value	Chi-square statistic	P-value
Intercept	4.10						4.3	0.038
Country (C)	12.1	28	65126.6	2325.9	70.2	0	1143.8	3.09E-222
Truck Class (C)	11.3	14	104,012.2	7429.4	224.1	0	1471.6	6.36E-306
NST-2007 (C)	4.4	19	5550.7	292.1	8.8	1.59E-25	204.8	3.69E-33
Operations (C)	0.4158	3	1963.7	654.6	19.7	9.33E-13	8.3	0.041
Distance	0.0006	1	3547.8	3547.8	107.0	5.91E-25	27.1	1.94E-07
Residual	-	9934	329,329.2	33.2			-	-
N=1,000,000								
Intercept	1.46						63.8	1.41E-15
Country (C)	10.8	30	2.96E+14	9.85E+12	8.35E+04	0	1.27E+05	0
Truck Class (C)	11.9	14	7.98E+13	5.70E+12	4.83E+04	0	1.62E+05	0
NST-2007 (C)	5.4	19	9.96E+12	5.24E+11	4.44E+03	0	21583.5	0
Operations (C)	0.3	3	5.08E+13	1.69E+13	1.44E+05	0	478.4	2.27E-103
Distance	0.0005	1	1.26E+14	1.26E+14	1.06E+06	0	4461.5	0
Residual	-	993,879	1.17E+14	1.18E+08			-	-

Notes:

- Regression coefficients for categorical (C) variables are given as delta between maximum and mininum value.
- Reg. Model: $\mathrm{Tons\ per\ Trip} \sim \mathrm{C(Country)} + \mathrm{C(Truck\ Class)} + \mathrm{C(NST_{2007})} + \mathrm{C(Ops)} + \mathrm{Distance_{Weekly}}$
- Generalized Linear Model with Gaussian error distribution models; R^2 OLS ≈ 0.27; R^2 GLM ≈ 0.3

Table S14: Driving profile simulation: Parameter dependency (share of laden trips)

N=10,000	Linear Regression (Ordinary Least Squares - OLS) and ANOVA						Wald test with GLM	
	Regr. coefficient	Degrees of freedom	Sum of squares	Mean square	F-statistic	P-value	Chi-square statistic	P-value
Intercept	0.413						41.0	1.54E-10
Country (C)	0.437	29	88.94	3.07	73.80	0	1948.4	0
Truck Class (C)	0.121	14	5.34	0.38	9.18	1.90E-20	88.2	8.37E-13
NST-2007 (C)	0.260	19	30.49	1.60	38.62	5.72E-138	579.0	1.38E-110
Operations (C)	0.05	3	0.96	0.32	7.67	4.07E-05	61.5	2.77E-13
Distance	1.489e-05	1	0.99	0.99	23.89	1.04E-06	42.1	8.76E-11
#Trips	-0.0014	1	7.11	7.11	171.12	8.82E-39	171.1	4.22E-39
Residual	-	9932	412.75	0.04			-	-
N=1,000,000								
Intercept	0.509						8288.4	0
Country (C)	0.498	29	9579.2	330.3	8059.6	0	208,476.0	0
Truck Class (C)	0.07	14	437.6	31.3	762.6	0	5930.8	0
NST-2007 (C)	0.264	19	2941.5	154.8	3777.4	0	58,359.5	0
Operations (C)	0.04	3	101.8	33.9	828.2	0	5966.5	0
Distance	1.237e-05	1	63.1	63.1	1540.6	0	3096.4	0
#Trips	-0.0016	1	861.6	861.6	21021.9	0	21,021.9	0
Residual	-	999,932	40,981.9	0.0				-

Notes:

- Regression coefficient for categorical (C) variables are given as delta between maximum and mininum value.
- Random sample with N=10,000 and N=1,000,000 taken from $data_{ERFT.}$
- Reg. model: % Laden $\mathrm{Trips} \sim \mathrm{C(Country)} + \mathrm{C(Truck\ Class)} + \mathrm{C(NST_{2007})} + \mathrm{C(Ops)} + \mathrm{Distance_W} + \mathrm{\#Trips_W}$
- GLM: Generalized Linear Model with Gaussian error distribution models; R^2 OLS ≈ 0.25; R^2 GLM ≈ 0.28

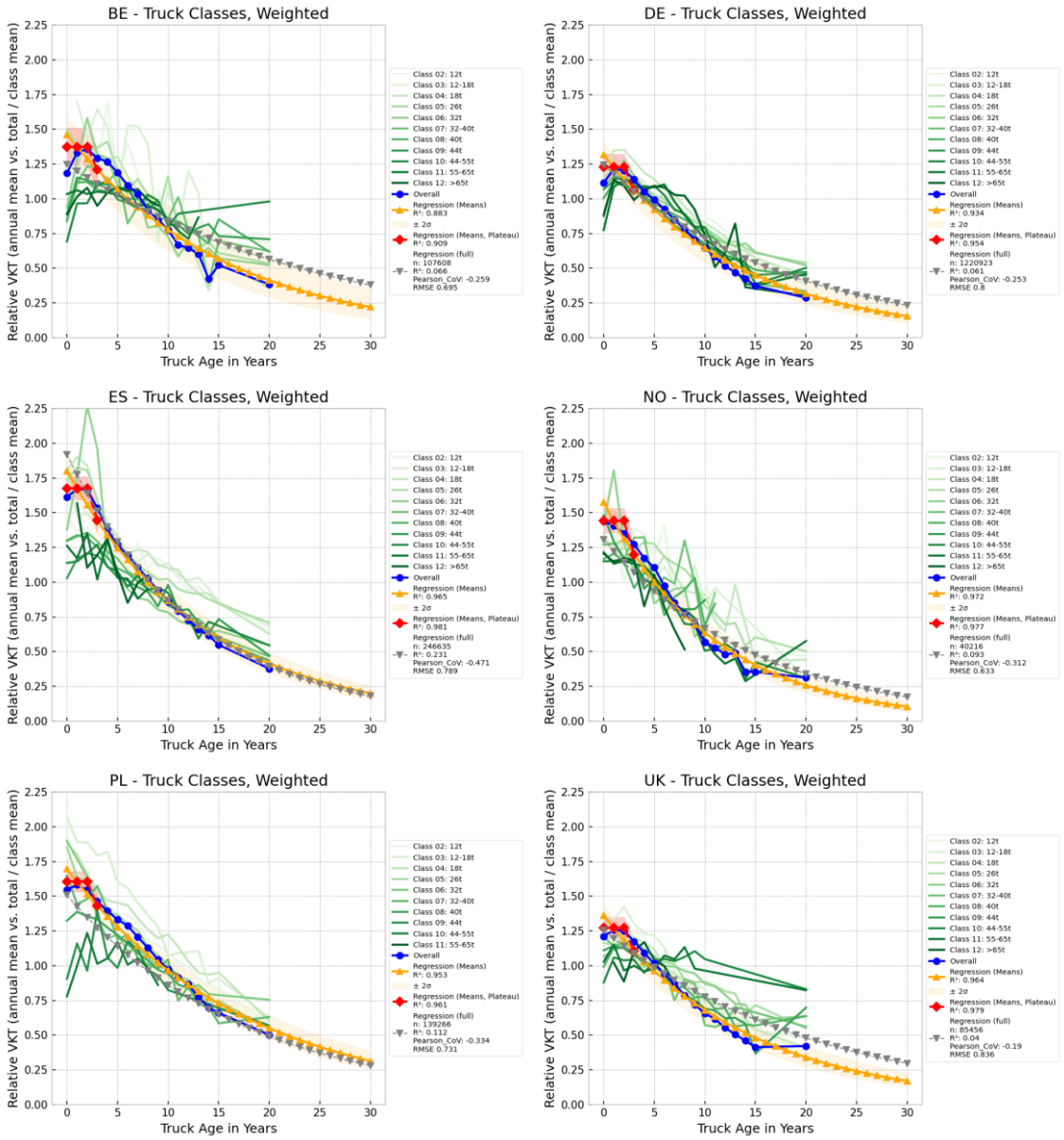

Figure S9: Weekly Module: Dependency of weekly mileage on truck age

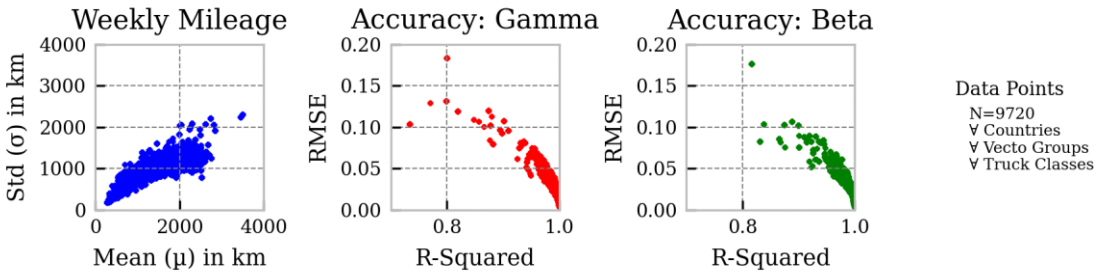

Figure S10: Weekly Module: Accuracy of determining the truck class

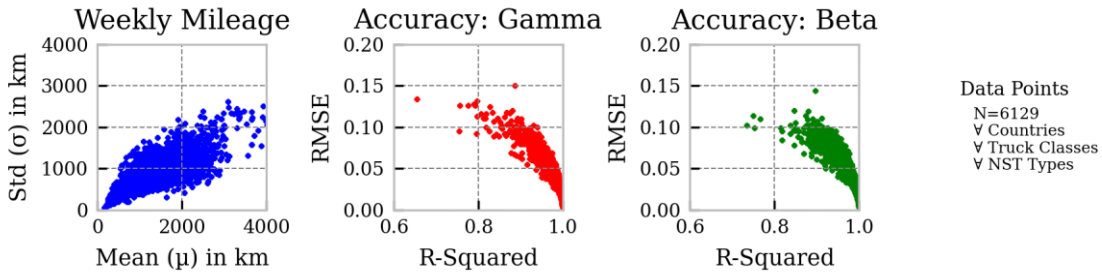

Figure S11: Weekly Module: Accuracy of determining the NST type.

Pseudo-Code to determine the individual trip distances, described by Equation (A.1):

Input:

- Probability distribution for trip lengths: $P\left(d_{Trip} \middle|\, cty, tc, nst, ops, f_{bin}(d_{week})\right)$ with $d_{trip,i} \sim D_{trip}\left(\alpha(\mu,\sigma), \beta(\mu,\sigma)\right)$
- Weekly distance: d_{week}
- Binning function: $f_{bin}(d_{week}) = \lfloor d_{week}/1000 \rfloor$
- Other defining parameters: cty, tc, nst, ops

Output:

- List of trip distances $\{d_{trip,i}\}_{i=1}^{n_{trips}}$ where $\sum_{i=1}^{n_{trips}} d_{trip,i} = d_{week}$
- Weekly number of trips: n_{trips}

Init: totat_distance ← 0; sampled_trips ← []

While total_distance < d_{week}:

    Sample trip length $d_{trip,i}$ from $P\left(d_{trip,i} \middle|\, cty, tc, nst, ops, f_{bin}(d_{week})\right)$

    Add $d_{trip,i}$ to sampled trips

    Update total_distance ← total_distance + $d_{trip,i}$

case1: keep last sampled trip and calculate total distance

case2: remove last sampled trip and calculate total distance

If case1 fits better (lower relative deviation from d_{week}):

    scaler ← d_{week}/ sum(case1)

    adj_trips ← [scaler * trip for trip in case1]

Else

    scaler ← d_{week}/ sum(case2)

    adj_trips ← [scaler * trip for trip in case2]

List of trip distances ← adj_trips

Return List of trip distances

(A.1)

Further Equations (*A.2*) to (*A.8*) to determine respective weekly parameters:

$$\begin{gathered}\mathrm{ops}^{*} = \arg\max_{\mathrm{ops}_x \in \mathrm{OPS_{All}}} \mathrm{P}(\mathrm{ops}_x|\mathrm{cty}, \mathrm{tc}, \mathrm{nst}, \mathrm{d_{week}}) \\ \text{with } \mathrm{P}(\mathrm{ops}_x|\mathrm{cty}, \mathrm{tc}, \mathrm{nst}, \mathrm{d_{week}}) = \mathrm{D_{ops}}\big(\alpha(\mu,\sigma), \beta(\mu,\sigma)\big) \\ \text{and } \mu = \mu(\mathrm{cty}, \mathrm{tc}, \mathrm{nst}, \mathrm{d_{week}}), \sigma = \sigma(\mathrm{cty}, \mathrm{tc}, \mathrm{nst}, \mathrm{d_{week}}) \\ \text{and } \mathrm{OPS_{All}} \in \{\mathrm{local}, \mathrm{regional}, \mathrm{national}, \mathrm{international}\}\end{gathered} \tag{A.2}$$

$$\begin{gathered}\mathrm{p}\big(\widehat{M}_{TKM}|\ \mathrm{cty}, \mathrm{tc}, \mathrm{nst}, \mathrm{f_{bin}}(\mathrm{d_{week}})\big) = \mathrm{D_{tkm}}\big(\alpha(\mu,\sigma), \beta(\mu,\sigma)\big) \\ \text{with } \mu = \mu(\mathrm{cty}, \mathrm{tc}, \mathrm{nst}, \mathrm{f_{bin}}(\mathrm{d_{week}})), \sigma = \sigma(\mathrm{cty}, \mathrm{tc}, \mathrm{nst}, \mathrm{f_{bin}}(\mathrm{d_{week}})) \\ \text{and } \mathrm{f_{bin}}(\mathrm{d_{week}}) = \lfloor \mathrm{d_{week}}/1000 \rfloor \text{ so that} \\ \widehat{M}_{TKM} \sim \mathrm{D_{tkm}}\big(\alpha(\mu,\sigma), \beta(\mu,\sigma)\big)\end{gathered} \tag{A.3}$$

$$\begin{gathered}\mathrm{p}\big(\mathrm{m_{PL,max}}|\ \mathrm{cty}, \mathrm{tc}\big) = \mathrm{D_{mpl}}\big(\alpha(\mu,\sigma), \beta(\mu,\sigma)\big) \\ \text{with } \mu = \mu(\mathrm{cty}, \mathrm{tc}) \text{ and } \sigma = \sigma(\mathrm{c}, \mathrm{tc}) \text{ so that} \\ \mathrm{m_{PL,max}} \sim \mathrm{D_{mpl}}\big(\alpha(\mu,\sigma), \beta(\mu,\sigma)\big)\end{gathered} \tag{A.4}$$

$$\begin{gathered}\mathrm{type_{trip},}_i = \arg\max_{\mathrm{type}_x \in \mathrm{TT_{All}}} \mathrm{P}\left(\mathrm{type}_x \middle| \mathrm{cty}, \mathrm{nst}, \mathrm{ops}, \mathrm{f_{bin}}\big(\mathrm{n_{trips}}\big)\right) \forall\ \mathrm{i} \in \mathrm{n_{trips}} \\ \text{with } \mathrm{P}\big(\mathrm{type}_x|\mathrm{cty}, \mathrm{nst}, \mathrm{ops}, \mathrm{f_{bin}}(\mathrm{n_{trips}})\big) = \mathrm{D_{tt}}\big(\alpha(\mu,\sigma), \beta(\mu,\sigma)\big) \\ \text{and } \mu = \mu\big(\mathrm{cty}, \mathrm{nst}, \mathrm{ops}, \mathrm{f_{bin}}(\mathrm{n_{trips}})\big), \sigma = \sigma\big(\mathrm{cty}, \mathrm{nst}, \mathrm{ops}, \mathrm{f_{bin}}(\mathrm{n_{trips}})\big) \\ \text{and } \mathrm{f_B}\big(\mathrm{n_{trips}}\big) = \begin{cases} \mathrm{low} & , \mathrm{n_{trips}} \le Q_1 \\ \mathrm{med} & , Q_1 < \mathrm{n_{trips}} \le Q_3 \text{ with Q1 and Q3 as quartiles} \\ \mathrm{high} & , \mathrm{n_{trips}} > Q_3 \end{cases} \\ \text{and } \mathrm{TT_{All}} \in \{\mathrm{single}, \mathrm{multi}, \mathrm{cdmr}\} \\ \text{which yields } \left\{\mathrm{type_{trip},}_i\right\}_{i=1}^{\mathrm{n_{trips}}}\end{gathered} \tag{A.5}$$

$$\begin{gathered}\mathrm{p}\big(\mathrm{n_{subtrip},}_i|\ \mathrm{cty}, \mathrm{tc}, \mathrm{nst}\big) = \mathrm{D_{sub}}\big(\alpha(\mu,\sigma), \beta(\mu,\sigma)\big) \\ \text{with } \mu = \mu(\mathrm{cty}, \mathrm{tc}, \mathrm{nst}), \sigma = \sigma(\mathrm{cty}, \mathrm{tc}, \mathrm{nst}) \text{ so that} \\ \mathrm{n_{subtrip},}_i \sim \mathrm{D_{sub}}\big(\alpha(\mu,\sigma), \beta(\mu,\sigma)\big)\ \forall\ i \in \mathrm{n_{trips}}, \text{if } \mathrm{type_{trip},}_i \in \{\mathrm{multi}, \mathrm{cdmr}\} \text{ else } 0 \\ \text{which yields } \left\{\mathrm{n_{subtrip},}_i\right\}_{i=1}^{\mathrm{n_{trips}}}\end{gathered} \tag{A.6}$$

$$\begin{gathered}\mathrm{p}(\mathrm{r_{Laden}}|\ \mathrm{cty}, \mathrm{nst}) = \mathrm{D_{load}}\big(\alpha(\mu,\sigma), \beta(\mu,\sigma)\big) \\ \text{with } \mu = \mu(\mathrm{cty}, \mathrm{nst}), \sigma = \sigma(\mathrm{cty}, \mathrm{nst}) \text{ so that} \\ \mathrm{r_{Loaded}} \sim \mathrm{D_{load}}\big(\alpha(\mu,\sigma), \beta(\mu,\sigma)\big) \text{ with} \\ \mathrm{n_{loaded}} = \lceil \mathrm{r_{loaded}} * \mathrm{n_{trips}} \rceil \text{ and} \\ \mathrm{n_{empty}} = \mathrm{n_{trips}} - \mathrm{n_{loaded}}\end{gathered} \tag{A.7}$$

$$\begin{gathered}\mathrm{p}\big(\mathrm{m_{tripPL},}_i|\ \mathrm{cty}, \mathrm{tc}, \mathrm{nst}\big) = \mathrm{D_{cargo}}\big(\alpha(\mu,\sigma), \beta(\mu,\sigma)\big) \\ \text{with } \mu = \mu(\mathrm{cty}, \mathrm{tc}, \mathrm{nst}), \sigma = \sigma(\mathrm{cty}, \mathrm{tc}, \mathrm{nst}) \text{ so that} \\ \mathrm{m_{tripPL},}_k \sim \mathrm{D_{cargo}}\big(\alpha(\mu,\sigma), \beta(\mu,\sigma)\big)\ \forall\ k \in \mathrm{n_{loaded}} \\ \text{and } \mathrm{m_{tripPL},}_j = 0\ \forall\ j \in \mathrm{n_{empty}} \\ \text{which yields } \left\{\mathrm{m_{tripPL},}_i\right\}_{i=1}^{n_{trips}} = \left\{\mathrm{m_{tripPL},}_k\right\}_{k=1}^{\mathrm{n_{loaded}}} + \left\{\mathrm{m_{tripPL},}_j\right\}_{j=1}^{\mathrm{n_{empty}}}\end{gathered} \tag{A.8}$$

Daily Module:

Pseudo-Code to allocate trips to days, described by Equation (*A.9*):

Input:

- Probability distribution for daily shares: $P(s_{day} | f_{bin}(d_{week}))$with $s_{day} \sim D_{dd}(\alpha(\mu,\sigma), \beta(\mu,\sigma))$ for $d \in [1, \dots, 7]$
- Weekly distance: d_{week}
- Binning function: $f_{bin}(d_{week}) = \lfloor d_{week}/1000 \rfloor$
- List trip distances $\{d_{trip,i}\}_{i=1}^{n_{trips}}$ and payloads $\{pl_{trip,i}\}_{i=1}^{n_{trips}}$

Output:

- Daily distances $\{d_{day,i}\}_{i=1}^{7}$ and a list of trips per day

Init:

total_share ← 0
sampled_shares ← []
num_days ← 0
While total_share < 1 and num_days < 7:
    Sample daily share s_{day} from $P(s_{day} | f_B(d_{week}))$
    Add s_{day} to sample_shares
    Update total_ share ← total_ share + s_{day}
    Update num_days ← num_days + 1
While num_days ≠ 7:
    Padding: Add 0 to sample_shares
    Update num_days ← num_days + 1
Normalize sampled_shares so that the sum equals 1

(A.9)

Frontloading:

- Rearrange order of sampled_shares to derive sorted_shares

Daily Target Distances:

- target_split ← [share * d_{week} for share in trip in sorted_shares]
- $\{\hat{d}_{day,i}\}_{i=1}^{7}$ <- target_split

Binsorting: Allocate trips to days

- listDailyTrips_perDay ← $f_{BinSort}(\{d_{trip,i}\}_{i=1}^{n_{trips}}, \{m_{tripPL,i}\}_{i=1}^{n_{trips}}$, target_split)

Mileage per day $\{d_{day,i}\}_{i=1}^{7}$:

- The daily mileage is the sum of the individual trip distances per day

Return Daily mileages, listDailyTrips_perDay

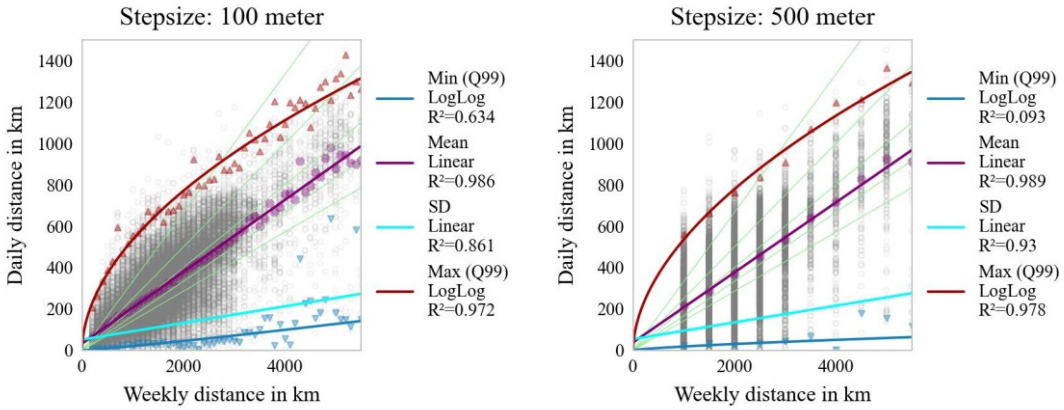

Note: Green reference lines split the weekly mileage equally among days (top: 3 days; lowest: 7 days)

Figure S12: Daily Module: Relationship between weekly and daily distances

Further generic Equation (*A.10*) to determine respective daily parameters:

$$\begin{gathered} P\left(x_i \mid f_{bin}(d_{day,i})\right) = D_x\left(\alpha(\mu,\sigma), \beta(\mu,\sigma)\right) \forall\, i \in \{Monday, \ldots, Sunday\} \\ \text{with } \mu = \mu\left(f_{bin}(d_{day,i})\right), \sigma = \sigma\left(f_{bin}(d_{day,i})\right) \\ \text{and } f_{bin}(d_{day,i}) = \lfloor d_{day,i}/100 \rfloor \text{ so that} \\ x_i \sim D_x\left(\alpha(\mu,\sigma), \beta(\mu,\sigma)\right) \\ \text{with } x_i \in \left\{v_i, r_{driving,i}, t_{DEP,i}, z_{tollRoad,i}\right\} \text{ and } D_x \text{ as respective distribution} \end{gathered} \tag{A.10}$$

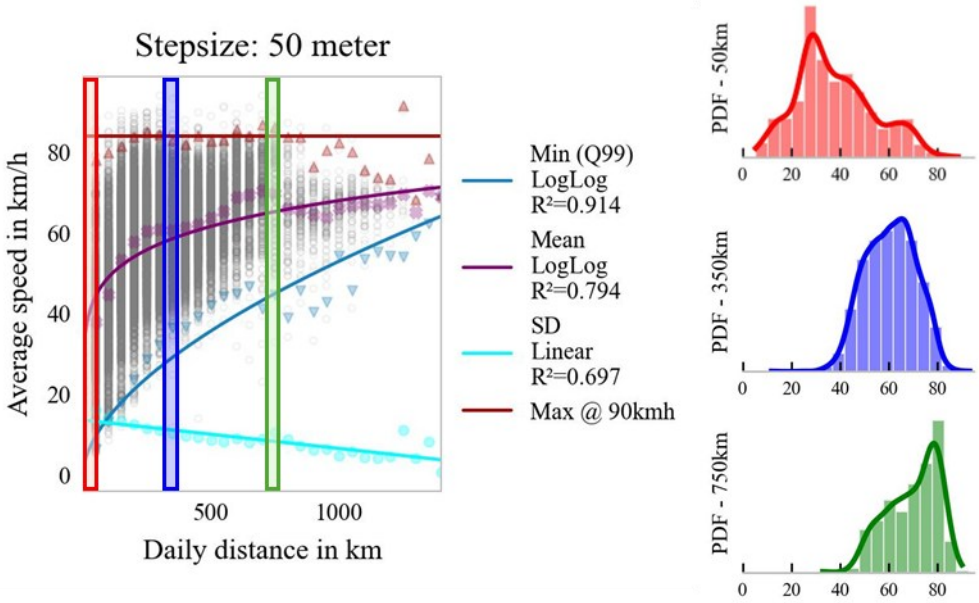

Figure S13: Daily Module: Relationship between daily distance and driving speed

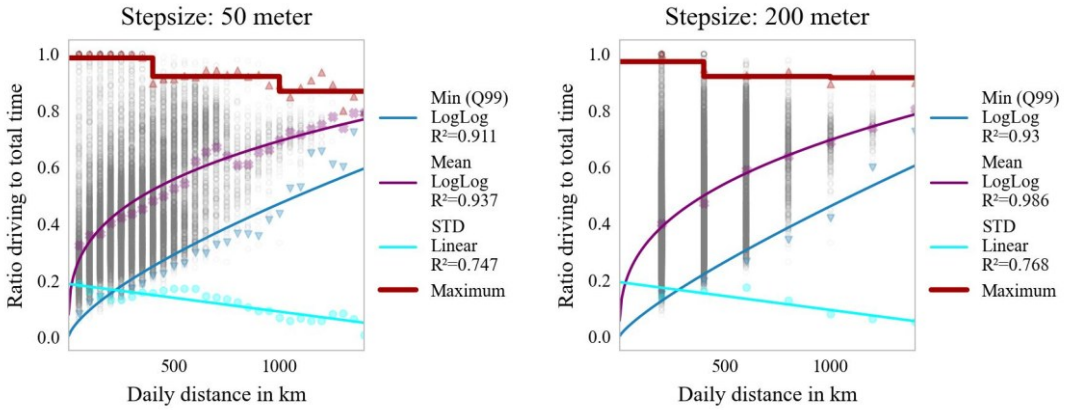

Figure S14: Daily Module: Relationship between daily distance and driving time

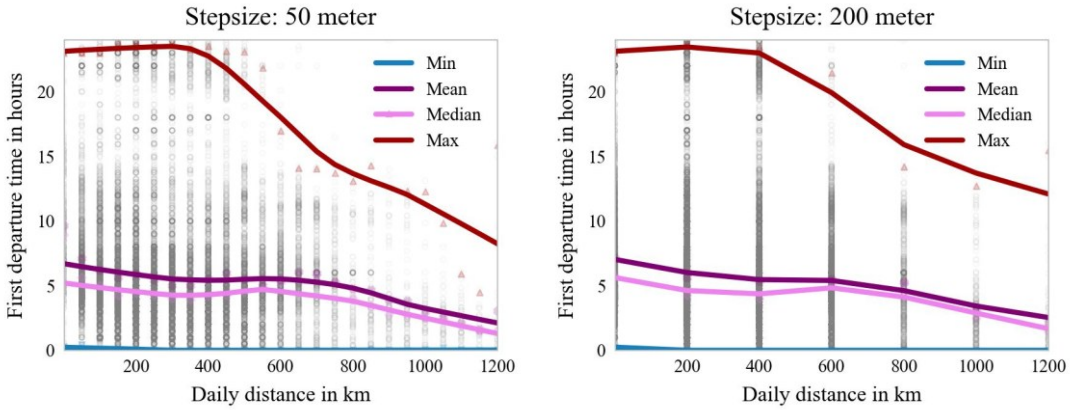

Note: Curves are derived via local polynomial regression (LOWESS - locally weighted scatterplot smoothing)

Figure S15: Daily Module: Relationship between daily distance and first departure

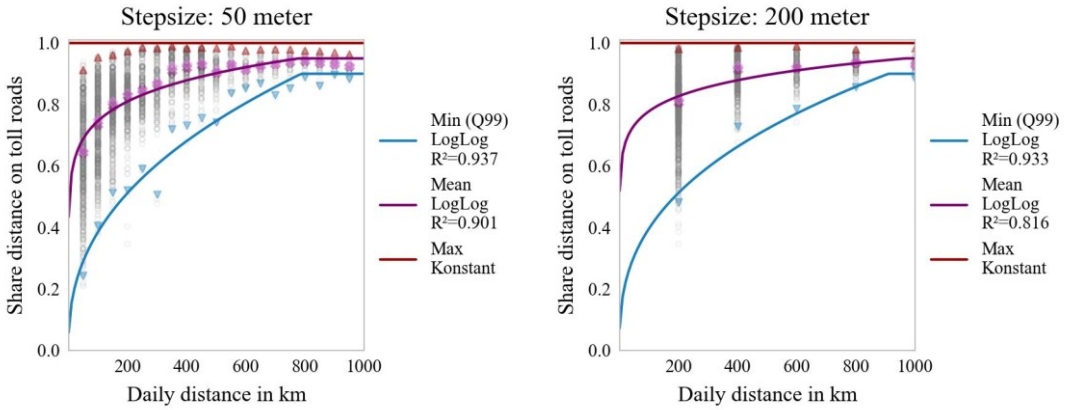

Figure S16: Daily Module: Relationship between daily distance and toll roads

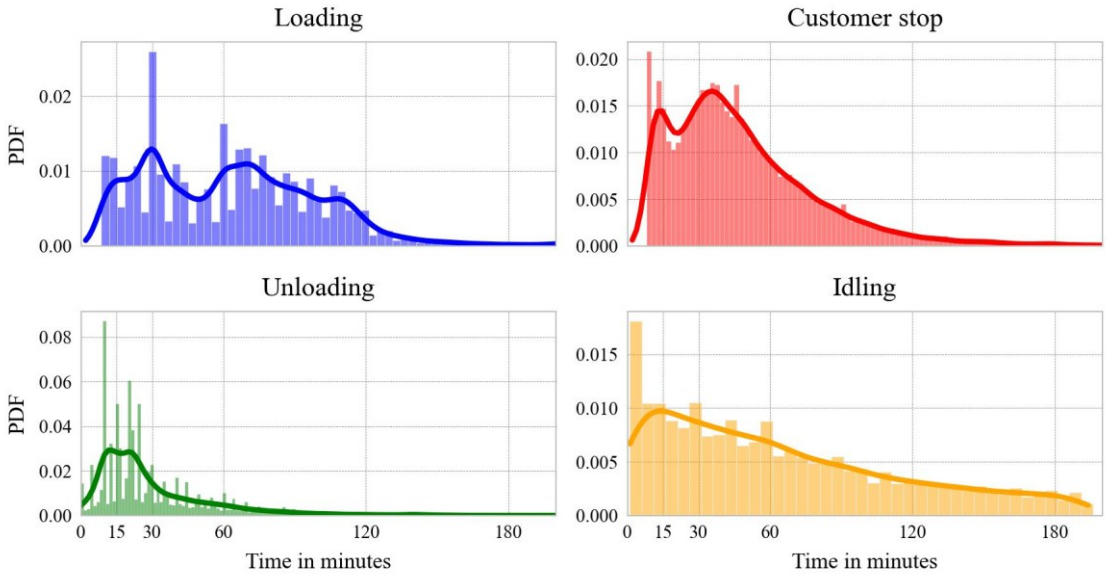

Figure S17: Daily Module: Additional time information for trip-related processes

Appendix to Section 4.2

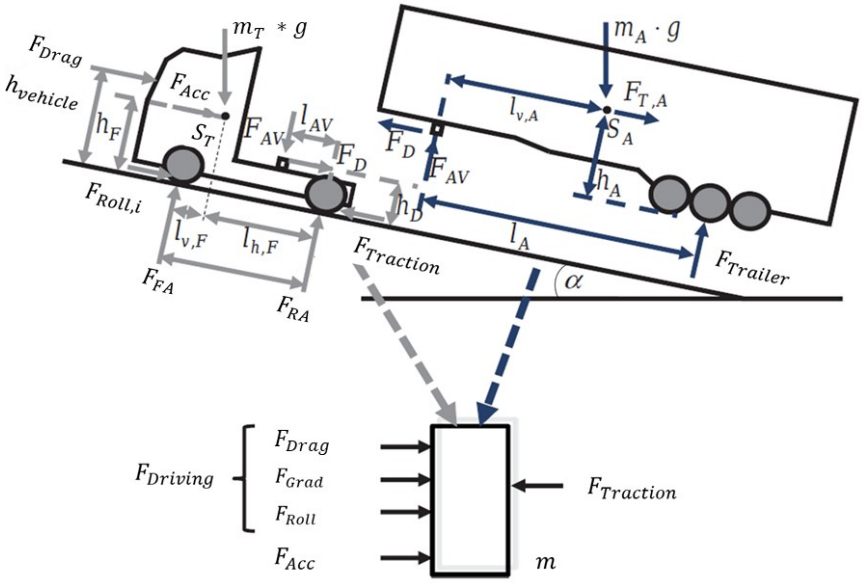

Note: Adjusted from Oberfell (2015)

Figure S18: Truck simulation: Point-mass model of a tractor-trailer combination

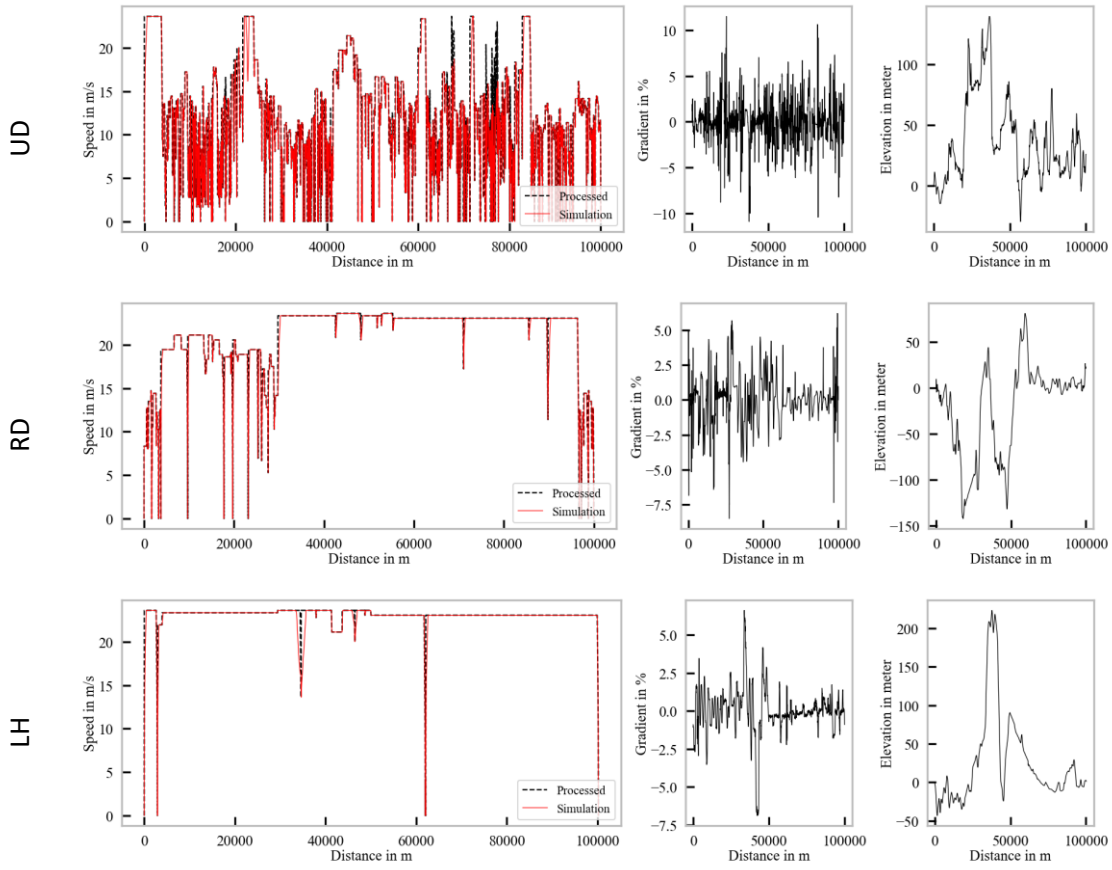

Figure S19: Truck simulation: VECTO mission profiles

Initialization of the rolling resistance coefficient:

Equation (*A.11*) describes the static correction of the tire rolling resistance. This implementation follows from the ISO 28580 testing procedure to include temperature effects – see Mioduszewski et al. (2015) and Greiner et al. (2018) – and the VECTO implementation (see Kies 2018) to include cargo weight effects. Note that the implementation assumes that the reported c_{rr} values from $data_{EEA}$ correspond to ISO-defined rolling resistance coefficient ($c_{rr,ISO}$).

$$c_{rr} = f_{wear} * \frac{\sum_{i=1}^{n} \frac{m_i}{m_{total}} * c_{rr,ISO,i} * \left(\frac{m_i * g}{w_i * F_{ISO,i}}\right)^{\beta - 1}}{1 - k_t \cdot (T_{amb} - T_{ISO})} \quad \text{(A.11)}$$

with the following parameter definition:

Parameter	Description	Unit
c_{rr}	Corrected rolling resistance coefficient	[N/kN]
f_{wear}	Tire wear correction factor – 0.88 (Kies 2018)	[-]
$c_{rr,ISO,i}$	ISO-defined c_{rr} for tires on axle i according to EU tire label	[N/kN]
m_i	Weight share per axle i	[kg]
m_{total}	Total truck weight	[kg]
w_i	Number of tires on axle i	[-]
$F_{ISO,i}$	Tire load on axle i according to ISO 28580 – 37,500 N (Kies 2018)	[N]
κ	Constant parameter – 0.9 (Kies 2018)	[-]
g	Gravitational constant – 9.81 m/s²	[m/s²]
T_{amb}	Ambient temperature	[°C]
k_t	Correction factor – 0.05 (Greiner et al. 2018)	[-]
T_{ISO}	ISO-defined norm temperature – 25°C (Greiner et al. 2018)	[°C]

Initialization of the air density:

Equation (*A.12*) describes the correction of the air density based on the empirical Magnus formula and the ideal gas law, where T_{amb} denotes the ambient temperature, p denotes the air pressure, R_f denotes the universal gas constant of humid air, R_d denotes the universal gas constant of steam, R_f denotes the universal gas constant of dry air), and φ denotes humidity.

$$\rho_{Air} = \frac{p_{Air}}{R_f \cdot T_{Amb}}$$
$$R_f = \frac{R_l}{1 - \left(\varphi \frac{p_d}{p}\right) \cdot \left(1 - \frac{R_l}{R_d}\right)} \quad \text{(A.12)}$$
$$p_d = 611.657 \cdot \exp\left(17.2799 - \frac{4102.99}{T_{Amb} - 35.719}\right)$$

Dynamic air drag factor:

The dynamic drag area adopts the speed-dependent correction formula by VECTO (VECTO 2025). The implementation is given by Kies (2018) and **Figure S20** visualizes the respective correction factor for different truck types.

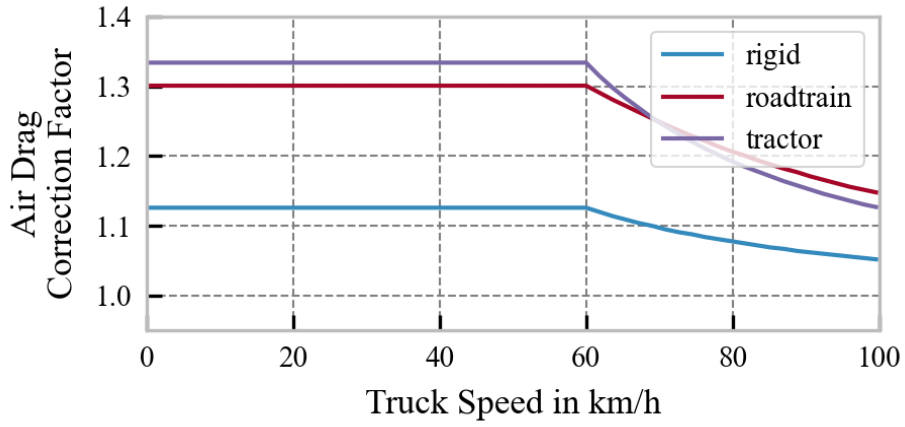

Figure S20: Truck simulation: Speed-dependent air drag correction

Table S15: Truck simulation: Parameter values

Parameter	Description	Value	Source
m_T	DT chassis curb mass (read-to-drive) in kg	Per $data_{EEA}$ (EEA 2024) and as visualized by *Figure 10*	
c_{rr}	Tire rolling resistance coefficient (ISO)		
A_{Drag}	Drag area in m²		
P_{rated}	Rated motor power in kW		
J_{wheels}	Total inertia of all tires in kg*m2	Per VECTO input data (VECTO 2025)	
r_{dyn}	Dynamic tire radius in m		
$m_{Trailer}$	Trailer mass	6,500-7,500 kg	(Norris et al. 2017) (VECTO 2025)
m_{eAx}	Weight of the e-axle	450-800 kg	(Mareev et al. 2018) (Wolff et al. 2021)
e_{ICE}	ICE power-to-weight ratio	3.3 kg/kW	(van Basshuysen 2015)
δ_{Diesel}	Diesel energy density	0.846 kg per liter 9.7 kWh per liter	
P_B	Auxiliary power by general consumers	1,800 W	(Tansini et al. 2019) (Heidt et al. 2019) (Zhao et al. 2013)

Electrical power demand by the HVAC system:

P_{HVAC} denotes the electrical power demand by the HVAC system of the driver cabin, which depends on the ambient temperature and driving speed. Following Steinstraeter et al. (2022) and Yang et al. (2022), an identical modern system design with heat pumps (heating or cooling) and an electric resistance heater (main heat source at low temperatures) is assumed for both DTs and BETs. However, the implementation accounts for a certain proportion of waste heat utilization by DTs, which results in reduced heating energy demand.

The electrical power demand by the HVAC system is described by Equation (*A.13*), where α_{cab} denotes the heat transfer coefficients multiplied by the cabin as a function of the driving speed, T_{Amb} denotes the ambient temperature, T_{cab} denotes the desired cabin temperature of 20°C, f_{WHR} denotes the waste heat recovery factor for DTs, $P_{H,max}$ denotes the maximum heating power defined by the electric resistance heater (PTC thermistor heater), and COP_C and COP_H denote the respective COP values for cooling or heating.

$$P_{HVAC} = \begin{cases} \min\left(P_{H,max}, \dfrac{(T_{cab} - T_{Amb}) * \alpha_{cab}}{COP_H} * f_{WHR}\right) & \text{if } T_{Amb} < T_{cab} \\ \dfrac{(T_{Amb} - T_{cab}) * \alpha_{cab}}{COP_C} & \text{if } T_{Amb} > T_{cab} \end{cases} \quad \text{(A.13)}$$

$$\text{with } \alpha_{cab} = f_{cab}(v)$$
$$COP_C = f_{copc}(T_{Amb})$$
$$COP_H = f_{coph}(T_{Amb})$$

Figure S21 visualizes the speed-dependent α_{cab} (adopted from Magnino et al. 2024) and values for $COP_{HVAC,C}$ and $COP_{HVAC,H}$ as a function of the ambient temperature, which follow general patterns and scales of modern air-source heat pumps. f_{WHR} is assumed at 67% for DTs, meaning that one third of the exhaust heat can be used for cabin temperature heating. The maximum heating power is limited to 5,500 Watts[1].

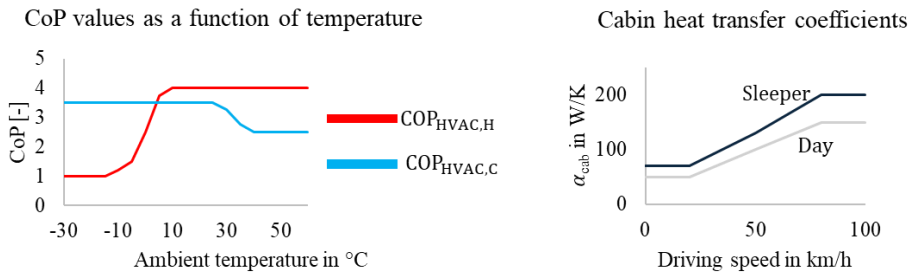

Figure S21: Truck simulation: HVAC system parameters

[1] Own assumption to limit the maximum power at low temperatures. Note that Neubauer et al. (2014) reported an electrical peak load of 4 kW for a 2010 Nissan Leaf cabin, so this thesis assumed that larger truck cabins (particularly sleeper cabins) require at least as this or more power.

Electrical power demand by the BTMS system:

The maximum electrical power demand by the BTMS system ($P_{BTMS,max}$) follows from the respective maximum of two scenarios.

Scenario S1 maps a fast-charge scenario at standard ambient temperature (25°C), where 70% of the battery capacity is recharged with a charging power of 2C, and the battery may heat up by a maximum of 20°C (derived from Teichert et al. 2022). Equation (*A.14*) formalizes the scenario, where $\mathrm{Q_{ch}}$ denotes the generated heat energy while charging (in kWh), $\mathrm{Q_{max}}$ the maximum heat energy stored in the battery in compliance with the permitted temperature increase (in kWh), $\mathrm{E_{bat}}$ denotes the total battery capacity (in kWh), $\mathrm{m_{bat}}$ the total battery weight (in kg), $\mathrm{P_{ch}}$ the charging power expressed as C-rate (in 1/h), $\Delta\mathrm{T_{max}}$ the maximum allowed temperature increase, $\mathrm{COP_C}$ denotes the respective COP value for cooling (assumed to be 2.5), $\eta_{\mathrm{ch,S1}}$ denotes the battery charge efficiency at 2C and 50% SOC, and $\mathrm{c_{p,bat}}$ denotes the specific heat capacity of the total battery[2].

$$\mathrm{P_{BTMS,S1}} = \frac{\max\left(0,\ \mathrm{Q_{ch}} - \mathrm{Q_{max}}\right)}{\mathrm{COP_C}} * \mathrm{P_{ch}}$$
$$\text{with } \mathrm{Q_{ch}} = 0.7 * \mathrm{E_{bat}} * \left(1 - \eta_{\mathrm{ch,S1}}\right) \text{ and } \mathrm{Q_{max}} = \frac{\mathrm{m_{bat}} * \mathrm{c_{p,bat}} * \Delta\mathrm{T_{max}}}{3600} \qquad \text{(A.14)}$$
$$\text{where } \eta_{\mathrm{ch,S1}} = \mathrm{f_{BAT}}(\mathrm{P_{bat}} = 2\mathrm{C}, \mathrm{T_{amb}} = 25°\mathrm{C}, \mathrm{SOC} = 50\%)$$

Scenario S2 maps a continuous discharge application, in which the truck operates permanently at the maximum rated power and the battery temperature must be maintained. Note that S2 neglects the cooling requirements for other powertrain components. Equation (*A.15*) formalizes the scenario, where η_{dis} denotes the battery discharge efficiency for the continuous discharge, E_{bat} denotes the total battery capacity (in kWh), and CoP_C denotes the respective COP value for cooling (assumed to be 2.5):

$$\mathrm{P_{BTMS,S2}} = \frac{\mathrm{P_{rated}} * \left(1 - \eta_{\mathrm{dis}}\right)}{\mathrm{COP_C}}$$
$$\text{where } \eta_{\mathrm{dis,S2}} = \mathrm{f_{BAT}}\left(\mathrm{P_{bat}} = \frac{\mathrm{P_{rated}}}{\mathrm{E_{bat}}}, \mathrm{T_{amb}} = 25°\mathrm{C}, \mathrm{SOC} = 50\%\right) \qquad \text{(A.15)}$$

Finally, Equation (A.16) describes how $\mathrm{P_{BTMS,max}}$ is transferred to an average power load using the non-linear temperature dependence (denoted via λ_T), which is derived from Tol et al. (2022) via polynomial regression to determine the respective coefficients ($\omega_1, \omega_2, \omega_3$):

$$\mathrm{P_{BTMS,max}} = \max\left(\mathrm{P_{BTMS,S1}}, \mathrm{P_{BTMS,S2}}\right)$$
$$\mathrm{P_{BTMS}} = \min\left(\mathrm{P_{BTMS,max}},\ \lambda_\mathrm{T} * \mathrm{E_{bat}}\right)$$
$$\text{where } \lambda_\mathrm{T} = \mathrm{f_T}(\mathrm{T_{amb}}) = \max\left(0, \omega_1 * \mathrm{T_{amb}^2} + \omega_2 * \mathrm{T_{amb}} + \omega_3\right) \qquad \text{(A.16)}$$
$$\text{with } \omega_1 = 0.000017, \omega_2 = -0.000561, \omega_3 = 0.004193$$

[2] The specific heat capacity is assumed to match the specific heat capacity of aluminum (896 J/kg/K)

Table S16: Truck simulation: Validation of DT fuel consumption.

	VECTO	Payload: Low		Payload: Reference		Payload: EMS Low		Payload: EMS Reference	
		simulated	reported	simulated	reported	simulated	reported	simulated	reported
UD	4	25.20 ± 1.18	29.00 ± 2.07	30.95 ± 1.21	34.45 ± 2.13	N/A	N/A	N/A	N/A
	5	39.70 ± 0.48	40.02 ± 1.38	57.54 ± 0.51	55.05 ± 1.72	N/A	N/A	N/A	N/A
	9	28.89 ± 0.88	N/A	34.63 ± 0.9	N/A	N/A	N/A	N/A	N/A
	10	41.58 ± 0.59	N/A	59.38 ± 0.68	N/A	N/A	N/A	N/A	N/A
RD	4	19.64 ± 1.34	21.71 ± 2.61	22.53 ± 1.33	23.79 ± 2.63	N/A	N/A	N/A	N/A
	5	26.17 ± 0.86	25.45 ± 1.44	35.29 ± 0.87	31.67 ± 1.52	33.92 ± 0.84	32.20 ± 1.49	44.81 ± 0.82	40.87 ± 1.67
	9	21.49 ± 1.32	22.50 ± 2.34	26.29 ± 1.33	25.79 ± 2.40	34.63 ± 1.42	34.04 ± 2.02	46.45 ± 1.36	42.78 ± 2.17
	10	26.85 ± 0.88	26.46 ± 1.48	35.99 ± 0.92	32.90 ± 1.54	34.67 ± 0.97	33.27 ± 1.56	45.14 ± 0.96	42.12 ± 1.7
LH	4	25.43 ± 1.66	29.01 ± 2.88	32.74 ± 1.68	34.53 ± 2.90	N/A	N/A	N/A	N/A
	5	23.05 ± 1.00	24.40 ± 1.65	33.05 ± 1.03	31.93 ± 1.80	29.95 ± 1.04	30.74 ± 1.68	44.06 ± 1.07	41.40 ± 1.88
	9	27.06 ± 1.65	29.34 ± 2.72	37.20 ± 1.69	36.92 ± 2.84	32.03 ± 1.80	32.63 ± 2.27	46.34 ± 1.80	43.43 ± 2.45
	10	23.68 ± 0.95	25.22 ± 1.69	33.72 ± 0.99	32.98 ± 1.80	30.58 ± 1.11	31.55 ± 1.77	44.67 ± 1.18	42.41 ± 1.95
CO	4	22.15 ± 1.30	25.19 ± 1.90	28.54 ± 1.35	28.36 ± 1.95	N/A	N/A	N/A	N/A
	5	31.61 ± 0.80	33.50 ± 4.64	43.50 ± 0.81	42.60 ± 5.00	N/A	N/A	N/A	N/A
	9	24.42 ± 1.26	29.22 ± 2.69	30.80 ± 1.26	34.29 ± 2.89	N/A	N/A	N/A	N/A
	10	32.88 ± 0.88	N/A	44.76 ± 0.92	N/A	N/A	N/A	N/A	N/A

Note: Values represent the mean value ± standard deviation

Appendix to Section 4.3

Battery sizing:

Equation (*A.17*) describes SOC and temperature dependence of the internal battery resistance, with power functions derived from Wassiliadis et al. (2022) and limited to valid ranges, where the ambient temperature (T_{amb} – in °C) is used to approximate the actual battery temperature:

$$R_{ref} = R_{ref,0} * f_{BAT,IR}(T_{amb}, SOC)$$

$$\text{where } f(T_{amb}) = \begin{cases} 1.6 & T_{amb} \leq 0 \\ \min\left(1.6, 1.5963 * T_{amb}^{-0.152}\right) & T_{amb} \in (0,40) \\ 0.9 & , T_{amb} > 40 \end{cases} \quad \text{(A.17)}$$

$$\text{where } f(SOC) = \begin{cases} 1.3 & SOC = 0 \\ \min(1.3, 1.6288 * SOC^{-0.132}) & T_{amb} \in (0,100] \end{cases}$$

Validation and simulation results:

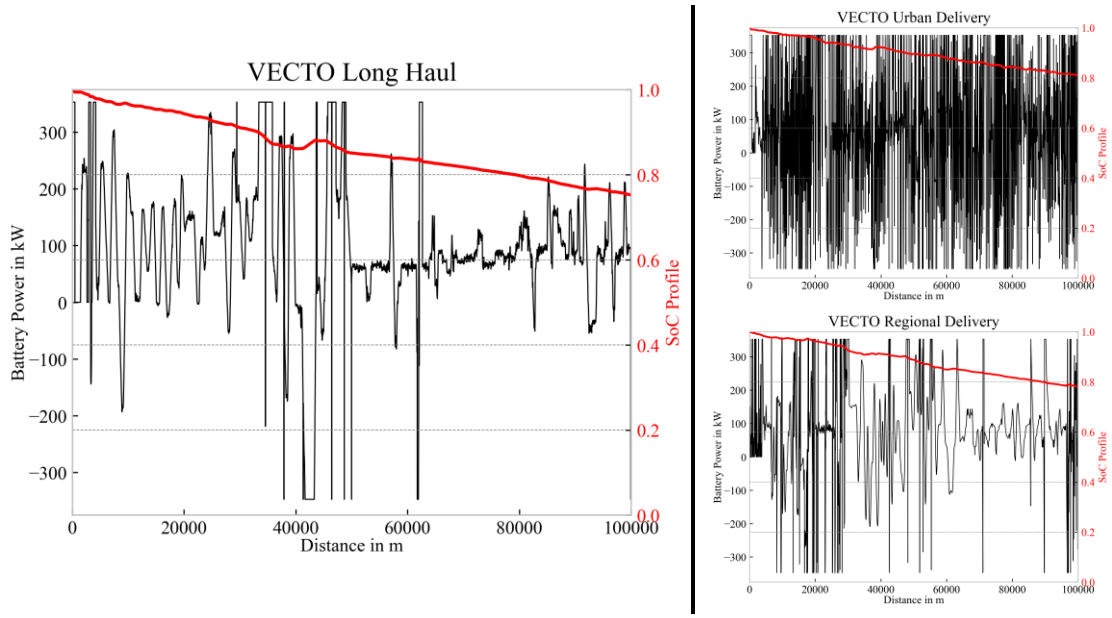

Note: Tractor 4x2 (VECTO-5); Battery: Pouch, NMC, 650 kWh, 180 Wh/kg; Ambient Temperature: 20°C; Payload: reference load

Figure S22: Truck simulation: Validation (power and SOC-profiles)

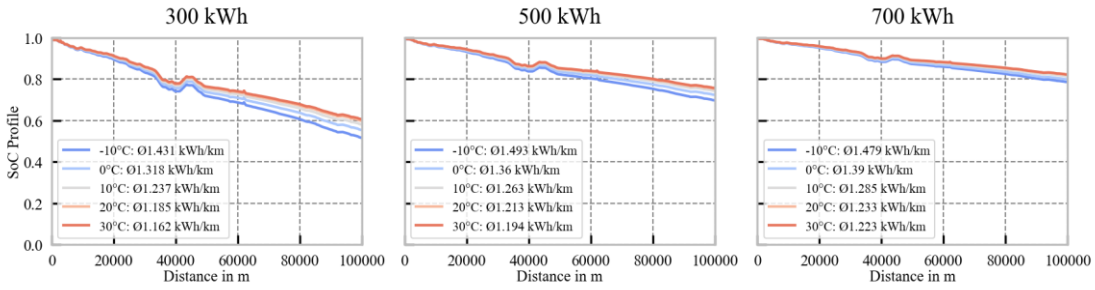

Note: Tractor 4x2 (VECTO-5); Battery: Prismatic, LFP; Payload: reference load; Mission Profile: VECTO-LH

Figure S23: Truck simulation: Validation (SOC-profiles)

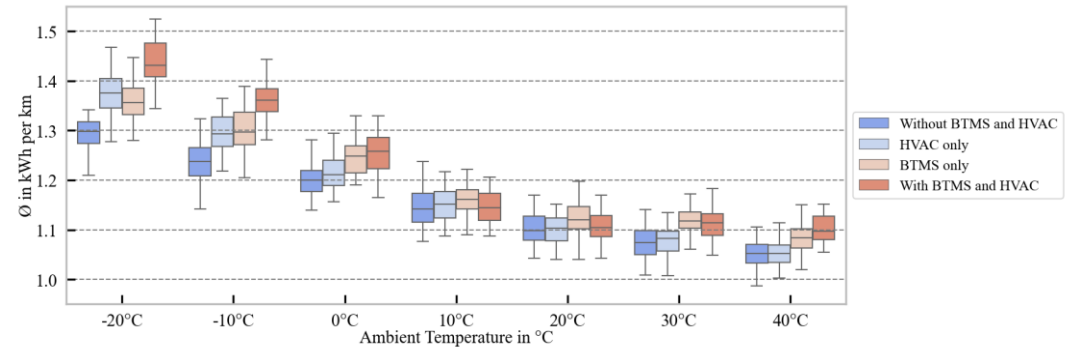

Note: Tractor 4x2 (VECTO-5); Battery: Prismatic, LFP; Payload: reference load; Mission Profile: VECTO-LH

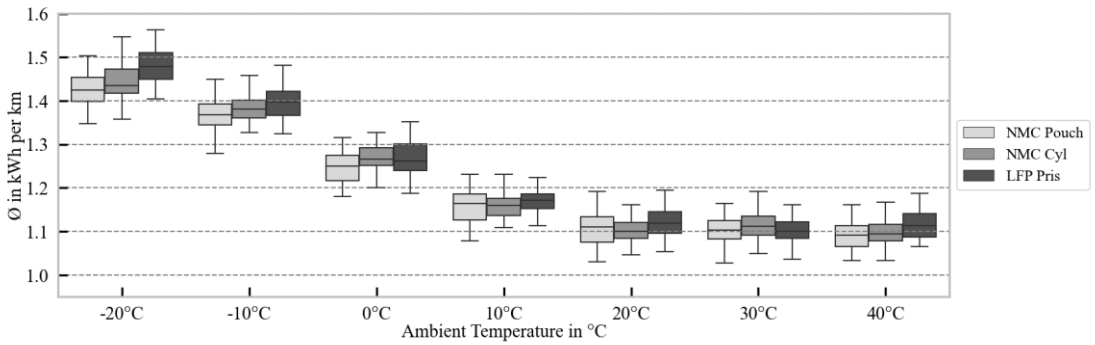

Note: Tractor 4x2 (VECTO-5); Payload: reference load; Mission Profile: VECTO-LH

Figure S24: Truck simulation: Validation (temperature effect)

Appendix to Section 4.4

Truck purchase costs and residual value

Table S17: Cost model: Scenario-dependent component costs

Component	Unit	*LOW*	*MEDIUM*	*HIGH*	Reference
c_{EM}	EUR_{2020}/kW	25	35	45	Link et al. (2024c)
c_{HV}	EUR_{2020}/kW	40	50	60	
c_{Bat}	EUR_{2020}/kWh	150	200	300	
c_{ICE}	EUR_{2020}/kW	61.2	72	82.8	(Plötz et al. 2023a)
c_{EAT}	EUR_{2020}/kW	15	19.8	25	

Table S18: Cost model: Chassis costs for rigid trucks per VECTO group

VECTO	Axles	Costs in $EURO_{2020}$ per body type		
		Normal	Chassis	Special
0	4x2	50,000	42,000	56,000
1	4x2	50,000	42,000	56,000
2	4x2	52,500	43,500	59,000
3	4x2	54,000	44,500	60,500
4	4x2	58,500	47,500	65,500
6	4x4	67,500	56,500	75,000
7	4x4	79,000	65,500	88,500
9	6x2	87,000	71,500	98,000
11	6x4	101,000	83,000	113,500
13	6x6	101,000	83,000	113,500
15	8x2	171,000	143,500	189,500
16	8x4	108,000	89,000	121,000
17	8x6	242,500	200,000	271,000

Note: Own calculation based on $data_{Resale}$

Table S19: Cost model: Chassis costs for tractors per VECTO group

VECTO	Axles	Costs in $EURO_{2020}$
1	4x2	38,500
2	4x2	40,500
3	4x2	41,500
5	4x2	60,500
8	4x4	82,000
10	6x2	76,500
12	6x4	107,000
14	6x6	140,000

Note: Own calculation based on $data_{Resale}$

Table S20: Cost model: Residual value (regression statistics)

Dependent variable: log (stated price)				
Term	**Tractors**		**Rigids**	
	Estimate	Standard error	Estimate	Standard error
(Intercept)	10.7202***	0.044	10.9547***	0.058
C(Axles) [T.4x2]	—	—	—	—
C(Axles) [T.4x4]	0.2070***	0.038	0.2304*	0.102
C(Axles) [T.6x2]	0.1493***	0.036	0.1515***	0.037
C(Axles) [T.6x4]	0.3***	0.025	0.1832*	0.063
C(Axles) [T.6x6]	0.5063***	0.073	0.1833	0.099
C(Axles) [T.8x2]	—	—	0.5992***	0.088
C(Axles) [T.8x4]	0.9329***	0.047	0.2341***	0.049
C(Axles) [T.8x6]	1.6382***	0.25	0.2084	0.108
C(Axles) [T.8x8]	—	—	0.3177*	0.122
C(Body) [Body]	—	—	—	—
C(Body) [Chassis]	—	—	-0.1437***	0.034
C(Body) [Special]	—	—	0.0872**	0.033
Age in years (β_1)	**-0.1361*** **	**0.003**	**-0.0769*** **	**0.045**
Mileage in million km (β_2)	**-0.5335*** **	**0.02**	**-0.9685*** **	**0.076**
Rated power in kW	2.7415***	0.117	2.4693***	0.025
Observations	4,446		812	
R^2	0.762		0.749	
Adjusted R^2	0.762		0.745	
F-Statistics	1582***		183.1***	
DF	9		13	

*p < 0.05; **p < 0.01; ***p < 0.001.

Truck maintainance costs

The maintainance costs for DTs cover lubricants, oil changes, Adblue refilling, components repair, and preventive maintenance. This thesis follows Basma et al. (2021b), who quantify the total costs at €0.0185/km. However, other studies reported lower values, such as Mareev et al. (2018) at €0.006/km, Craglia (2022) at €0.0074/km, Kampker et al. (2018) at €0.01/km, Kleiner et al. (2017) at €0.0147/km, Jöhrens et al. (2018) at €0.0156/km, Hunter et al. (2021) at €0.0047/km to €0.0094/km and €0.0187/km for their low, medium, and high range scenario.

The maintainance costs for BETs are typical lower than for DTs, although the level varies. Basma et al. (2021b) assumed an advantage of 28%, Hunter et al. (2021) assumed 21% to 52% for their scenarios, Kleiner et al. (2017) assumed 33%, and Craglia (2022) assumed 36%. Accordingly, typical ranges may be quantified to between 20% and 40%.

Table S21: Cost model: Maintainance costs

Powertrain	**Unit**	***LOW***	***MEDIUM***	***HIGH***	**Reference**
BET	EUR_{2020} ct/km	11.1	13.3	15.7	See assessment above
DT	EUR_{2020} ct/km	18.5	18.5	18.5	Basma et al. (2021b)

Toll costs:

Table S22: Cost model: Distance-based toll rates per country and truck class

Country	Unit	Light trucks	Medium trucks	Heavy Trucks	Note
AT	km	0.132 €	0.203 €	0.423 €	
BE	km	0.088 €	0.135 €	0.149 €	
BG	km	0.068 €	0.105 €	0.105 €	
HR	km	0.082 €	0.126 €	0.251 €	
CY	—	—	—	—	
CZ	km	0.049 €	0.075 €	0.202 €	
DK	km	0.083 €	0.128 €	0.154 €	
EE	yr	390 €	600 €	1,000 €	
FI	—	—	—	—	
FR	km	0.201 €	0.309 €	0.347 €	
DE	km	0.203 €	0.313 €	0.333 €	Based on toll rates without CO_2 charge (200 €/t, depending on the emission class) plus factor 1.75
EL	km	0.100 €	0.154 €	0.215 €	
HU	km	0.063 €	0.097 €	0.241 €	
IE	km	0.098 €	0.150 €	0.191 €	
IT	km	0.083€	0.128€	0.152€	
LV	yr	278€	427€	711€	
LT	yr	489€	753€	753€	
LU	yr	488€	750€	1,250€	
MT	—	—	—	—	
NL	km	0.082€	0.126€	0.130€	
PL	km	0.036€	0.055€	0.055€	
PT	km	0.075€	0.116€	0.166€	
RO	yr	364€	560€	1,210€	
SK	km	0.109€	0.167€	0.176€	
SI	km	0.120€	0.185€	0.428€	
ES	km	0.120€	0.185€	0.185€	
SE	yr	488€	750€	1,250€	
UK	yr	495€	762€	1,172€	
CH	km	0.148€	0.228€	0.433€	
NO	km	0.069€	0.106€	0.106€	
EUROPE	**km**	**0.096€**	**0.148€**	**0.215€**	**Cross-country mean value**

References: Basma et al. (2021b), Tol et al. (2022), Noll et al. (2022), and Toll Collect (2025)
Light: Trucks with a GVW between 3.5 and 12 tons
Medium: Trucks with a GVW between 12 to 18 tons
Heavy: Trucks with a GVW above 18 tons

Truck energy costs (diesel):

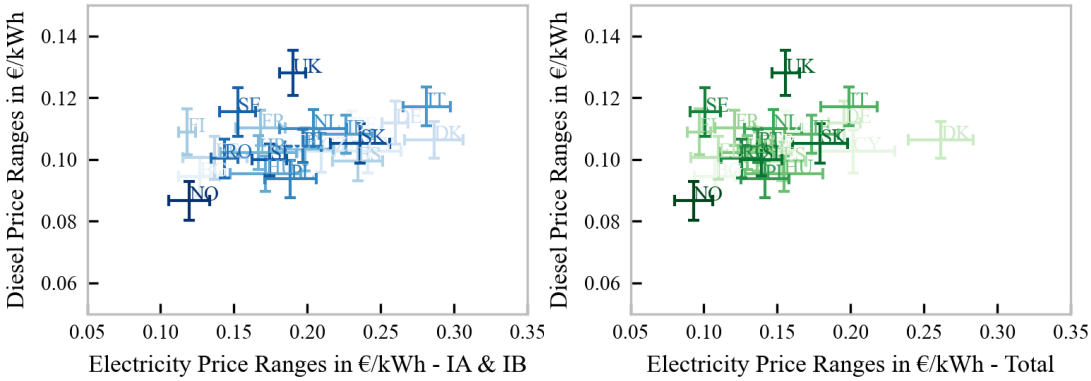

Note: Markers (mean value and error bars) represent mean values ± half standard deviation

Figure S25: Cost model: Differential prices of diesel and electricity

Table S23: Cost model: Historical diesel prices

Country	Mean	STD	Lower quartile	Upper quartile	Minimum	Maximum
AT	0.104	0.013	0.094	0.113	0.079	0.146
BE	0.109	0.013	0.100	0.118	0.083	0.150
BG	0.095	0.013	0.086	0.104	0.067	0.124
CH	0.156	0.015	0.144	0.168	0.128	0.192
CY	0.103	0.014	0.093	0.113	0.074	0.137
CZ	0.103	0.014	0.093	0.112	0.077	0.137
DE	0.112	0.014	0.102	0.120	0.084	0.155
DK	0.106	0.012	0.098	0.116	0.084	0.146
EE	0.101	0.014	0.089	0.110	0.073	0.139
EL	0.103	0.014	0.091	0.112	0.076	0.142
ES	0.099	0.013	0.090	0.109	0.077	0.139
FI	0.109	0.015	0.097	0.119	0.084	0.156
FR	0.110	0.011	0.102	0.118	0.086	0.147
HR	0.102	0.011	0.094	0.109	0.077	0.132
HU	0.095	0.012	0.089	0.103	0.068	0.124
IE	0.108	0.012	0.099	0.119	0.085	0.142
IS	0.099	0.013	0.090	0.107	0.074	0.133
IT	0.117	0.012	0.109	0.123	0.093	0.148
LI	0.100	0.013	0.091	0.109	0.073	0.137
LT	0.095	0.014	0.084	0.106	0.072	0.135
LU	0.098	0.013	0.088	0.106	0.074	0.146
LV	0.097	0.014	0.085	0.107	0.071	0.139
MT	0.102	0.012	0.091	0.110	0.082	0.124
NL	0.110	0.012	0.101	0.118	0.087	0.152
NO	0.087	0.013	0.078	0.095	0.062	0.123
PL	0.094	0.012	0.085	0.103	0.068	0.126
PT	0.104	0.011	0.097	0.111	0.081	0.136
RO	0.100	0.013	0.093	0.110	0.073	0.132
SE	0.115	0.016	0.104	0.125	0.085	0.168
SI	0.100	0.010	0.093	0.107	0.078	0.125
SK	0.105	0.013	0.097	0.115	0.080	0.137
UK	0.128	0.015	0.116	0.141	0.100	0.157

Note: Values in EUR_{2020} per kWh

Source: Weekly Oil Bulletin by Eurostat -https://energy.ec.europa.eu/data-and-analysis/weekly-oil-bulletin_en

Table S24: Cost model: Parameters for future diesel costs

Parameter	Unit	PERT parameter	2020	2025	2030	2035	2040	2045	2050	Ref
Non-ETS CO2	$EURO_{2020}$ per ton CO_2	-	0	60	115	210	300	300	300	[1]
Biodiesel costs	$EURO_{2020}$ per kWh	*Max*	0.177	0.218	0.251	0.273	0.288	0.285	0.264	[2]
		Most likely	0.162	0.189	0.212	0.230	0.244	0.248	0.242	
		Min	0.147	0.160	0.174	0.187	0.199	0.211	0.220	
Biodiesel share	%	*Max*	8%	-	15%	-	35%	-	60%	[2]
		Most likely	8%	-	10%	-	25%	-	50%	
		Min	8%	-	8%	-	15%	-	40%	
Synthetic diesel costs (Pt-Diesel)	$EURO_{2020}$ per kWh	*Max*	0.370	0.349	0.328	0.307	0.286	0.264	0.243	[2]
		Most likely	0.370	0.345	0.320	0.295	0.270	0.244	0.219	
		Min	0.370	0.341	0.312	0.283	0.254	0.224	0.195	
Synthetic diesel share	%	*Max*	0%	-	3%	-	35%	-	60%	[2]
		Most likely	0%	-	1%	-	25%	-	50%	
		Min	0%	-	0%	-	15%	-	40%	
Diesel cost index versus 2020	-	-	1.00	1.07	1.00	1.04	1.05	1.06	1.08	[2]

References: [1] (Gnann et al. 2023) [2] (Plötz et al. 2023a)

Truck energy costs (electricity):

Table S25: Cost model: Parameters for future electricity costs

Parameter	Unit	PERT parameter	2020	2025	2030	2035	2040	2045	2050	Ref
Energy Supply and Generation – Cost index vs. 2020	-	*Max*	1.00	1.00	1.00	0.80	0.75	0.73	0.70	[1]
		Most likely	1.00	1.00	0.85	0.70	0.58	0.57	0.57	
		Min	1.00	1.00	0.55	0.47	0.43	0.42	0.42	
Network costs – Cost index vs. 2020	-	*Max*	1.00	1.17	1.25	1.33	1.42	1.50	1.60	[1]
		Most likely	1.00	1.08	1.17	1.25	1.33	1.42	1.50	
		Min	1.00	1.00	1.10	1.15	1.20	1.30	1.35	

References: [1] (Plötz et al. 2023a)

Appendix to Section 4.5

Charging infrastructure costs:

The parameters used in Plötz et al. (2023a) were developed in consultation with the European Automobile Manufacturers' Association (ACEA) and based on scientific publications. Their calculated charging infrastructure costs followed the scheme by Basma et al. (2021b) and the calculated grid expansion costs followed the assessment by Burges et al. (2021). This thesis implements scenario variations by assuming a ten-year delay (*HIGH*) and a five-year advance (*LOW*) compared to the medium scenario, which is calculated accordingly.

For depot charging stations with four to ten chargers, costs per CCS charger start at around €50,000 by 2020 and decrease by 10% per five-year increment, which yields around €22,000 by 2050. The charger`s service life is assumed to be 15 years and OPEX are calculated as 3% of the CAPEX. The assumed charging efficiency is 90% and the interest rate is 9.5%. The utilization (6 weeks per day and 50 weeks per year) increases from 18% by 2020 to 33% by 2030 and beyond. Grid expansion costs are likely around €0.04 per kWh (Burges et al. 2021; Burges et al. 2022), but probably not every depot needs to expand its grid connection since the existing capacity may be sufficient. The final values are summarized in **Table S26.**

Table S26: Charging infrastructure: Cost parameters for depots

Parameter	Unit	PERT parameter	2020	2025	2030	2035	2040	2045	2050	Ref
Charging infrastructure costs	ct/kWh	*Max*	5.75	5.75	5.75	4.96	4.16	3.75	3.37	
		Most likely	5.75	4.96	4.16	3.75	3.37	3.04	2.73	[1,2]
		Min	4.96	4.16	3.75	3.37	3.04	2.73	2.46	
Local grid expansion	ct/kWh	*Max*	5.50	5.50	5.50	5.50	5.50	5.50	5.50	
		Most likely	4.00	4.00	4.00	4.00	4.00	4.00	4.00	[1,3]
		Min	0.50	0.50	0.50	0.50	0.50	0.50	0.50	

References: [1] (Plötz et al. 2023a) [2] (Basma et al. 2021b) [3] (Burges et al. 2021; Burges et al. 2022)

For public charging stations with four to eight chargers, costs per MCS charger start at around €485,000 by 2020 and decrease by 10% per five-year increment, which yields around €260,000 by 2050. The charger`s service life is assumed to be 15 years and OPEX are calculated as 3% of the CAPEX. The assumed charging efficiency is 90% and the interest rate is 9.5%. The utilization (6 weeks per day and 52 weeks per year) increases from 1% by 2020 to 4% by 2025 and coverges slowly towards 20% by 2050. Grid expansion costs are likely around €0.05 per kWh (Burges et al. 2021; Burges et al. 2022). The final values are summarized in **Table S27.**

Table S27: Charging infrastructure: Cost parameters for public locations

Parameter	Unit	PERT parameter	2020	2025	2030	2035	2040	2045	2050	Ref
Charging infrastructure costs	ct/kWh	*Max*	—	29.40	29.40	29.40	13.20	8.60	5.70	
		Most likely	—	29.40	13.20	8.60	5.70	4.30	3.50	[1,2]
		Min	—	13.20	8.60	5.70	4.30	3.50	2.80	
Local grid expansion	ct/kWh	*Max*	6.50	6.50	6.50	6.50	6.50	6.50	6.50	
		Most likely	5.00	5.00	5.00	5.00	5.00	5.00	5.00	[1,3]
		Min	3.50	3.50	3.50	3.50	3.50	3.50	3.50	

References: [1] (Plötz et al. 2023a) [2] (Basma et al. 2021b) [3] (Burges et al. 2021; Burges et al. 2022)

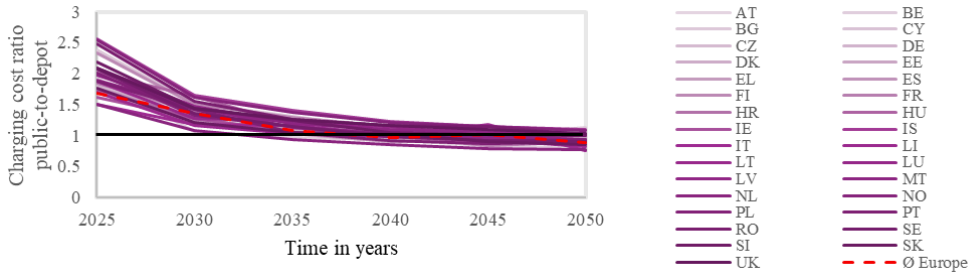

Note: Overlapping color scheme - only to visualize trends and scales.

Figure S26: Charging infrastructure: Cost ratio public-to-depot (MEDIUM scenario)

Charging infrastructure locations:

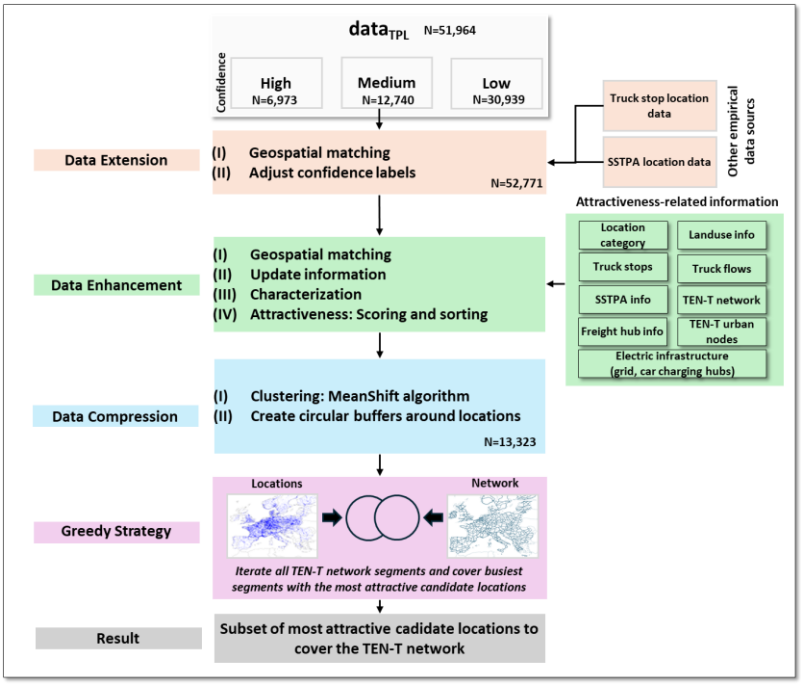

Figure S27: Charging infrastructure: Allocation approach

A4: Supplemental information to Chapter 5

Appendix to Section 5.1

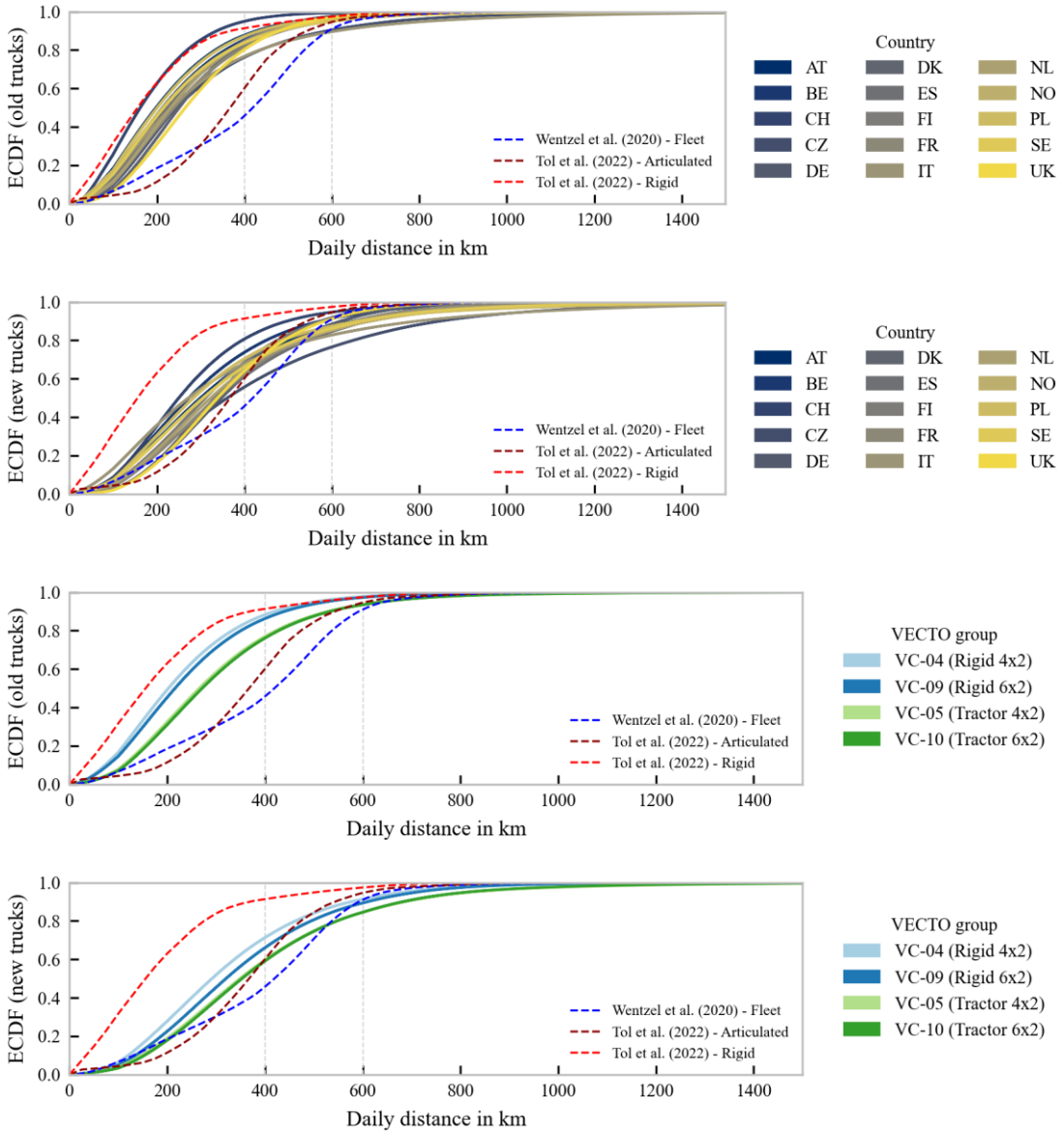

Figure S28: Results: Simulated daily mileage distributions by truck age

Appendix to Section 5.2

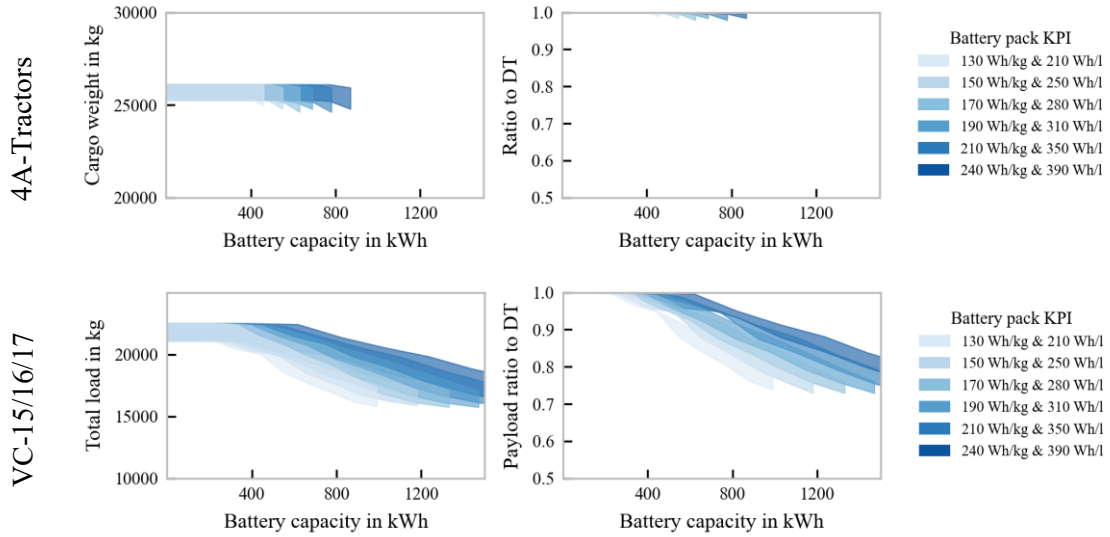

Figure S29: Results: Installable battery capacities (four-axle trucks)

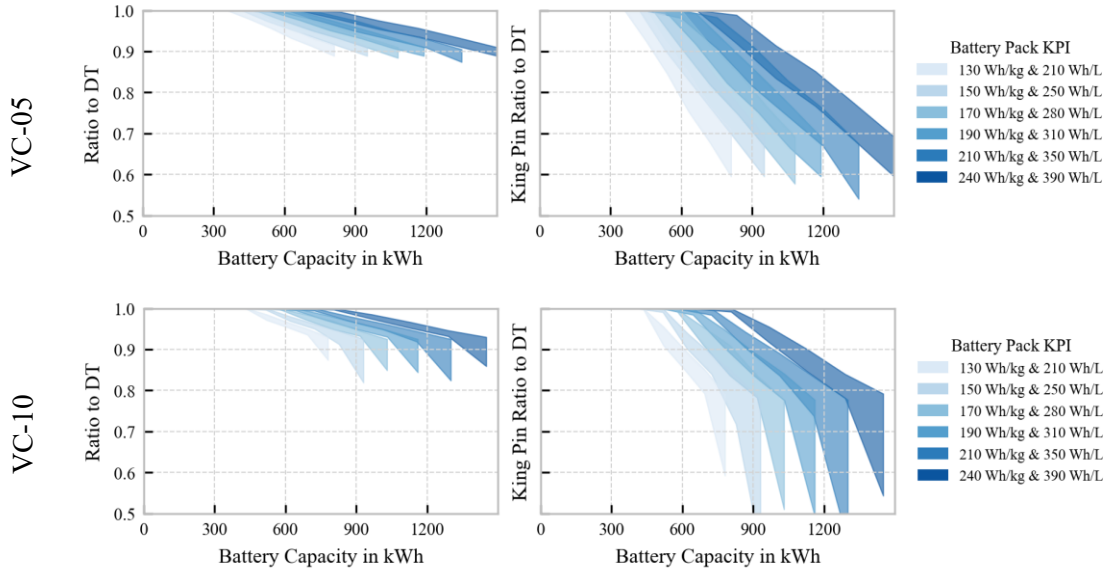

Figure S30: Results: Fifth-wheel load for tractors

Table S28: Results: Simulated energy consumption by country

Country	Mean	90th percentile	Upper quartile
AT	1.20 (1.01-1.29)	1.57 (1.19-1.80)	1.37 (1.08-1.55)
BE	1.34 (1.17-1.49)	1.63 (1.34-1.93)	1.49 (1.27-1.73)
CH	1.14 (0.99-1.20)	1.51 (1.21-1.76)	1.24 (1.04-1.36)
CZ	1.29 (1.12-1.34)	1.63 (1.52-1.84)	1.44 (1.22-1.57)
DE	1.22 (1.13-1.26)	1.62 (1.52-1.77)	1.37 (1.27-1.43)
DK	1.26 (1.16-1.33)	1.69 (1.54-1.95)	1.43 (1.30-1.59)
ES	1.17 (1.03-1.26)	1.51 (1.26-1.69)	1.32 (1.12-1.49)
FI	1.32 (1.02-1.55)	1.77 (1.18-2.36)	1.54 (1.09-1.98)
FR	1.22 (1.11-1.28)	1.59 (1.35-1.87)	1.39 (1.26-1.53)
IT	1.30 (1.20-1.39)	1.49 (1.37-1.57)	1.40 (1.30-1.50)
NL	1.13 (0.98-1.24)	1.44 (1.18-1.70)	1.24 (1.04-1.36)
NO	1.26 (1.02-1.38)	1.59 (1.17-1.92)	1.41 (1.07-1.63)
PL	1.12 (1.01-1.32)	1.33 (1.17-1.59)	1.23 (1.09-1.47)
SE	1.28 (1.01-1.42)	1.58 (1.18-1.96)	1.43 (1.07-1.69)
UK	1.17 (0.98-1.27)	1.52 (1.17-1.82)	1.31 (1.03-1.50)

Notation: Mean (Maximum – Minimum). All values in kWh/km

Table S29: Results: Simulated energy consumption by VECTO group

VECTO	Mean	90th percentile	Upper quartile
4	1.12 (0.98-1.27)	1.42 (1.17-1.71)	1.24 (1.04-1.48)
9	1.22 (1.03-1.49)	1.68 (1.28-2.16)	1.40 (1.13-1.81)
5	1.26 (1.15-1.39)	1.56 (1.41-1.69)	1.40 (1.24-1.54)
10	1.26 (1.17-1.41)	1.57 (1.46-1.85)	1.40 (1.26-1.62)

Notation: Mean (Maximum – Minimum). All values in kWh/km

Table S30: Results: Simulated daily energy requirements by country

Country	Mean	90th percentile	Upper quartile
AT	380 (160-570)	1,090 (480-1,460)	820 (350-1,120)
BE	380 (240-570)	1,070 (690-1,530)	820 (520-1,160)
CH	270 (150-470)	820 (480-1,320)	590 (340-1,010)
CZ	510 (290-670)	1,370 (1060-1,670)	1,080 (740-1,300)
DE	430 (250-580)	1,090 (780-1,380)	850 (560-1,090)
DK	410 (280-570)	1,020 (790-1,360)	790 (600-1,080)
ES	420 (190-610)	1,100 (540-1,500)	860 (400-1,160)
FI	420 (170-680)	1,100 (480-1,760)	840 (370-1,310)
FR	420 (280-570)	1,110 (820-1,430)	870 (620-1,130)
IT	450 (230-690)	1,220 (770-1,660)	960 (560-1,350)
NL	380 (180-590)	1,020 (500-1,480)	790 (380-1,190)
NO	430 (160-660)	1,160 (480-1,650)	910 (360-1,280)
PL	350 (180-670)	950 (540-1,580)	730 (400-1,260)
SE	440 (160-670)	1170 (480-1740)	910 (360-1310)
UK	410 (230-560)	970 (640-1260)	760 (480-1010)

Notation: Mean (Maximum – Minimum). All values in kWh

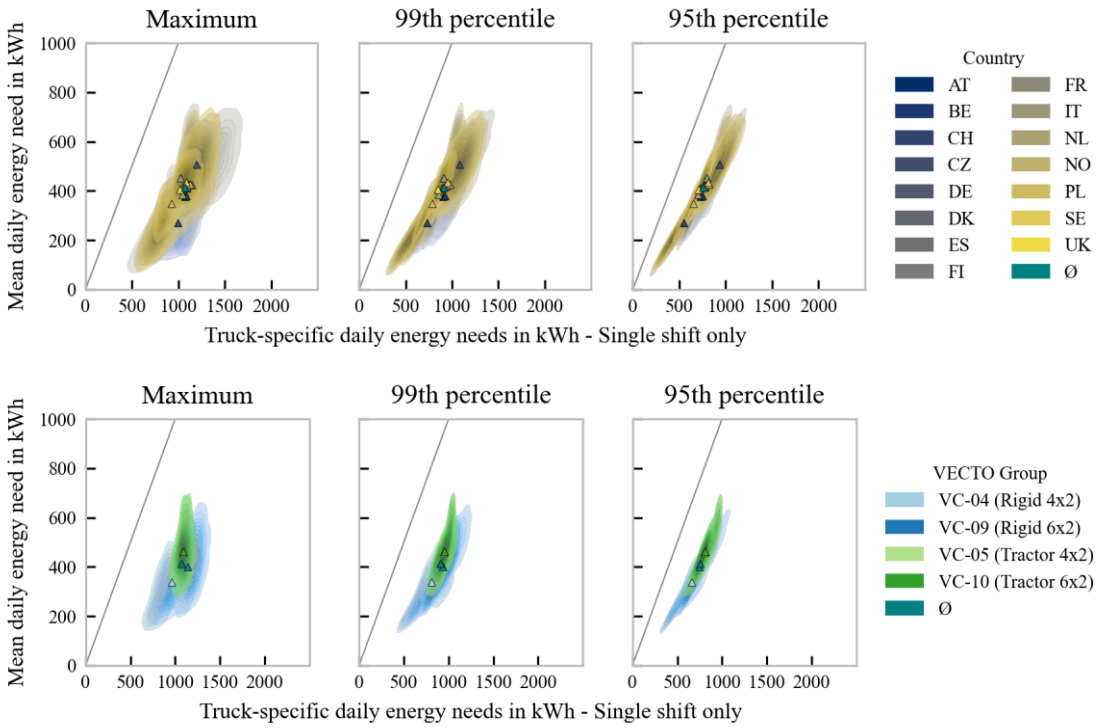

Figure S31: Results: Variation of daily energy requirements (single shift)

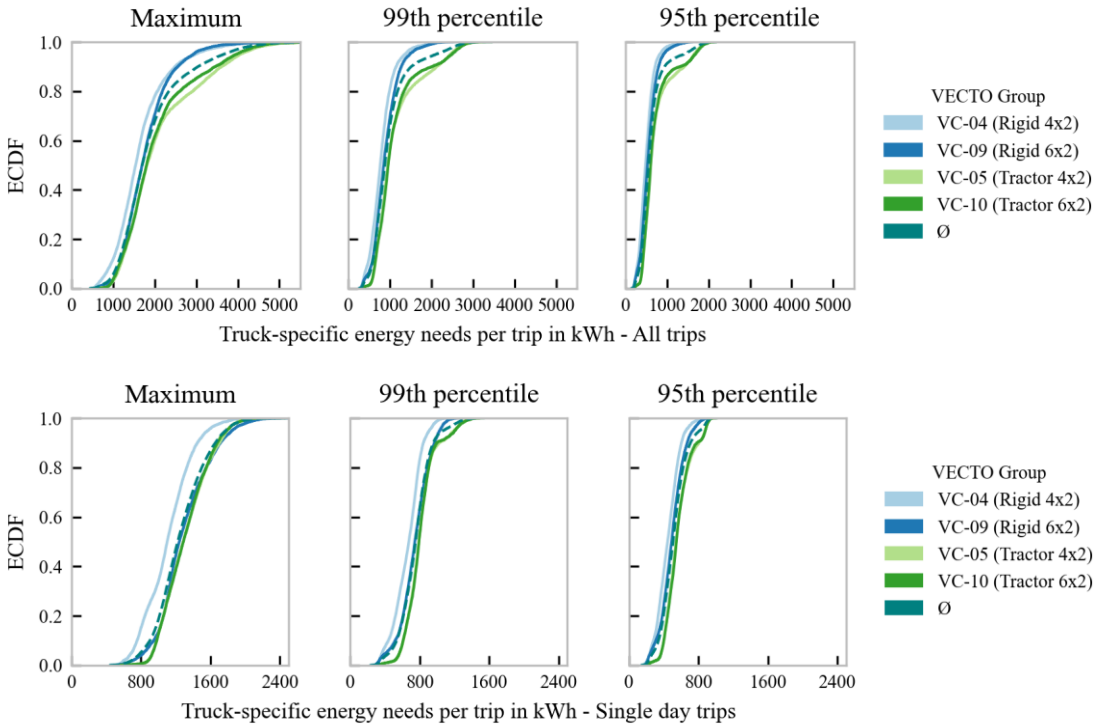

Figure S32: Results: Truck-specific maximum energy requirements per trip by VECTO group

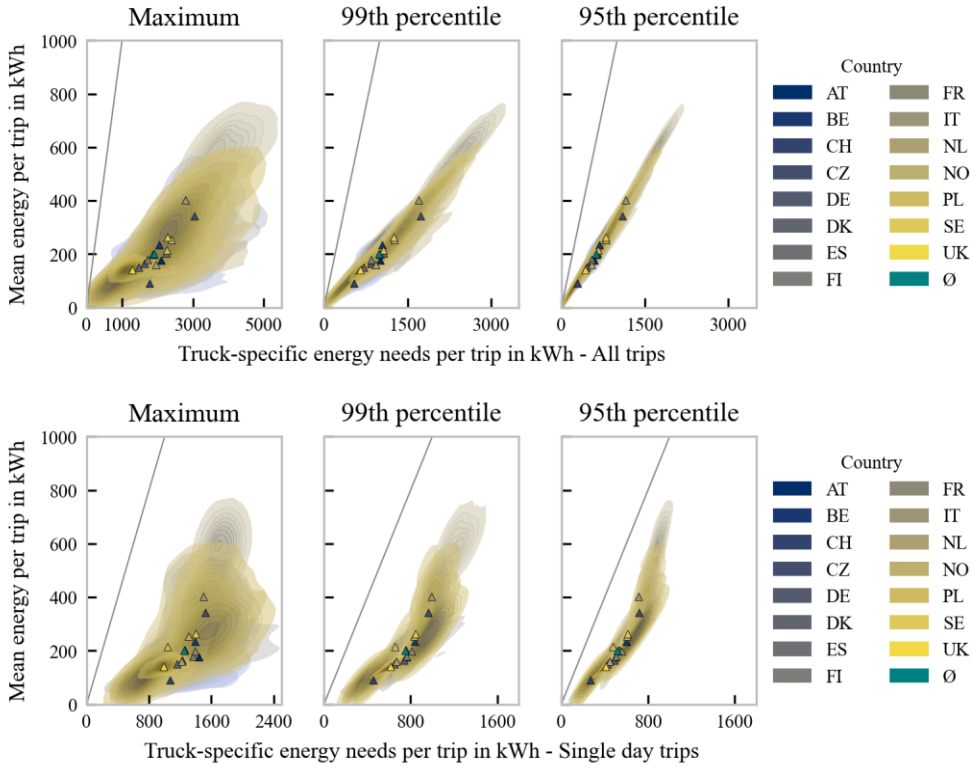

Figure S33: Results: Variation of truck-specific energy requirements per trip by country

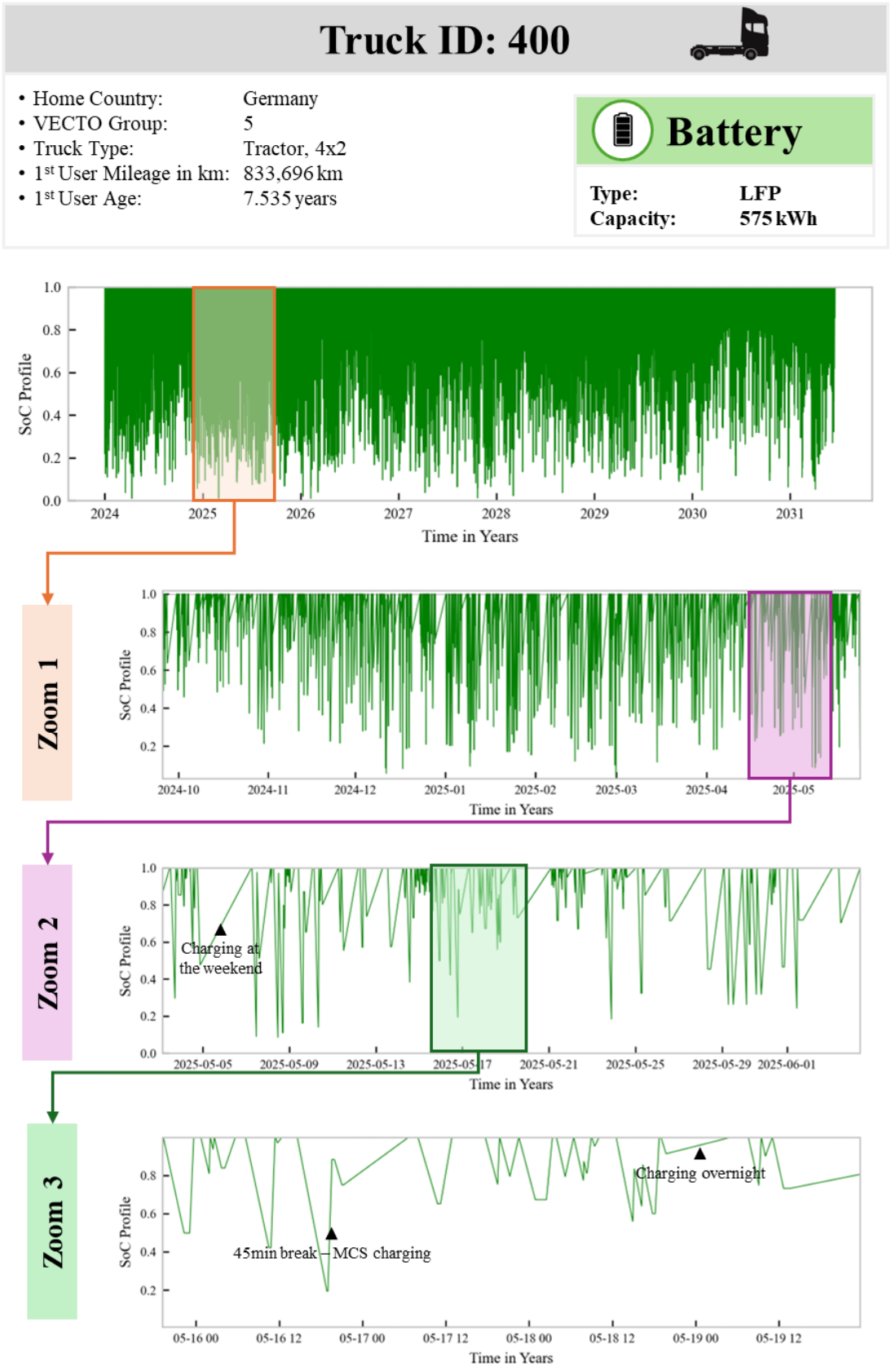

Figure S34: Results: Operational schedule expressed as SOC diagram

Figure S35: Results: Technical feasibility by selected countries for the unlimited scenario

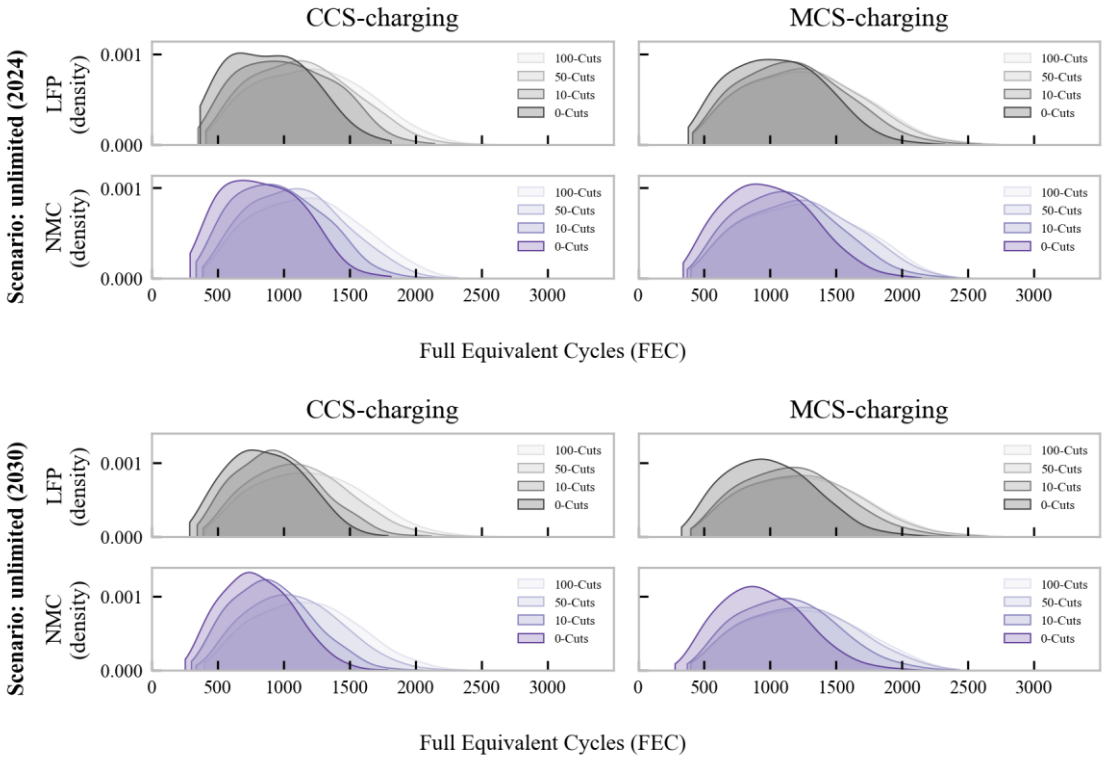

Figure S36: Results: Resulting FEC for the unlimited scenario

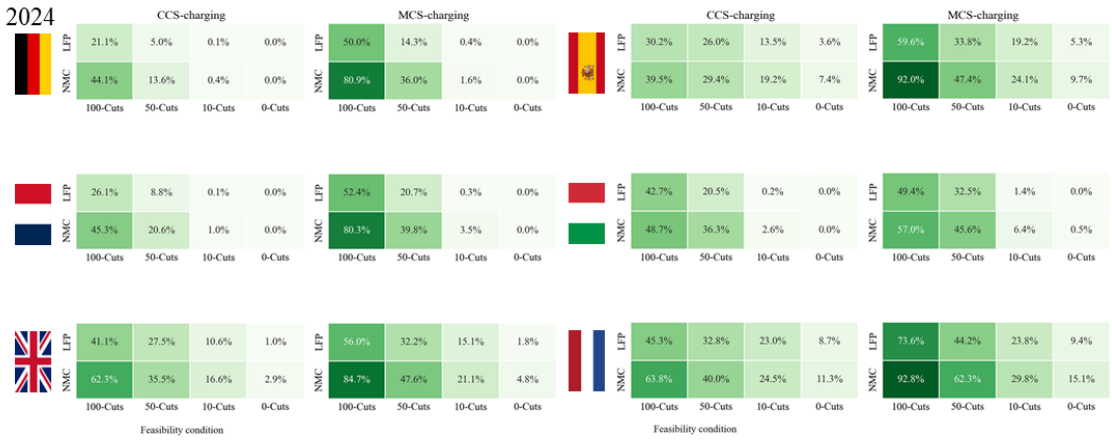

Figure S37: Results: Technical feasibility by selected countries for the limPrivate scenario

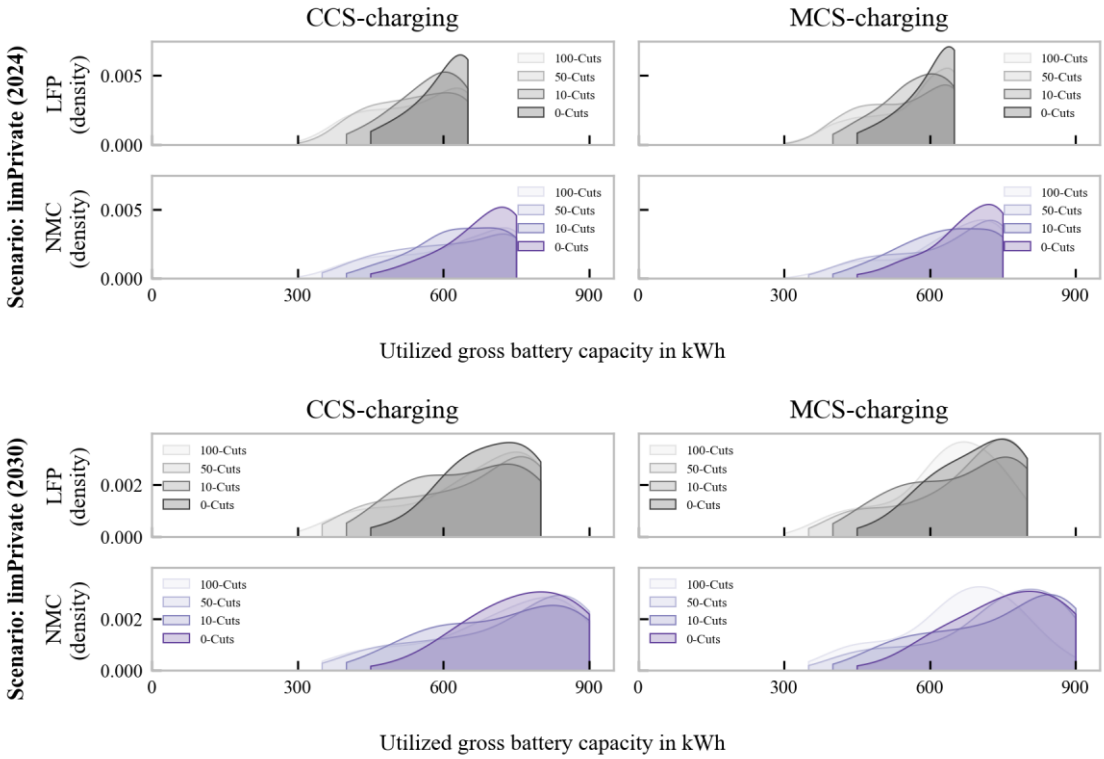

Figure S38: Results: Utilized battery capacities for the limPrivate scenario

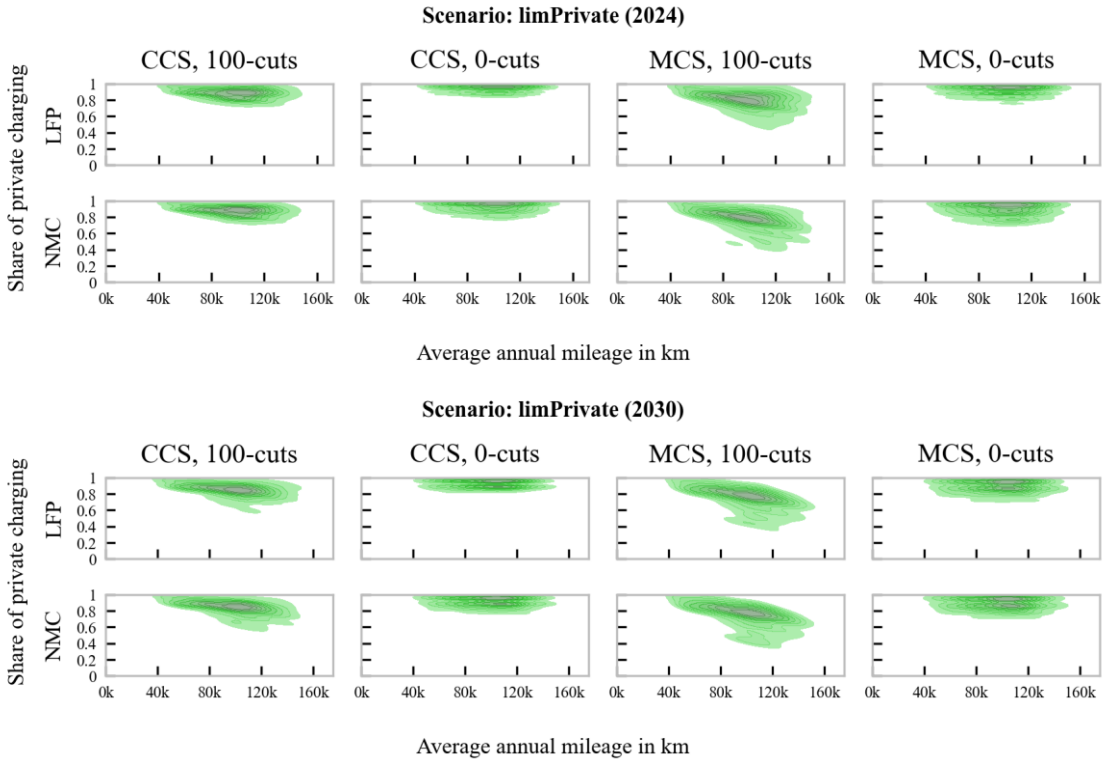

Figure S39: Results: Relevance of charging at private locations for the limPrivate scenario

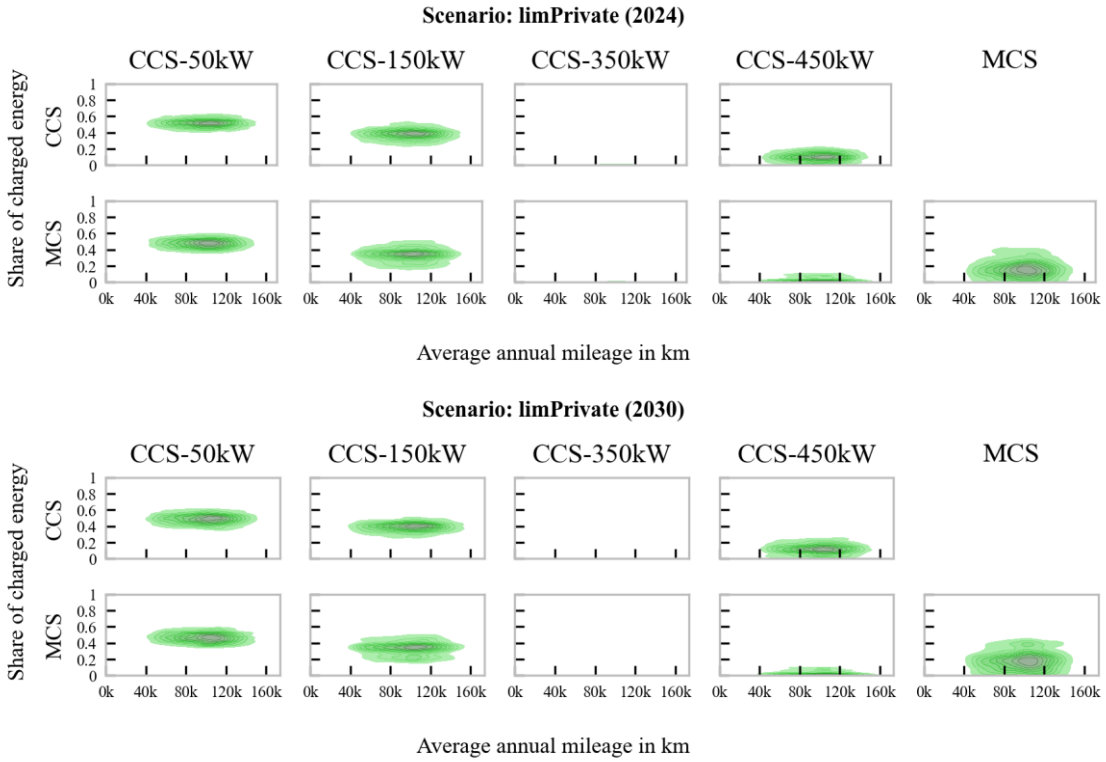

Note: Overlay of battery chemistry (LFP and NMC) and feasibility condition (*100-cuts* and *0-cuts*)

Figure S40: Results: Relevance of charging power for the limPrivate scenario

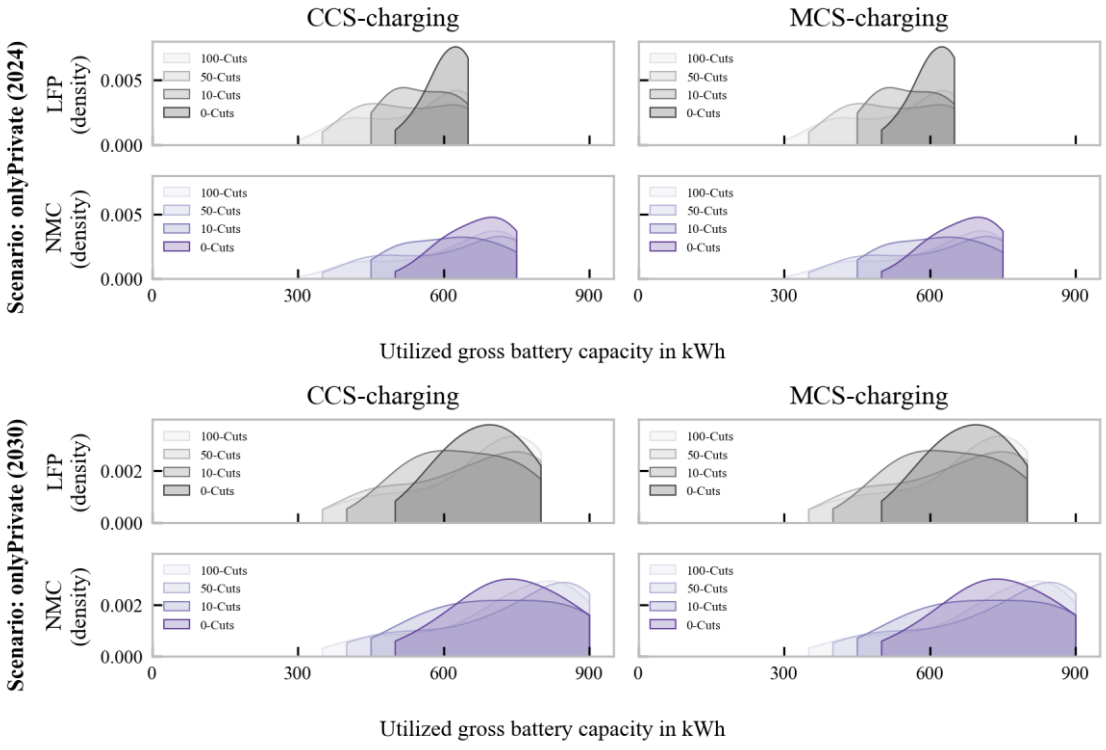

Figure S41: Results: Utilized battery capacities for the onlyPrivate scenario

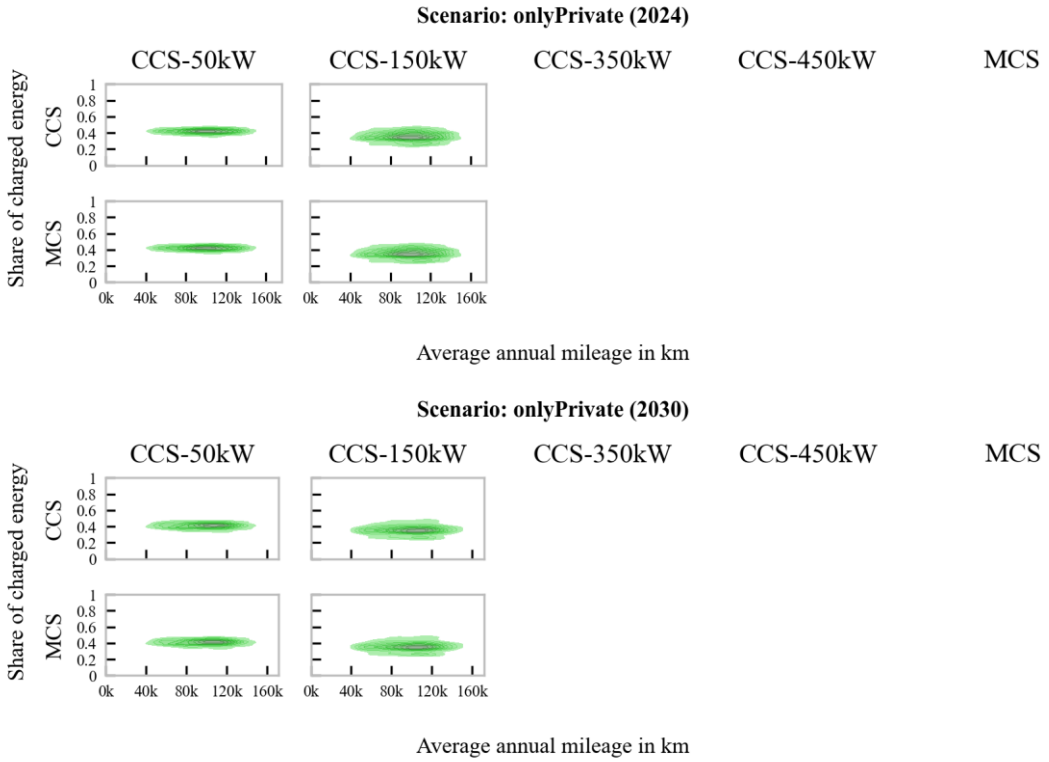

Note: Overlay of battery chemistry (LFP and NMC) and feasibility condition (*100-cuts* and *0-cuts*)

Figure S42: Results: Relevance of charging power for the onlyPrivate scenario

Appendix to Section 5.4

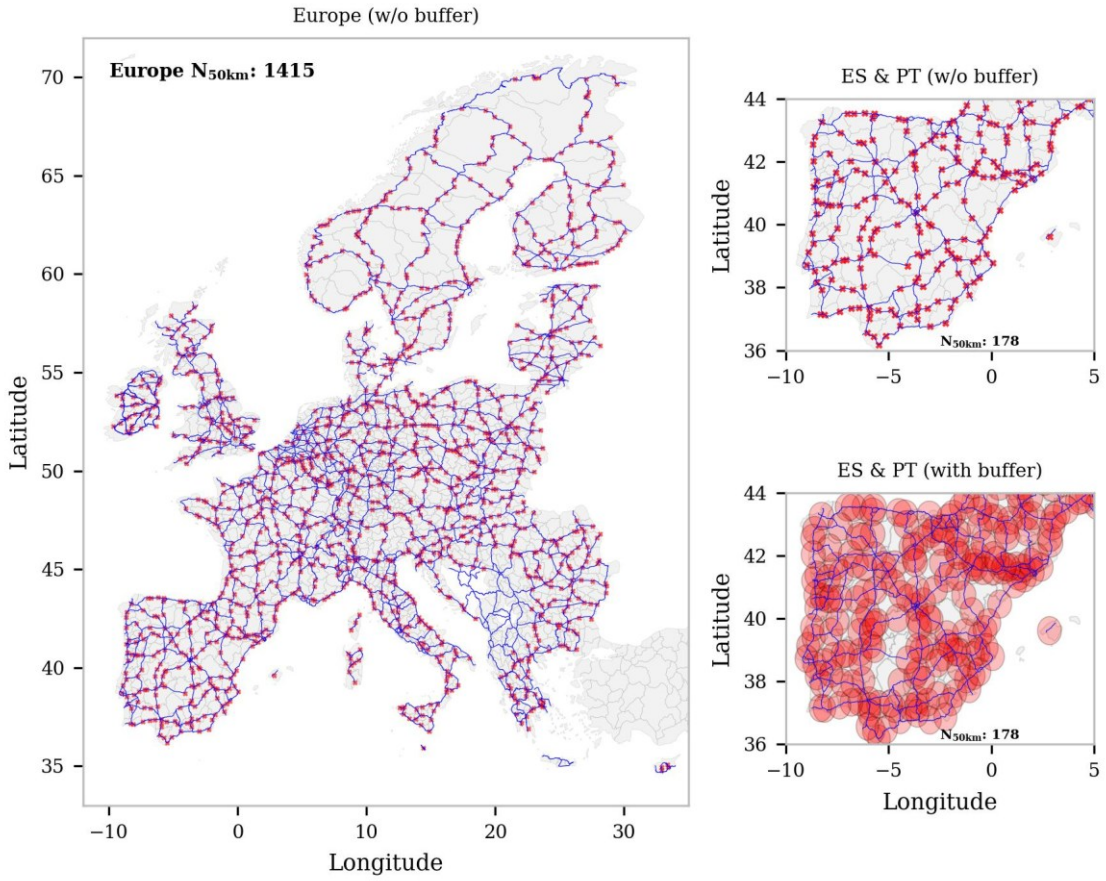

Figure S43: Results: Wide-meshed charging network (50 km)

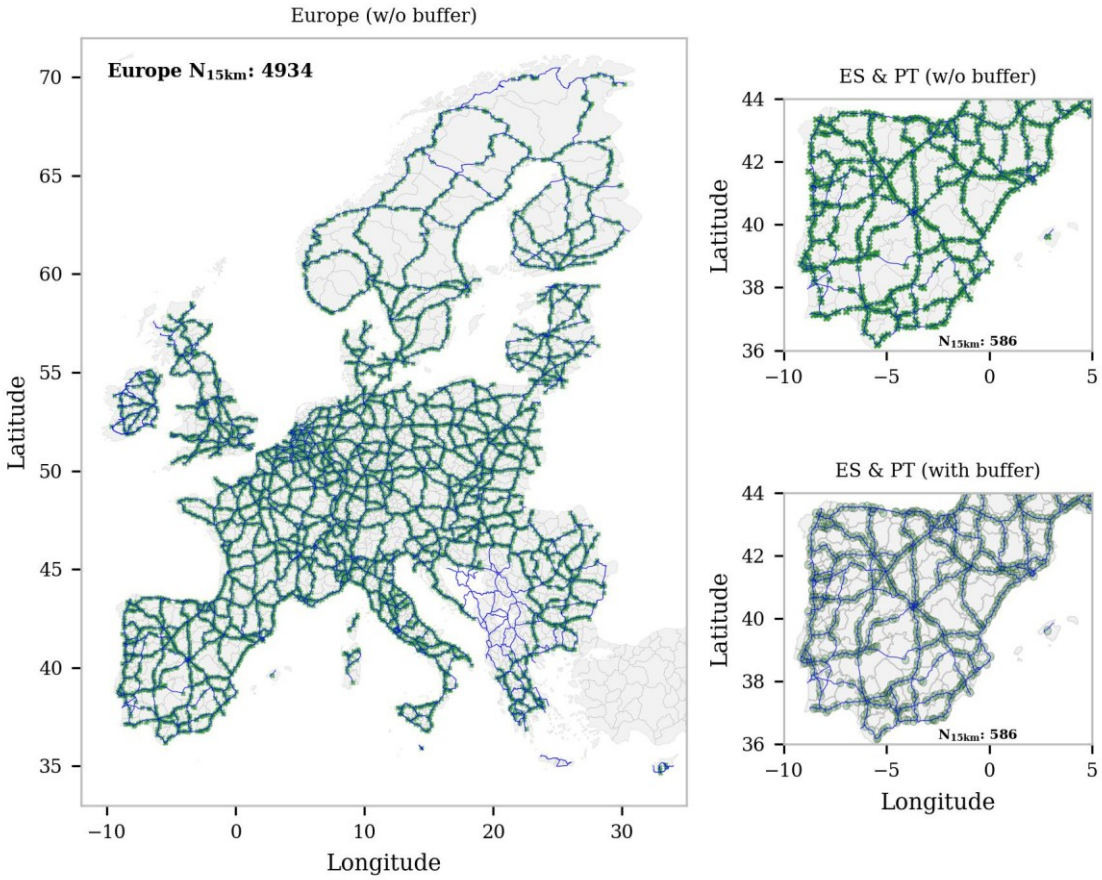

Figure S44: Results: High-dense charging network (15 km)

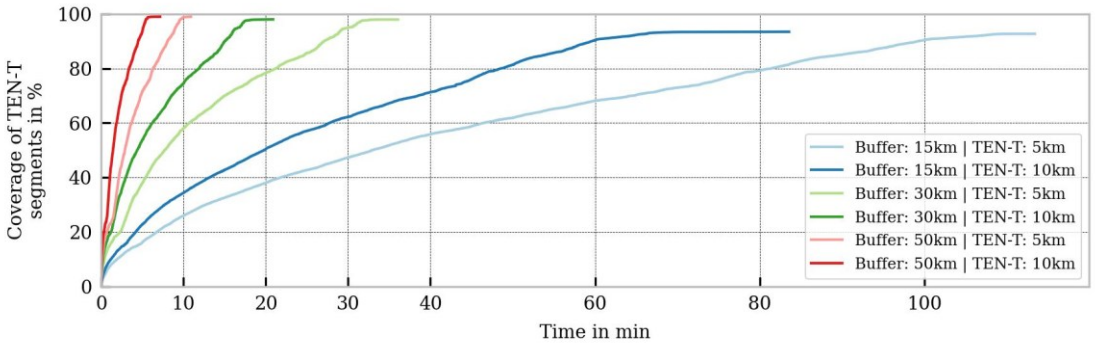

Figure S45: Results: Greedy algorithm: convergence and computing time

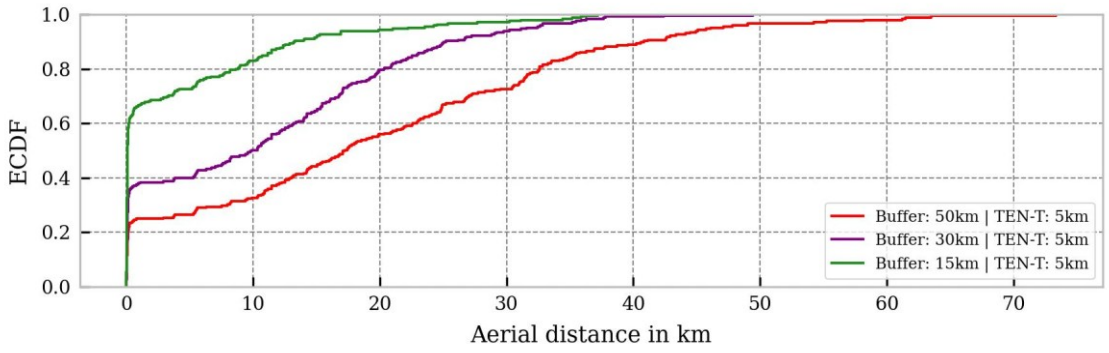

Figure S46: Results: Aerial distance versus NLL charging locations in Germany

Table S31: Results: Country-specific number of charging locations

Country	Number of charging locations per country		
	50 km (wide-meshed)	30 km (medium-dense)	15 km (high-dense)
AT	21 (21)	35 (34)	76 (74)
BE	19 (18)	30 (28)	73 (72)
BG	29 (29)	47 (46)	91 (88)
BY	0 (0)	1 (1)	1 (1)
CH	16 (16)	30 (29)	70 (71)
CY	4 (3)	5 (4)	5 (5)
CZ	28 (28)	45 (44)	89 (89)
DE	134 (135)	222 (219)	507 (506)
DK	20 (20)	35 (35)	79 (78)
EE	16 (15)	29 (28)	58 (56)
EL	41 (39)	68 (72)	111 (108)
ES	149 (147)	225 (229)	492 (476)
FI	79 (76)	122 (124)	213 (213)
FR	159 (167)	288 (284)	631 (630)
HR	20 (18)	35 (34)	67 (65)
HU	27 (26)	49 (47)	115 (107)
IE	29 (29)	44 (43)	68 (67)
IT	109 (104)	198 (189)	426 (414)
LT	23 (21)	46 (45)	89 (85)
LU	2 (2)	2 (2)	3 (3)
LV	17 (16)	35 (36)	59 (60)
MD	1 (1)	1 (1)	1 (1)
MT	1 (1)	1 (1)	1 (1)
NL	15 (14)	29 (30)	70 (70)
NO	65 (64)	92 (85)	187 (183)
PL	99 (96)	172 (172)	372 (355)
PT	29 (29)	41 (39)	94 (92)
RO	61 (58)	96 (93)	182 (172)
SE	90 (91)	137 (137)	282 (279)
SI	10 (9)	14 (13)	25 (26)
SK	14 (13)	28 (28)	62 (62)
UK	88 (86)	141 (141)	335 (326)
Europe	**1,415 (1,392)**	**2,343 (2,313)**	**4,934 (4,835)**
Coverage:	**99.01% (99.03%)**	**97.99% (98.05%)**	**92.73% (93.50%)**

Notation: $N_{5km\ TENT}$ ($N_{10km\ TENT}$)

List of prior publications

During the development of this thesis, several related publications and student theses were written in which distinct aspects and excerpts of this work were already presented. Please find a complete list in chronological order below.

Peer-reviewed journal publications (listed in Scopus / Web of Science)

- **Link, S.**, & Plötz, P. (2022). Technical Feasibility of Heavy-Duty Battery-Electric Trucks for Urban and Regional Delivery in Germany—A Real-World Case Study. World Electric Vehicle Journal, 13 (9), 161. https://doi.org/10.3390/wevj13090161
- **Link, S.**, Neef, C., & Wicke, T. (2023). Trends in Automotive Battery Cell Design: A Statistical Analysis of Empirical Data. Batteries, 9 (5), 261. https://doi.org/10.3390/batteries9050261
- Plötz, P., Wachsmuth, J., Sprei, F., Gnann, T., Speth, D., Neuner, F., & **Link, S.** (2023). Greenhouse gas emission budgets and policies for zero-carbon road transport in Europe. Climate Policy, 23(3), 343–354. https://doi.org/10.1080/14693062.2023.2185585
- Teichert, O., **Link, S.**, Schneider, J., Wolff, S., Lienkamp, M. (2023): Techno-economic cell selection for battery-electric long-haul trucks. eTransportation Journal, Volume 16. https://doi.org/10.1016/j.etran.2022.100225
- **Link, S.** & Plötz, P. (2024). Geospatial truck parking locations data for Europe. Data in Brief Journal, Volume 54. https://doi.org/10.1016/j.dib.2024.110277
- **Link, S.**, Stephan, A., Speth, D., Plötz P. (2024). Declining costs imply fast market uptake of zero-emission trucks. Nature Energy 9, 924–925. https://doi.org/10.1038/s41560-024-01555-1
- **Link, S.**, Stephan, A., Speth, D., Plötz P. (2024). Rapidly declining costs of truck batteries and fuel cells enable large-scale road freight electrification. Nature Energy 9, 1032–1039 (2024). https://doi.org/10.1038/s41560-024-01531-9
- **Link, S.**, Stephan, M., Weymann, L., & Hettesheimer, T. (2024). Techno-Economic Suitability of Batteries for Different Mobile Applications—A Cell Selection Methodology Based on Cost Parity Pricing. World Electric Vehicle Journal, 15 (9), 401. https://doi.org/10.3390/wevj15090401
- **Link, S.**, Schneider, L., Stephan, A., Weymann, L., Plötz, P. (2025). Feasibility of meeting future battery demand via domestic production in Europe. Nature Energy 10, 526–534. https://doi.org/10.1038/s41560-025-01722-y
- **Link, S.**, Schneider, L., Stephan, A., Weymann, L., Plötz, P. (2025). Reliable industrial policies required to support the ramp-up of European battery production. Nature Energy 10, 433-434. https://doi.org/10.1038/s41560-025-01741-9

Peer-reviewed journal publications (drafts/under review)

- Zackrisson, A., Engholm, A., Bengtsson, T., **Link, S.**, Plötz, P. (2025): Quantifying the Impact of Fleet Planning Re-Optimization on Truck Electrification in Distribution Logistics. *Under review - npj Sustainable Mobility and Transport*.
- Plötz, P., Sgaramella, A., **Link, S.**, Speth, D., Gnann, T., de Santoli, L. (2025/26): Hydrogen Refuelling and Charging Infrastructure for Trucks in Europe - a Cost Comparison. *Draft – to be submitted*.
- Hoppe, J., Pietzcker, R., Ueckerdt, F., Plötz, P., **Link, S.**, Speth, D., Zhao, P. (2025/26): Electrifying the haul: On the cost competitiveness of zero-emission heavy-duty trucks *Draft – to be submitted*.
- Plötz, P., Sgaramella, A., **Link, S.**, Speth, D., Gnann, T., de Santoli, L. (2025/26): Hydrogen Refuelling and Charging Infrastructure for Trucks in Europe - a Cost Comparison. *Draft – to be submitted*.
- **Link, S.**, Frank, F., Plötz, P.; Wietschel, M., Doppelbauer, M. (2025/26). From few to many: Creating detailed spatiotemporal operating profiles for heavy-duty trucks from empirical data. *Draft – to be submitted*.
- **Link, S.**, Speth, D., Plötz, P.; Wietschel, M., Doppelbauer, M. (2025/26). Evaluation of battery design strategies for heavy-duty trucks in Europe based on representative driving patterns and user-centric techno-economic battery selection. *Draft – to be submitted*.

Other publications (conferences, working paper)

- **Link., S.**, Speth, D., Griener, J., George, J. (2021): H2 mobility via fuel cell or IC engine: alternatives for heavy-duty vehicles in Germany and India? Eceee Summer Study Proceedings (2021). 711–721.
- Moll, C., **Link., S.** (2021): Attractiveness of electric vehicles under current tax and incentive schemes in Germany: a total cost of ownership calculation from the customer's perspective? Eceee Summer Study Proceedings (2021). 691–700.
- Gnann, T., Speth, D., **Link, S.**, Plötz, P. (2022). What is the right battery size for an electric truck with respect to its charging infrastructure? EVS35 Conference Proceedings. https://doi.org/10.24406/publica-618
- **Link, S.**, & Plötz, P. (2022). Link, S., & Plötz, P. (2022). Technical Feasibility of Heavy-Duty Battery-Electric Trucks for Urban and Regional Delivery in Germany. EVS35 Conference Proceedings. https://doi.org/10.24406/publica-271
- Plötz, P., Speth, D., **Link, S.** (2023). Locations for Battery Electric Truck Charging based on Truck Stop Location Data. EVS35 Conference Proceedings. https://doi.org/10.24406/publica-2253
- **Link, S.**, Auer, J., Plötz, P. (2023). Where to charge battery-electric trucks in Germany: A GIS-based statistical analysis using real-world truck data. EVS35 Conference Proceedings. https://doi.org/10.24406/publica-2252

- **Link, S.** (2023). Tailored battery design for heavy-duty trucks in Europe based on real-world operating patterns. Conference Proceedings – AABC Europe 2023.
- Scherrer, A., Helferich, M., Speth, D., **Link, S.** (2024): Requirements of German logistics companies for charging battery-electric trucks. Results of a combined survey and interview study. Fraunhofer ISI Working Paper. https://doi.org/10.24406/publica-2615
- Speth, D., **Link, S.**, Wietschel, M. (2024). Infrastructure Requirements for Electrified Heavy Road Transport in Germany and the EU. PCIM Europe 2024 – Conference Proceedings. https://doi.org/10.30420/566262481
- **Link, S.** & Neef, C. (2025). Cell and Battery Design – An Overview. Encyclopedia of Electrochemical Power Sources (Second Edition). Volume 2. Pages 522-531. https://doi.org/10.1016/B978-0-323-96022-9.00202-4
- Gnann, T., **Link, S.**, Speth, D., Scherrer, A. (2025). Powerfuels for Heavy-Duty Road Transportation. Book chapter. Powerfuels Status and Prospects. https://doi.org/10.1007/978-3-031-62411-7_28.
- Engholm, A., Zackrisson, A., Bengtsson, T., **Link, S.**, Plötz, P. (2025): Beyond replacing diesel trucks. How optimized fleet planning increases electrification and lowers transporation costs. Fraunhofer ISI Working Paper. https://doi.org/10.24406/publica-4574
- Plötz, P., Sgaramella, A., **Link, S.**, Speth, D., Gnann, T. (2025): Future Demand and Costs of Megawatt Charging for Battery Electric Trucks. EVS38 Conference.
- Speth, D., **Link, S.**, Plötz, P. (2025): Truck data for the future design of road freight transport. EVS38 Conference.
- **Link, S.**, Hendreich, S., Lincoln, S., Speth, D., Plötz, P. (2025): Empirical insights on usage trends and patterns of public fast-charging stations in Germany. EVS38 Conference.

Student theses

The following student theses were written within the framework of this dissertation under the supervision of the author in terms of content, technical and scientific support. Many thanks to the authors of the respective theses for their extensive support and contribution to my research.

- Griener, J. (2021): Alternative Antriebstechnologien im Kontext schwerer Nutzfahrzeuge: Techno-ökonomische Bewertung von Brennstoffzellen- und Wasserstoffmotoren-Lkw in Deutschland und Indien bis 2050. Karlsruhe Institute of Technology (KIT). Master Thesis. Examiner: Prof. Dr. Martin Wietschel (KIT-IIP).
- Auer, J. (2022): Gegenwärtige LKW-Halteorte und Eignung zukünftiger Ladeinfrastrukturstandorte für batterieelektrische LKW in Deutschland - Eine Untersuchung mittels GIS-basierter MCDA und Archetypenanalyse. Karlsruhe Institute of Technology (KIT). Master Thesis. Examiner: Prof. Dr. Martin Wietschel (KIT-IIP).
- Strohmaier, L. (2022): Nutzungsmuster von schweren Nutzfahrzeugen und Ableitung synthetischer Fahrprofile. Karlsruhe Institute of Technology (KIT). Master Thesis. Examiner: Prof. Dr. Martin Wietschel (KIT-IIP).

- Schneider, L. (2023/24): Comparison of Battery Supply and Demand for Battery Electric Passenger Vehicles in Europe until 2035 - A Scenario-Based Modeling Approach. Karlsruhe Institute of Technology (KIT). Master Thesis. Examiner: Prof. Dr. Martin Wietschel (KIT-IIP).
- Lincoln, S. (2024/25): Empirical Study of Battery Storages for Local Grid Integration at Electric Vehicle Charging Stations in Germany. Technical University of Darmstadt (TUD). Master Thesis. Examiner: Prof. Dr.-Ing. Clemens Rohde (TUD-ESE).
- Uhl, F. (2025): Towards sustainable batteries in Europe: Advancing circular economy along the battery value chain. Technical University of Darmstadt (TUD). Master Thesis. Examiner: Prof. Dr.-Ing. Clemens Rohde (TUD-ESE).

Eidesstattliche Versicherung

Eidesstattliche Versicherung gemäß § 13 Absatz 2 Ziffer 3 der Promotionsordnung des Karlsruher Instituts für Technologie (KIT) für die KIT-Fakultät für Elektrotechnik und Informationstechnik:

Bei der eingereichten Dissertation zu dem Thema

> *Assessing the techno-economic feasibility of battery-electric trucks in Europe: A model-based analysis of lithium-ion batteries and public charging infrastructure*

handelt es sich um meine eigenständig erbrachte Leistung.

Ich habe nur die angegebenen Quellen und Hilfsmittel benutzt und mich keiner unzulässigen Hilfe Dritter bedient. Insbesondere habe ich wörtlich oder sinngemäß aus anderen Werken übernommene Inhalte als solche kenntlich gemacht.

Die Arbeit oder Teile davon habe ich bislang nicht an einer Hochschule des In- oder Auslands als Bestandteil einer Prüfungs- oder Qualifikationsleistung vorgelegt.

Die Richtigkeit der vorstehenden Erklärungen bestätige ich.

Die Bedeutung der eidesstattlichen Versicherung und die strafrechtlichen Folgen einer unrichtigen oder unvollständigen eidesstattlichen Versicherung sind mir bekannt.

Ich versichere an Eides statt, dass ich nach bestem Wissen die reine Wahrheit erklärt und nichts verschwiegen habe.

Davis, Kalifornien - 21.11.2025	*Steffen Fabian Link*
Ort und Datum	Signatur / Name

References

Aggarwal, A.; Mittal, M.; Battineni, G. (2021): Generative adversarial network: An overview of theory and applications. In: International Journal of Information Management Data Insights, 1 (1), p. 100004, doi: 10.1016/j.jjimei.2020.100004

Al-Hanahi, B.; Ahmad, I.; Habibi, D.; Masoum, M. (2021): Charging Infrastructure for Commercial Electric Vehicles: Challenges and Future Works. In: IEEE Access.

Ananda, S.; Mulholland, E.; Musa, A. (2024): European Heavy-Duty Vehicle Market. Development Quarterly (January-December 2023). Market Spotlight - Race to Zero. Brussels: International Council on Clean Transportation.

Anderhofstadt, B.; Spinler, S. (2019): Factors affecting the purchasing decision and operation of alternative fuel-powered heavy-duty trucks in Germany – A Delphi study. In: Transportation Research Part D: Transport and Environment, 73, pp. 87–107, doi: 10.1016/j.trd.2019.06.003

Ank, M.; Sommer, A.; Abo Gamra, K.; Schöberl, J.; Leeb, M.; Schachtl, J.; Streidel, N.; Stock, S.; Schreiber, M.; Bilfinger, P.; Allgäuer, C.; Rosner, P.; Hagemeister, J.; Rößle, M.; Daub, R.; Lienkamp, M. (2023): Lithium-Ion Cells in Automotive Applications: Tesla 4680 Cylindrical Cell Teardown and Characterization. In: Journal of The Electrochemical Society, 170 (12), p. 120536, doi: 10.1149/1945-7111/ad14d0

Aryanpur, V.; Rogan, F. (2024): Decarbonising road freight transport: The role of zero-emission trucks and intangible costs. In: Scientific Reports, 14 (1), p. 2113, doi: 10.1038/s41598-024-52682-4

Auer, J.; Link, S.; Plötz, P.; :unav (2022): Public charging locations for battery electric trucks: A GIS-based statistical analysis using real-world truck stop data for Germany, doi: 10.24406/PUBLICA-1198

Bae, Y.; Mitra, S. K.; Rindt, C. R.; Ritchie, S. G. (2022): Factors influencing alternative fuel adoption decisions in heavy-duty vehicle fleets. In: Transportation Research Part D: Transport and Environment, 102, p. 103150, doi: 10.1016/j.trd.2021.103150

Baek, D.; Chen, Y.; Chang, N.; Macii, E.; Poncino, M. (2020): Optimal Battery Sizing for Electric Truck Delivery. In: Energies, 13 (3), p. 709, doi: 10.3390/en13030709

Balke, G.; Adenaw, L. (2023): Heavy commercial vehicles' mobility: Dataset of trucks' anonymized recorded driving and operation (DT-CARGO). In: Data in brief, 48, p. 109246, doi: 10.1016/j.dib.2023.109246

Basma, H.; Beys, Y.; Rodriguez, F. (2021a): Battery electric tractor-trailers in the European Union: A vehicle technology analysis. Working Paper. Berlin: International Council on Clean Transportation.

Basma, H.; Rodríguez, F. (2023): The European Heavy-Duty Vehicle Market until 2040: Analysis of decarbonization pathways. White Paper. Berlin: International Council on Clean Transportation.

Basma, H.; Saboori, A.; Rodríguez, F. (2021b): Total Cost of Ownership for tractor-trailres in Europe: Battery-electric versus Diesel. White Paper. Available at https://theicct.org/wp-content/uploads/2021/11/tco-bets-europe-1-nov21.pdf.

Berndard, M. R.; Hall, D. (2021): Efficient planning and implementation of public chargers: Lessons learned from European cities. Working Paper 2021-05. Brussels: International Council on Clean Transportation.

Berndard, M. R.; Tankou, A.; Cui, H.; Ragon, P.-L. (2022): Charging Solutions for battery-electric trucks. Washington, D.C.: International Council on Clean Transportation.

Birkl, C. R.; Roberts, M. R.; McTurk, E.; Bruce, P. G.; Howey, D. A. (2017): Degradation diagnostics for lithium ion cells. In: Journal of Power Sources, 341, pp. 373–386, doi: 10.1016/j.jpowsour.2016.12.011

BloombergNEF (2024): Lithium-Ion Battery Pack Prices See Largest Drop Since 2017, Falling to $115 per Kilowatt-Hour. Washington, D.C.

Boer, E. den; Aarnink, S.; Kleiner, F.; Pagenkopf, J. (2013): Zero emissions trucks. An overview of state-of-the-art technologies and their potential. Delft: CE Delft; Deutsches Zentrum für Luft- und Raumfahrt.

Borlaug, B.; Muratori, M.; Gilleran, M.; Woody, D.; Muston, W.; Canada, T.; Ingram, A.; Gresham, H.; McQueen, C. (2021): Heavy-duty truck electrification and the impacts of depot charging on electricity distribution systems. In: Nature Energy, 6 (6), pp. 673–682, doi: 10.1038/s41560-021-00855-0

Brooker, A.; Gonder, J.; Wang, L.; Wood, E.; Lopp, S.; Ramroth, L. (2015): FASTSim: A Model to Estimate Vehicle Efficiency, Cost and Performance, doi: 10.4271/2015-01-0973

Bstieler, M. (2021): Package-Analysis for the Evaluation of Zero-Emission Technologies for Heavy-Duty Vehicle Concepts, Technische Universität München (Ed.).

Burges, K.; Kippelt, S. (2021): Grid-related challenges of high-power and megawatt charging stations for battery-electric long-haul trucks. Brussels.

Burges, K.; Kippelt, S.; Probst, F. (2022): Grid-related challenges of high power charging stations for battery electric long haul trucks. In: IET Conference Proceedings, 2021 (10), pp. 144–148, doi: 10.1049/icp.2021.2517

Burke, A.; Fulton, L. (2019): Analysis of advanced battery-electric long haul trucks: batteries, performance, and economics. Working Paper. UC Davis STEPS+ Sustainable Freight Research Center.

Çabukoglu, E.; Georges, G.; Küng, L.; Pareschi, G.; Boulouchos, K. (2018): Battery electric propulsion: An option for heavy-duty vehicles? Results from a Swiss case-study. In: Transportation Research Part C: Emerging Technologies, 88, pp. 107–123, doi: 10.1016/j.trc.2018.01.013

Calstart (2024): Drive to Zero's Zero-emission Technology Inventory (ZETI) Tool. Version 9.0. California.

Cheng, X.; Lin, J. (2024): Is electric truck a viable alternative to diesel truck in long-haul operation? In: Transportation Research Part D: Transport and Environment, 129, p. 104119, doi: 10.1016/j.trd.2024.104119

Craglia, M. (2022): Decarbonising Europe's Trucks How to Minimise Cost Uncertainty. Case-Specific Policy Analysis. Policy Paper No. 107. Available at https://www.itf-oecd.org/sites/default/files/docs/decarbonising-europes-trucks-minimise-cost-uncertainty.pdf.

Creutzig, F.; Jochem, P.; Edelenbosch, O. Y.; Mattauch, L.; van Vuuren, D. P.; McCollum, D.; Minx, J. (2015): Energy and environment. Transport: A roadblock to climate change mitigation? In: Science (New York, N.Y.), 350 (6263), pp. 911–912, doi: 10.1126/science.aac8033

Daimler Trucks (2024): Daimler eActros600 Product Page. Stuttgart.

Deb, S.; Tammi, K.; Kalita, K.; Mahanta, P. (2018): Review of recent trends in charging infrastructure planning for electric vehicles. In: WIREs Energy and Environment, 7 (6), doi: 10.1002/wene.306

Demissie, M. G.; Kattan, L. (2022): Estimation of truck origin-destination flows using GPS data. In: Transportation Research Part E: Logistics and Transportation Review, 159, p. 102621, doi: 10.1016/j.tre.2022.102621

Deng, J.; Bae, C.; Denlinger, A.; Miller, T. (2020): Electric Vehicles Batteries: Requirements and Challenges. In: Joule, 4 (3), pp. 511–515, doi: 10.1016/j.joule.2020.01.013

Depcik, C.; Gaire, A.; Gray, J.; Hall, Z.; Maharjan, A.; Pinto, D.; Prinsloo, A. (2019): Electrifying Long-Haul Freight—Part II: Assessment of the Battery Capacity. In: SAE International Journal of Commercial Vehicles, 12 (2), doi: 10.4271/02-12-02-0007

Dimatulac, T.; Maoh, H.; Carriveau, R. (2023): An archetypal routing network model to help identify potential charging locations for long-haul electric vehicles in Ontario, Canada. In: Transportation Research Interdisciplinary Perspectives, 19, p. 100825, doi: 10.1016/j.trip.2023.100825

Doppelbauer, M. (2020): Grundlagen der Elektromobilität. Technik, Praxis, Energie und Umwelt. Wiesbaden: Springer Fachmedien Wiesbaden; Imprint Springer Vieweg.

Earl, T.; Mathieu, L.; Cornelis, S.; Kenny, Samuel, Ambel, Carlos Calvo; Niix, J. (2018): Analysis of long haul battery electric trucks in EU. Marketplace and technology, economic, environmental, and policy perspectives. 8th Commerical Vehicle Workshop: Transport and Environment.

Ecker, M.; Gerschler, J. B.; Vogel, J.; Käbitz, S.; Hust, F.; Dechent, P.; Sauer, D. U. (2012): Development of a lifetime prediction model for lithium-ion batteries based on extended accelerated aging test data. In: Journal of Power Sources, 215, pp. 248–257, doi: 10.1016/j.jpowsour.2012.05.012

Edge, J. S.; O'Kane, S.; Prosser, R.; Kirkaldy, N. D.; Patel, A. N.; Hales, A.; Ghosh, A.; Ai, W.; Chen, J.; Yang, J.; Li, S.; Pang, M.-C.; Bravo Diaz, L.; Tomaszewska, A.; Marzook, M. W.; Radhakrishnan, K. N.; Wang, H.; Patel, Y.; Wu, B.; Offer, G. J. (2021): Lithium ion battery degradation: what you need to know. In: Physical chemistry chemical physics : PCCP, 23 (14), pp. 8200–8221, doi: 10.1039/d1cp00359c

electrive.com (Ed.) (2025). *CATL to open 300 battery exchange stations for electric trucks by the end of the year*. Available at https://www.electrive.com/2025/05/19/catl-plans-to-open-300-battery-exchange-stations-for-e-trucks-by-the-end-of-the-year/.

Engholm, A.; Zackerisson, A.; Bengtsson, T.; Link, S.; Plötz, P. (2025): Beyond replacing diesel trucks: how optimized fleet planning increases electrification and lowers transportation costs. Karlsruhe: Einride AB; Fraunhofer ISI.

Environmental Protection Agency (2024): Greenhouse Gas Emissions Standards for Heavy-Duty Vehicles—Phase 3. Washington, D.C.

European Climate Assessment and Datasets (2024): Daily temperature data. Brussels.

European Commission (2024): EU Transport in Figures - Statistical Pocketbook. Mobility and Transport. Brussels.

European Environment Agency (2024): Monitoring of CO2 emissions from heavy-duty vehicles. Brussels.

Eurostat (2008): Road freight transport methodology: Reference Manual for the implementation of Council Regulation No. 1172/98 on statistics on the carrage of goods by road. Luxembourg: Statistical Office of the European Communities.

Eurostat (2016a): Anonymised Road Carriage (RC) micro-data: User Manual. Brussels.

Eurostat (2016b): Road freight transport methodology. 2016 edition. Luxembourg: Publications Office.

Gaete-Morales, C.; Kramer, H.; Schill, W.-P.; Zerrahn, A. (2021): An open tool for creating battery-electric vehicle time series from empirical data, emobpy. In: Scientific Data, 8 (1), p. 152, doi: 10.1038/s41597-021-00932-9

Gallagher, K.; Charvin, K.; Nielsen, S. B.; Sambridge, M.; Stephenson, J. (2009): Markov chain Monte Carlo (MCMC) sampling methods to determine optimal models, model resolution and model choice for Earth Science problems. In: Marine and Petroleum Geology, 26 (4), pp. 525–535.

Garrido, J.; Hidalgo, E.; Barth, M.; Boriboonsomsin, K. (2023): Home-Base Charging Load Profiles of Battery Electric Trucks Considering Tour Completion and Time-of-Use Rates. In: 2023 IEEE Transportation Electrification Conference & Expo (ITEC). 21-23 June 2023 : conference location: Detroit, MI, USA (2023 IEEE Transportation Electrification Conference & Expo (ITEC)), 6/21/2023 - 6/23/2023, Detroit, MI, USA.

Geslin, A.; Le Xu; Ganapathi, D.; Moy, K.; Chueh, W. C.; Onori, S. (2024): Dynamic cycling enhances battery lifetime. In: Nature Energy, doi: 10.1038/s41560-024-01675-8

Gnann, T.; Link, S.; Speth, D.; Scherrer, A. (2025): Powerfuels for Heavy-Duty Road Transportation. In: 1865-3537, pp. 821–847, doi: 10.1007/978-3-031-62411-7_28

Gnann, T.; Speth, D.; Krail, M.; Wietschel, M. (2023): Langfristszenarien für die Transformation des Energiesystems in Deutschland 3: T45-Szenarien. Modul Verkehr. Berlin: Fraunhofer ISI; ifeu GmbH; TU Berlin; Consentec GmbH.

Göckeler, K.; Hacker, F.; Ziegler, L.; Heinzelmann, J.; Lesemann, L.; Bernecker, T. (2022): Anforderungen der Logistikbranche an einen Umstieg auf klimaschonende Fahrzeugtechnologien. StratES Ergebnisbericht. Berlin: Öko-Institut e.V.; Hochschule Heilbronn.

Goodfellow, I.; Pouget-Abadie, J.; Mirza, M.; Xu, B.; Warde-Farley, D.; Ozair, S.; Courville, A.; Bengio, Y. (2020): Generative adversarial networks. In: Communications of the ACM, 63 (11), pp. 139–144, doi: 10.1145/3422622

Gray, N.; O'Shea, R.; Wall, D.; Smyth, B.; Lens, P. N.; Murphy, J. D. (2022): Batteries, fuel cells, or engines? A probabilistic economic and environmental assessment of electricity and electrofuels for heavy goods vehicles. In: Advances in Applied Energy, 8, p. 100110, doi: 10.1016/j.adapen.2022.100110

Greiner, M.; Unrau, H.-J.; Gauterin, F. (2018): A model for prediction of the transient rolling resistance of tyres based on inner-liner temperatures. In: Vehicle System Dynamics, 56 (1), pp. 78–94, doi: 10.1080/00423114.2017.1343955

Günter, F. J.; Wassiliadis, N. (2022): State of the Art of Lithium-Ion Pouch Cells in Automotive Applications: Cell Teardown and Characterization. In: Journal of The Electrochemical Society, 169 (3), p. 30515, doi: 10.1149/1945-7111/ac4e11

Han, X.; Lu, L.; Zheng, Y.; Feng, X.; Li, Z.; Li, J.; Ouyang, M. (2019): A review on the key issues of the lithium ion battery degradation among the whole life cycle. In: eTransportation, 1, p. 100005, doi: 10.1016/j.etran.2019.100005

Hasselwander, S.; Meyer, M.; Österle, I. (2023): Techno-Economic Analysis of Different Battery Cell Chemistries for the Passenger Vehicle Market. In: Batteries, 9 (7), p. 379, doi: 10.3390/batteries9070379

Heidt, C.; Biemann, K.; Dünnebeil, F.; Jamet, M.; Lambrecht, U.; Althaus, H.-J.; Wüthrich, P.; Hausberger, S. (2019): Entwicklung und Bewertung von Maßnahmen zur Verminderung von CO2-Emissionen von schweren Nutzfahrzeugen. Berlin.

Hesse, H.; Schimpe, M.; Kucevic, D.; Jossen, A. (2017): Lithium-Ion Battery Storage for the Grid—A Review of Stationary Battery Storage System Design Tailored for Applications in Modern Power Grids. In: Energies, 10 (12), p. 2107, doi: 10.3390/en10122107

Hettesheimer, T.; Neef, C.; Rosellón Inclán, I.; Link, S.; Schmaltz, T.; Schuckert, F.; Stephan, A.; Stephan, M.; Thielmann, A.; Weymann, L.; Wicke, T.; :unav (2022): Lithium-Ion Battery Roadmap - Industrialization Perspectives toward 2030. Karlsruhe: Fraunhofer ISI, doi: 10.24406/PUBLICA-2153

Hildermeier, J.; Jahn, A.; Rodriguez, F. (2020): Electrifiying EU city logistics. An analysis of energy demand and charging cost. Regulatory Assistance Project; International Council on Clean Transportation.

Hilgers, M. (2016): Gesamtfahrzeug. Wiesbaden: Springer Vieweg.

Hilgers, M. (2023): Vocational vehicles and applications. Berlin: Springer Vieweg.

Hlawatsch, S.; Reichling, P. (2010): Konstruktion und Anwendung von Copulas in der Finanzwirtschaft, Otto-von-Guericke University Magdeburg, Faculty of Economics and Management (Ed.).

Hoepke, E.; Breuer, S. (2016): Nutzfahrzeugtechnik. Grundlagen, Systeme, Komponenten. Wiesbaden: Springer Vieweg.

Hunter, C.; Penev, M.; Reznicek, E.; Lustbader, J.; Birky, A.; Zhang, C. (2021): Spatial and Temporal Analysis of the Total Cost of Ownership for Class 8 Tractors and Class 4 Parcel Delivery Trucks. Golden, Colorado: National Renewable Energy Laboratory.

ITF (2023): How governments can bring low-emission trucks to our roads – and fast. International Transport Forum Policy Papers, No. 127, OECD Publishing. Paris.

Jaramillo, P.; Kahn Ribeiro, S.; Newman, N.; Dhar, S.; Diemuodeke, O.; Kajino, T.; Lee, D. S.; Nugroho, S. B.; Ou, X.; Strømman, A. H.; Whitehead, J. (2023): Climate Change 2022: Mitigation of Climate Change.: Contribution of

Working Group III to the Sixth Assessment Report of the Intergovernmental Panel on Climate Change. Chapter 10: Transport. In: Cambridge University Press, doi: 10.1017/9781009157926.012

Jöhrens, J.; Rücker, J.; Kräck, J.; Allekotte, M.; Lambrecht, U.; Waßmuth, Volker, Paufler-Mann, Daniela; Veres-Homm, U.; Schwemmer, M. (2018): Roadmap OH-Lkw: Potentialanalyse 2020-2030. Kurzfristig realisierbare Potenziale für den wirtschaftlichen Betrieb von OH-Lkw. Berlin: ifeu gGmbH; Fraunhofer; PTV.

Kairies, K.-P.; Sauer, D. U. (2019): Alterungsmechanismen von Lithium-Ionen Batterien. Elektrotechnisches Kolloquium an der TU Paderborn. RWTH Aachen.

Kampker, A.; Krciskother, K.; Buning, M. K.; Dorantes Gomez, J. G. (2018): Technological and Total Cost of Ownership Analysis of Electric Powertrain Concepts for Long-Haul Transport in Comparison to Traditional Powertrain Concepts. In: 2018 8th International Electric Drives Production Conference (E|DPC). 4 and 5 December 2018, Schweinfurt, Germany : proceedings (2018 8th International Electric Drives Production Conference (EDPC)), 12/4/2018 - 12/5/2018, Schweinfurt, Germany.

Karlsson, J.; Grauers, A. (2023a): Case Study of Cost-Effective Electrification of Long-Distance Line-Haul Trucks. In: Energies, 16 (6), p. 2793, doi: 10.3390/en16062793

Karlsson, J.; Grauers, A. (2023b): Energy Distribution Diagram Used for Cost-Effective Battery Sizing of Electric Trucks. In: Energies, 16 (2), p. 779, doi: 10.3390/en16020779

Kaur, D.; Sobiesk, M.; Patil, S.; Liu, J.; Bhagat, P.; Gupta, A.; Markuzon, N. (2021): Application of Bayesian networks to generate synthetic health data. In: Journal of the American Medical Informatics Association : JAMIA, 28 (4), pp. 801–811, doi: 10.1093/jamia/ocaa303

Keil, P.; Jossen, A. (2012): Aufbau und Parametrierung von Batteriemodellen.

Khanna, N.; Lu, H.; Fridley, D.; Zhou, N. (2021): Near and long-term perspectives on strategies to decarbonize China's heavy-duty trucks through 2050. In: Scientific reports, 11 (1), p. 20414, doi: 10.1038/s41598-021-99715-w

Kies, A. (2018): A contribution to the analysis of fuel efficiency measures for heavy-duty vehicles. Graz: Verlag der Technischen Universität Graz.

Kippelt, S.; Probst, Felix, Greve; Marco; Burges, K. (2022): Einfach laden an Rastanlagen. Auslegung des Netzanschlusses für E-Lkw-Lade-Hubs. Berlin: ef.Ruhr GmbH; RE-xpertise.

Kleiner, F.; Friedrich, H. (2017): Maintenance & Repair Cost Calculation and Assessment of Resale Value for Different Alternative Commercial Vehicle Powertrain Technologies. EVS30 Symposium.

Lain, M. J.; Brandon, J.; Kendrick, E. (2019): Design Strategies for High Power vs. High Energy Lithium Ion Cells. In: Batteries, 5 (4), p. 64, doi: 10.3390/batteries5040064

Lange, J.-H.; Speth, D.; Plötz, P. (2024): Optimized demand-based charging networks for long-haul trucking in Europe. In: Environmental Research: Infrastructure and Sustainability, 4 (4), p. 45004, doi: 10.1088/2634-4505/ad889e

Li, K.; Luo, S. (2019): Bayesian Functional Joint Models for Multivariate Longitudinal and Time-to-Event Data. In: Computational statistics & data analysis, 129, pp. 14–29, doi: 10.1016/j.csda.2018.07.015

Liimatainen, H.; van Vliet, O.; Aplyn, D. (2019): The potential of electric trucks – An international commodity-level analysis. In: Applied Energy, 236, pp. 804–814, doi: 10.1016/j.apenergy.2018.12.017

Link, S.; Neef, C.; Wicke, T. (2023): Trends in Automotive Battery Cell Design: A Statistical Analysis of Empirical Data. In: Batteries, 9 (5), p. 261, doi: 10.3390/batteries9050261

Link, S.; Plötz, P. (2022): Technical Feasibility of Heavy-Duty Battery-Electric Trucks for Urban and Regional Delivery in Germany—A Real-World Case Study. In: World Electric Vehicle Journal, 13 (9), p. 161, doi: 10.3390/wevj13090161

Link, S.; Plötz, P. (2024a): Geospatial truck parking locations data for Europe. In: Data in brief, 54, p. 110277, doi: 10.1016/j.dib.2024.110277

Link, S.; Plötz, P.; Griener, J.; Moll, C. (2021): Lieferverkehr mit Batterie-Lkw: Machbarkeit 2021. Fallbeispiel REWE Group - Region Nordost. Karlsruhe: Transport & Environment; European Climate Foundation.

Link, S.; Plötz, P.; Speth, D.; Gnann, T. (2025a): European Truck Parking Locations. Zenodo. Available at https://zenodo.org/records/14643147/files/EuropeanTruckStopLocations_Documentation_KamoUpdate_v04.pdf.

Link, S.; Schneider, L.; Stephan, A.; Weymann, L.; Plötz, P. (2025b): Feasibility of meeting future battery demand via domestic production in Europe. In: Nature Energy.

Link, S.; Stephan, A.; Speth, D.; Plötz, P. (2024b): Declining costs imply fast market uptake of zero-emission trucks. In: Nature Energy, 9 (8), pp. 924–925, doi: 10.1038/s41560-024-01555-1

Link, S.; Stephan, A.; Speth, D.; Plötz, P. (2024c): Rapidly declining costs of truck batteries and fuel cells enable large-scale road freight electrification. In: Nature Energy, 9 (8), pp. 1032–1039, doi: 10.1038/s41560-024-01531-9

Magnino, A.; Marocco, P.; Saarikoski, A.; Ihonen, J.; Rautanen, M.; Gandiglio, M. (2024): Total cost of ownership analysis for hydrogen and battery powertrains: A comparative study in Finnish heavy-duty transport. In: Journal of Energy Storage, 99, p. 113215, doi: 10.1016/j.est.2024.113215

Mareev, I.; Becker, J.; Sauer, D. (2018): Battery Dimensioning and Life Cycle Costs Analysis for a Heavy-Duty Truck Considering the Requirements of Long-Haul Transportation. In: Energies, 11 (1), p. 55, doi: 10.3390/en11010055

Margaritis, D. (2003): Learning Bayesian network model structure from data. Dissertation, CMU School of Computer Science (Ed.).

Mauler, L.; Dahrendorf, L.; Duffner, F.; Winter, M.; Leker, J. (2022): Cost-effective technology choice in a decarbonized and diversified long-haul truck transportation sector: A U.S. case study. In: Journal of Energy Storage, 46, p. 103891, doi: 10.1016/j.est.2021.103891

Meng, J.; Luo, G.; Ricco, M.; Swierczynski, M.; Stroe, D.-I.; Teodorescu, R. (2018): Overview of Lithium-Ion Battery Modeling Methods for State-of-Charge Estimation in Electrical Vehicles. In: Applied Sciences, 8 (5), p. 659, doi: 10.3390/app8050659

Menter, J.; Fay, T.-A.; Grahle, A.; Göhlich, D. (2023): Long-Distance Electric Truck Traffic: Analysis, Modeling and Designing a Demand-Oriented Charging Network for Germany. In: World Electric Vehicle Journal, 14 (8), p. 205, doi: 10.3390/wevj14080205

Meszler, D.; Delgado, O.; Rodríguez, F.; Muncrief, R. (2018): European Heavy-Duty Vehicles: Cost-Effectiveness of Fuel-Efficiency Technologies for Long-Haul Tractor-Trailers in the 2025–2030 Timeframe. White Paper. Available at https://theicct.org/wp-content/uploads/2021/06/ICCT_EU-HDV-tech-2025-30_20180424_updated.pdf.

Metais, M.-O.; Jouini, O.; Perez, Y.; Berrada, J.; Suomalainen, E. (2021): Too much or not enough? Planning electric vehiclecharging infrastructure: a review of modeling options. Université Paris-Saclay.

Milence (2024): Charging and payment. Amsterdam.

Mioduszewski, P.; Ejsmont, J.; Taryma, S.; Woźniak, R. (2015): Temperature influence on tire/road noise evaluated by the drum method. The Institute of Noise Control Engineering/USA (INCE/USA.

Mulholland, E.; Miller, J.; Braun, C.; Sen, A.; Ragon, P.-L.; Rodríguez, F. (2023): The CO2 standards required for trucks and buses for Europe to meets its climate targets. White Paper. Brussels: International Council on Clean Transportation.

Mulholland, E.; Ragon, P.-L. (2024): European Heavy-Duty Vehicle Market. Development Quarterly (January-September 2024). Brussels: International Council on Clean Transportation.

Muratori, M.; Borlaug, B.; Ledna, C.; Jadun, P.; Kailas, A. (2023): Road to zero: Research and industry perspectives on zero-emission commercial vehicles. In: iScience, 26 (5), p. 106751, doi: 10.1016/j.isci.2023.106751

Naumann, M.; Schimpe, M.; Keil, P.; Hesse, H. C.; Jossen, A. (2018): Analysis and modeling of calendar aging of a commercial LiFePO4/graphite cell. In: Journal of Energy Storage, 17, pp. 153–169, doi: 10.1016/j.est.2018.01.019

Naumann, M.; Spingler, F. B.; Jossen, A. (2020): Analysis and modeling of cycle aging of a commercial LiFePO4/graphite cell. In: Journal of Power Sources, 451, p. 227666, doi: 10.1016/j.jpowsour.2019.227666

Nelsen, R. B. (2006): An introduction to copulas. New York: Springer.

Neubauer, J.; Wood, E. (2014): Thru-life impacts of driver aggression, climate, cabin thermal management, and battery thermal management on battery electric vehicle utility. In: Journal of Power Sources, 259, pp. 262–275, doi: 10.1016/j.jpowsour.2014.02.083

Neuhausen, J.; Foltz, C.; Rose, P.; Thalmair, A.; Kasseroler, T.; Kehrbein, L. (2024): Truck Study 2024: Battery-electric trucks on the rise.

Newsom, G. (2023): Office of Governor Gavin: California Approves World's First Regulation to Phase Out Dirty Combustion Trucks and Protect Public Health. Available at https://www.gov.ca.gov/2023/04/28/california-approves-worlds-first-regulation-to-phase-out-dirty-combustion-trucks-and-protect-public-health/, accessed 01.08.2023.

Noll, B.; Del Val, S.; Schmidt, T. S.; Steffen, B. (2022): Analyzing the competitiveness of low-carbon drive-technologies in road-freight: A total cost of ownership analysis in Europe. In: Applied Energy, 306, p. 118079, doi: 10.1016/j.apenergy.2021.118079

Norris, J.; Escher, G. (2017): Heavy duty vehicles technology potential and cost study. Brussels: International Council on Clean Transportation.

NOW GmbH (2022): Einfach laden an Rastanlagen. Auslegung des Netzanschlusses für E-Lkw-Lade-Hubs. Berlin.

NOW GmbH (2024a): Market development of climate-friendly technologies in the heavy-road freight transport in Germany and Europe. Evaluation of the 2024 Cleanroom Talks with truck manufacturers. Berlin.

NOW GmbH (2024b): Standorte für das LKW-Schnellladenetz an Rastanlagen mit benötigten Netzanschlussleistungen. Stand 13.09.2024. Berlin.

Nykvist, B.; Olsson, O. (2021): The feasibility of heavy battery electric trucks. In: Joule, 5 (4), pp. 901–913, doi: 10.1016/j.joule.2021.03.007

Oberfell, R. (2015): Stochastische Simulation von Energieflüssen im Nutzfahrzeug - Ein einsatzorientiertes Bewertungs- und Optimierungsverfahren. Dissertation, Karlsruhe Institute of Technology (Ed.), Karlsruhe.

Ortúzar, J. d. D. (2011): Modelling transport. Chichester: Wiley.

Pagany, R.; Ramirez Camargo, L.; Dorner, W. (2019): A review of spatial localization methodologies for the electric vehicle charging infrastructure. In: International Journal of Sustainable Transportation, 13 (6), pp. 433–449, doi: 10.1080/15568318.2018.1481243

Phadke, A.; Khandekar, A.; Abhyankar, N.; Wooley, D.; Rajagopal, D. (2021): Why Regional and Long-Haul Trucks are Primed for Electrification Now, doi: 10.2172/1834571

Pishvaee, M. S.; Kianfar, K.; Karimi, B. (2010): Reverse logistics network design using simulated annealing. In: The International Journal of Advanced Manufacturing Technology, 47 (1-4), pp. 269–281, doi: 10.1007/s00170-009-2194-5

Plötz, P. (2022): Hydrogen technology is unlikely to play a major role in sustainable road transport. In: Nature Electronics, 5 (1), pp. 8–10, doi: 10.1038/s41928-021-00706-6

Plötz, P.; Link, S.; Weißenburger, B.; Speth, D.; Ueckert, F.; Hoppe, J.; Pietzker, R. (2023a): Expanding the Blue Slide - Paris compatible pathways to 100% fossil free vehicles from 2040. Karlsruhe: Fraunhofer ISI; PIK; ACEA.

Plötz, P.; Speth, D. (2021): Truck Stop Locations in Europe - Final Report. Karlsruhe: Fraunhofer ISI.

Plötz, P.; Speth, D.; Kappler, L.; Klausmann, F.; Satvat, B. (2024): Megawatt charging in long-haul trucking: First findings on challenges and solutions. Karlsruhe: Fraunhofer ISI.

Plötz, P.; Wachsmuth, J.; Sprei, F.; Gnann, T.; Speth, D.; Neuner, F.; Link, S. (2023b): Greenhouse gas emission budgets and policies for zero-carbon road transport in Europe. In: Climate Policy, 23 (3), pp. 343–354, doi: 10.1080/14693062.2023.2185585

Qian, Q.; Gan, M.; Wei, L.; Yao, Z.; He, Y. (2024): Behavior-Driven Planning of Electric Truck Charging Infrastructure for Intercity Operations. In: IEEE Transactions on Intelligent Transportation Systems, 25 (9), pp. 12049–12065, doi: 10.1109/TITS.2024.3375458

Ragon, P.-L.; Mulholland, E.; Basma, H.; Rodriguez, F. (2022a): A review of the AFIR proposal: Public infrastructure needs to support the transition to a zero-emission truck fleet in the European Union. Brussels: International Council on Clean Transportation.

Ragon, P.-L.; Rodríguez, F. (2022b): Road freight decarbonization in Europe. Readiness of the European fleets for zero-emission trucking. White Paper. Available at https://theicct.org/wp-content/uploads/2022/09/road-freight-decarbonization-europe-sep22.pdf.

Rogozhin, A.; Gallaher, M.; Helfand, G.; McManus, W. (2010): Using indirect cost multipliers to estimate the total cost of adding new technology in the automobile industry. In: International Journal of Production Economics, 124 (2), pp. 360–368, doi: 10.1016/j.ijpe.2009.11.031

Rosenberger, N.; Rosner, P.; Bilfinger, P.; Schöberl, J.; Teichert, O.; Schneider, J.; Abo Gamra, K.; Allgäuer, C.; Dietermann, B.; Schreiber, M.; Ank, M.; Kröger, T.; Köhler, A.; Lienkamp, M. (2024): Quantifying the State of the Art of Electric Powertrains in Battery Electric Vehicles: Comprehensive Analysis of the Tesla Model 3 on the Vehicle Level. In: World Electric Vehicle Journal, 15 (6), p. 268, doi: 10.3390/wevj15060268

Saldaña, G.; San Martín, J. I.; Zamora, I.; Asensio, F. J.; Oñederra, O. (2019): Analysis of the Current Electric Battery Models for Electric Vehicle Simulation. In: Energies, 12 (14), p. 2750, doi: 10.3390/en12142750

Scania.com (Ed.) (2025). *Scania and DHL to test electric truck with fuel-powered range extender*. Available at https://www.scania.com/group/en/home/newsroom/press-releases/press-release-detail-page.html/4993330-scania-and-dhl-to-test-electric-truck-with-fuel-powered-range-extender.

Schmalstieg, J.; Käbitz, S.; Ecker, M.; Sauer, D. U. (2014): A holistic aging model for Li(NiMnCo)O2 based 18650 lithium-ion batteries. In: Journal of Power Sources, 257, pp. 325–334, doi: 10.1016/j.jpowsour.2014.02.012

Schneider, J.; Teichert, O.; Zähringer, M.; Balke, G.; Lienkamp, M. (2023): The novel Megawatt Charging System standard: Impact on battery size and cell requirements for battery-electric long-haul trucks. In: eTransportation, 17, p. 100253, doi: 10.1016/j.etran.2023.100253

Schneider, J.; Teichert, O.; Zähringer, M.; Götz, K.; Lienkamp, M. (2024): Spoilt for Choice: User-Centric Choice of Battery Size and Chemistry for Battery-Electric Long-Haul Trucks. In: Energies, 17 (1), p. 158, doi: 10.3390/en17010158

Schoch, J. (2018): Battery Life Optimal Operation of Electric Vehicles, doi: 10.5445/IR/1000083119

Seaman, A.; Dao, T.-S.; McPhee, J. (2014): A survey of mathematics-based equivalent-circuit and electrochemical battery models for hybrid and electric vehicle simulation. In: Journal of Power Sources, 256, pp. 410–423, doi: 10.1016/j.jpowsour.2014.01.057

Seemungal, L.; Arrigoni, A.; Davies, J.; Weidner, E.; Hodson, P. (2021): Decarbonisation of heavy duty vehicle transport : zero emission heavy goods vehicles : workshop summary report (28 October 2020, JRC Petten, Netherlands). Luxembourg: Publications Office of the European Union.

Seidenova, U.; Hundenborn, J.; Keuchel, S. (2022): Costs and capabilities of innovative concepts of long and heavy vehicles in Germany. In: Research in Transportation Business & Management, 44, p. 100518, doi: 10.1016/j.rtbm.2020.100518

Shoman, W.; Yeh, S.; Sprei, F.; Plötz, P.; Speth, D. (2023): Battery electric long-haul trucks in Europe: Public charging, energy, and power requirements. In: Transportation Research Part D: Transport and Environment, 121, p. 103825, doi: 10.1016/j.trd.2023.103825

Speth, D.; Plötz, P. (2024): Depot slow charging is sufficient for most electric trucks in Germany. In: Transportation Research Part D: Transport and Environment, 128, p. 104078, doi: 10.1016/j.trd.2024.104078

Speth, D.; Plötz, P.; Wietschel, M. (2025): An optimal capacity-constrained fast charging network for battery electric trucks in Germany. In: Transportation Research Part A: Policy and Practice, 193, p. 104383, doi: 10.1016/j.tra.2025.104383

Speth, D.; Sauter, V.; Plötz, P. (2022a): Where to Charge Electric Trucks in Europe—Modelling a Charging Infrastructure Network. In: World Electric Vehicle Journal, 13 (9), p. 162, doi: 10.3390/wevj13090162

Speth, D.; Sauter, V.; Plötz, P.; Signer, T. (2022b): Synthetic European road freight transport flow data. In: Data in brief, 40, p. 107786, doi: 10.1016/j.dib.2021.107786

Speth, D. W. (2024): Electrification of road freight transport – public fast charging infrastructure and the market diffusion of battery electric trucks. Karlsruher Institut für Technologie (KIT).

Spiller, B.; Lohawala, N.; DeAngeli, E. (2023): Medium- and Heavy-Duty Vehicle Electrification: Challenges, Policy Solutions, and Open Research Questions. Available at https://media.rff.org/documents/Report_23-03_v3.pdf.

Sripad, S.; Viswanathan, V. (2017): Performance Metrics Required of Next-Generation Batteries to Make a Practical Electric Semi Truck. In: ACS Energy Letters, 2 (7), pp. 1669–1673, doi: 10.1021/acsenergylett.7b00432

Sripad, S.; Viswanathan, V. (2019): Quantifying the Economic Case for Electric Semi-Trucks. In: ACS Energy Letters, 4 (1), pp. 149–155, doi: 10.1021/acsenergylett.8b02146

Steinstraeter, M.; Buberger, J.; Minnerup, K.; Trifonov, D.; Horner, P.; Weiss, B.; Lienkamp, M. (2022): Controlling cabin heating to improve range and battery lifetime of electric vehicles. In: eTransportation, 13, p. 100181, doi: 10.1016/j.etran.2022.100181

Stock, S.; Hagemeister, J.; Grabmann, S.; Kriegler, J.; Keilhofer, J.; Ank, M.; Dickmanns, J. L.; Schreiber, M.; Konwitschny, F.; Wassiliadis, N.; Lienkamp, M.; Daub, R. (2023): Cell teardown and characterization of an automotive prismatic LFP battery. In: Electrochimica Acta, 471, p. 143341, doi: 10.1016/j.electacta.2023.143341

Suneson, A.; Herlt, A.; Begon, C.; Hans, M.; Becker, H. (2024): The bumpy road to zero-emission trucks. Stockholm: McKinsey & Company.

Suzan, S.; Mathieu, L. (2021): Unlocking Electric Trucking in the EU: Recharging long highways. Electrification of long-haul trucks. Brussels: Transport & Environment.

Szimba, E.; Kraft, M.; Ihrig, J.; Schimke, A.; Schnell, O.; Fermi, F. (2012): ETISplus Database Content and Methodology, doi: 10.13140/RG.2.2.16768.25605

Tamilselvi, S.; Gunasundari, S.; Karuppiah, N.; Razak RK, A.; Madhusudan, S.; Nagarajan, V. M.; Sathish, T.; Shamim, M. Z. M.; Saleel, C. A.; Afzal, A. (2021): A Review on Battery Modelling Techniques. In: Sustainability, 13 (18), p. 10042, doi: 10.3390/su131810042

Tansini, A.; Fontaras, G.; Ciuffo, B.; Millo, F.; Rujas, I. P.; Zacharof, N. (2019): Calculating Heavy-Duty Truck Energy and Fuel Consumption Using Correlation Formulas Derived From VECTO Simulations. In: SAE technical paper series.

Teichert, O. (2024): Battery Design for Battery-Electric Long-Haul Trucks. Dissertation, Technische Universität München (Ed.). Available at https://mediatum.ub.tum.de/doc/1705700/document.pdf.

Teichert, O.; Link, S.; Schneider, J.; Wolff, S.; Lienkamp, M. (2023): Techno-economic cell selection for battery-electric long-haul trucks. In: eTransportation, 16, p. 100225, doi: 10.1016/j.etran.2022.100225

Teichert, O.; Müller, F.; Lienkamp, M. (2022): Techno-economic design of battery thermal management systems in different climates. In: Journal of Energy Storage, 48, p. 103832, doi: 10.1016/j.est.2021.103832

Tinsley, H. E.; Brown, S. (2006): Handbook of applied multivariate statistics and mathematical modeling. San Diego: Academic Press.

Tol, D.; Frateur, T.; Verbeek, M.; Rimersma, I.; Mulder, H. (2022): Techno-economic uptake potential of zero-emission trucks in Europe. Available at https://www.agora-verkehrswende.de/fileadmin/Veranstaltungen/2022/Elektrische-Lkw/TNO_2022_R11862_Techno-economic_uptake_potential_of_zero-emission_trucks_in_Europe.pdf.

Toll Collect (2025): Toll rates 2024. Berlin.

Tomasov, M.; Kajanova, M.; Bracinik, P.; Motyka, D. (2019): Overview of Battery Models for Sustainable Power and Transport Applications. In: Transportation Research Procedia, 40, pp. 548–555, doi: 10.1016/j.trpro.2019.07.079

Tong, F.; Wolfson, D.; Jenn, A.; Scown, C. D.; Auffhammer, M. (2021): Energy consumption and charging load profiles from long-haul truck electrification in the United States. In: Environmental Research: Infrastructure and Sustainability, 1 (2), p. 25007, doi: 10.1088/2634-4505/ac186a

Ueckerdt, F.; Verpoort, P. C.; Anantharaman, R.; Bauer, C.; Beck, F.; Longden, T.; Roussanaly, S. (2024): On the cost competitiveness of blue and green hydrogen. In: Joule, 8 (1), pp. 104–128, doi: 10.1016/j.joule.2023.12.004

van Basshuysen, R. (2015): Handbuch Verbrennungsmotor. Grundlagen, Komponenten, Systeme, Perspektiven. Wiesbaden: Springer Vieweg. in Springer Fachmedien Wiesbaden GmbH.

VECTO (2025): Vehicle Energy Consumption calculation Tool. Brussels.

Vermeer, W.; Chandra Mouli, G. R.; Bauer, P. (2022): A Comprehensive Review on the Characteristics and Modeling of Lithium-Ion Battery Aging. In: IEEE Transactions on Transportation Electrification, 8 (2), pp. 2205–2232, doi: 10.1109/TTE.2021.3138357

Volvo Trucks (2022): Volvo`s heavy-duty electric truck put to the test: Excels in range and energy efficiency. Gothenburg.

Walz, K.; Rudion, K. (2024): Charging Profile Modeling of Electric Trucks at Logistics Centers. In: Energies, 17 (22), p. 5613, doi: 10.3390/en17225613

Wang, Y.; Tian, J.; Sun, Z.; Wang, L.; Xu, R.; Li, M.; Chen, Z. (2020): A comprehensive review of battery modeling and state estimation approaches for advanced battery management systems. In: Renewable and Sustainable Energy Reviews, 131, p. 110015, doi: 10.1016/j.rser.2020.110015

Wang, Z.; Acha, S.; Bird, M.; Sunny, N.; Stettler, M. E.; Wu, B.; Shah, N. (2024): A total cost of ownership analysis of zero emission powertrain solutions for the heavy goods vehicle sector. In: Journal of Cleaner Production, 434, p. 139910, doi: 10.1016/j.jclepro.2023.139910

Wassiliadis, N.; Steinsträter, M.; Schreiber, M.; Rosner, P.; Nicoletti, L.; Schmid, F.; Ank, M.; Teichert, O.; Wildfeuer, L.; Schneider, J.; Koch, A.; König, A.; Glatz, A.; Gandlgruber, J.; Kröger, T.; Lin, X.; Lienkamp, M. (2022): Quantifying the state of the art of electric powertrains in battery electric vehicles: Range, efficiency, and lifetime from component to system level of the Volkswagen ID.3. In: eTransportation, 12, p. 100167, doi: 10.1016/j.etran.2022.100167

Wentzel, H. (2020): Battery Electric and Plug-in Hybrid Vehicles. Paris: Scania.

Wermuth, M.; et al. (2012): Mobilitätsstudie "Kraftfahrzeugverkehr in Deutschland 2010" (KiD 2010) - Ergebnisse im Überblick. Braunschweig.

Whitehead, J.; Whitehead, J.; Kane, M.; Zheng, Z. (2022): Exploring public charging infrastructure requirements for short-haul electric trucks. In: International Journal of Sustainable Transportation, 16 (9), pp. 775–791, doi: 10.1080/15568318.2021.1921888

Wolff, S.; Kalt, S.; Bstieler, M.; Lienkamp, M. (2021): Influence of Powertrain Topology and Electric Machine Design on Efficiency of Battery Electric Trucks—A Simulative Case-Study. In: Energies, 14 (2), p. 328, doi: 10.3390/en14020328

AI statement:

During the preparation of this thesis the author used the following AI-assisted technologies for English editing (spelling, grammar and style; sorted alphabetically): AJE.com, Chatgpt.com, DeepL Write, FhGenie, and Grammarly. After using these tools, the author reviewed and edited the content as needed and takes full responsibility for the content of the publication.